University of Groningen

Novel hybrid materials based on graphene

Spyrou, Konstantinos

IMPORTANT NOTE: You are advised to consult the publisher's version (publisher's PDF) if you wish to cite from it. Please check the document version below.

Document Version
Publisher's PDF, also known as Version of record

Publication date:
2012

Link to publication in University of Groningen/UMCG research database

Citation for published version (APA):
Spyrou, K. (2012). *Novel hybrid materials based on graphene: synthesis and characterization*. s.n.

Copyright
Other than for strictly personal use, it is not permitted to download or to forward/distribute the text or part of it without the consent of the author(s) and/or copyright holder(s), unless the work is under an open content license (like Creative Commons).

The publication may also be distributed here under the terms of Article 25fa of the Dutch Copyright Act, indicated by the “Taverne” license. More information can be found on the University of Groningen website: https://www.rug.nl/library/open-access/self-archiving-pure/taverne-amendment.

Take-down policy
If you believe that this document breaches copyright please contact us providing details, and we will remove access to the work immediately and investigate your claim.

Downloaded from the University of Groningen/UMCG research database (Pure): http://www.rug.nl/research/portal. For technical reasons the number of authors shown on this cover page is limited to 10 maximum.

Download date: 04-05-2023

Novel hybrid materials based on graphene: synthesis and characterization

Konstantinos Spyrou

University of Groningen
Zernike Institute
for Advanced Materials

The work described in this thesis was performed in the group “Surfaces and Thin Films” (part of the Zernike Institute for Advanced Materials) of the University of Groningen, the Netherlands.

Cover: Image of the Acropolis, the greatest monument of ancient Athens.

Printed by: Gildeprint Drukkerijen, Enschede

ISBN: 978-90-367-5740-9 (print)

ISBN: 978-90-367-5739-3 (digital)

ISSN 1570-1530

Zernike Institute for Advanced Materials Ph.D.-thesis series 2012-19

RIJKSUNIVERSITEIT GRONINGEN

Novel hybrid materials based on graphene

Synthesis and characterization

Proefschrift

ter verkrijging van het doctoraat in de
Wiskunde en Natuurwetenschappen
aan de Rijksuniversiteit Groningen
op gezag van de
Rector Magnificus, dr. E. Sterken,
in het openbaar te verdedigen op
vrijdag 16 November 2012
om 11.00 uur

door

Konstantinos Spyrou

geboren op 1 Juni 1984
te Ioannina, Griekenland

Promotor :	Prof. dr. P. Rudolf
Copromotor:	Prof. dr. D. Gournis

Beoordelingscommissie:	Prof. dr. M. Prato Prof. dr. J. A. Loontjens Prof. dr. K. U. Loos

ISBN: 978-90-367-5740-9

Dedicated to Vasileios Papaefthimiou

Prof. University of Ioannina

Contents

Chapter 1

Introduction

"Carbon has this genius of making a chemically stable, two-dimensional, one-atom-thick membrane in a three-dimensional world. And that, I believe, is going to be very important in the future of chemistry and technology in general." - Richard Smalley

1.1 Motivation

This thesis contains a representative part of my research efforts aimed at producing new knowledge on the creation and functionalization of graphene, as well on the intercalation of graphite and clay. The target of this work was to produce layered nanostructures based on graphene and aluminosilicate minerals as main building blocks to establish the properties of these new nanocomposite materials in view of innovative applications.

The various chapters of this thesis demonstrate the potential of those nanostructures for future use in diverse fields like catalysis, energy storage as well as biomedical and environmental applications; I also try to give the reader an overview of the advances that have been made till now.

The ideas in part inspired by previous works, emanate from my years of studies in the area of carbon allotropes and layered nanostructures.

1.2 Carbon and its allotropes

Carbon takes its name from the Latin word 'carbo' meaning charcoal, and forms the more known stable allotropes than any other element. Elemental carbon with $-sp^3$ hybridization builds up a tetrahedral lattice, giving rise to diamond (Figure 1.2), while sp^2 hybridized extended networks are responsible for the formation of graphite (Figure 1.2). Both structures have been known from the ancient times (the word diamond comes from the ancient Greek, 'adamad' meaning impossible to tame) and possess unique physical properties like hardness, thermal conductivity, lubrication behaviour.[1]

The last 30 years have brought the discovery of many other allotropes of carbon, where the periodic binding networks alternate $-sp^3$, $-sp^2$ and sp hybridized carbon atoms. Among the most famous is buckminsterfullerene (C_{60}), carbon nanotubes (CNTs) and graphene. Buckminsterfullerene was discovered at Rice University in September 1985 by Kroto, Smalley, Heath, Curl and O'Brian (Figure 1.2).[2]They observed that laser ablation of graphite lead to the formation of closed cages consisting of carbon atoms connected in pentagonal and hexagonal rings.[3]Fullerenes and their derivatives were found to be superconductors when combined with alkali metals as M_3C_{60} (M is an alkali metal),[4-7]and organic ferromagnets,[8] but they also proved useful in organic electronics and photovoltaics,[9,10] thin film transistors,[11,12]catalysts[13] and biological applications.[14] The discovery was awarded with the Nobel Prize in Chemistry in 1996.

Contemporarily with the rise of fullerene research came the discovery of carbon nanotubes by Iijima in (1991).[15]The single wall carbon nanotube (SWCNT) consists of two regions with different physical and chemical properties, the sidewall of the tube and the end cap of the tube (Figure 1.1). Multi walled carbon nanotubes (MWCNTs) consist of a collection of SWCNTs with different diameters, arranged in the fashion of Russian dolls one inside the other, and as a consequence have different properties. CNTs can be produced in various ways; the most successful of them are arc discharge,[16,17]laser ablation[18] and chemical vapour deposition (CVD).[19] Their strength, small dimensions, physical properties, electronic, optical and chemical properties open the way to innovative applications including, field emission devices,[20,21] nanoprobes and sensors, [22,23] hydrogen storage media, [24,25] semiconductor devices, composites materials, [26-28] and templates.[29,30]

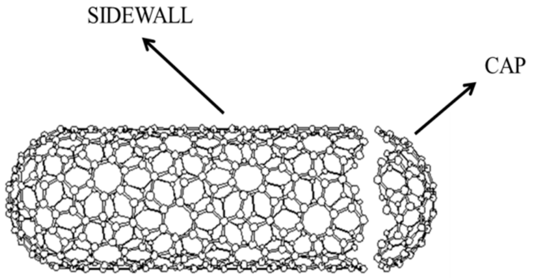

Figure 1.1. Schematic representation of a single wall carbon nanotube

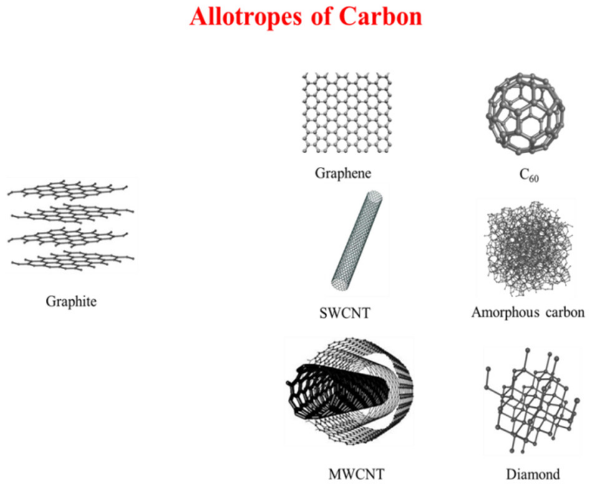

Figure 1.2. Schematic representation of some allotropes of carbon including graphite, graphene, SWNT, MWNT, C_{60}, amorphous carbon and diamond

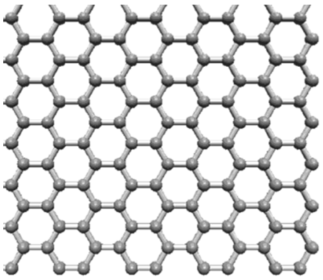

Figure 1.3. Schematic representation of graphene

There are many more allotropes of carbon like amorphous carbon, carbon nanofibers and nanoonions, all with interesting properties depending on the shape and the type of hybridization. However, a big revolution of carbon arises with the discovery of graphene, the first stable two dimensional (2-D) material ever found with extraordinary properties.

1.3 Graphene

Graphene is a monolayer of sp^2-bonded carbon atoms tightly packed into a honeycomb two dimensional (2-D) crystal lattice (Figure 1.3). Graphene has fascinated physicists and chemists because of its extraordinary properties. Graphene sheets exhibit excellent electronic properties,[31-33]thermal conductivity,[34] very high specific area (calculates value 2,630 m^2 g^{-1}),[35] transport phenomena such as the quantum Hall effect,[36] and outstanding mechanical stiffness,[37]thus this material has been extensively studied for applications like nanoelectronics,[38] sensors[38] and gas separation,[39] polymer composites,[40] supercapacitors,[41] and energy storage materials.[35]

Graphene can be obtained by various methods, each with different advantages and disadvantages (discussed extensively in Chapter 3). Some of them include micromechanical cleavage of graphite,[31] chemical exfoliation,[42] chemical vapour deposition[43] and epitaxial growth.[44]

An obstacle to the exploitation of the properties of graphene is aggregation. Graphene sheets have the natural tendency to re-aggregate by weak Van Der Waals interactions and to form graphite. Hence the high surface area, associated with individual graphene layers, becomes inaccessible due to stacking. Inserting robust stabilizers between the flakes contributes to separation and therefore allows for building strong graphene composites for applications like catalysis[45] and energy storage[46], through the well-established intercalation chemistry.

1.4 Intercalation

The term intercalation refers to the accommodation of guest molecules or ions (called the intercalants) into a host lattice, possessing, in most of the cases, a layered structure. An example concerning this process is presented in Figure 1.4. Host materials are classified in two main categories: insulating materials including zeolites, clays, layered double hydroxides, acid phosphates, and layered

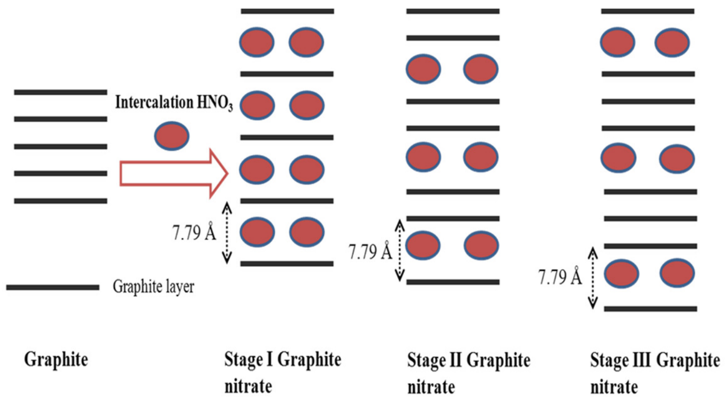

Figure 1.4. Schematic representation of three different stages of graphite intercalated with HNO_3

oxides and conducting hosts such as graphite, C_{60}, carbon nanotubes, transition metal chalcogenides, metal phosphorus trisulfides, metal oxyhalides, metal nitride halides, and metal oxides.[47] The insertion of guest species into the host matrix is exploited by the well-known 'intercalation chemistry'. According to the type of interaction between intercalant and host material, intercalation may occur through (a) electrostatic interaction, due to ion exchange of interlayer metal cations with organic/or inorganic cations (usually in clay minerals), (b) covalent bonding via chemical grafting reactions within the interlayer space (*e.g.* of graphite) or (c) weaker interactions like Van Der Waals forces, hydrogen bonding, ion dipole and coordination, electron transfer, through absorption of neutral molecules by interaction with external or internal surfaces.[47]

Graphite occupies a dominant place among the host matrixes due to the high degree of structural ordering, leading to well defined structures. The most important ordering property of graphite intercalation compounds is the staging phenomenon, which consists in intercalate layers alternating periodically with graphene layers in sequences like 1 intercalant - 1 graphene or 1 intercalent – 2 graphene etc. as schematically illustrated forstage I, II, III compounds of graphite nitrate in Figure 1.4. The first synthesis of intercalated graphite was reported by Schaffäult in 1841. However detailed studies of graphite intercalation compounds (GIC) began in the 1930s, with Hoffman and Frenzel in 1931, as well Schleede and Wellman in 1932, introducing for the first time X-ray diffraction techniques in order to investigate the structure of the hybrid compounds.[48] The recent years GIC have attracted the scientific interest due to their fascinating applications like highly electrically conductive compounds,[49-51] lithium-ion battery anodes,[52] hydrogen storage materials,[53-56] electrochemical storage media,[57] sorbents for separation processes and gas sensors.[58]

GICs have been used extensively as starting materials for obtaining colloidal dispersions of single-layer graphene sheets.[47,48] Ideally the use of a GIC allows the production of high quality graphene as will be illustrated in this thesis.

1.5 The Pillaring Method

Pillaring is the process by which an intercalated layered compound is transformed into a thermally stable, mesoporous material with high surface area, retaining the layered structure. The pillaring

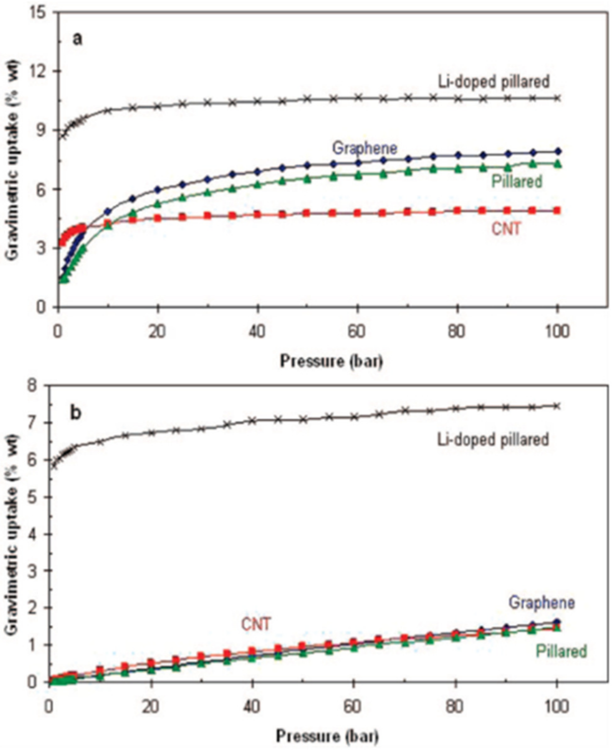

Figure 1.5. Gravimetric hydrogen uptake for graphene (diamonds), (6.6) carbon nanotubes (squares), pillared material (triangles), and Li-doped pillared (stars) at (a) 77 K and (b) 300 K. Adapted from Dimitrakakis, G. K.; Tylianakis, E.; Froudakis, G. E. Nano Letters 2008, 8, 3166–3170.

species which keeps the distance between graphene sheets can be either inorganic or organic and such structures are considered very promising as hydrogen storage media. A theoretical approach by Dimitrakakis *et al.*[5] suggests a novel three dimensional[9] (3-D) material consisting of parallel graphene layers at a variable distance, stabilized by carbon nanotubes (CNTs) placed vertically onto the graphene planes and supporting the graphene layers like 'pillars'. This material is predicted to adsorb hydrogen under ambient conditions, almost reaching the U.S. Department of Energy's (DOE) volumetric requirement for mobile applications. Figure 1.5 presents the gravimetric hydrogen uptake predicted for graphene, CNTs, pillared material and Li-doped pillared material.

1.6 Outline of the thesis

The research work described in this thesis is organized in eight chapters and three appendixes as follows.

Chapter 2 is dedicated to the experimental techniques used to characterize both starting material and hybrid composites which were the result of these four years of work. The chapter also reports in detail all the steps in the synthesis/or purification of the starting materials and is complemented by Appendixes A, B and C, which offer a brief explanation of X-ray photoelectron spectroscopy and porosimetry measurements, as well a small introduction to clay minerals and their chemical and physical properties.

Chapter 3 is devoted to our review article entitled “Roadmap to high quality chemically prepared graphene” giving a broad overview of the chemical attempts for producing graphene. We describe the different approaches and discuss the quality of the obtained product. Some recent developments are also added here.

Chapter 4 presents the successful functionalization of few layers graphene using the 1,3-dipolar cycloaddition of azomethide ylides, by amino-terminated organic groups. Through this work we demonstrated that the internal parts of the sheets are as reactive as the edges contrary to common belief, as well opens new perspectives for the control functionalization of graphene nanoplatelets acting as scaffolds for the creation of nanocomposites nanomaterials.

Chapter 5 concerns a new approach based on the synthesis of graphite intercalation compounds without the utilization of any oxidation treatments, with the help of co-intercalant molecules. Through this work we demonstrated the successful incorporation of fullerene (C_{60}) molecules between the graphene sheets with the help of nitric acid. This effort constitutes an innovative method for the intercalation of various guest molecules in graphite without disturbing the long range order of the hexagonal lattice.

Chapter 6 details a new approach for the synthesis of multi-functional materials by the intercalation of adamantylamine molecules into the host matrix of layered structures. We showed that adamantylamine can be successfully incorporated into the interlayer space of graphite oxide, montmorillonite and laponite clay. The final hybrid materials exhibit excellent properties in diverse fields like gas adsorption, environmental remediation and anticancer properties.

In Chapter 7 we describe the direct formation of multiwall carbon nanotubes by ultrasonication of graphite in dimethylformamide with the addition of ferrocene aldehyde. Carbon nanotubes are considered as rolled up graphene sheets and for the first time a chemical experimental procedure matches that concept. The proposed mechanism is general and will lead to the controlled production of carbon nanostructures by simple ultrasonication treatments.

Chapter 8 reports the successful intercalation of aluminium speices into the interlayer space of graphite oxide, after interaction with Keggin ion $[Al_{13}(O)_4(OH)_{24}(H_2O)_{12}{}^{7+}]$, and subsequent heating of this hybrid nanostructure up to 370°C. With the help of X-ray diffraction we could demonstrate the intercalation of the Al clusters and show that upon heating a pillared graphene oxide structure is formed, while with X-ray photoelectron spectroscopy we could identify the type of aluminium clusters incorporated between the graphene oxide layers.

In Chapter 9 we focus on the intercalation mechanism of cyclic aromatic molecules into graphite oxide. We investigated two molecules of this family, aniline and naphthalene amine and observed that anilene prefers to covalently bind to the graphene oxide matrix via chemical grafting, while napthalene amine binds with the graphene oxide surface through π-π electrostatic interactions. This work opens new perspectives for the interaction of various aromatic molecules with graphite oxide and the so-called “intercalation chemistry”.

References

[1] Hirsch, A. *Nat. Mater.* **2010**, 9, 868–871.

[2] Kroto, H. W.; Heath, J. R.; O'Brien, S. C.; Curl, R. F.; Smalley, R. E.*Nature* **1985**, 318, 162–163.

[3] Krätschmer, W.; Huffman, D. R.; Jura, M.; Leach, S. *Phil. Trans. R. Soc. Lond. (A Phys. Sci. Eng.)* **1993**, 343, 33–38.

[4] Hebard, A. F.; Rosseinski, M. J; Haddon, R. C.; Murphy, D. W.; Wong, T. *Tetrahedron Lett.* **1996**, 37, 6153-6156.

[5] Holczer, K.; Klein, O.; Huang, S. –M.; Kaner, R. B.; Fu, K. –J.; Whetten R. L.; Diederich, F. *Science*, **1991**, 252, 1154-1157.

[6] Haddon, R. C. *Acc. Chem. Res.* **1992**, 25, 127-133.

[7] Rosseinsky, M. J. J. *Mater. Chem.* **1995**, 5, 1497.

[8] Allemand, P. M.; Khemani, K. C.; Koch, A.; Wudl, F,; Holczer, K.; Donovan, S.; Gruner , G.; Thompson, J. D. *Science* **1991**, 253, 301-302.

[9] Bendikov, M.; Wudl, F.; Perepichka, D. F.; *Chem. Rev.* **2004**, 104, 4891–4945.

[10] Imahori, H.; Fukuzumi, S. *Adv. Funct. Mater.* **2004**, 14, 525-536.

[11] Haddon, R. C.; Perel, A. S.; Morris, R. C.; Palstra, T. T. M.; Hebard, A. F.; Fleming, R. M. *Appl. Phys. Lett.* **1995**, 67, 121-123.

[12] Anthopoulos, T. D.; Singh, B.; Marjanovic, N.; Sariciftci, N. S.; Montaigne Ramil, A.; Sitter, H.; Cölle, M.; De Leeuw, D. M. *Appl. Phys. Lett.* **2006**, 89, 213504.

[13] Gan, L.; Huang, S.; Zhang, X.; Zhang, A.; Cheng, B.; Cheng, H.; Li, X.; Shang, G. *J. Am. Chem. Soc.* **2002**, 124, 13384–13385.

[14]. Bosi, S.; Da Ros, T.; Spalluto, G.; Prato, M. *Eur. J. Med.Chem.* **2003**, 38, 913–923.

[15] Iijima, S. *Nature* **1991**, 354, 56–58.

[16] Bethune, D. S.,; Kiang, C. H.; De Vries, M. S.; Gorman, G.; Savoy, R.; Vazquez, J.; Beyers, R.; *Nature* **1993**, 363, 605–607.

[17] Ebbesen, T. W.; Ajayan, P. M. *Nature* **1992**, 358, 220–222.

[18] Journet, C.; Maser, W. K.; Bernier, P.; Loiseau, A.; Lamy de la Chapelle, M.; Lefrant, S.; Deniard, P.; Lee, R.; Fischer, J. E. *Nature* **1997**, 388, 756–758.

[19] Cassell, A. M.; Raymakers, J. A.; Kong, J.; Dai, H. *J. Phys. Chem. B* **1999**, 103, 6484–6492.

[20] De Heer, W. A.; Châtelain, A.; Ugarte, D. *Science* **1995**, 270, 1179–1180.

[21] Rinzler, A.G.; Hafner, J. H.; Nikolaev, P.; Nordlander, P.; Colbert, D. T.; Smalley, R. E.; Lou, L.; Kim, S. G.; Tománek, D. *Science* **1995**, 269, 1550–1553.

[22] Wong, S. S.; Joselevich, E.; Woolley, A. T.; Cheung, C. L.; Lieber, C. M. *Nature* **1998**, 394, 52-55.

[23] Kim, P.; Lieber, C. M. *Science* **1999**, 286, 2148.

[24] Chen, Y.; Shaw, D. T.; Bai, X. D.; Wang, E. G.; Lund, C.; Lu, W. M.; Chung, D. D. L.; *App. Phys. Lett.* **2001**, 78, 2128–2130.

[25] Dillon, A. C.; Heben, M. J. *Appl. Phys. A* **2001**, 72, 133–142.

[26] The Web site of Hyperion Catalysis International, Inc. is available at www.fibrils.com

[27] Biercuk, M. J.; Llaguno, M. C.; Radosavljevic, M.; Hyun, J. K.; Johnson, A. T.; Fischer, J. E. *App. Phys. Lett.* **2002**, 80, 2767–2769.

[28] Thompson, B. C.; Fréchet, J. M. J. *Ang. Chem. – Int. Ed* .**2008**, 47, 58–77.

[29] Braun, E.; Eichen, Y.; Sivan, U.; Ben-Yoseph, G. *Nature* **1998**, 391, 775–778.

[30] Che, G.; Lakshmi, B. B.; Fisher, E. R.; Martin, C. R. *Nature* **1998**, 393, 346–349.

[31] Novoselov, K. S.; Geim, A. K.; Morozov, S. V.; Jiang, D.; Zhang, Y.; Dubonos, S. V.; Grigorieva, I. V.; Firsov, A. A. *Science* **2004**, 306, 666–669.

[32] Novoselov, K. S.; Geim, A. K.; Morozov, S. V.; Jiang, D.; Katsnelson, M. I.; Grigorieva, I. V.,; Dubonos, S. V.; Firsov, A. A. *Nature* **2005**, 438, 197–200.

[33] Zhang, Y.; Tan, Y.-W.; Stormer, H. L; Kim, P. *Nature* **2005**, 438, 201–204

[34] Balandin, A. A.; Ghosh, S.; Bao, W.; Calizo, I.; Teweldebrhan, D.; Miao, F.; Lau, C. N. *Nano Lett.* **2008**, 8, 902–907.

[35] Stoller, M. D.; Park, S.; Zhu, Y.; An, J.; Ruoff, R. S. *Nano Lett.* **2008**, 8, 3498–3502.

[36] Zhang, Y.; Tan, Y.-W.; Stormer, H. L.; Kim, P. *Nature* **2005**, 438, 201–204.

[37] Geim, A. K.; Novoselov, K. S.; *Nat. Mater.* **2007**, 6, 183–191.

[38] Berger, C.; Song, Z.; Li, T.; Li, X.; Ogbazghi, A. Y.; Feng, R.; Dai, Z.; Alexei, N.; Conrad, M. E. H.; First, P. N.; De Heer, W. A. *J. Phys. Chem. B* **2004**, 108, 19912–19916.

[39] Schedin, F.; Geim, A. K.; Morozov, S. V.; Hill, E. W.; Blake, P.; Katsnelson, M. I.; Novoselov, K. S. *Nat. Mater.* **2007**, 6, 652–655.

[40] Stankovich, S.; Dikin, D. A.; Dommett, G. H. B.; Kohlhaas, K. M.; Zimney, E. J.; Stach, E. A.; Piner, R. D.; Nguyen, S. T.; Ruoff, R. S. *Nature* **2006**, 442, 282–286.

[41] Vivekchand, S. R. C.; Rout, C. S.; Subrahmanyam, K. S.; Govindaraj, A.; Rao, C. N. R. *J. Chem. Sci.* **2008**, 120, 9–13.

[42] Hernandez, Y.; Nicolosi, V.; Lotya, M.; Blighe, F. M.; Sun, Z.; De, S.; McGovern, I. T.; Holland, B.; Byrne, M.; Gun'ko, Y. K.; Boland, J. J.; Niraj, P.; Duesberg, G.; Krishnamurthy, S.; Goodhue, R.; Hutchison, J.; Scardaci, V.; Ferrari, A. C.; Coleman, J. N. *Nat. Nanotechnol.* **2008**, 3, 563–568.

[43] Park, S.; Ruoff, R. S. *Nat. Nanotechnol.* **2009**, 4, 217–224.

[44] Eizenberg, M.; Blakely, J. M. *Surf. Sci.* **1970**, 82, 228–236

[45] Serp, P.; Figueiredo, J. L. '*Carbon Materials for Catalysis*' (John Wiley & Sons, Inc, Hoboken, New Jersey, 2008).

[46] Boukhvalov, D. W.; Katsnelson, M. I.; Lichtenstein, A. I. *Phys. Rev. B* **2008**, 77, 033101.

[47] Dresselhaus, M. S.; Dresselhaus, G. *Adv. Phys.* **1981**, 30, 139–326.

[48] Dresselhaus M. S.; Dresselhaus G. *Adv. Phys.* **2002,** 51, 1-186 .

[49] Vogel, F. L. *Bull. Am. Phys. Soc*. **1976**, 21, 262; *J. Mater. Sci.* **1977**, 12, 982-986.

[50] Inagaki, M. *Hyoumen* **1982**, 20, 130.

[51] Matsubara, H.; Yamaguchi, Y.; Shioya, J.; Murakami, S. *Synth. Met.***1987**, 18, 503-507.

[52] Winter M; Besenhard J. O; Spahr M. E; Novak P. *Adv Mater* **1998**, 10, 725–763.

[53] (a) Watanabe, K.; Soma, M.; Ohishi, T.; Tamaru, K. *Nature* **1971**, 233, 160-161; (b) Watanabe, K.; Kondow, T.; Soma, M.; Onishi, T.; Tamaru, K. *Proc. Roy. Soc. A* **1973**, 333, 51-67.

[54] (a) Lagrange, P.; Metrot, A.; Herold, A. Compt. Rend. 1972, 275, C-765; (b) Lagrange P.; Herold, A. *ibid*.**1975**, 281, C-381.

[55] Akuzawa, N.; Katano, K.; Ohmura, Y.; Konishi, T.; Amemiya, T.; Terai, T.; and Takahashi, Y. *TANSO* **1988** [No. 133], 100.

[56] Kayiran, S. B.; Lamari Darkrim, F.; Levesque, D. *J Phys. Chem.B* **2004**, 108, 15211-15215.

[57] Frackowiak, E.; Béguin, F. *Carbon* **2001**, 39, 937-950.

[58] Rodríguez-Reinoso, F. *Carbon* **1998**, 36, 159-175.

[59] Dimitrakakis, G. K.; Tylianakis, E.; Froudakis, G. E. *Nano Lett.* **2008**, 8, 3.

Chapter 2

Experimental details

This chapter describes all the experimental details, introducing the characterization techniques as well as the procedures that have been used to obtain the starting materials for the synthesis of the hybrid nanocomposites object of this thesis. In the beginning of this chapter we report the instrumental parameters and conditions used when applying X-ray photoelectron spectroscopy, Raman spectroscopy, Fourier transform infrared spectroscopy, ultraviolet-visible spectroscopy, X-ray diffraction, porosimetry and transmission electron microscopy. In the second part we explain all the steps in the synthesis and/or purification of the starting materials.

2.1 Characterization techniques

2.1.1 X-ray photoelectron spectroscopy (XPS)

X-ray photoelectron spectroscopy (XPS) data were collected using an SSX-100 (Surface Science Instruments) spectrometer equipped with a monochromatic Al Kα X-ray source (hν=1486.6 eV). The photoelectron take-off angle was 37° and the energy resolution was set to 1.2 eV in order to minimize data acquisition time. For insulating samples, an electron flood gun was used to compensate for sample charging. The base pressure during the measurement was $3x10^{-10}$ mbar. Binding energies were referenced to the Au $4f_{7/2}$, Al 2p,

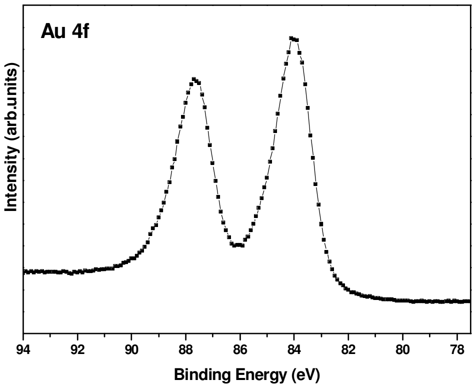

Figure 2.1 X-ray photoelectron spectrum of a gold substrate, which shows the separated Au $4f_{7/2}$ (~84 eV) and $4f_{5/2}$(~87 eV) orbitals.

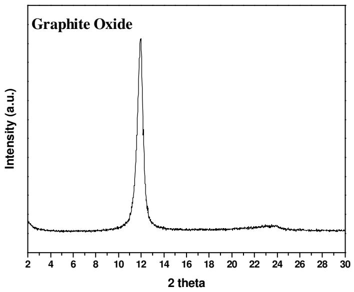

Figure 2.2 Typical XRD pattern for graphite oxide

Ag 2p and C 1s core levels[1, 2] of the substrates on which the material was deposited (see Figure 2.1 as an example). Spectral analysis included a Shirley background subtraction and peak separation using mixed Gaussian-Lorentzian functions in least-squares curve-fitting program (Winspec) developed in the LISE laboratory of the Facultés Universitaires Notre-Dame de la Paix, Namur, Belgium. For the N 1s line, we employed a linear background subtraction due to low peak intensity, which does not allow for Shirley background subtraction. The photoemission peak areas of each element used to estimate the amount of each species within the probed volume were normalized by the sensitivity factors of each element tabulated for the spectrometer used. The substrates were either evaporated gold films supported on mica (cleaned in an ozone discharge for 15 min), Ag or Al foil (purity 99.99%, Goodfellow, UK), which was polished (Brasso metal polish, Reckitt Benckiser UK Ltd., UK) to remove most of the impurities from the surface, sonicated in ethanol for 20 min, and dried in an oven (Thermo Electron Corporation, USA) at 65 °C immediately before being employed. All the measurements were peformed on freshly prepared samples in order to guarantee the reproducibility of the results. The reader is referred to Appendix A for a brief description of the XPS technique.

2.1.2 X-ray diffraction (XRD)

XRD patterns of thin films were collected using a Philips PANanlytical X'Pert MRD diffractometer with a Cu Kα (λ=1.5418 Å) radiation source (40kV, 40mA), a 0.25° divergent slit and a 0.125° antiscattering slit. The reflectivity patterns were recorded in the 2-Theta (2θ) range from 0.5 to 30° with a 0.02° step and a counting time of 15 s per step for the non-ambient measurements recorded in a temperature range of 25 ºC to 320 ºC. For the preparation of the films, aqueous suspensions of the samples were deposited on silicon substrates, and the solvent was evaporated at ambient conditions.

X-ray powder diffraction data were collected on a D8 Advance Bruker diffractometer using Cu-Kα radiation and a secondary beam graphite monochromator. The patterns were recorded in the 2-theta (2q) range from 20 ° to 90 °, with steps of 0.02 ° and a counting time of 2 s per step. Samples were in the form of films supported on glass substrates. For the preparation of the films, aqueous dispersions of the samples were deposited on glass plates, and the solvent was allowed to evaporate slowly at ambient temperature. Figure 2.2 shows the XRD pattern of graphite oxide as an example.

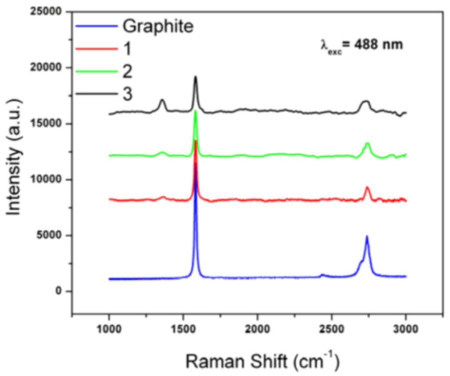

Figure 2.3 Raman spectra of graphite (blue line), few layer graphene (red line) and few layer graphene after functionalization with α-amino acid ($BocNHCH_2CH_2OCH_2CH_2OCH_2CH_2NHCH_2COOH$) (green and black line) at λ_{exc}=488nm.(for details see chapter 4)

2.1.3 Raman spectroscopy

Raman spectra covering Raman shifts in the range of 1000-2400 cm^{-1} were recorded with two systems. (a) an InVia Renishaw microspectrometer (50x) equipped with He-Ne laser at 633 nm and Ar laser at 488 nm and (b) a Micro-Raman system RM 1000 RENISHAW using a laser excitation line at 532 nm (Nd-YAG). In the second case a 0.5-1 mW laser was used with 1 mm focus spot in order to avoid photodecomposition of the samples.Samples were prepared by dropcasting dispersions of graphene products in NMP on glass surfaces and leaving them to dry under vacuum. Figure 2.3 shows the Raman spectra of graphite, few layer graphene, and few layer graphene after functionalization with α-amino acid as an example.

2.1.4 Fourier transform infraredspectroscopy (FTIR)

Infrared spectra covering the spectral range 400–4000 cm^{-1} were measured with a Shimadzu FT-IR 8400 infrared spectrometer, equipped with a deuterated triglycine sulphate (DTGS) detector. Each spectrum was the average of 128 scans collected at 2 cm^{-1} resolution. Samples were in the form of KBr pellets containing ca. 2 wt% of the compound of interest.

2.1.5 Ultaviolet-visible spectroscopy (UV/vis)

The optical characterization in the ultraviolet and visible range was carried out with a Cary 5000 spectrophotometer using 10mm path length quartz cuvettes. All spectra are normalized at 400 nm for better comparison. Samples measured were dispersed in DMF (dimethylformamide) in order to avoid aggregation. Figure 2.4 shows an example of a UV/vis spectrum.

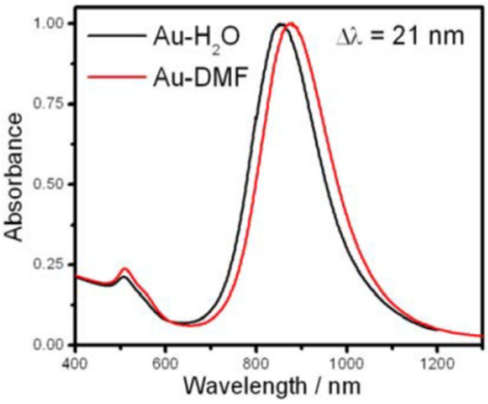

Figure 2.4 UV-vis spectra of Au nanorods in the water (black line) and after transfer into dimethylformamide (red line).

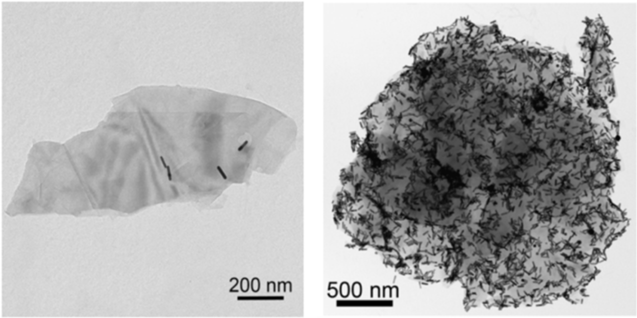

Figure 2.5 TEM image of (left) exfoliated graphite and (right) functionalized few layer graphene mixed with Au nanorods (see chapter 4)

2.1.6 Transmission electron microscopy (TEM)

TEM measurements were performed on two a TEM Philips EM208, using an accelerating voltage of 100 kV. Samples were prepared by drop casting from the dispersion onto a TEM grid (200 mesh, nickel, carbon only). Figure 2.5 shows a typical micrograph.

An aberration corrected TEM (FEI TITAN 50-80) was used at 80 kV in order to visualize the atomic structure of the graphene sheets.

2.1.7 Porosimetry measurement

The nitrogen adsorption-desorption isotherms were recorded at 77 K using a Thermo Finnigan Sorptomatic 1C1990 porosimeter. The specific surface area SBET was calculated using standard Brunauet-Emmed-Teller (BET) method.[3]A relative pressure p/p_0 range (where p and p_0 denote the equilibrium and saturation pressures of nitrogen, respectively) between 0 and 0.33 was used for the BET surface area calculation. The pore volume was calculated from the desorption isotherms, the distribution of the pores with the Barret-Jaynor-Halenda (BJH) method. All the samples used for surface area measurements were degassed at 120 ^{o}C for 10 hours under high vacuum (10^{-4} mbar).The reader is referred to Appendix B for a brief description of the porosimetry technique with the BET method.

2.2 Material preparation

2.2.1 Preparation of graphite oxide (GO)

The first report on the on the preparation of GO comes from Brodie in 1859.[4]GO was prepared by treating natural graphite (Ceylon) with an oxidation mixture consisting of potassium chlorate and fuming nitric acid, for reaction times of 3–4 days with the solution kept at a temperature of 60 °C, until no further change was observed. Staudenmaier[5] proposed a variation to Brodie's method, where the graphite is oxidized in concentrated sulfuric and nitric acids with potassium chlorate. These methods have been adapted over the years to exfoliate graphite and make it soluble as described elsewhere.[6,7,8]Our starting material consisted in exfoliated hydrophilic single-layer flakes of graphene oxide (GO),[*]prepared following Staudenmaier's method[1] for oxidizing powdered graphite. In detail, 10 g of powdered graphite (purum, powder ≤0.2 mm; Fluka) were added to a mixture of concentrated sulphuric acid (400 mL, 95–97 wt%) and nitric acid (200 mL, 65 wt%) while cooling in an ice-water bath. Potassium chlorate powder (200 g, purum, >98.0%; Fluka) was added to the mixture in small portions while stirring and cooling. The reactions were quenched after 18 h by pouring the mixture into distilled water and the oxidation product was washed until the pH reached the value 6. The sample was then dried at room temperature.

A schematic representation of the reactions followed for the synthesis of GO is presented in Figure 2.6.

2.2.2 Clay as host material and purification

The clay used in this work was a natural Wyoming montmorillonite (SWy-2) obtained from the Source Clay Minerals Repository, University of Missouri, Coloumbia, with a cation exchange capacity (CEC) of 76.4 meq/100 g clay and composition $[(Al_{3.07}Ti_{0.01}Fe(III)_{0.40}Mg_{0.49})(Si_{7.79}Al_{0.12})O_{20}OH_{4}]Na_{0.75}$.[9]

The cation exchange capacity (CEC) is defined as the amount of exchangeable cations that a clay mineral can adsorb at a specific pH.The clay was fractionated to <2 μm by gravity sedimentation and purified by standard methods in clay science.[10] Sodium exchanged samples (Na^{+}-SWy-2) were prepared by immersing the clay in an aqueous solution of sodium chloride 1mol/L. The cation exchange was completed by washing and centrifuging four times with NaCl solution. The samples were finally washed with double distilled deionized water, transferred into dialysis tubes in order to obtain chloride-free clays and then dried at room temperature. In Figure 2.7 a schematic structure of montmorillonite before and after the exchange with Na^{+} cations is presented.

---

[*] Synthesis by E. Diamanti, University of Ioannina.

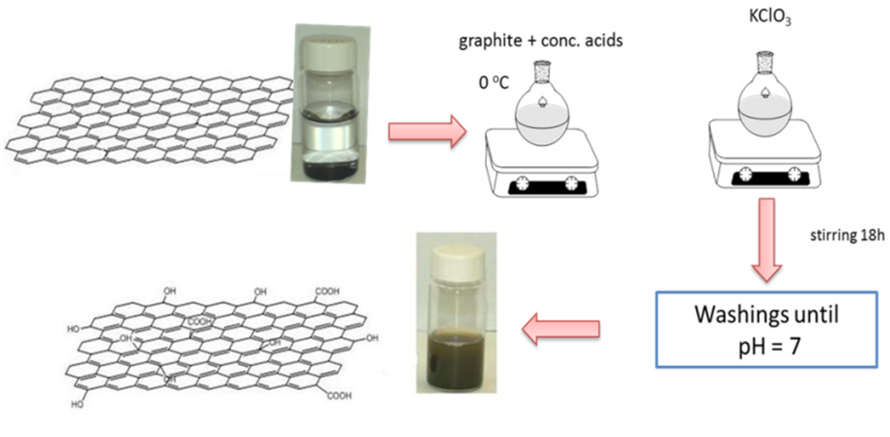

L. Staudenmaier, Ber. deut. *Chem. Ges.* 31, 1481, (1899).

Figure 2.6 Schematic representation of the synthetic procedure for obtaining an aqueous dispersion of GO.

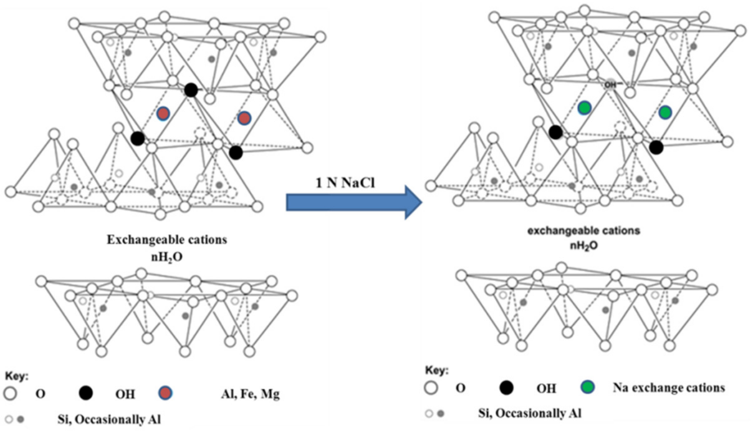

Figure 2.7. Schematic representation of Wyoming montmorillonite (SWy-2) before and after exchange with sodium cations

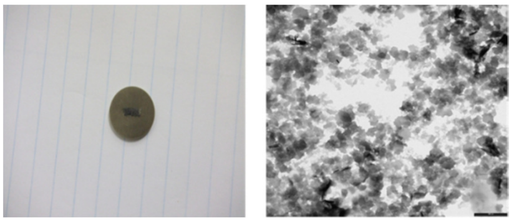

Figure 2.8 Graphite after intercalation with nitric acid (left) and TEM image of Graphite-HNO_3 (right)

2.2.3 Preparation of graphite nitrate (GN)

In a typical procedure,[†] which follows the method of Inagaki at al,[11] graphite powder (4 gr) was suspended in 20 mL of fuming nitric acid (≥99.5 %) under vigorous stirring at ambient conditions for 30 min, and the mixture was left to rest for 90 min. After the top yellow solution (redundant nitric acid) was removed by siphoning, 50 mL of anhydrous acetonitrile was added and the mixture was stirred for another 5 min. The solid phase was separated by filtration through a PTFE membrane with average pore size of 0.45 μm. Finally, the film was washed twice with anhydrous acetonitrile (20 mL each time) and dried under vacuum. The final product (GN) was placed in a brown glass bottle and stored at RT. The weight gain of starting graphite due to reaction of nitrates was about 30%. Figure 2.8 shows graphite after the intercalation of nitric acid (left) and TEM image of graphite nitrate (right).

2.2.4 Preparation of graphene

24 mg of graphite were dispersed in 200 mL of N-methylpyrrolidone (NMP) and sonicated for 30 min in a low power sonic bath (2510 Branson).[‡] The resultant dispersion was then centrifuged using a Hettich Universal 320 centrifuge for 90 min at 500 rpm. Thereafter, decantation was carried out by pipetting off the top half of the dispersion. Figure 2.9 shows a TEM micrograph of the obtained material.

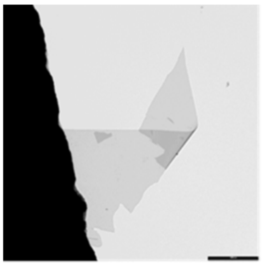

Figure 2.9. TEM image of Graphene in NMP

References

[1] Moulder, J. K.; Stickle, W. F.; Sobol, P. E.; Bomben, K. D. **1995** '*Handbook of X-ray photoelectron Spectroscopy*', Physical Electronics, Inc. (Eden Prairie, Minnesota,).

[2] Lotya, M.; Hernandez, Y.; King, P. J.; Smith, R. J.; Nicolosi, V.; Karlsson, L. S.; Blighe, F. M.; De, S.; Wang, Z.; McGovern, I. T.; Duesberg, G. S.; Coleman, J. N. *J. Am. Chem. Soc.* **2009**, 131, 3611-3620.

[3] Brunauer, S.; Emmett, P. H.; Teller, E. *J. Am. Chem. Soc.* **1938**, 60, 309–319.

[†] Synthesis by Longtian Kang, Zernike Institute for Advanced Materials

[‡] Synthesis by Mildred Quintana, University of Trieste

[4] Brodie, B. *Phil. Trans.*.**1869** 149, 249.

[5] Staudenmaier, L. *Berichte der deutschen chemischen Gesellschaft* **1898**, 31, 1481-1487.

[6] Dekany, I.; Kruger-Grasser, R.; Weiss, A. *Colloid Polym. Sci.* **1998**, 276, 570.

[7] Stankovich, S.; Dikin, D. A.; Piner, R. D.; Kohlhaas, K. A.; Kleinhammes, A.; Jia, Y.; Wu, Y.; Nguyen, S. T.; Ruoff, R. S. *Carbon* **2007**, 45, 1558.

[8] Stathi, P.; Litina, K.; Gournis, D.; Giannopoulos, T. S.; Deligiannakis, Y. J. *Colloid Interface Sci.* **2007**, 316, 298.

[9] Auerbach, S. M.; Carrado, K. A.; Dutta, P. K.; **2004**. *Handbook of layered materials.* M. Dekker.

[10] King, R. D.; Nocera, D. G.; Pinnavaia, T. J. J. *Electroanal. Chem.* **1987**, 43, 23

[11] Inagaki, M.; Rouillon, J. C.; Füg, G., Delhaes, P. *Carbon* **1977**, 15, 181–185.

Chapter 3

The roadmap to high quality chemically prepared graphene[§]

This chapter is devoted to our review article entitled "Roadmap to high quality chemically prepared graphene" and gives a broad overview of the chemical methods for producing graphene. We describe the different approaches and discuss the quality of the obtained product. Some recent developments are also added here.

3.1 Introduction

In the past few years much interest has focused on graphene, a flat monolayer of carbon atoms tightly packed into a two dimensional (2D) honeycomb lattice. K.S Novoselov and A.K.Geim's discovery, that micromechanical cleavage of bulk graphite allows us to isolate graphene,[1] has triggered a tremendous amount of scientific interest in this new material, at first mainly for its electronic properties. Graphene was immediately seen as the successor of the current silicon-based technology since the 2-D honeycomb carbon structure features semimetallic behaviour and high carrier motilities, which are ideal for a potential implementation as computing element. Therefore, graphene sheets, if processable, could be used in classical computer technology, even though examples of use as qubit elements or for spintronics potentially extend its use further then to purely classical transistor-based microprocessors. Alongside with this main research stream, pure graphene was found to exhibit outstanding mechanical,[2] thermal[3] an optical properties,[4] while graphene derivatives like graphene oxide or other types of functionalized graphene display remarkable catalytic, mechanical, sensing and electronic properties.

Although graphene has so far been explored mainly in fundamental research, creating or depositing high quality graphene for application purposes has been one of the main challenges. Without realizing the future impact of his research, Brodie was the first to produce exfoliated graphite (through oxidation).[5] The final product was not graphene but graphene oxide (noticed by Brodie because of the increased mass of the reaction product).[5] More than a century later, a drastically different method, micromechanical cleavage,[1] used to produce isolated graphene sheets, stimulate new interests in graphene. Since then chemists and physicists

---

[§] This chapter is based on: Gengler, R.Y.N.; Spyrou, K.; Rudolf, P. 2010. A roadmap to high quality chemically prepared graphene. Journal of Physics D: Applied Physics 43, 374015.

have used a plethora of (more or less successful) methods, among which chemical vapour deposition (CVD) is one of the most promising[6] in terms of coverage and layer quality. In fact, while micromechanical cleavage has been very successful in producing samples for fundamental studies, its extremely low yield and lack of control in placement of the sheets limits future in application. Other methods based on the use of SiC as a substrate and as a precursor have excellent potential in the pursuit of the best quality synthetic graphene.[7-11] An alternative road is chemically prepared graphene, which we review in this chapter, focusing on properties and quality as a function of the production method (electronic properties, transparency, ambipolar behaviour, sheet size and related features such as defect/impurity level and coverage on various substrates). Chemical preparation processes of graphene sheets use graphite as starting material and delaminate it by various means, namely by chemical functionalization, oxidation or by intercalation. To give a good representation of today's scientific landscape concerning chemical methods for graphene production we divided the subject into two subcategories, the preponderant graphene oxide (GO) production as a first one and all the other methods (intercalation with N-methylpyrrolidone (NMP), functionalized surfactants, perfluorinated aromatic molecules, etc.) as a second one.

3.2 Graphene from graphene oxide

The first reports on the production of GO date from 1840 by Schafhäutl[12] and 1859 by Brodie.[5] In the latter GO was prepared by treating natural graphite (Ceylon) with an oxidation mixture consisting of potassium chlorate and fuming nitric acid, for reaction times of 3–4 days with the solution kept at a temperature of 60 ºC, until no further change was observed. Interestingly, the author, Brodie, proposed also an alternative method, where the heating was replaced by exposing the oxidation mixture flasks to sunlight and described it as advantageous because it was faster. Staudenmaier[13] proposed a variation to Brodie's method, where the graphite is oxidized in concentrated sulfuric and nitric acids with potassium chlorate. 99 years after Brodie's first experiments, Hummers and Offeman[14] presented a method where the oxidation of graphite to graphitic oxide is accomplished by treating graphite with a water-free mixture of concentrated sulfuric acid, sodium nitrate and potassium permanganate. This process requires less than 2 h for completion and rather low temperatures (below 45 ºC). In the pursuit of high quality graphene these three methods have been used extensively over the past few years. Based on the results obtained with a variety of modern analysis techniques such as NMR,[15] XPS,[16-18] TEM[19] and Raman,[20,21] the most recent model of GO's structure is the one depicted schematically in Figure 3.1, where hydroxyl and

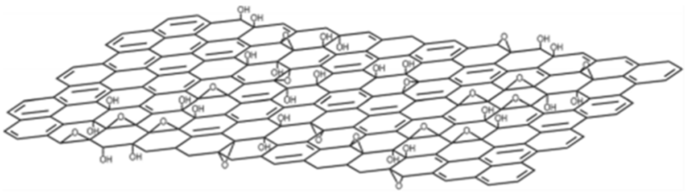

Figure.3.1. Schematic representation of the structure of graphene oxide sheets (GO); grafted hydroxyl and epoxide groups disrupt the sp^2-bonded carbon mesh of pure graphene. Scheme taken from Park and Ruoff. Reprinted with permission from Macmillan Publishers Ltd: Nature Nanotechnology[23] Copyright (2009).

epoxide groups are grafted randomly (for older structural models of GO and details of derivation of this model see ref.[22]) to the carbon mesh alter the sp^2-bonded carbon network of pure graphene sheets.[23]Owing to the presence of such hydrophilic polar groups, the GO presents swelling and intercalation properties very similar to clay.[24] In the next four sections, we shall review some of the characteristics of this new material.

3.3 Ambipolar behaviour – the quest for high field effect mobility

While an incredibly large number of publications on graphene have appeared in the last 3–4 years, very few actually testify to the truly amazing properties of this material. In particular, most of the recent publications concerning the development of new synthesis methods for graphene, comprising exfoliation, reduction, deposition, etc., omit giving evidence for ambipolar behaviour by recording the Dirac curve, as the conductivity, resistivity or drain–source current versus gate voltage measured in a field effect transistor [FET] device configuration is called. Transmission electron microscopy and atomic force microscopy, often used to demonstrate the graphene character of newly produced material, are very local probes and do not inform on the overall graphene quality. If one wants to compare chemically produced material with high quality graphene created by micromechanical cleavage, the Dirac curve is the best non-local probe. Both graphene and graphite display a good conductivity; therefore measuring high flake conductivity without gate voltage dependence does not prove a bipolar behaviour. To the best of our knowledge, the measurements reported by Gomez-Navarro et al.[20] were the first to actually show the ambipolar character of the deposited chemically prepared material, i.e. reduced graphene oxide (RGO). The room-temperature field effect mobilities of 2–200 $cm^2\ V^{-1}\ s^{-1}$ for holes and 0.5– 30 $cm^2\ V^{-1}\ s^{-1}$ for electrons reported for these reduced GO samples are approximately 2 orders of magnitude lower than those of mechanically cleaved graphene[1] and definitely lower than the 200000 $cm^2\ V^{-1}\ s^{-1}$ field effect mobility of free-standing graphene[25] because of the defective nature of the reduced layers. More detailed data about the ambipolar behaviour of graphene and reduced graphene oxide are presented on the invited review article: “Roadmap to high quality chemically prepared graphene” Journal of Physics D: Applied Physics 43, 37, p.3745015.

3.4 Structural integrity

Reduced Graphene Oxide (RGO) shows the typical ambipolar behaviour expected for graphene but strongly influenced by the presence of defects/impurities. The structural integrity of the RGO can be investigated by several methods as described hereafter. Low energy electron diffraction and selected area electron diffraction (SAED) have been the methods of choice to reveal local and global high crystallinity of reduced GO and exfoliated samples (see last section for the latter) because the cross section for interaction with electrons is 105 times higher than that with X-rays, electrons can be focused on very small spots and these techniques do not require access to large-scale facilities like synchrotron or neutron sources. STM and HRTEM are probably today’s most powerful tools to investigate, locally, the structural integrity of a given material. Therefore, we review hereafter some of the most relevant studies realized on GO and reduced GO. Figure 3.2(a) shows the STM image of a GO sheet deposited onto HOPG after dispersion in water with the help of soft sonication.[20]The hexagonal lattice of graphene is clearly

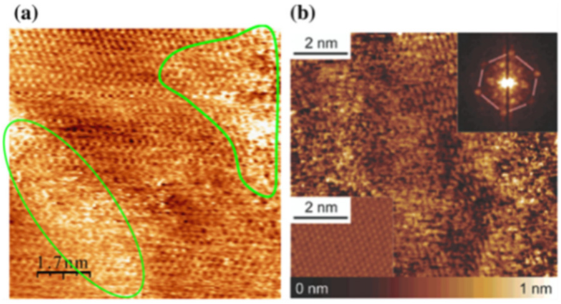

Figure 3.2 (a) STM image of a graphene oxide monolayer on HOPG. Oxidized regions are marked by green contours, reprinted with permission from Gomez-Navarro et al.[20] Copyright 2007 American Chemical Society. (b) 10 × 10 nm STM image of a different type of oxidized graphene on HOPG, Fourier transform of the image shows that the hexagonal order is present (inset on the right top), and inset on the left bottom shows an STM image of HOPG recorded with identical scan conditions, reprinted with permission from Kudin et al.[21] Copyright 2008 American Chemical Society.

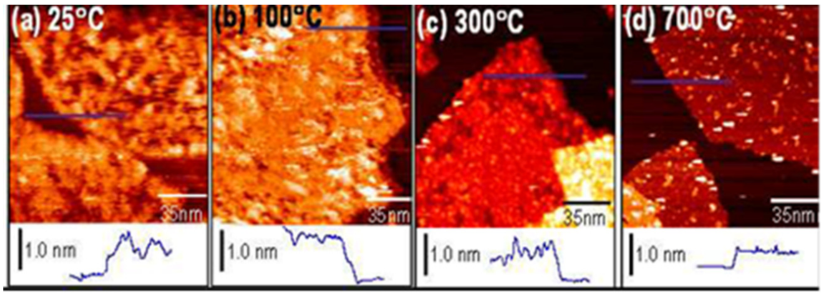

Figure 3.3 (left) STM image from Chua et al[29] of octadecylamine functionalized GO and representative line profile after thermal treatment at different temperatures. (a) Pristine, (b) after 10 min 100 °C in N_2, (c) after 10 min 300 °C in N_2, and (d) after 15 min 700 °C in N_2. Conditions: $V_{tip} = 2.0V$, $i_{tunnel} = 100$ pA and T = 77 K. Image vertical scale: 1.0 nm (bright is high and dark is low). Reprinted with permission from Chua et al,[29] copyright 2008 American Institute of Physics.

preserved in some parts of the sheet while the regions marked by green contours presumably contain functional groups from the oxidation process and appear disordered. The degree of oxidation/defect level of this type of sheets was calculated from a range of measurements and agrees with spectroscopic data.[20] The STM image in Figure 3.2(b) shows similar features for different GO, called functionalized graphene in the original report, prepared through rapid heating of GO in solution[21] and subsequent deposition on HOPG and is also clearly distinguishable from pristine graphene (shown in the inset of Figure 3.2(b)). Even though Figure 3.2(b) does not reveal large regions with a honeycomb lattice as seen in Figure 3.2(a), a Fourier transform of the image (see inset Figure 3.2(b)) shows a clear hexagonal structure, signature of a graphitic backbone. The observed separation of pristine graphene and disordered regions in these GO sheets agrees with the theoretical prediction that these functional groups should arrange in islands and rows.[26]

GO shown in Figure 3.2 appears quite rough with a peak to peak distance of about 1 nm, most likely due to the presence of random –O and –OH or defects. However, a model for the possible bonding

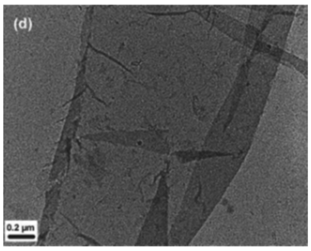

Figure 3.4 Transmission electron micrograph of water soluble functionalized GO, Reprinted with permission from Si et al.[30] Copyright 2008 American Chemical Society.

sites of –O and –OH on a graphene layer[27] reproduced in Figure 3.3 (right panel) shows a possible arrangement where top and bottom –O and –OH groups are attached to the graphene sheet in a periodic fashion. Such a structure has been observed by Pandey et al.[28] in STM images of GO prepared following the classic Hummers and Offeman's method as illustrated in the left panel of Figure 3.3. This is the first atomically resolved image of a graphene oxide sheet which seems, nevertheless, to refer to rather small areas since the reported STM field of view is only of ~2 nm^2.This periodic structure can therefore be regarded as a minority phase of GO while the randomly attached functional groups discussed before constitute the majority phase.

Surface functionalization of GO can be a means to introduce desired chemical groups for control of the surface properties and for integration into devices. In this context it is not only important to understand the functionalization process itself but also to identify how the introduced groups influence the graphene properties. As a representative example,[29] STM images GO nanosheets functionalized with octadecylamine are displayed in Figure 3.4; the line profile across the sheet edge extracted from these images is also shown. The authors argue that by adding the van der Waals radius of graphene to twice that of octadecylamine since the molecules are grafted on both sides of the nanosheet, one obtains a total van der Waals radius of 1.0–1.2 nm, in agreement with the observed STM image. Note that this value also agrees with atomic force microscopy (AFM) data[11] of octadecylamine-functionalized GO. The series of STM images in Figure 8 displays the thickness and morphology evolution as a function of the temperature. No changes in morphology/coverage of grafted groups are observed for annealing at 373 K, while annealing beyond this temperature results in a progressive diminution of the bright features on top of graphene, identified as the grafted groups as well as a decrease in the average thickness. This trend is observed up to a temperature of 973 K where very few bright features remain. One can conclude from these observations that the octadecylamine functionalities progressively detach from the graphene sheet.

Additional proof of the graphene-like structure of the graphene oxide and functionalized graphene oxide is provided by TEM images and diffraction patterns (SAED). Figure 3.5 shows a TEM image of functionalized graphene oxide obtained by reducing exfoliated graphite oxide in the presence of poly(sodium-4 styrene sulfonate).[30] The large single sheet appears transparent and folded over at the edges, with isolated small graphene fragments on its surface, similarly to what one observes for micromechanically cleaved graphene.[31] Figure 10 presents instead the TEM images and diffraction pattern of graphene oxidized with benzoyl peroxide after reduction.[32] Again single sheets with a hexagonal diffraction pattern are evident. This is the only GO not produced using Hummers and Offeman's, Brodie's or Straudemair's methods and the flakes are significantly smaller than what one can obtain using the 'classical oxidation routes'.

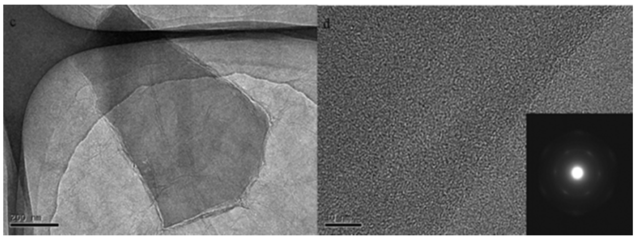

Figure 3.5 Transmission electron micrographs of benzoyl peroxide oxidized graphene oxide. Scale bar 200 nm (left) and 10 nm (right). Reprinted with permission from Shen et al.[32] Copyright 2009 American Chemical Society.

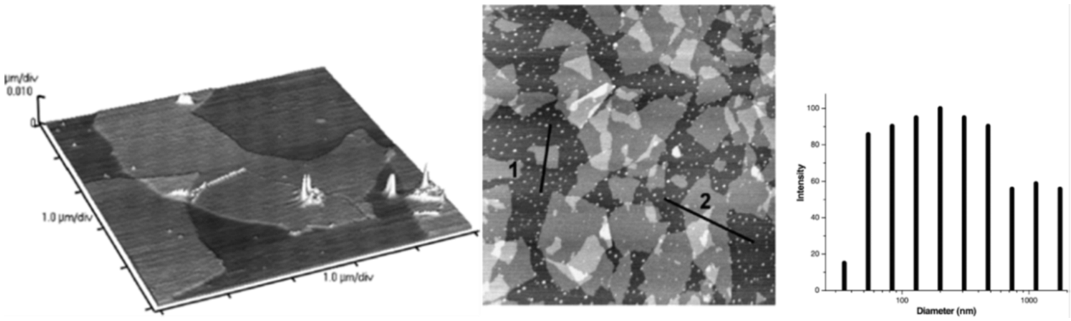

Figure 3.6 Non-contact mode AFM image of isolated exfoliated single layer graphene oxide; from Stankovich et al.,[33] reproduced with permission from the Royal Society of Chemistry. A non-contact AFM image of nanoplatelets deposited on a mica surface from a dispersion of phenyl isocyanate-treated GO in DMF; line 1 = 0.7μm , line 2 = 1.0 μm and CONTIN analysis showing the intensity-weighted hydrodynamic diameter distribution of phenyl isocyanate-treated GO nanoplatelets exfoliated in DMF. Reprinted from Stankovich et al.[34] with permission from Elsevier.

3.5 Going large-scale

While in the previous section we mainly focused on the properties and quality of the graphene flakes prepared by various methods, in this section we review which approaches can be considered best in terms of 'large-scale' production. To this end we compared various preparation methods on the basis of different microscopies or optical images of the produced material. In this comparison we consider first the chemically exfoliated flakes and then how controllably surfaces can be covered with single graphene sheets. Figure 3.6 shows one of the first AFM images of isolated exfoliated single layer GO, namely a ~ 10 μm^2 sheet deposited from a colloidal suspension onto a mica substrate and measured to be ~1 nm thick.[33] In the central panel of Figure 3.6, one can see the size distribution of the first chemically derivatized graphite oxide exfoliated in organic solvents (also deposited on mica).[34] These two examples of single layers of pure and chemically functionalized GO are among the first where complete exfoliation was achieved and have therefore been chosen to illustrate the starting point of a rapid evolution. In these pioneering results neither the coverage nor the number of deposited layers was controlled (see Figure 3.6).

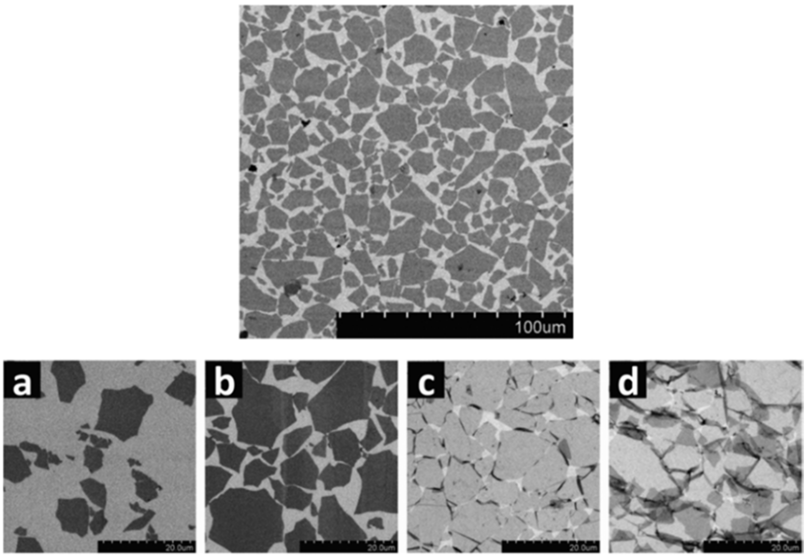

Figure 3.7 (Top) SEM images of the monolayers of highly covered sample. Scale bars represent 100 µm. (bottom) Langmuir–Blodgett assembly of graphite oxide single layers. (a)–(d) SEM images showing the collected graphite oxide monolayers on a silicon wafer in different regions of the isotherm. The packing density was continuously tuned: (a) dilute monolayer of isolated flat sheets, (b) monolayer of close-packed GO, (c) overpacked monolayer with sheets folded at interconnecting edges and (d) over packed monolayer with folded and partially overlapped sheets interlocking with each other. Image reprinted with permission from L.J. Cote et al.[35] Copyright 2009 American Chemical Society.

A few years later, still using the same Hummers and Offeman's method to produce the starting GO, new deposition procedures were developed to achieve larger flake size, high controllability of the packing and, last but not least, single layer deposition. Two examples of optimal results obtained so far for the deposition of chemically prepared graphene are illustrated in Figure 3.7 top and bottom. Cote et al.[35] used a Langmuir–Blodgett method first reported in Li et al.[36] but achieved a drastic improvement in terms of flake size and controlled deposition. Similar control alongside with proof of the true graphene quality was reported shortly after by Gengler et al.[37]. Since one can monitor the surface pressure on top of the water in the Langmuir–Blodgett trough, the packing of the graphene oxide sheets floating at the air/water interface is controlled very easily. As illustrated by the sequence of images (a)–(d) in the bottom panel of Figure 3.7, the more or less compacted floating layer can be transferred to a variety of substrates by vertical or horizontal dipping. One can see an increased coverage; in the first image (Figure 3.7 bottom) where flakes with lateral dimensions of 4–10µm are well dispersed with a distance of 5–20µm between them. With increasing surface pressure, the packing increases from image (b), where the inter-flake distance is 1–2µm to less than 1µm with some contact between the flakes in image (c), to finally the most dense case in image (d), where the GO flakes are so compressed that they start to overlap at the borders. GO flakes reaching millimeter sizes for use as thin film electrodes when reduced were reported by Su et al.[38]

A last example of deposition we review here is one where selectivity is achieved through surface modification, namely a study by Wei et al.[39] of GO transferred from a colloidal dispersion to a patterned

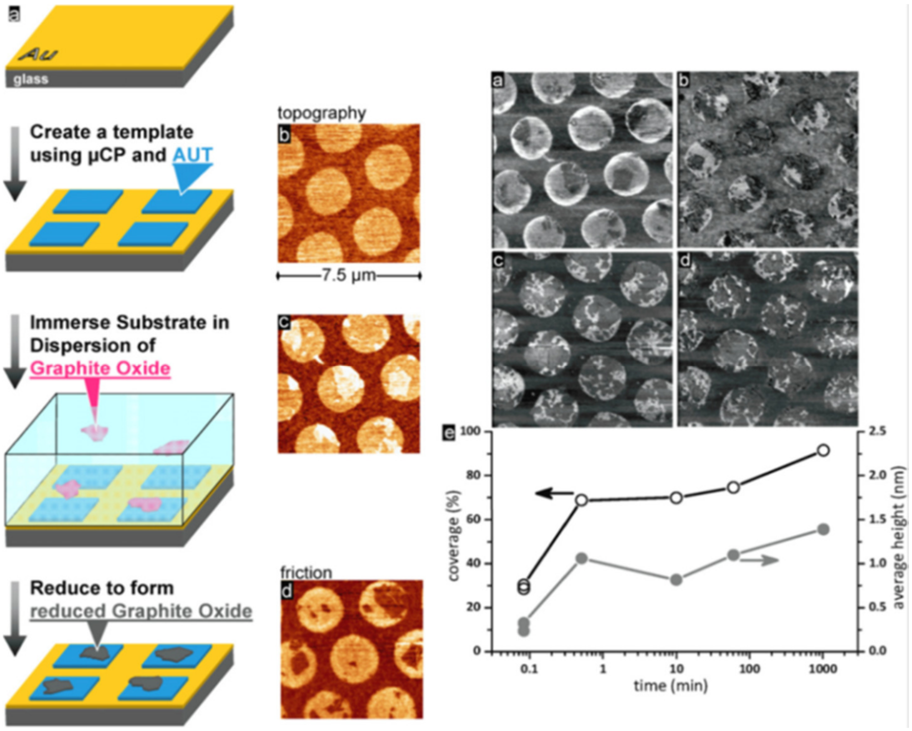

Figure 3.8 (Left) A scheme of the templating process that shows the formation of the amino-terminated template on mica-peeled gold, followed by immersion in a dispersion of graphite oxide to the reduction of the captured GO to form reduced graphite oxide. (Right (a)–(d)) Friction images of 11-amino 1-undecanethiol (AUT)-patterned Au following 5 s (a), 30 s (b), 10 min (c) and 17 h (d) immersion times in GO dispersions, respectively. All images are 10µm wide and show the bright (high friction) 11-amino 1-undecanethiol (AUT) being covered with the lower friction GO. (e) Plot of the per cent coverage and average height of the GO films as a function of time. There is a quick adsorption period followed by a much longer and slower adsorption. Reprinted with permission from Wei et al.[39] Copyright 2008 American Chemical Society.

substrate. As summarized in Figure 3.8, the authors show that a charged molecular template created using microcontact printing can direct the attachment of a single graphene oxide layer. The method is based on a few simple steps: first the desired template is printed using microcontact printing; the molecule chosen by the authors was 11-amino-1-undecanethiol. Then the gold substrate printed with the pattern of self-assembled molecules is immersed in a GO solution. The authors show that this later step is critical: time, pH and GO concentration influence drastically the quality of the deposition. Once this attachment is achieved, the adsorbed layer can be processed further—for example with a reduction treatment of GO to obtain graphene. Figure 3.8 documents the success of this method, since in the AFM image on the left (labeled c) selective adsorption can be clearly distinguished. The images on the right of Figure 3.8 show instead the influence of the dipping time on the coverage of the patterned surface, in fact, a dipping time of 5 s (Figure 3.8(a)) produces a coverage of ~50% while immersion for 17 h (Figure3.8(d)) covered the patterned surface up to ~90%. A similar templated deposition was reported by Li et al.[40] and in principle one can envision other methods for producing the template such as dip pen lithography.[41]

3.6 The roadmap to high quality graphene

The scientific landscape has been flooded in the few last years by a huge amount of reports on new methods in terms of production, deposition, reduction or exfoliation of graphene, supposedly one better than the other. In this last section we draw up a condensed summary of the most relevant examples and point out what we believe to be the best currently available ways to prepare graphene. Scheme 3.1, our roadmap to high quality graphene, displays CVD, mechanical cleavage, Si carbide and other methods defined previously but we shall focus our attention on the methods using chemically derived graphene. Graphite is on top of this scheme and represents today's reality: all or a huge majority of the chemical approaches are top down; in opposition to bottom up approaches so commonly used in material science. Bottom up approaches for graphene-like 2D polymers are not the scope of this review but we refer the reader to Junji Sakamoto et al.[42]

Anyone getting started in graphene production can choose from many different routes leading to the goal but requiring/involving a series of procedures that will result in the same end material, though of various quality. Starting from graphite, one has two options, going through oxidation or avoiding it. The ease and relatively high yield of the graphite oxide approach lead a lot of research groups to follow that path. The starting point is in this first case the oxidation of graphite (any type) by means of potassium chlorate and fuming nitric acid treatment(s) as described by Brodie in 1859[5] or, as proposed by

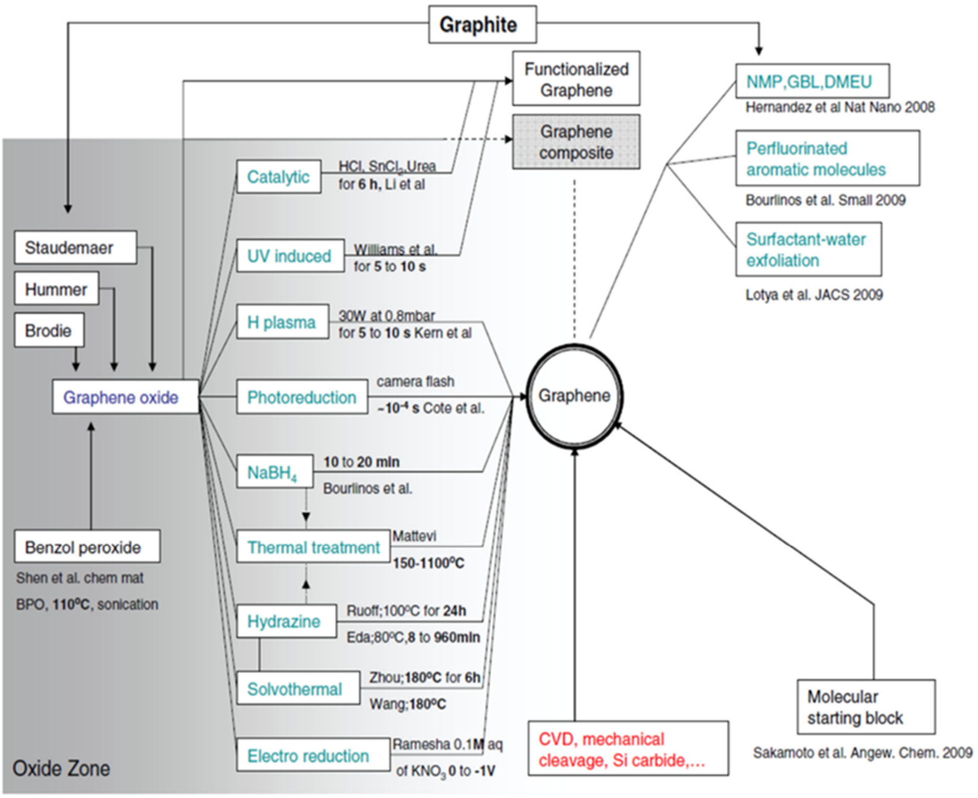

Scheme 3.1 The roadmap to high quality graphene

Staudenmaier,[13] by use of sulphuric and nitric acid combined with potassium chlorate or still, as suggested by Hummers and Offeman[14], using concentrated sulfuric acid, sodium nitrate and potassium permanganate as explained in the first section of this review. This last method is the most commonly used for the synthesis of graphite oxide and accepted as the most efficient. To the best of our knowledge, Shen et al.[32] is the only report of a recent alternative method where benzoyl peroxide is reacted with graphite at moderate temperature and under sonication to produce exfoliated graphene oxide sheets. Depending on the application or fundamental study graphene/graphene oxide is destined for, a number of processing steps is then needed in order to achieve the desired properties, i.e. in many cases to recover a decent conductivity—while still keeping transparency. Other studies report on the creation of composite material, which either consists of stacked pure GO, GO mixed with a polymer alone or combined with other layered material like clay.[43,44] Some of these composite materials do not require any reduction treatment and use graphene oxide as it is, the GO paper discovered by Ruoff et al.[45,46] being a famous example of such composite film. On the other hand, years concentrates on the reconversion of GO to graphene and its deposition for various purposes. Scheme 1 lists the most relevant reduction methods. To the best of our knowledge, the flash photoreduction discovered by Cote et al.[47] is the fastest reduction process ever (10^{-4} s) and involves, in terms of equipment, only a conventional flash of a digital camera. The reduction occurs because the very large photon flux induces a thermal deoxygenation. Unfortunately, little evidence supports the graphene-like behaviour of the product. Nevertheless, we believe this approach to be promising. Today's most efficient procedure for the reduction of GO seems to be the H plasma reduction method proposed by Kern et al,[48] even though it requires more time (5–10 s) and more equipment is needed. The optimized conditions were found to be 5–10 s of exposure to a plasma operating at 0.8 mbar of H and 30W of power. Ranking next in terms of proven efficiency are purely thermal treatments or heat treatments in vacuum or controlled atmosphere preceded by hydrazine or the $NaBH_4$ reduction process (for further reading, we recommend recent theoretical works[49,50] which present possible models for the hydrazine induced deoxygenation). Once more, the reduction effectiveness is clearly proven by the Dirac curves of devices prepared by various groups.[51,52,17,53,37,49,54,55,56] The most suitable temperature for annealing is still undefined: some groups report on the damage of the ambipolar characteristic after annealing above ~200 ◦C,[17] others report on an improved ambipolar behaviour for temperatures up to 500–600 °C (accompanied by ethylene exposure).[37] Two additional methods leading to RGO are listed in the lower part of Scheme 1: firstly, solvothermal reduction (including hydrothermal reduction) which proceeds in a solvent (water when hydrothermal) while applying mild annealing. The trick is to keep single layers suspended in the solution after reduction. Zhou et al.[57] showed such an example of hydrothermal reduction and proved, using Raman spectroscopy, X-ray photoelectron spectroscopy (XPS) and AFM that the material was substantially reduced but still single or bilayer. Other examples of solvothermal reduction procedures can be found in the literature;[58,59] Wang et al.[60]reported Dirac curves of a solvothermally reduced material, whereas Fan et al.[61] prepared a graphene suspension through deoxygenation by simply heating an exfoliated-GO suspension under strongly alkaline conditions at moderate temperatures (50–90 °C). Based on these results hydro/solvothermal reduction can be considered a good candidate for reduced GO production if the single layer character can be preserved, for example by depositing the layer beforehand. An alternative approach reported by Liu et al.,[62]Ganganahalli et al.,[63] Zhou et al.[64] and Wang et al.[65](most probably without knowing of each other's work) is the reduction of graphene oxide using electrochemistry. While voltametry seems to prove an irreversible transformation of the oxidized material, preventing the single layers from aggregating is once more a central issue. Ganganahalli et al.[63] is the only group actually showing that their electrochemical reduced GO consists of single layers. Though electrochemical methods seem promising, a lot of effort is still needed to develop procedures for a more complete reduction while conserving monolayer characteristics if one actually wants to produce graphene and not very thin graphite! We complete our review of GO deoxygenation with two examples of catalytic reduction. The first, reported by Williams et al.,[66] describes how graphene oxide suspended in ethanol undergoes reduction as it accepts electrons from UV-irradiated TiO_2 suspensions. The second[67] involves the use of $SnCl_2$ in HCL and urea, the reaction that creates SnO_2 nanoparticles. The reduced nature of the end product was established by XPS in the SnO_2 case and qualitatively proven by a color change in the TiO_2 suspensions. The effect of such a nanoparticle overlayer on the electrical properties is unfortunately not documented.

3.7 Alternative routes

While so far we have concentrated on the ambipolar behaviour, structural properties and the coverage analysis concerning RGO, this section is devoted to the chemical preparation of graphene without oxidation (listed in the right part of our roadmap to graphene (Scheme 1)). A very effective method for the exfoliation of graphite with the help of organic solvents such as N methylpyrrolidone (NMP), N,N-dimethylacetamide (DMA), g-butyrolactone (GBL) and 1,3-dimethyl-2-imidazolidinone (DMEU) was proposed by Hernandez et al.[68] This exfoliation takes place because the energy required to exfoliate graphene matches the solvent–graphene interaction energy and extra energy provided through sonication activates the process. It works for solvents which have an interaction energy with graphene that is equal to graphene–graphene interaction energy,[1,69,70] resulting in a minimal energy cost to overcome the Van Der Waals forces between the graphene sheets. High quality graphene is produced in this way but the very low concentration of single layer graphene in the suspension (0.01 mg mL^{-1})[68] is a drawback. Some of the best TEM images using the solvent exfoliation route are displayed in Figure 3.9 where one can distinguish monolayer graphene with sizes in the range 0.5–1µm. Among the proposed solvents NMP seems to yield the best results since one can clearly see graphene single layers in the corresponding TEM images. Figure 3.9(h) displays a histogram of the number of layers per sheet for the exfoliation of graphite in NMP which is peaked between 1 and 4 layers.

SAED of the exfoliated material is in Figure 3.10, and shows a hexagonal pattern illustrative of the hexagonal carbon honeycomb arrangement of graphite. The existence of monolayer and bilayer graphene arrangements is as well demonstrated by {2 1 1 0} spots appearing more intense relative to the {1 1 0 0}. An alternative route, still NMP based but avoiding the sonication step to afford bigger flakes, was proposed by Vallés et al.[71] Inspired by carbon nanotube processing technology,[72] they showed that the exposure of graphite to an ternary potassium salt K(THF) × C 24 (THF) tetrahydrofurane, × (1–3) in NMP leads to stable exfoliation of graphite. An alkali metal graphite intercalation compound is formed, which, thanks to its charge, helps the exfoliation of graphite in NMP and leads to a stable suspension of negatively charged graphene in NMP mixed with the alkaline salt. As expected for this mild exfoliation method, yields drastically improved flake size as compared with the results reported in Figures 3.9 and 3.10.

One of the best STM images of chemically exfoliated graphene produced without oxidation is shown in Figure 3.11. The height of 0.3 nm confirms the single layer character of the graphene flake.

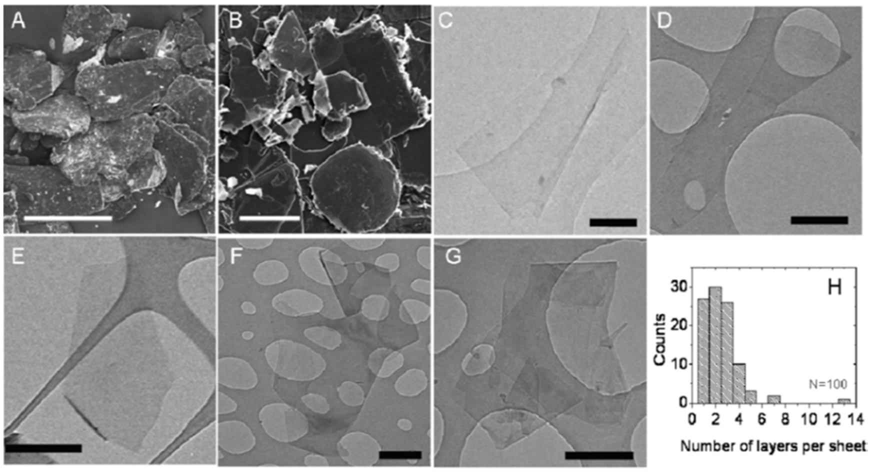

Figure 3.9 Electron microscopy of graphite and graphene. (a) SEM image of sieved, pristine graphite (scale bar: 500 mm). (b) SEM image of sediment after centrifugation (scale bar: 25 mm). (c)–(e) Bright-field TEM images of monolayer graphene flakes deposited from GBL (c), DMEU (d) and NMP (e), respectively (scale bars: 500 nm). (f), (g) Bright-field TEM images of a folded graphene sheet and multilayer graphene, both deposited from NMP (scale bars: 500 nm). (h) Histogram of the number of visual observations of flakes as a function of the number of monolayers per flake for NMP dispersions. Images and graph reprinted with permission from Macmillan Publishers Ltd: Nature Nanotechnology, Hernandez et al. [76], Copyright 2008.

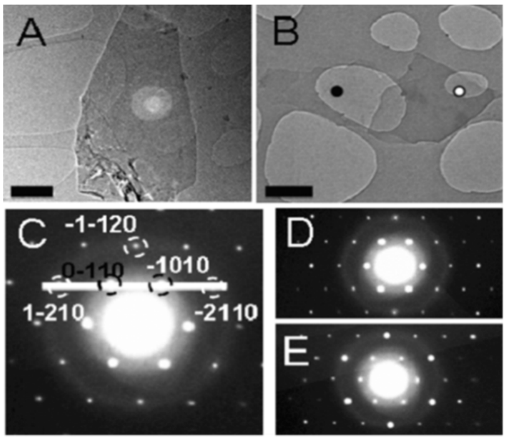

Figure 3.10 Evidence of monolayer graphene from TEM. (a), (b) High-resolution TEM images of solution-cast monolayer (a) and bilayer (b) graphene (scale bar 500 nm). (c) Electron diffraction pattern of the sheet in (a), with the peaks labeled by Miller–Bravais indices. (d), (e) Electron diffraction patterns taken from the positions of the black (d) and white spots (e), respectively, of the sheet shown in (b), using the same labels as in (c). The graphene is clearly one layer thick in (d) and two layers thick in (e). Reprinted with permission from Macmillan Publishers Ltd: Nature Nanotechnology, Hernandez et al[77], Copyright 2008.

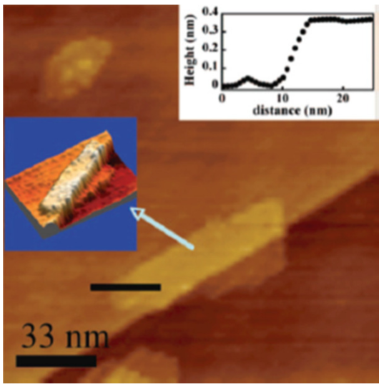

Figure 3.11 Ambient STM image of a filed-down graphite deposit drop casted from solution on a HOPG substrate, showing a graphene flake, lying on a HOPG step. Height scan inset shows a height difference of 0.36 nm between substrate and flake. Similar results have been obtained on a vast number of flakes. Image reprinted with permission from Vallés et al[80] Copyright 2008 American Chemical Society.

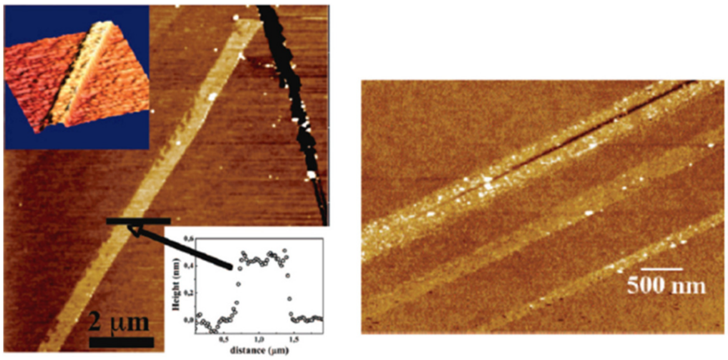

Figure 3.12 Tapping mode AFM image of a deposit performed by dip-coating of a graphene solution (from expanded graphite) onto mica. Height measurements of the ribbon show a height of 0.4 nm; the full length of the ribbon is ca. 40µm. (right) Tapping mode AFM image of a deposit performed by dip-coating of a graphene solution (from expanded graphite) onto Si/SiO$_2$ wafer. Height measurements give between 0.8 and 1.3 nm for the three ribbons (multilayer). Image reprinted with permission from Vallés et al[80] Copyright 2008 American Chemical Society.

Tapping mode AFM images show large-scale monolayer graphene ribbons as reported in Figure 3.12. Again, a height of 0.3 nm was measured on the ribbon. Unfortunately no characterization of the electrical properties was performed on the produced material.

Very recently Bourlinos et al.[73] presented an approach following the idea of Hernandez et al.[68] for the exfoliation of graphite with the help of solvents with a surface energy that matches the graphene–graphene interaction energy.[1,69,70] Some of the solvents of this approach belong to a peculiar class of perfluorinated aromatic molecules[74,75]and include hexafluorobenzene (C_6F_6), octafluorotoluene ($C_6F_5CF_3$), pentafluorobenzonitrile (C_6F_5CN) and pentafluoropyridine (C_5F_5N). Aside from the aromatic compounds Bourlinos et al.[73] also found that some non-aromatic solvents tested successfully for dispersing graphite, namely ethyl acetate, vinyl acetate, methyl chloroacetate, 2-methoxyethyl ether, acetylacetone

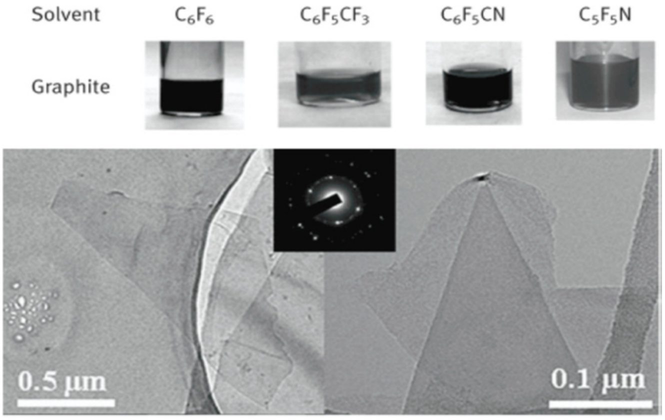

Figure 3.13 (Top) Colloidal dispersions obtained after liquid-phase exfoliation of graphite using the perfluorinated aromatic solvents below. (Bottom) TEM images of some pentafluorobenzonitrile-etched thin sheets. The SAED pattern is included as inset. Images reprinted with the permission from Bourlinos et al[82] Copyright 2009 Wiley-VCH.

and N-tetramethylmethylenediamine, which all exhibited remarkable colloidal stabilities and concentrations of 0.2– 0.3 mg ml^{-1}. Examples of the dispersions and TEM images are presented in Figure 3.13. Uniform dark dispersions testify to the absence of aggregation, while single to 2–3 layer thick graphene with flake size in the order of few micrometers were observed by TEM.

Lotya et al.[76] proposed a liquid-phase exfoliation of graphene which does not require oxidation or high temperature, avoids expensive solvents and is even, according to the author, safe and user friendly. Here graphite was dispersed in surfactant-water solutions in a manner similar to surfactant aided carbon nanotube dispersion.[77-81]The dispersed graphitic/graphene flakes are stabilized against reaggregation by Coulomb repulsion between the adsorbed surfactant molecules. Electrical measurements on such flakes show a conductivity of 35 Sm^{-1}, a low value attributed to the presence of residual surfactant molecules which are difficult to remove even after several washing treatments. After annealing at 250 ^{o}C, as expected, the conductivity rose to 1500 Sm^{-1} (the sheet resistance fell from 920 to 22.5KΩ) while optical measurements demonstrated that the transparency did not vary throughout the processing. However, this conductivity value is still far from those resulting after the reduction of graphene oxide, which vary from 7200[82] to 10000 Sm^{-1}[15] and is also significantly lower than the conductivity of graphene derived from exfoliation in NMP (6500 Sm^{-1}).[76] Nevertheless, HRTEM with atomic resolution reproduced in Figure 3.14(a) shows the monolayers to be well graphitized and largely defect free. The authors observed large flakes were of monolayers and bilayers but also reaggregation of thin layers. SAED images reveal the hexagonal lattice of graphene and from the analysis of images like that reproduced in Figure 3.14(b) one can deduce from the number of lines in the edge of the flake that it is a three layer graphite sheet.[83] The relative amount of the multilayer structures is illustrated in the histogram of the number of layers per flake for dispersions from original sieved graphite and from recycled sediment shown in Figure 3.15 (the very large flakes are ignored in this histogram) from which one deduces that ~43% of flakes have less than 5 layers and about ~3% of the flakes were monolayer graphene. While this value is considerably smaller than that observed for graphene/solvent dispersions, working in aqueous systems has its own advantages. In general, the majority of these few-layer flakes had lateral dimensions

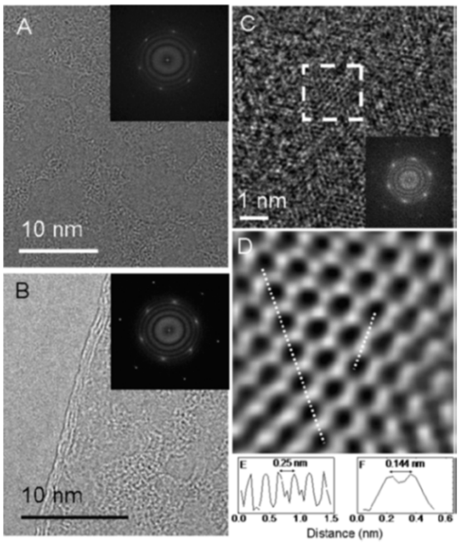

Figure 3.14 High-resolution TEM images of surfactant exfoliated graphene flakes. (a) A HRTEM image of a section of a graphene monolayer. Inset: fast Fourier transform (equivalent to an electron diffraction pattern) of the image. (b) HRTEM image of a section of a trilayer. Inset: fast Fourier transform of the image. (c) HRTEM image of part of a graphene monolayer. Inset: fast Fourier transform of the region enclosed by the white square. The scale bar is 1 nm. (d) A filtered image of part of the region in the white square. (e) Intensity analysis along the left white dashed line shows a hexagon width of 2.4 Å. (F) Intensity analysis along the right white dashed line shows a C–C bond length of 1.44 Å. Reprinted with permission from Lotya et al[76] Copyright 2009 American Chemical Society.

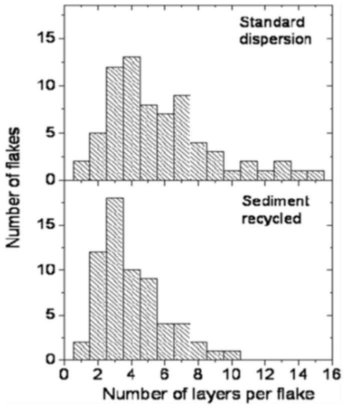

Figure 3.15 Histograms of the number of layers per flake for dispersions from original sieved graphite and from recycled sediment graphs reprinted with permission from Lotya et al[76] Copyright 2009 American Chemical Society.

of~1µm. Although these results do not compete with the top quality of the RGO, we believe that today's research is only a beginning and much more can be expected from such an approach. Characterization of the electrical properties would be of great help to learn more about the true quality of the prepared material and it is obvious that efforts are still needed to conserve larger flake sizes with this kind of approach.

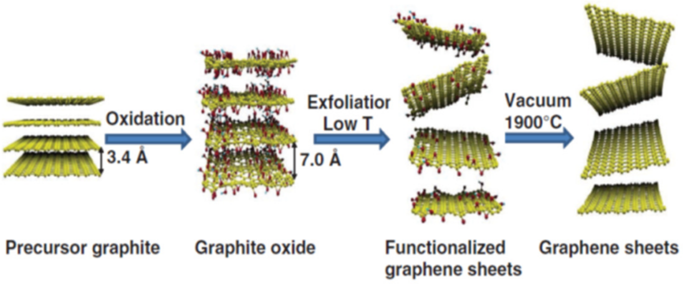

Figure 3.16 Schematic of experimental procedures used to produce Graphene Sheets via high temperature and high vacuum annealing. Advanced Functional Materials, Jin et al.[84] Copyright 2011.

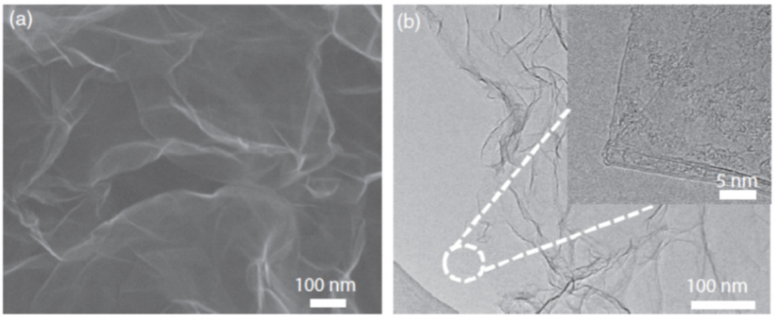

Figure 3.17 (a) FE-SEM image of Graphene Sheets and (b) HR-TEM image of Graphene Sheets. Advanced Functional Materials, Jin et al.[84] Copyright 2011.

3.8 Latest developments

Various attempts for the large scale chemical production of high quality graphene have been reported in the last few years. Some of them follow the path of chemical oxidation of graphite to graphene oxide and subsequent exfoliation and reduction, to obtain reduced graphene oxide (RGO) nanosheets. Among the most noticeable ones is the report by Jin et al.[84] who obtained highly crystalline graphene sheets with low oxygen content similar to the precursor graphite by annealing exfoliated functionalized graphene sheets at very high temperature (1900 ^{o}C) under high vacuum (10^{-6} Torr) (Figure 3.16). Figure 3.17 presents FE-SEM and HR-TEM image of graphene sheets after the exfoliation process of graphite oxide.

A novel method for the exfoliation of graphite oxide to achieve chemically reduced graphene oxide sheets was put forward by Tang et al.[85] This method employs glucose as sole reagent and utilizes a bottom-up assembly technique to grow graphene oxide with a controllable number of layers from monolayer to multilayer (Figure 3.18). An alternative and effective route was proposed by Kumaret al.[86] for the preparation of polyaniline-decorated reduced graphene oxide nanosheets (called PANI-g-rGO). A schematic representation of this method is shown in Figure 3.19 while the FE-SEM and HR-TEM images are displayed in Figure 3.20.

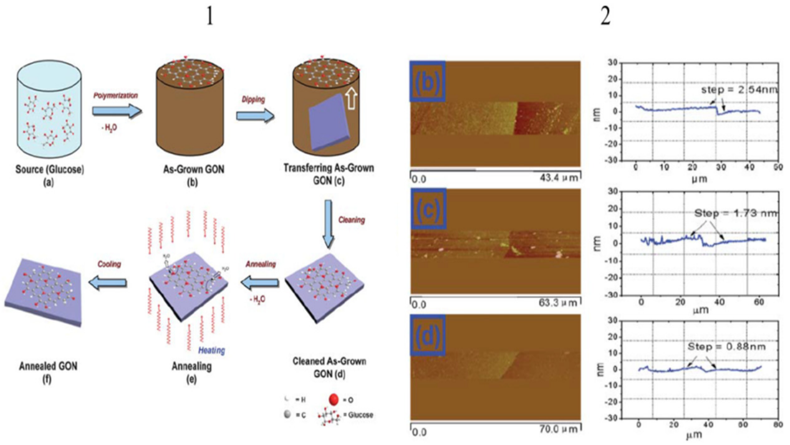

Figure 3.18 (1) Schematic illustration of preparing graphene oxide nanoplatelets (2) (b) the graphene oxide nanoplatelets annealed at 700 ^{o}C for 2 min with a thickness of 2.54 nm(trilayer), (c) After one cycle of Al sputtering (8 nm) and HCL (2 mol L^{-1}) etching, the thickness is reduced to 1.73 nm,(d) After two cycles of Al sputtering and HCL etching, the thickness of the graphene oxide nanoplatelets are further reduced to 1.73 nm (monolayer). Journal of Materials Chemistry, Tang et al.[85] Copyright 2012.

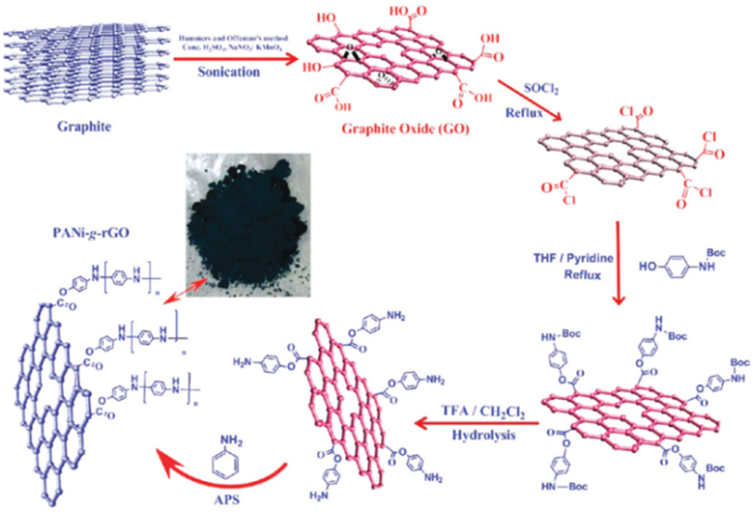

Figure 3.19 Schematic governing the preparation of PANi-g-rGO with a digital picture of the sample in the middle. ACS Nano, Kumar et al.[86] Copyright 2012.

Very recently the Ruoff group[87] proposed the exfoliation and dispersion of graphite oxide in propylene carbonate (PC) by bath sonication. Highly reduced graphene oxide (GO) nanoplatelets were obtained after heating of graphene oxide suspensions at 150 °C; paper samples comprising such reduced graphene oxide platelets had an electrical conductivity of 5230 S/m. Figure 3.21 shows the TEM and SEM images of graphene oxide and reduced graphene oxide platelets. Finally Zhao et al.[88] prepared large-area graphene oxide (GO) sheets by mild oxidation and sonication following a protocol which prevents small graphene oxide flakes due to overcracking of graphite during oxidation and exfoliation. The SEM

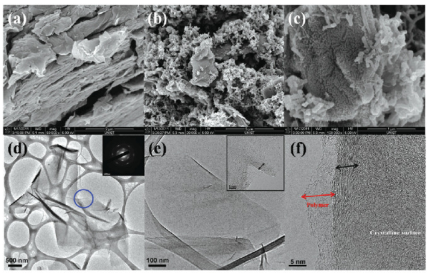

Figure 3.20 Typical FE-SEM images: (a) GO; (b and c) the surface of the PANI-g-rGO hybrid. HR-TEM images: (d) GO. Inset image is of a selected-area electron diffraction (SAED) pattern; (e) rGO-NH_2. Inset image is at higher magnification; (f) PANI-g-rGO. ACS Nano, Kumar et al.[86] Copyright 2012.

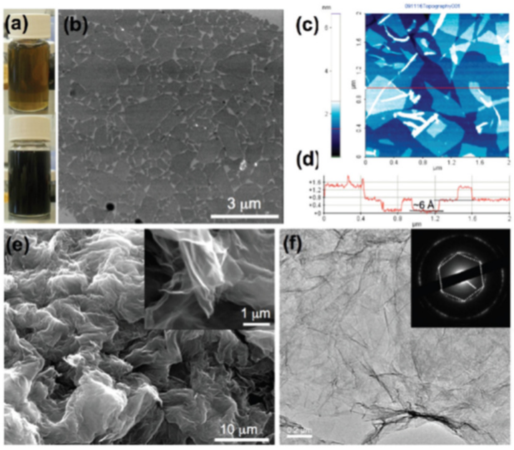

Figure 3.21 (a) Optical images of a graphene oxide suspension in PC (top) before and (bottom) after heating at 150 °C for 12 h. (b) SEM image of graphene oxide platelets deposited on a Si substrate. (c) AFM image of graphene oxide platelets dispersed on mica and (d) corresponding line profile. (e) SEM image of the reduced graphene oxide powder obtained by heating graphene oxide in PC at 150 °C with a high magnification SEM image in the inset. (f) TEM image of the reduced graphene oxide platelets from the 150 °C treatment and the corresponding SAED pattern. ACS Nano, Zhu et al.[87] Copyright 2010.

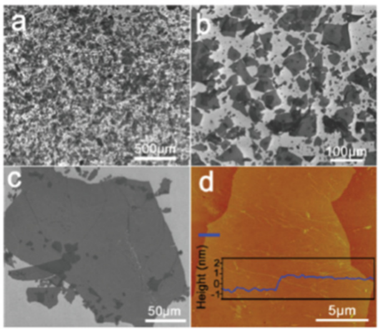

Figure 3.22 (a-c) SEM and (d) AFM images of large-area GO sheets. The inset of panel d shows that the thickness of the measured GO sheets is approximately 1.2 nm. ACS Nano, Zhao et al.[88] Copyright 2010.

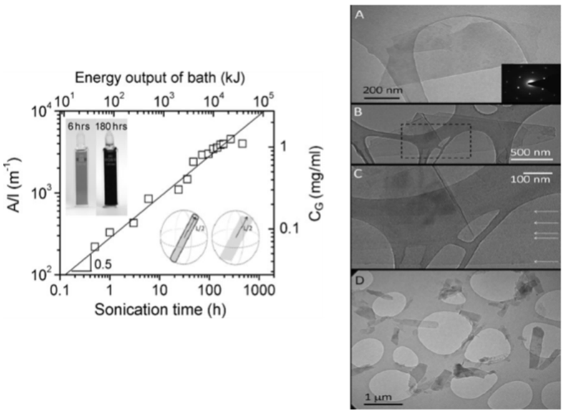

Figure 3.23 On the left concentration of graphene after centrifugation as a function of sonication time. The left Axis shows the measured absorbance per cell length, A/l, while the right axis shows the concentration calculated using an absorption coefficient of 3620 ml mg^{-1} m^{-1}. On the right TEM images of graphene flakes are presented. A) A typical monolayer. Inset: a diffraction pattern taken from a monolayer. B) A multilayer and C) a magnified version of the portion of (B) in the dashed box. The arrows in this image show the position of the edges of the individual flakes comprising this multilayer. Five edges can be seen showing that this is a 5-layer flake. D)A wide-field image showing the large quantities of flakes observed after long sonication times (180 h).Small, Khan et al.[89] Copyright 2010.

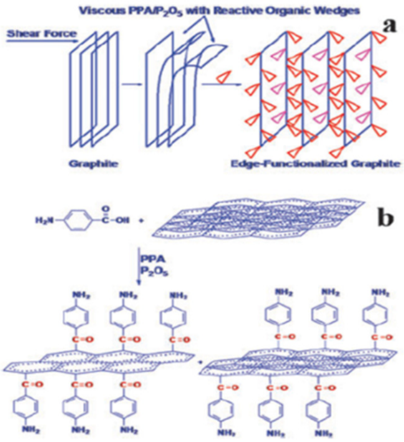

Figure 3.24 (a) Schematic presentation of a graphite exfoliation mechanism. (b) Schematic representation of the reaction between graphite and 4-aminobenzoic acid as a molecular wedge via Friedel–Crafts acylation in PPA/P_2O_5 medium. Chemical Communications, Choi et al.[90] Copyright 2010.

and AFM images presented in Figure 3.22 clearly testify to the success of this method in delivering large area of GO sheets.

Considerable effort has been dedicated to the chemical exfoliation of graphite without the oxidation of the graphene flakes, avoiding in such way severe damage of the graphene lattice. The group of Coleman[89] succeeded in increasing the graphene concentration in N-methyl-pyrrolidone (NMP) to

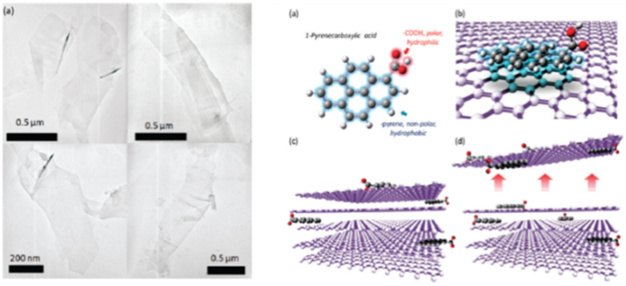

Figure 3.25 (**Left**) TEM images of graphene flakes showing typical size, shape, and morphology of the graphene flakes obtained by our proposed "molecular wedging" of graphite. (**Right**) (a) molecular structure of 1-pyrenecarboxylic acid with its polar (hydrophilic) and nonpolar (hydrophobic) parts indicated (b) a 1-pyrenecarboxylic acid molecule can form π-stacking bond with graphitic surfaces. (c) In polar medium (H_2O) and with agitation, the nonpolar pyrene part prefer to attach itself on top of the graphitic surface via the π-stacking mechanism, or penetrates within the layers of graphite to reduce hydrophobic interactions with water. With continuous agitation, more of such molecules enter between the layers and move in deeper, breaking the π-bonding of the graphene layers of graphite (d) Continuing this process releases single or few layer graphene. The COOH groups of the 1-pyrenecarboxylic acid molecules (attached to the released graphene flakes) prefer the polar medium and keep the graphene layers stably suspended in the water. Nano Letters, An et al.[92] Copyright 2010.

approximately 1mg mL^{-1} (Figure 3.23) by mild sonication of graphite for long times. Exfoliation in the same solvent N-methyl-pyrrolidone (NMP) was carried out by Choi et al.[90] via a ''direct'' covalent attachment of organic molecular wedges and lead to high-yield exfoliation of the three-dimensional graphite into two-dimensional graphene-like sheets (Figure 3.24). Bourlinos et al.[91] attempted the liquid-phase exfoliation of graphite-fluoride in dimethylformamide (DMF) solvent providing colloidal graphene fluoride by mild sonication. Fluorine elimination was achieved by reduction of the dispersed layers with Et_3Si-H or Zn particles. A scalable and facile technique for non-covalent functionalization of graphene with the help of 1-pyrenecarboxylic acid that exfoliates single-, few-, and multilayered graphene flakes into stable aqueous dispersions was proposed by An et al.[92] based on the π-stacking bond of this molecule with the graphitic surfaces. The -COOH groups of the 1-pyrenecarboxylic acid molecules (attached to the released graphene flakes) prefer the polar medium and keep the graphene flakes stably suspended in water. Dhakate et al.[93] described an approach to produce single and double layer clean large area graphene from re-exfoliation of expanded graphite. In this approach dried natural graphite is mixed with saturated acid consisting of concentrated H_2SO_4 and HNO_3 to form the graphite intercalated compound (GIC). The GIC is then rapidly expanded at temperatures between 800 and 900 ^{o}C to form expandable graphite which is then dispersed in an organic solvent like N,N-dimethylformamide (DMF) by ultra-sonication and centrifuged to obtain a stable suspension. Re-exfoliation of expandable graphite gives the clean large area single and double layers of graphene (Figure 3.26).

High-yield synthesis of few-layer graphene flakes through electrochemical expansion of graphite in propylene carbonate electrolyte has been reported by Wang et al.[94] They demonstrate a solution route inspired by the lithium rechargeable battery for the high-yield (>70%) exfoliation of graphite into

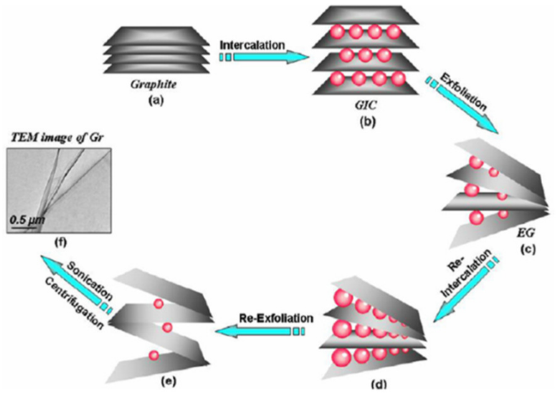

Figure 3.26 The steps involved in the synthesis of graphene-sheets. (a) naturel graphite (NG), (b) formation of graphite intercalation compound (GIC) on acid treatment, (c) formation of expandable graphite (EG) on thermal exfoliation, (d) re-intercalation of EG, (e) re-exfoliation of EG and (f) formation of single and double layer graphene-sheets after ultra-sonication and centrifugation. Carbon, Dhakarte et al.[93] Copyright 2011.

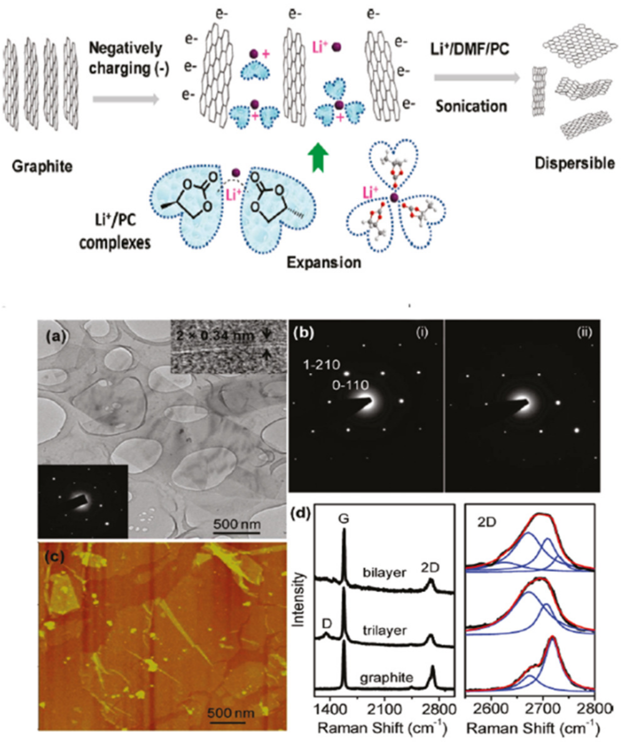

Figure 3.27 (**Above**) Exfoliation of graphite into few layer graphene via Intercalation of Li^+ Complexes. (**Below**) (a) TEM images and electron diffraction pattern of few layer graphene (FLG) (b) Electron diffraction patterns of (i) single and (ii) bilayer sheets. (c) AFM image of FLG spin-coated onto a Si substrate. The thickness was ~1.5 nm corresponding to a bilayer. (d) (left) Raman spectra (532 nm laser) of FLG on Si substrates compared with the spectrum of graphite; (right) Lorentzian peak fitting of the 2D bands of the bilayer and trilayer. J. Am. Chem. Soc., Wang et al.[94] Copyright 2011.

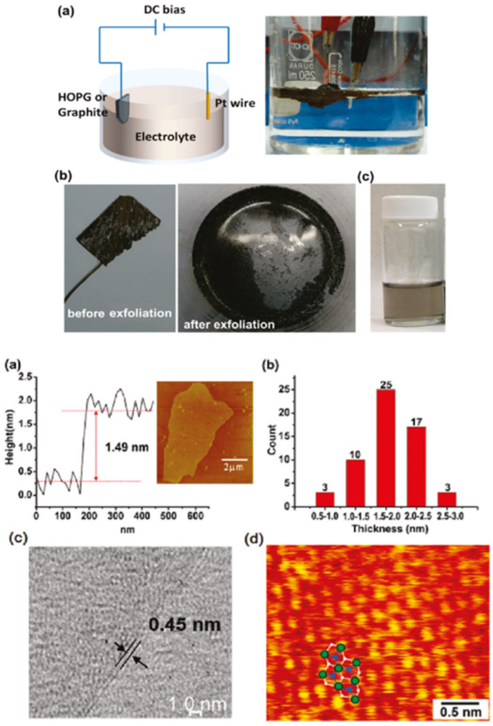

Figure 3.28.(a) Schematic illustration and photo for electrochemical exfoliation of graphite. (b) Photos of the graphite flakes before and after electrochemical exfoliation. (c) Photo of the dispersed graphene sheets in a DMF solution.(a) Typical AFM image for an electrochemically exfoliated graphene thin sheet cast on a SiO_2 substrate. (b) Statistical thickness analysis for the graphene sheet ensemble (randomly selected 58 sheets were measured by AFM). (c) Typical TEM image for an exfoliated bilayered graphene. (d) Corresponding STM image of a bilayered graphene, where hexagons indicate the atom configuration of the two layers. ACS Nano, Su et al.[95] Copyright 2011.

highly conductive few-layer graphene flakes (average thickness <5 layers). A negative graphite electrode can be electrochemically charged and expanded in an electrolyte of Li salts and organic solvents under high current density and exfoliated efficiently into few-layer graphene sheets with the aid of sonication (Figure 3.27).

Another innovative one-step approach for the production of high quality thin graphene films from fast electrochemical exfoliation has been reported by Su et al.[95] Figure 3.28 shows that the lateral size of their exfoliated graphene sheets ranges from several up to 30 μm, which significantly reduces the number of intersheet junctions for making percolative transparent conductive films. These films exhibits excellent conductivity (sheet resistance is 210 ohm/sq at 96% transparency), however, the effective field-effect mobility extracted from the single-sheet device remains rather low, namely 17 cm^2/V^3 s.

References

[1] Novoselov, K. S.; Geim, A. K.; Morozov, S. V.; Jiang, D.; Zhang, Y.; Dubonos, S. V.; Grigorieva, I. V.; Firsov, A. A. *Science* **2004**, 306, 666-669.

[2] Lee, C.; WWei, X.; Kysar, J. W.; Hone, J. *Science* **2008**, 321, 385-388.

[3] Balandin, A. A.; Ghosh, S.; Bao, W.; Calizo, I.; Teweldebrhan, D.; Miao, F.; Lau, C. N. *Nano Lett.* **2008**, 8, 902-907.

[4] Nair, R. R.; Blake, P.; Grigorenko, A. N.; Novoselov, K. S.; Booth, T. J.; Stauber, T.; Peres, N. M. R.; Geim, A. K. *Science* **2008**, 320, 1308.

[5] Brodie, B. C. *Philos. Trans. R. Soc. London* **1859**, 149, 249-259

[6] Kim, K. S.; Zhao, Y.; Jang, H.; Lee, S.Y.; Kim, J. M.; Kim, K. S.; Ahn, J.; Kim, P.; Choi, J.; Hong, B. H. *Nature* **2009**, 457, 706-710.

[7] Van Bommel, A.; Crombeen, J; Van Tooren, A. *Surf.Sci.* **1975**, 48, 463-472

[8] Forbeaux, I.; Themlin, J.; Debever, *Phys. Rev. B* **1998**, 58, 16396.

[9] Berger, C.; Song, Z.; Li, T.; Li, X.; Ogbazghi, A. Y.; Feng, R.; Dai, Z.*J.Phys.Chem.B* **2004**, 108, 19912-19916.

[10] Seyller, T.; Emtsev, K. V.; Speck, F.; Gao, K.; Ley, L. *Appl.Phys.Lett.* **2006**, 88, 242103

[11] Emtsev, K. V.; Bostwick, A.; Horn, K.; Jobst, J.; Kellog, G. L.; Ley, L.; McChesney, J. L.; Ohta, T.; Reshanov, S. A.; Rohrl, J.; Rotenberg, E.; Schmid, A. K.; Waldmann, D.; Weber, H. B.; Seyller, T. *Nat*ure *Mater.* **2009**, 8, 203-207.

[12] Schafhaeult, C. *Phil.Mag.* **1840**, 16, 570-590.

[13] Staudenmaier, L. *Ber. DeutschenChem.Ges.* **1898**, 31, 1481-1487.

[14] Hummers, W. S.; Offeman, R. E. *J. Am. Chem. Soc.***1958**, 80, 1339.

[15] Cai, W.; Piner, R. D.; Stadermann, F. J.; Park, S.; Shaibat, M. A.; Ishii, Y.; Yang, D.; Velamakanni, A.; An, S. J.; Stoller, M.; An, J.; Chen, D.; Ruoff, R. S. *Science* **2008**, 321, 1815-1817.

[16] Becerril, H. A.; Mao, J.; Liu, Z.; Stoltenberg, R. M.; Bao, Z.; Chen, Y. *ACSNano* **2008**, 2, 463-470.

[17] Mattevi, C.; Eda, G.; Agnoli, S.; Miller, S.; Mkhoyan, K. A.; Celik, O.; Mastrogiovanni, D.; Granozzi, G.; Garfunkel, E.; Chhowalla, M. *AdvFunctMater.* **2009**, 19, 2577-2583.

[18] Yang, D,; Velamakanni, A.; Bozoklu, G.; Park, S.; Stoller, M.; Piner, R. D.; Stankovich, S.; Jung, I.; Field, D. A.; Ventrice Jr., C. A.; Ruoff, R. S. *Carbon* **2009**, 47, 145-152.

[19] Mkhoyan, K. A.; Contryman, A. W.; Silcox, J.; Stewart, D. A.; Eda, G.; Mattevi, C.; Miller, S.; Chhowalla, M. *NanoLett.* **2009**, 9, 1058-1063.

[20] Gomez-Navarro, C.; Weitz, RE. T. ; Bittner, A. M.; Scolari, M.; Mews, A.; Burghard, M.; Kern, K. *NanoLett.* **2007**, 7, 3499-3503.

[21] Kudin, K. N.; Ozbas, B.; Schniepp, H. C.; Prud'homme, R. K.; Aksay, I. A.; Car, R. *NanoLett.* **2008**, 8, 36-41.

[22] Dreyer, D. R.; Park , S.; Bielawaski, C. W.; Ruoff, R. S. *Chem.Soc.Rev.* **2010**, 39, 228.

[23] Park, S.; Ruoff, R. S. *Nat.Nanotechnol.* **2009**, 4, 217-224.

[24] Karaborni, S.; Smit, B.; Heidug, W.; Wurai, J.; Oort, E. V. *Science* **1996**, 271, 1102-1104.

[25] Bolotin, K.; Sikes, K.; Jiang, Z.; Klima, M.; Fudenberg, G.; Hone, J.; Kim, P.; Stroner, H. *SolidStateCommun.* **2008**, 146, 351-355.

[26] Li, J.; Kudin, K. N.'McAllister, M. J.; Prud'homme, R. K.; Aksay, I. A.; Car, R. *Phys.Rev.Lett.* **2006**, 96, 176101.

[27] Buchsteiner, A.; Lerf, A.; Pieper, J. *J. Phys. Chem. B* **2006**, 110, 22328-22338.

[28] Pandey, D.; Reifenberger, R.; Piner, R. *Surf.Sci.* **2008**, 602, 1607-1613.

[29] Chua, L.; Wang, S.; Chia, P.; Chen, L.; Zhao, L.; Chen, W.; Wee, A. T.; Ho, P. K. *J.Chem.Phys.* **2008**, 129, 114702-6.

[30] Si, Y.; Samulski, E. T. *Nano Lett.* **2008**, 8, 1679-1682.

[31] Meyer, J. C.; Girit, C. O.; Crommie, M. F.; Zettl, A. *Nature* **2008**, 454, 319-322.

[32] Shen, J.; Hu, Y.; Shi, M.; Lu, X.; Qin, C.; Li, C.; Ye, M. *Chem Mater* **2009**, 21, 3514-3520.

[33] Stankovich, S.; Piner, R. D.; Chen, X.; Wu, N.; Nguyen, S. T. ; Ruoff, R. S. *J. Mater. Chem.* **2006**, 16, 155-158.

[34] Stancovich, S.; Piner, R. D.; Nguyen, S. T.; Ruoff, R. S. *Carbon* **2006**, 44, 3342-3347.

[35] Cote, L. J.; Kim, F.; Huang, J. *J. Am. Chem. Soc.* **2009**, 131, 1043-1049.

[36] Li, X.; Zhang, G.; Bai, X.; Sun, X.; Wang, E.; Dai, H. *Nat. Nanotechnol.* **2008**, 3, 538-542.

[37] Gengler, R. Y. N.; Velingura, A.; Enotiadis, A.; Diamanti, E. K.; Gournis, D.; Józsa, C.; Wees, B. J. V.; Rudolf, P. *Small* **2010**, 6, 35-39.

[38] Su, C.; Xu, Y.; Zhang, W.; Zhao, J.; Tang, X.; Tsai, C.; Li, L. Chem. of Mater. **2009**, 21, 5674-5680.

[39] Wei, Z.; Barlow, D. E.; Sheehan, P. E. *Nano Lett.* **2008**, 8, 3141-3145.

[40] Li, B.; Lu, G.; Zhou, X.; Cao, X.; Boey, F.; Zhang, H. *Langmuir* **2009**, 25, 10455-10458.

[41] Wang, Y.; Maspoch, D.; Zou, S.; Schatz, G. C.; Smalley, R. E.; Mirkin, C. A. *Proc. Natl. Acad. Sci. USA* **2006**, 103, 2026-2031.

[42] Sakamoto, J.; van Heijst, J.; Lukin, O.; Schlüter, A. D.*, Two-Dimensional Polymers: Just a Dream of Synthetic Chemists? *Angew. Chem. Int. Ed.* **2009**, *48*, 1030-1069.

[43] Nethravathi, C.; Rajamathi, J. T.; Ravishankar, N.; Shivakamura, C.; Rajamathi, M. *Langmuir* **2008**, 24, 8240-8244.

[44] Nethravathi, C.; Viswanath, B.; Shivakumara, C.; Mahadevaiah, N.; Rajamathi, M. *Carbon* **2008**, 46, 1773-1781.

[45] Dikin, D. A.; Stankovich, S.; Zimney, E. J.; Piner, R. D. ; Dommett, G. H. B.; Evmenenko, G.; Nguyen, S. T.; Ruoff, R. S. *Nature* **2007**, 448, 457-460.

[46] Park, S.; Lee, K.; Bozoklu, G.; Cai, W.; Nguyen, S. T.; Ruoff, R. S. *ACS Nano* **2008**, 2, 572-578.

[47] Cote, L. J.; Cruz-Silva, R.; Huang, J. *J. Am. Chem. Soc.* **2009**, 131, 11027-11032.

[48] Kaiser, A. B.; Gomez-Navarro, C.; Sundaram, R. S.; Burghard, M.; Kern, K. *Nano Lett.* **2009**, 9, 1787-1792.

[49] Kim, M. C.; Hwang, G. S.; Ruoff, R. S. *J. Chem. Phys.* **2009**, 131, 11027-11032.

[50] Gao, X.; Jang, J.; Nagase, S. *J. Phys.Chem.* C **2010**, 114, 832-842.

[51] Bourlinos, A. B.; Gournis, D.; Petridis, D. A.; Szabo, T.; Szeri, A.; Decany, I. *Langmuir* **2003**, 19, 6050-6055.

[52] Stankovich, S.; Dikin, D. A.; Piner, R. D.; Kohlhaas, K. A.; Kleinhammes, A.; Jia, Y.; Wu, Y.; Nguyen, S. T.; Ruoff, R. S. *Carbon* **2007**, 45, 1558-1565.

[53] Jung, I.; Dikin, D.; Piner, R. D.; Ruoff, R. S. *Nano Lett.* **2008**, 8, 4283-4287.

[54] Gilje, S.; Han, S.; Wang, M.; Wang, K. L.; Kaner, R. B. *Nano Lett.* **2007**, 7, 3394-3398.

[55] Eda, G.; Lin, Y.; Miller, S.; Chen, C.; Su, W.; Chhowalla, M. *Appl. Phys. Lett.* **2008**, 92, 233305-3.

[56] Lomeda, J. R.; Doyle, C. D.; Kosynkin, D. V.; Hwang, W.; Tour, J. M. *J. Am. Chem. Soc.* **2008**, 130, 16201-16206.

[57] Zhou, Y.; Bao, Q.; Tang, L. A. L.; Zhong, Y.; Loh, K. P. *ChemMater.* **2009**, 21, 2950-2956.

[58] Choucair, M.; Thordarson, P.; Stride, J. A. *Nat. Nanotechnol.* **2009**, 4, 30-33.

[59] Wang, G.; Wang, B.; Park. J.; Yang, J.; Shen, X.; Yao, J. *Carbon* **2009**, 47, 68-72.

[60] Wang, H.; Robinson, J. T.; Li, X.; Dai, H. *J. Am. Chem. Soc.* **2009**, 131, 9910-9911.

[61] Fan, X.; Peng, W.; Li, Y.; Li, X.; Wang, S.; Zhang, G.; Zhang, F. *Adv. Mater.* **2008**, 20, 4490-4493.

[62] Liu, N.; Luo, F.; Wu, H.; Liu, Y.; Zhang, C.; Chen, J. *Adv. Funct. Mater.* **2008**, 18, 1518-1525.

[63] Ramelsha, G. K.; Sampath, S. *J Phys. Chem. C* **2009**, 113, 7985-7989.

[64] Zhou, M.; Wang, Y.; Zhai, Y.; Zhai, J.; Ren, W.; Wang, F.; Dong, S. *Chem Eur J* **2009**, 15, 6116-6120.

[65] Wang, Z.; Zhou, X.; Zhang, J.; Boey, F.; Zhang, H. *J Phys. Chem. C* **2009**, 113, 14071-14075.

[66] Williams, G.; Seger, B.; Kamat, P. V. *ACS Nano* **2008**, 2, 1487-1491.

[67] Li, F.; Song, J.; Yang, H.; Zhang, Q.; Han, D.; Ivaska, A.; Niu, L. *Nanotechnol.* **2009**, 20, 455602.

[68] Hernandez, Y.; Nikolosi, V.; Lotya, M.; Blighe, F. M.; Sun, Z.; De, S.; McGoverni, T.; Holland, B.; Byrne, M.; Gun'Ko, Y. K.; Boland, J. J.; Niraj, P.; Duesberg, G.; Krishnamurthy, S.; Goodhue, R.; Hutchison, J.; Scardaci, V.; Ferrari, A. C.; Coleman, J. N. *Nat. Nanotechnol.* **2008,** 3, 563-568.

[69] Geim, A. K.; Novoselov, K. S. *Nat. Mater.* **2007**, 6, 183-191.

[70] Novoselov, K. S.; Jiang, D.; Schedin, F.; Booth, T. J.; Khotkevich, V. V.; Morozov, S. V.; Geim, A. K. *Proc Natl Acad Sci US*A **2005**, 102, 10451-10453.

[71] Vallés, C.; Drummond, C.; Saadaoui, H.; Furtado, C. A.; He, M.; Roubeau, O.; Ortolani, L.; Monthioux, M.; Pénicaud, A. *J. Am. Chem. Soc.* **2008**, 130, 15802-15804.

[72] Penicaud, A.; Poulin, P.; Derre, A.; Anglaret, E.; Petit, P. *J. Am. Chem. Soc.* **2005**, 127, 8-9.

[73] Bourlinos, A. B.; Georgakilas, V.; Zboril, R.; Steriotis, T. A.; Stubos, A. K. *Small* **2009**, 5, 1841-1845.

[74] Züchner, K.; Richardson, T. J.; Glemser, O.; Bartlett, N. *Ang. Chem. Int. Ed.* **1980**, 19, 944-945.

[75] Langer, J.; Dabkowska, I.; Zhang, Y.; Illenberger, E. *Phys. Chem. Chem. Phys.* **2008**, 10, 1523-1531.

[76] Lotya, M.; Hernandez, Y.; King, P. J.; Smith, R. J.; Nicolosi, V.; Karlsson, L. S.; Blighe, F. M.; De, S.; Wang, Z.; McGovern, I. T.; Duesberg, G. S.; Coleman, J. N. *J. Am. Chem. Soc.* **2009**, 131, 3611- 3620.

[77] Moore, V. C.; Strano, M. S.; Haroz, E. H.; Hauge, R. H.; Smalley, R. E.; Schmidt, J.; Talmon, Y. *Nano Lett.* **2003**, 3, 1379-1382.

[78] O'Connell, M. J.; Bachilo, S. M.; Huffman, C. B.; Moore, V. C.; Strano, M. S.; Haroz, E. H.; Rialon, K. L.; Boul, P. J.; Noon, W. H.; Kittrell, C.; Ma, J.; Hauge, R. H.; Weisman, R. B.; Smalley, R. E. *Science* **2002**, 297, 593-596.

[79] O'Connell, M. J.; Boul, P.; Ericson, L. M.; Huffman, C.; Wang, Y.; Haroz, E.; Kuper, C.; Tour, J.; Ausman, K. D.; Smalley, R. E. *Chem. Phys. Lett.* **2001**, 342, 265-271.

[80] Bergin, S. D.; Nicolosi, V.; Cathcart, H.; Lotya, M.; Rickard, D.; Sun, Z.; Blau, W. J.; Coleman, J. N. *J. Phys. Chem. C* **2008**, 112, 972-977.

[81] Sun, Z.; Nicolosi, V.; Rickard, D.; Bergin, S. D.; Aherne, D.; Coleman, J. N. *J. Phys. Chem. C* **2008**, 112, 10692-10699.

[82] Li, D.; Muller, M. B.; Gilje, S.; Kaner, R. B.; Wallace, G. G. *Nat. Nanotechnol.* **2008**, 3, 101-105.

[83] Meyer, J. C.; Geim, A. K.; Katsnelson, M. I.; Novoselov, K. S.; Booth, T. J.; Roth, S. *Nature* **2007**, 446, 60-63.

[84] Jin, M.; Kim, T. H.; Lim, S. C.; Duong, D. L.; Shin, H. J.; Jo, Y. W.; Jeong, H. K.; Chang, J.; Xie, S.; Lee, Y. H. *Adv. Funct. Mater.* **2011**, 21, 3496–3501.

[85] Tang, L.; Li, X.; Ji, R.; Teng, K.S.; Tai, G.; Ye, J.; Wei, C.; Lau, S. P. *J. Mater. Chem.* **2012**, 22, 5676–5683.

[86] Kumar, N.A.; Choi, H. -J.; Shin, Y. R.; Chang, D. W.; Dai, L.; Baek, J. -B. *ACS Nano* **2012**, 6, 1715–1723.

[87] Zhu, Y.; Stoller, M. D.; Cai, W.; Velamakanni, A.; Piner, R. D.; Chen, D.; Ruoff, R. S. *ACS Nano* **2010**, 4, 1227–1233.

[88] Zhao, J.; Pei, S.; Ren, W.; Gao, L.; Cheng, H. -M. *ACS Nano* **2010**, 4, 5245–5252.

[89] Khan, U.; O'Neill, A.; Lotya, M.; De, S.; Coleman, J. N. *Small* **2010**, 6, 864–871.

[90] Choi, E. -K.; Jeon, I. -Y.; Bae, S.-Y.; Lee, H. -J.; Shin, H. S.; Dai, L.; Baek, J. -B. *Chem. Commun.* **2010**, 46, 6320–6322.

[91] Bourlinos, A. B.; Safarova, K.; Siskova, K.; Zbořil, R.*Carbon* **2012**, 50, 1425–1428.

[92] An, X.; Simmons, T.; Shah, R.; Wolfe, C.; Lewis, K. M.; Washington, M.; Nayak, S. K.; Talapatra, S.; Kar, S.*Nano Lett.* **2010**, 10, 4295–4301.

[93] Dhakate, S. R.; Chauhan, N.; Sharma, S.; Tawale, J.; Singh, S.; Sahare, P. D.; Mathur, R. B. *Carbon* **2011**, 49, 1946–1954.

[94] Wang, J.; Manga, K. K.; Bao, Q.; Loh, K. P.*J. Am. Chem. Soc.* **2011**, 133, 8888–8891.

[95] Su, C. -Y.; Lu, A. -Y.; Xu, Y.; Chen, F. -R.; Khlobystov, A. N.; Li, L. -J. *ACS Nano* **2011**, 5, 2332–2339.

Chapter 4

Functionalization of graphene via 1,3-dipolar cycloaddition[**]

In this chapter we report how few-layer graphene produced by dispersion and exfoliation of graphite in N-methylpyrrolidone were successfully functionalized using the 1,3-dipolar cycloaddition of azomethide ylides. The amino functional groups attached to graphene sheets were quantified by the Kaiser test. These amino groups selectively bind to gold nanorods, which were introduced as contrast markers for the identification of the graphene reactive sites. The intercalation between gold nanorods and functionalized graphene was followed by UV-vis spectroscopy. The presence of the organic groups was confirmed by X-ray photoelectron spectroscopy and thermogravimetric analysis. The sheets were characterized by transmission electron microscopy, demonstrating the presence of gold nanorods distributed uniformly all over the graphene surface. This observation indicates that reaction has taken place not just at the edges but also at the internal C=C bonds of graphene. Our results identify exfoliated graphene as considerably more reactive structure than graphite and hence open the possibility to control the functionalization for use a scaffold in the construction of organized composite nanomaterials.

4.1 Introduction

Graphene is a single layer of carbon atoms arranged in a hexagonal lattice and one of the few structures that are stable in two dimensions.[1] Its extraordinary properties, such as high carrier mobility, half-integer quantum Hall effect at room temperature,[2] spin transport[,3] high elasticity,[4] electromechanical modulation, and ferromagnetism,[5] have made graphene a very promising candidate as a robust atomic-scale scaffold in the design of new nanomaterials.[6] The integration of graphene sheets with metal or semiconductor nanoparticles for the creation of new biosensors,[7] energy storage materials,[8] and fuel cells[9] has been proposed. Modification of the carbon network by grafting atoms or molecules is important in the design of graphene-based nanoelectronics because this provides a means to dope the material.[10] For the development of optoelectronic devices, functionalization of graphene with photoactive molecules can provide interesting donor-acceptor nanohybrids.[11]

Before one can chemically manipulate graphene and transform it into various functional structures or integrate it with other materials to form nanodevices, two preliminary steps are necessary: first, graphite has to

---

[**] This chapter is based on: Quintana, M.; Spyrou, K.; Grzelczak, M.; Browne, W. R.; Rudolf, P.; Prato, M.; ACS Nano **2010**, 4, 3527–3533.

be chemically exfoliated into individual or few-layer sheets, and second, the graphene sheets have to be stabilized. Recently, high-yield liquid-phase exfoliation of graphite into individual sheets by stabilization through interactions with the solvent was reported.[12] This methodology opens the way to carry out different organic reactions on graphene in order to produce specific structures for functional devices. An interesting reaction to test on graphene is the 1,3-dipolar cycloaddition of azomethine ylides because this reaction has been extensively used for the chemical modification of carbon nanotubes[13] (CNTs) and fullerenes[14] with applications in different fields such as solar energy conversion and biosensors.[15] CNTs and fullerenes differ from graphene in that they present a curvature which mixes some sp^3 character into the sp^2 hybridization. In fullerenes and CNTs, the curvature has been put in relation with the reactivity of the carbon nanostructure: the stronger the curvature, the higher the reactivity.[16] In graphene instead, the sheet edges are considered the most reactive sites.[17]

With the results reported in this chapter, we demonstrate that even if the reactivity of graphene differs from that of fullerenes and CNTs, the 1,3-dipolar cycloaddition can be performed efficiently and yields a highly functionalized material.[18] To prove this, we identified the reactive sites on graphene layers by introducing amino groups quantified by the Kaiser test. These free amino groups selectively bind to gold nanorods (AuNRs), which were employed as contrast markers.

The interaction between AuNRs and functionalized graphene was followed by UV-vis spectroscopy, while the morphological changes were characterized by transmission electron microscopy (TEM). The presence of the organic groups and their interaction with AuNRs were verified by X-ray photoelectron spectroscopy (XPS). Thermogravimetric analysis (TGA) confirmed the functionalization degree of the products. In short, here we prove that 1,3-dipolar cycloaddition of azomethine ylides on graphene produces a highly functionalized material that provides a platform for the construction of a nanocomposite material using AuNRs.

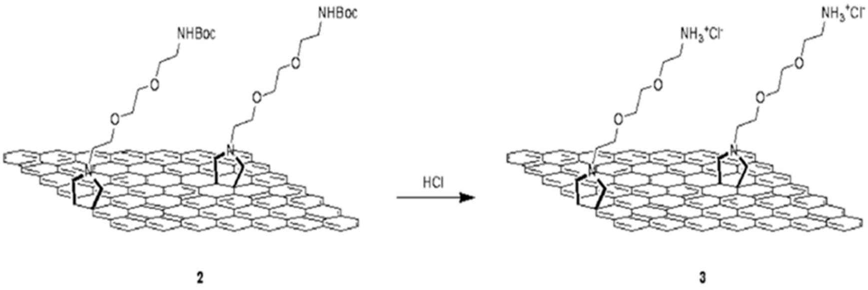

Scheme 4.1 Representation of functionalized graphene derivatives before and after the cleavage of the Boc protecting groups

4.2 Results and discussion

4.2.1 Experimental[††]

To obtain graphene sheets **1**, we have used the solvent extraction procedure[12] because by this technique it is possible to effectively produce single and few graphene layers without the use of intercalants,[19] polymers,[20] or surfactants,[21] which might interfere with the organic reaction.

Graphite Exfoliation, Product 1*:*(See chapter 2.2.4). Thereafter, decantation was carried out by pipetting off the top half of the dispersion. Functionalized graphene **2** was prepared by condensation of paraformaldehyde with a modified α-amino acid ($BocNHCH_2CH_2OCH_2CH_2OCH_2CH_2NHCH_2COOH$), followed by the deprotection of the t-butyl carbamate group (Boc group) to afford **3** (Scheme 4.1).

1,3-Dipolar Cycloaddition on Graphene, Product *2:* Fifty mL of exfoliated graphite solution was used to carry out the reaction. The graphene concentration of the solution was calculated by the optical characterization reported by Coleman and co-workers.[12] The concentration was normally found to range from 0.01 ± 005 mg/mL. To perform the organic reaction, 1.5 equiv with respect to graphene of modified amino acid[35] and paraformaldehyde was added to the graphene dispersion. The reaction mixture was heated at 125 °C under magnetic stirring, while the reagents were added each 24 h for 5 days. The resulting mixture was filtered with a Millipore system (JH 0.45 μm filter), and the solid was washed thoroughly with methanol until the solvent was clear. The product was dispersed in 20 mL of DMF by mild sonication.

Deprotection of the Boc Group, Product 3*:* To cleave the Boc group from functionalized graphene, product **2** was dispersed by sonication in a 4 M solution of HCl in dioxane. The solution was stirred magnetically for 5 h and then was filtered and washed thoroughly first with DMF and finally with methanol. After drying the solvent, the solid was dispersed in 20 mL of DMF, and the final concentration of few layer graphene (FLG) was measured by UV-vis spectroscopy and found to range between 0.025 ± 0.005 mg/mL.

To verify the presence of free amino groups in the products, we have performed the quantitative Kaiser test.[22] For graphenes **1** and **2**, we obtained a negative test value, while following the cleavage of the Boc group, the amount of amine functions in **3** was calculated in the range of 640 ± 70 μmol/g of material. This is a high value if one takes into account only the functionalization of the edges of graphene sheets considered as the most reactive sites. This is the first indication that 1,3-dipolar cycloaddition must take place also in the central carbon-carbon bonds of graphene layers.

The presence of organic groups on the graphene sheets was further analyzed by TGA. TGA plots under N_2 of graphite and products **1** and **2** are shown in Figure 4.1. The overall weight loss of exfoliated graphite, product **1**, is ~1.5%, which can be attributed mostly to the solvent molecules stabilizing graphene sheets.[12] The observed weight loss for product **2** was 15%. The degree of functionalization was estimated to be approximately 1 functional group in 128 carbon atoms and is in good agreement with the Kaiser Test amine content.

[††] Synthesis by Mildred Quintana and Marek Grzelczak, University of Trieste.

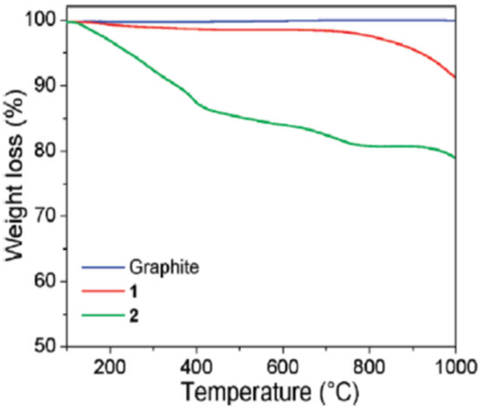

Figure 4.1 Thermographs of graphite, along with products **1** and **2**, conducted in a nitrogen atmosphere.

To visualize the functional groups on the graphene sheets, we have used gold NRs which not only can be attached to free amino group[23] but also possess interesting optical properties arising from localized surface-plasmon resonances.[24]

For the gold nanorod preparation (AuNRs): A solution of gold seed was prepared by borohydride (30 mM, 0.3 mL) reduction of $HAuCl_4$ (0.25 mM, 5 mL) in aqueous cetyltrimethylammonium bromide (CTAB) solution (0.1 M). An aliquot of the seed solution (24 µL) was added to a growth solution (10mL) containing CTAB (0.1 M), $HAuCl_4$ (0.5 mM), ascorbic acid (0.8 mM), silver nitrate (0.12 mM), and HCl (18.6 mM). The mixture was left undisturbed for 4 h at 27 °C.

Surface Functionalization of Gold Nanorods-PVP (polyvinylpyrrolidone) Coating: Typically, a suspension of as-prepared gold nanorods (10 mL) was centrifuged at 8000 rpm for 15 min, and the precipitate was redispersed in Milli-Q water (5 mL). Subsequently, 5 mL of CTAB-coated gold nanorods was mixed with an aqueous solution of PVP (1.2 mM, 5 mL) and stirred overnight. The mixture was centrifuged at 4500 rpm for 60 min, and the precipitate was redispersed in 5 mL of DMF under sonication.

Graphene-AuNR Composites: One milliliter of solutions of products 1, 2, and 3 was separately mixed with 2 mL of AuNR solution each. After 6 h of incubation, the graphene-AuNR composite solution was washed by centrifugation (1500 rpm, 20 min) and redispersed in DMF.

4.2.2. UV/vis spectroscopy

Due to the shape anisotropy of NRs, two well-defined types of plasmon resonances occur, parallel and transversal to the long axis of the rod. The sensitivity of the longitudinal plasmon band to inter-particle interaction gives rise to strong changes in the absorption spectra, which are directly related to a plasmon coupling effect.[25] Taking advantage of this behaviour, we have used AuNRs as contrast marker agents sensitive to aggregation. To this purpose, prior to the graphene conjugation experiment, CTAB was exchanged with poly(vinylpyrrolidone) (PVP) as previously reported[26] to allow for transfer into DMF without aggregation. The AuNR solution was then mixed with **1**, **2**, or **3** in DMF and monitored by UV-vis-NIR spectroscopy for 6 h, as shown in Figure 4.2. The maximum of the longitudinal plasmon band (LPB) of initial,

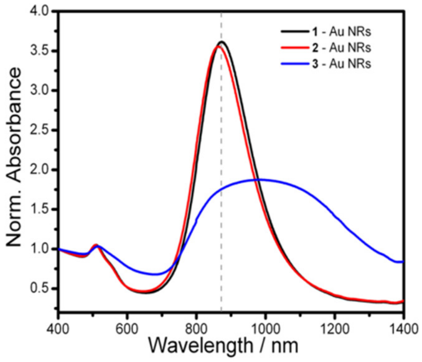

Figure 4.2. UV-vis-NIR absorption spectra of Au NRs mixed with **1** (black), **2** (red) and **3** (blue), showing aggregation of nanorods on amine functionalized graphene sheets. The dashed line at 871 nm corresponds to the position of the longitudinal plasmon band of isolated gold nanorods in DMF. All spectra are normalized at 400 nm for better comparison.

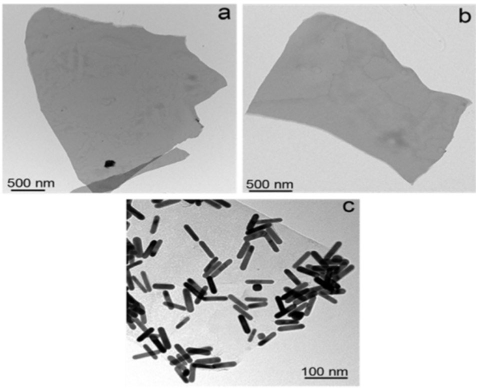

Figure 4.3 TEM images of (a) **1** stabilized graphene in NMP, (b) **2** functionalized Boc-protected graphene, (c) **3** functionalized graphene after the cleavage of the Boc group and mixed with AuNRs

well-dispersed AuNRs is marked with a dashed line. The LPB of AuNRs mixed with **1** and **2** remains unchanged, indicating no further interaction with either as-exfoliated or NH-Boc-functionalized graphene sheets. Conversely, in the case of rods mixed with **3**, the LPB was broadened and red-shifted by about 110 nm, a behaviour that indicates aggregation on the flat surface.[27]

4.2.3. Transmission electron microscopy

TEM analysis confirmed that AuNRs were indeed grafted onto the graphene sheets. Figure 4.3 shows the TEM images of all products; a difference observed in the morphology of products **1** (Figure 4.3a) and **2** (Figure 4.3b) is a decrease in the average size of functionalized products, which was found to be 2.69 ± 1.39 μm (31 images). The reduction in the average size after the reaction is possibly a consequence of the higher reactivity of graphene borders. Most importantly, the distribution of AuNRs all over the graphene surfaces

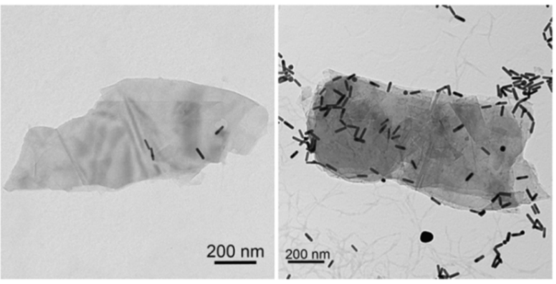

Figure 4.4. TEM images the product **1** and **2** mixed with nanoparticles showing no selective interactions

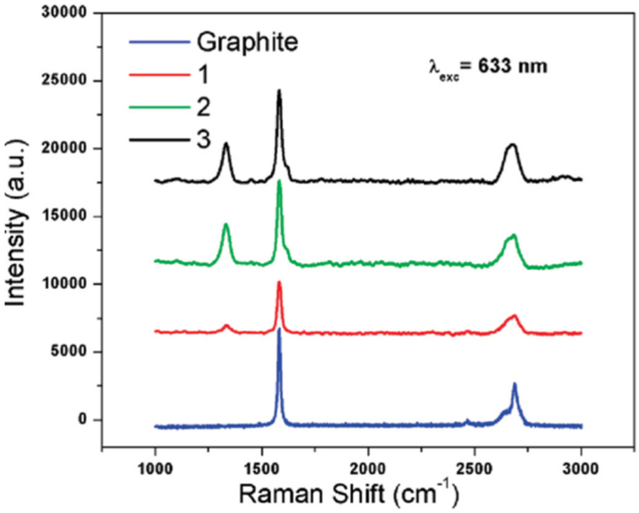

Figure 4.5 Raman spectra of initial graphite and few-layer graphenes before and after functionalization.

was seen only for **3** (Figure 4.3c). To confirm the specific affinity of AuNRs to product **3**, control experiments were performed in which products **1** and **2** were mixed with nanoparticles, showing no interaction (Figure 4.4), which is consistent with the observations from UV-vis-NIR experiments (Figure 4.2). Uniform distribution of the nanoparticles on the functionalized FLG indicates that the reaction has taken place not just at the edges of the graphene sheets but also at the central CAC. This is a very interesting result since it identifies exfoliated graphene as a considerably more reactive structure than graphite and hence opens the possibility to control the degree of graphene functionalization to obtain specific nanostructures.

4.2.4. Raman spectroscopy

Figure 4.5 shows the Raman spectra of the graphene products compared to graphite. In the graphite spectra, there are two intense features, which are the vibrational G band and the two-phonon 2D band. The second-order Raman 2D band is sensitive to the number of layers in graphene, as has been proposed in the literature.[28] Unfortunately, in our Raman spectra, we are not able to identify single-layer graphenes, which have a very sharp and symmetric band. Nevertheless, by the position and the shape of the 2D band at about

2700 cm^{-1} and the relative intensity of the G and 2D bands, we observe most of the aggregates as few-layer graphenes (FLG), as reported in Figure 4.5. A clear difference between functionalized and nonfunctionalized FLG is the appearance of the disorder D band at about 1350 cm^{-1}. In **1**, the D band is weak and may arise from the presence of defects at the graphene edges and the interaction with the substrate. An important feature of the D band is that its intensity decreases with the

increase of graphene thickness and is invisible for bulk graphite, demonstrating that defects are more easily introduced into thinner graphene sheets,[29] allowing the organic functionalization preferentially on monolayers and FLG. As observed, for products **2** and **3**, there is an increase in the intensity of the D band associated with the presence of defects on the lattice as a result of the organic functionalization. As a consequence, after 1,3-dipolar cycloaddition, it is possible to increase the concentration of graphene layers obtaining stable dispersions of 0.1 mg/mL, as calculated by UV-vis spectroscopy.

4.2.5. X-ray photoelectron spectroscopy

To confirm the presence of the organic groups involved in the reaction, all products were characterized by X-ray photoelectron spectroscopy, a direct method for determining the surface elemental composition of a material. The C 1s core level photoemission spectra of **2** and of the graphite used as starting material are shown in Figure 4.6a,b, respectively. The spectral analysis procedure consists of mathematically reconstructing the spectrum with a minimum number of peaks consistent with the raw data and the molecular structure, with the simplification of assuming equivalent carbon atoms depending on their environment. On this basis, four contributions to the carbon 1*s* core level region recorded for the functionalized graphene can be identified: A first main peak at a binding energy of 284.8 eV is assigned to the C-C bonds of the graphene sheet. A second peak due to carbons bound to oxygen and to nitrogen is seen at 286.2 eV, while the C=O and O-C=O contributions are found at 287.5 and 289.0 eV, respectively.

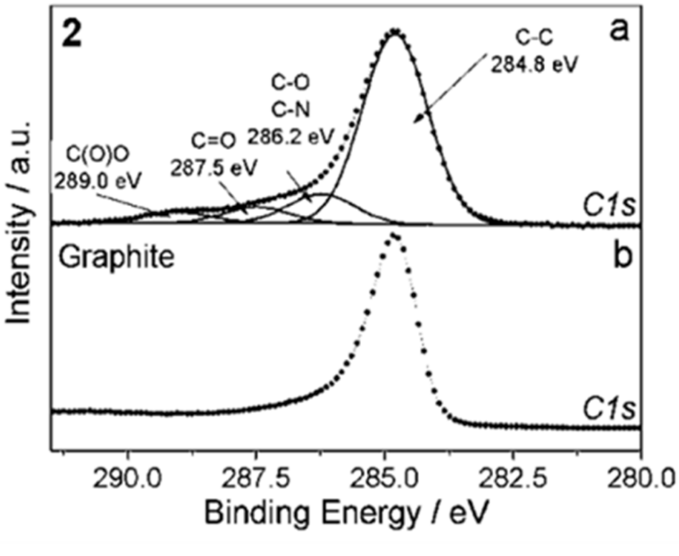

Figure 4.6. Photoemission spectra and fit of the C 1s core level region and fit of (a) product **2** and (b) graphite dispersed on Au/mica.

The presence of these carbon atoms clearly confirms the successful functionalization of graphene. The graphite C 1s spectrum (Figure 4.6b) plotted for comparison verifies the good quality of the sample. Figure 4.7 shows the photoemission spectra and fit of the C 1s core level region of two types of functionalized graphene after exposure to Au nanorods: (a) **2**-Au and (b) **3**-Au. Comparison with the C1 speak of functionalized graphene discussed above (Figure 4.7a) demonstrates that only the spectrum of product **3**-Au (Figure 4.7b) shows an additional peak at 283.9 eV binding energy, attributed to the C-N-Au bond.[30,31] This means that the amino groups recognize the AuNRs, as previously shown by UV-vis-NIR spectroscopy. The other difference between the spectra in Figure 4.6 is that, of course, the carbonyl peak is more intense for **2** due to the Boc group (Figure 4.7a).

Additional evidence for the presence of the Boc groups comes from the O 1s core level photoemission spectra for **2** and **3** shown in Figure 4.8. In fact, as expected, the contributions from carbonyl and carboxyl groups are more important for product **2** (Figure 4.8a). From the fit of the O 1s and the C 1s spectra, we can deduce the intensities of the different contributions and find that the carbonyl and carboxyl group intensities in the O 1s spectra totally agree with the corresponding C 1s intensities. From these intensities, we can calculate the atomic percentages of the elements present after application of the two functionalization procedures. This quantitative analysis is reported in Table 1 and shows a decrease of the oxygen levels from ~15 atomic % in product **2** to ~4 atomic % in product **3**.

Figure 4.9 shows the N 1s core level photoemission spectra of products **2** and **3**. In Figure 4.9a, the N-Boc nitrogen is identified at 400.4 eV, in analogy to a similar fullerene derivative,[32] while the pyrrolidine nitrogen is located at 398.9 eV. Therefore, from the fit of the spectra for **3** (Figure 4.9b), we can identify the positively charged (NH_3^+) species of the amine group at a binding energy of 401.1 eV as well as the nitrogen of the pyrrolidine at 399.7 eV, whose shift with respect to **2** is probably due to partial protonation. On the basis of the XPS analysis, we can assume that the interactions between Au nanoparticles with **3** are driven by two different interactions, the formation of amine-gold bonding[33] (Figure 4.7b) and the electrostatic recognition between protonated amine and PVP stabilizer.[34]

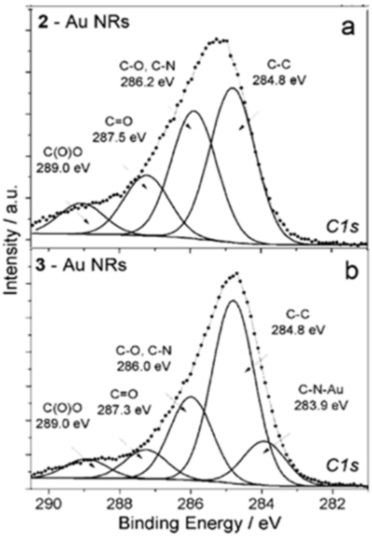

Figure 4.7. Photoemission spectra and fit of the C 1s core level region of (a) **2**-AuNRs (b) **3**-AuNRs, dispersed on Al.

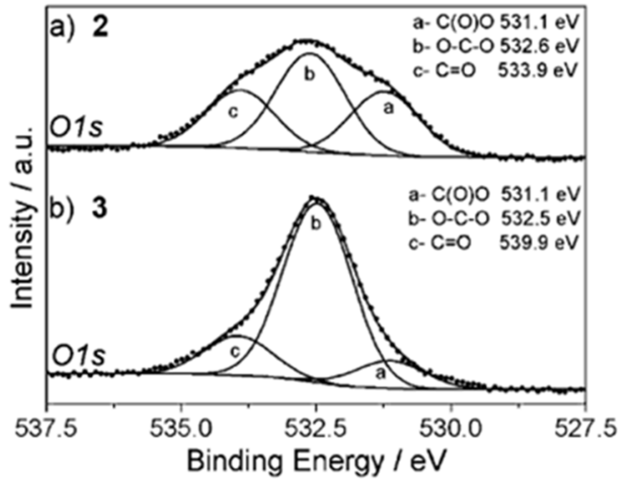

Figure 4.8. Photoemission spectra and fit of the O 1s core level region of (a) **2** and (b) **3** dispersed on Au/mica.

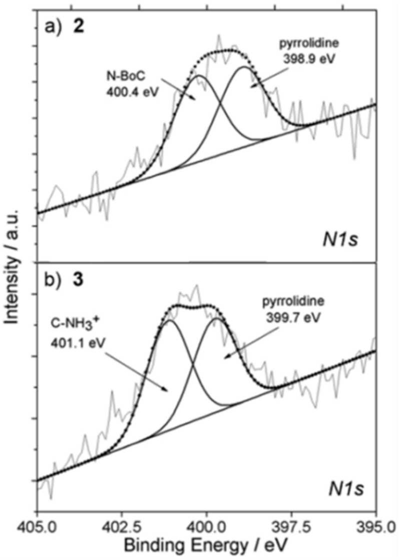

Figure 4.9. Photoemission spectra and fit of the N 1*s* core level region of (a) **2** and (b) **3** dispersed on Au/mica.

Table 1. Atomic composition of functionalized graphene

Atomic %	Product 3	Error %	Product 2	Error %
carbon	95.2	±1.9	82.9	±1.7
Oxygen	4.1	±0.3	15.2	±0.9
Nitrogen	0.7	±0.1	1.9	±0.2

4.3 Conclusion

In summary, we have illustrated how one can successfully produce functionalized graphene layers by condensation of a protected α-amino acid and paraformaldehyde followed by the deprotection of the Boc group. This derivative can be easily integrated with AuNRs that served as contrast markers for the identification of the reactive sites and produced a nanocomposite material that can be used for diverse applications.

Further chemical modifications of graphene functionalized **3** can be easily envisioned, such as introduction of photoexcitable donor-acceptor groups for photoinduced charge-transfer studies in photovoltaic devices.

References

[1] (a) Bernard, A. S.; Shook, I. K. *J. Chem. Phys.* **2008**, 128, 094707. (b) Meyer, J. C.; Geim, A. K.; Katsnelson, M. I.; Novoselov, K. S.; Booth, T. J.; Roth, S. *Nature* **2007**, 446, 60-63.

[2] Novoselov, K. S.; Geim, A. K.; Morozov, S. V.; Jiang, D.; Katsnelson, M. I.; Grigorieva, I. V.; Dubonos, S. V.; Firsov, A. A. *Nature* **2005**, 438, 201-204.

[3] Tombros, N.; Jozsa, C.; Popinciuc, M.; Jonkman, H. T.; van Wees, B.J. *Nature* **2007**, 448, 571-574.

[4] Kim, K.S.; Zhao, Y.; Jang, H.; Lee, S. Y.; Kim, J. M.; Kim, K. S.; Ahn, J. –H.; Kim, P.; Choi, J.; Hong, B. H. *Nature***2009**, 457, 706-710.

[5] Wang, Y.; Huang, Y.; Song, Y.; Zhang, X. Y.; Ma, Y. F.; Liang, J. J.; Chen, Y. S. *Nano Lett.***2009**, 9, 220–224.

[6] Elias, D. C.; Nair, R. R.; Mohiuddin, T. M. G.; Morozov, S.; Blake, V. P.; Halsall, M. P.; Ferrari, A. C.; Boukvalov, D. W.; Katsnelson, M. I.; Geim, A. K.; Novoselov, K. S. *Science* **2009**, 323, 610–613.

[7] (a) Schedin, F.; Geim, A. K.; Morozov, S. V.; Hill, E. W.; Blake, P.; Katsnelson, M. I.; Novoselov, K, S. Nat. Mater. 2007, 6, 652–655. (b) Lu, J.; Do, I.; Drzal, L. T.; Worden, R. M.; Lee, I. *ACS Nano* **2008**, 2, 1825–1832.

[8] Stoller, M. D.; Park, S.; Zhu, Y.; An, J.; Ruoff, R. S. *Nano Lett.* **2008**, 8, 3498–3502.

[9] Si, Y.; Samulski, E. T. *Chem. Mater.* **2008**, 20, 6792–6797.

[10] (a) Westervelt, R. M. Science 2008, 320, 324–325. (b) Chen, W.; Chen, S.; Qi, D. C.; Gao, X. Y.; Wee, A. T. S. *J. Am. Chem. Soc.* **2007**, 129, 10418–10422.

[11] (a) Williams, G.; Seger, B.; Kamat, P. V. *ACS Nano* **2008**, 2, 1487–1491. (b) Xu, Y.; Liu, Z.; Zhang, X.; Wang, Y.; Tian, J.; Huang, Y.; Ma, Y.; Zhang, X. Y.; Chen, Y. A. *Adv. Mater.* **2009**, 21, 1275–1279.

[12] Hernandez, Y.; Nicolosi, V.; Lotya, M.; Blighe, F. M.; Sun, Z.; De, S.; McGovern, I. T.; Holland, B.; Byrne, M.; Gunko, Y. K.; Boland, J. J.; Niraj, P.; Duesberg, G.; Krishnamurthy, S.; Goodhue, R.; Hutchison, J.; Scardaci, V.; Ferrari, A. C.; Coleman, J. N. *NatureNanotechnol.***2008**, 3, 563–568.

[13] (a) Georgakilas, V.; Kordatos, K.; Prato, M.; Guildi, D. M.; Holzinger, M.; Hirsch, A. *J. Am. Chem. Soc* **2002**, 124, 760–761. (b) Tasis, D.; Tagmatarchis, N.; Bianco, A.; Prato, M. *Chem. Rev.***2006**, 106, 1105–1136.

(c) Singh, P.; Campidelli, S.; Giordani, S.; Bonifazi, D.; Bianco, A.; Prato, M. *Chem. Soc. Rev*. **2009**, 38, 2214–2230.

[14] (a) Maggini, M.; Scorrano, G.; Prato, M. J. Am. Chem. Soc. 1993, 115, 9798–9799. (b) Tagmatarchis, N.; Prato, M. *Synlett*. **2003**, 6, 768–779.

[15] (a) Prato, M. *J. Mater. Chem.***1997**, 7, 1097–1109. (b) Tagmatarchis, N.; Prato, M. *J. Mater. Chem.* **2004**, 14, 437–439.

[16] Lin, T.; Zhang, W. D.; Huang, J.; He, C. *J. Phys. Chem. B* **2005**, 109, 13755–13760.

[17] Jiang, D.; Sumpter, B. G.; Dai, S. *J. Chem. Phys*. **2007**, 126, 134701.

[18] After the present work was completed, an article describing a similar procedure appeared in the literature: Georgakilas, V.; Bourlinos, A. B.; Zboril, R.; Steroptos, T. A.; Dallas, P.; Stubos, A. K.; Traplis, C. *Chem. Commun*. **2010**, 46, 1766–1768.

[19] (a) Yoshida, A.; Hishiyama, Y.; Inagaki, M. *Carbon* **1991**, 29, 1227–1231. (b) Valles, C.; Drummond, C.; Saadaoui, H.; Furtado, C. A.; Maoshuai, H.; Roubeau, O.; Ortolani, L.; Monthioux, M.; Penicaud, A. *J. Am. Chem. Soc*. **2008**, 130, 15802–15804.

[20] (a) Stankovich, S.; Dikin, D. M. G.; Dommett, H. B.; Kohlhaas, K. M.; Zimney, E. J.; Stach, E. A.; Piner, R. D.; Nguyen, S. T.; Ruoff, R. S. *Nature* **2006**, 442, 282–286.

[21] Lomeda, J. R.; Doyle, C. D.; Kosynkin, D. V.; Hwang, W. F.; Tour, J. M. *J. Am. Chem. Soc***2008**, 130, 16201–16206.

[22] Sarin, V. K.; Kent, S. B. H.; Tam, J. P.; Merrifield, R. B. *Anal. Biochem.***1981**, 117, 147–157.

[23] (a) Leff, D.; Brandt, V. L.; Heath, J. R. *Langmuir* **1996**, 12, 4723–4730. (b) Kumar, A.; Mandal, S.; Pasricha, R.; Mandale, A. B.; Sastry, M. *Langmuir* **2003**, 19, 6277–6282. (c) Zhong, Z.; Patskovsky, S.; Bouvrette, P.; Luong, H. T. J.; Gedanken, A. *J. Phys. Chem. B***2004**, 108, 4046–4052.

[24] Pérez-Juste, J.; Pastoriza-Santos, I.; Liz-Marzá´n, L. M.; Mulvaney, P. *Coord.Chem. Rev*. **2005**, 249, 1870–1901.

[25] (a) Jain, P. K.; Eustis, S.; El-Sayed, M. A. *J. Phys. Chem. B***2006**, 110, 18243–18253. (b) Pramod, P; Thomas, K. G. *Adv. Mater.* **2008**, 20, 4300–4305. (c) Funston, A. M.; Novo, C.; Davis, T. J.; Mulvaney, P. *Nano Lett.* **2009**, 9, 1651–1658

[26] Pastoriza-Santos, I.; Gomez, D.; Pérez-Juste, J.; Liz-Marzán, L. M.; Mulvaney, P. *Phys. Chem. Chem. Phys.***2004**, 6, 5056– 5060.

[27] Vial, S.; Pastoriza-Santos, I.; Pérez-Juste, J.; Liz-Marzán, L. M. *Langmuir* **2007**, 23, 4606–4611.

[28] Ferrari, A. C.; Meyer, J. C.; Scardaci, V.; Casiraghi, C.; Lazzeri, M.; Mauri, F.; Piscanec, S.; Jiang, D.; Novoselov, K. S.; Roth, S,; Geim, A. K. *Phys. Rev. Lett.* **2006**, 97, 187401-1- 253113-3.

[29] Gupta, A.; Chen, G.; Joshi, P.; Tadigadapa, S.; Eklund, P. C. *Nano Lett.* **2006**, 6, 2667–2673.

[30] Richardson, M. J.; Johnston, J. H.. *J. Colloid Interface Sci.* **2007**, 310, 425–430.

[31] Gomez-Navarro, C.; Weitz, R. T.; Bittner, A. M.; Scolari, M.; Mews, A.; Burghard, M.; Kern, K. *Nano Lett.* **2007**, 7, 3499–3503.

[32] Benne, D.; Maccallini, E.; Rudolf, P.; Sooambar, C.; Prato, M. *Carbon* **2006**, 44, 2896–2903.

[33] Kumar, A.; Mukherjee, P.; Guha, A.; Adyantaya, S. D.; Mandale, A. B.; Kumar, R.; Sastry, M. *Langmuir* **2000**, 16, 9775–9783.

[34] Correa-Duarte, M. A.; Pe´rez-Juste, J.; Sa´nchez-Iglesias, A.; Giersig, M.; Liz-Marza´n, L. M. *Angew. Chem., Int. Ed.* **2005**, 44, 4375–4378.

[35] Kordatos, K.; Da Ros, T.; Bosi, S.; Vazquez, E.; Bergamin, M.; Cusan, C.; Pellarini, F.; Tomberli, V.; Pantarotto, D.; Georgakilas, V.; Spalluto, G.; Prato, M. *J. Org. Chem.* **2001**, 66, 4915–4920.

Chapter 5

A novel route towards high quality fullerene-pillared graphene

In this chapter, we propose a new approach for the synthesis of graphite intercalation compounds (GICs)based on the use of co-intercalant molecules. We demonstrate the successful incorporation of fullerene (C_{60}) molecules between the graphene sheets with the help of nitric acid. The presence of intercalated C_{60} between the graphene sheets is deduced from the X-ray diffraction patterns, while Raman and X-ray photoelectron spectroscopy (XPS) serve to verify that the quality of the graphene layers is not compromised by the intercalation. A quantification of the interaction yield was derived from thermogravimetric analysis and XPS studies, giving 25wt% of intercalated fullerene molecules in the pillared structure. The present method opens new perspectives for the intercalation of various guest molecules in graphite also because graphite nitrate allows for functionalization processes following the very well established carbon chemistry.

5.1 Introduction

Carbon is the element with the greatest number of known allotropes. The three best-known ones are amorphous carbon, graphite, and diamond. In the past 30 years, new forms have been synthesized, including carbon nanotubes, graphene, and fullerenes, all of which have had a significant scientific and technological impact due to their unique properties, such as high surface area, good thermal and chemical stability, low mass, chemical inertness and unusual electronic properties.[1-4] These materials have been extensively used as electrochemical storage capacitors, catalytic substrates, sorbents for separation processes, gas sensors, gas storage materials at high temperatures (*e.g.* for hydrogen, CO_2, methane).[5-8] On the other hand, the big challenge in the field of nanoporous materials is the creation of mesoporous structures with controlled porosity and very high/tunable surface area,[9] since both are decisive factors for applications in catalysis and energy storage.[10] Graphene, the one atom thick layer of sp^2-hybridized carbon atoms, with its very high surface area, (2500 m^2/g), is an excellent candidate for the development of novel hybrid nanoporous materials since it is also easily modifiable (chemically) and presents excellent mechanical and thermal stability.[11] To create a porous material, one has to prevent graphene layers from stacking to form graphite driven by weak van der Waals interaction between the aromatic π-systems, and a way to do this is to insert robust organic/inorganic species as columns/pillars in between them, using the so-called 'pillaring method'.[12] This method has been successfully employed with other layered materials like clays,[13] and layered double hydroxides.[14] By choosing the right guest molecules which are stable

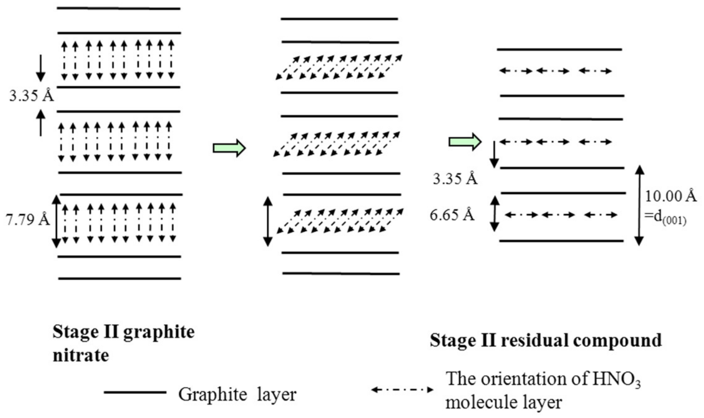

Scheme 1. Schematic representation of stage II intercalation of HNO_3[21-23]

enough to keep the graphene layers separate, the appropriate distance for achieving a high surface area can be obtained. To succeed in making such a pillared structure starting from graphite, two basic steps must be accomplished prior to intercalation of the pillaring moieties: the 3-D structure of graphite must be opened with the help of a co-intercalant and this primarily hybrid structure must be dispersed in an organic solvent. The role of the co-intercalant is essential because once the graphite planes are pushed apart, guest molecules easily penetrate between the layers with the help of the appropriate solvent.[15-17] Graphite oxide (GO) holds a foremost place in intercalation strategies applied to date, because of its well-ordered structure in combination with excellent hydrophilic and swelling properties.[18] The functional oxygen groups (such as hydroxyl, epoxy and carbonyl) give rise to the absorption of polar molecules forming GO-intercalation compounds, however upon reduction the quality of graphene layers is low due to both formation of holes in the hexagonal lattice and the presence of some remaining oxygen-groups.

An alternative is provided by graphite nitrate (GN) whose structure was quite difficult to unravel.[19] The final solution to the puzzle was given by Fuzellier,[20]according to whom there are two arrangements of the nitric acid during the intercalation process. The first phase (α crystalline phase) with stoichiometry $C^{+}_{24n}\bullet NO_3^{-}\cdot 5HNO_3$ for the nth stage compound, and interlayer distance of 0.78 nm, corresponds to an arrangement where the triangular planar nitric acid molecules stay perpendicular to the graphite planes. This phase spontaneously converts into a second 'residual' phase (β crystalline phase) with stoichiometry $C^{+}_{24n}\bullet NO_3^{-}\cdot 2HNO_3$ and an interlayer distance of 0.66 nm, where the molecules lie down between the graphite planes (Scheme 1).[21-23] The great benefit of using GN as a host matrix, for the insertion of suitable robust molecules in the graphite lattice, is the sufficient opening of the graphene layers without any oxidation treatment. Thus, the quality of the graphene flakes after the intercalation remains high and this allows for the development of a new class of hybrid structures with high specific surface area and a defect free lattice.

In this chapter, we report the successful incorporation of pure fullerene molecules into graphite nitrate by a simple intercalation reaction using toluene as solvent. Nitrate molecules/anions play the role of co-intercalant, enabling C_{60} molecules to penetrate between the graphene layers. As a result pillared fullerene graphene structures are formed upon thermal treatment at relative low temperatures (below 100 °C). The final hybrid materials, as well as the intermediate products, were characterized by X-ray diffraction and differential thermal and thermogravimetric (DTA-TGA) analysis, in conjunction with X-ray photoelectron and Raman spectroscopies. The possibility of stabilizing graphite nitrate by intercalation of organic compounds have been tried in the past,[24,25] but here we report for the first time the insertion of a robust organic molecule acting as pillar between the graphene layers to create a hybrid structure with good thermal stability.

5.2 Experimental Section

Materials High purity graphite powder was purchased from Carbon Bay (Grade: SP1, Batch no. 04100; Lot No. 011705) and toluene (99.99%) from Acros Organics. Nitric acid (fuming, ≥99.5%, d=1.502 g/cm^3), anhydrous acetonitrile (water < 10 ppm) and fullerene C_{60} (99.5%) were purchased from Sigma-Aldrich. All chemicals were used as received.

Preparation of graphite nitrate(See chapter 2.2.3).

Intercalation of fullerene in graphite nitrate In a typical experiment, 10 mg of graphite nitrate were dispersed in 100 mL of toluene and the mixture was stirred for 5 days at ambient conditions. A solution of C_{60} (10 mg) in toluene (100 mL) was then added dropwise to the graphite nitrate suspension and the mixture was stirred for another 5 days at room temperature. During this progress the initial purple color of the dispersion progressively darkened (after the 3 days) and finally became black indicative of the successful intercalation of C_{60} into the graphite nitrate host material. The mixture was filtered with an Ederol Filter (15-65 g/m^2 110 mm), washed three times with toluene and the final powder was collected (sample denoted as GN/C_{60}).

Characterization techniques

X-ray diffraction (XRD): (see chapter 2.1.2)

Raman spectra: (see chapter 2.1.3 b)

X-ray photoelectron spectroscopy (XPS): (see chapter 2.1.1)

Thermogravimetric (TGA): (see chapter 2.1.6)

5.3 Results and discussion

5.3.1 X-ray diffraction

The X-ray diffraction (XRD) patterns of pristine graphite and graphite-nitrate are presented in Figure 1. The pattern of pure graphite exhibits an intense peak at 26.5±0.2° corresponding to a basal spacing of d_{002}= 3.35 Å followed by the weak 100, 101 and 004 reflection peaks at 42.4±0.4°, 44.6±0.4° and 54.6±0.4°. For graphite-nitrate a new 001 reflection peak appears at 8.8±0.6° equaling d_{001}=10.03±0.5 Å. The latter corresponds to an inter-sheet separation of 10.03-3.35= 6.68 Å, where 3.35 Å is the thickness between two adjacent graphene layers and denotes the formation of a so-called stage II residual compound of graphite-nitrate whose structure is illustrated in Scheme 1.[23] The stability of this compound

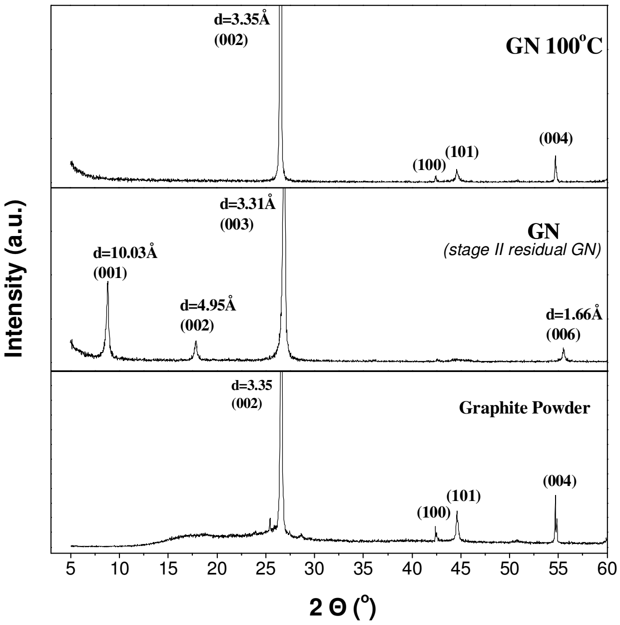

Figure 5.1 XRD patterns of graphite, graphite nitrate and graphite nitrate after heating at 100 °C.

depends mainly on temperature; in fact, as demonstrated by the diffraction patterns in Figure 5.1, upon heating GN at 100 °C, the nitrate molecules/anions disappear from the graphite galleries and the graphene layers restack forming graphite.

The intercalation of fullerene into the interlayer space of GN was demonstrated by temperature dependent X-ray diffraction measurements. Figure 5.2 displays the XRD patterns of a GN/C_{60} film recorded in a temperature range between 25 °C to 125 °C. At room temperature, the X-ray diffractogram of GN/C_{60} shows that the main 001 reflection of GN is superimposed on a new broader peak centered at ~9.5°. The existence of the 001 peak reveals that the nitrate molecules remain within the graphite galleries (stage II residual compound) while the broad peak is due to insertion of C_{60} molecules between graphene layers, which gives rise to the formation of a new intercalated graphite derivative. As the temperature increased, the 001 peak due to stage II residual GN progressively vanished. At 75 °C only the broad peak due to intercalated C_{60} between graphene sheets remained and no changes were observed upon further heating, indicating that fullerenes acted as robust pillar molecules between the graphene layers. From the value of the basal d_{001}spacing of 9.3 Å of this compound an inter-sheet separation of L = 9.3 – 3.3 = 6.0 Å was deduced, where the value of 3.3 Å represents the thickness of a graphene sheet. This value is reasonably close to the size of C_{60} (~7 Å) and a similar interlayer spacing has been observed upon intercalation of fulleropyrrolidine derivatives in smectite nanoclays.[27] Employing the Debye-Scherrer equation, the thickness of the coherently diffracting domains or mean crystalline dimension, t, can be calculated: $t = K\lambda/\beta \cos\theta$,[13] where K is a constant near unity (K = 0.91), λ is the X-ray wavelength (λ = 1.5418 Å), θ is the angular position of the first diffraction peak, and β is the broadening of the 001 line

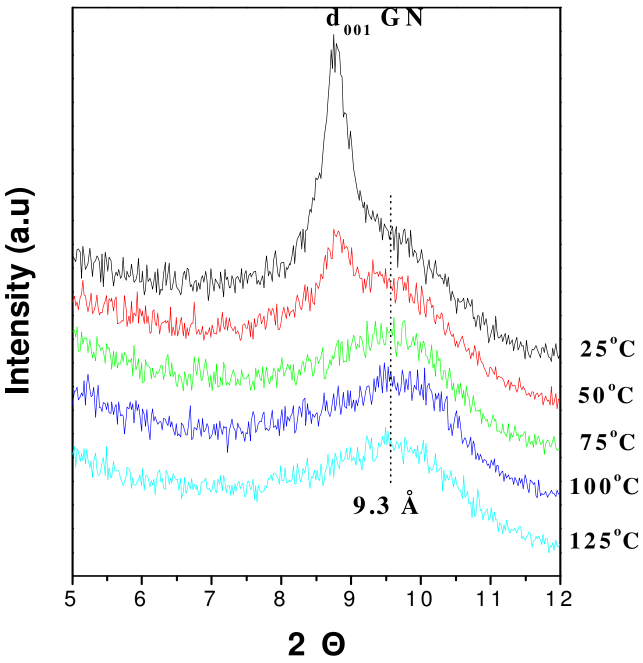

Figure 5.2. Temperature dependent X-ray diffraction patterns of GN/C_{60}

diffraction line (calculated as full width at half of the peak height and expressed in radians). Thus the crystalline dimension of the GN/C_{60} hybrids were estimated as 19.3 Å. As a consequence, the average stacking height of the layers, estimated by the formula N = t/d, where N is the number of diffracting layers along the c-axis and d is the 001 spacing of one layer (in Å), was found to be equal to 2.This suggests that an important exfoliation has occurred and that the intercalated hybrid is present as bilayers.

5.3.2 X-ray photoelectron spectroscopy

To gain insight into the elemental composition and the chemical state of the elements that make up the pillared compound, XPS spectra of graphite, GN and of the GN/C_{60} hybrid were collected before and after heating at 400 °C (under vacuum) and are presented in Figure 5.3. The C 1s core level region of the XPS spectrum of natural graphite displays only one narrow peak at a binding energy of 285.0 eV, indicative of the good quality of the starting material. After intercalation of nitric acid, the C 1s line of GN exhibits four contributions at 285.0 eV, 286.2 eV, 287.2 eV and 289.0 eV. The peak at 285.0 eV (C1) originates from the carbon-carbon bonds of the hexagonal lattice, and accounts for 87.5% of the total carbon intensity. The contribution at 286.2 eV (C2) is due to in C-N and C-O bonds (7.8% of the total carbon intensity), while the spectral intensity at 287.2 eV (C3) and 289.0 eV (C4) arises from the carbonyl (3.6%) and carboxyl groups (1.3%), respectively. The data suggest that the synthesis of GN did

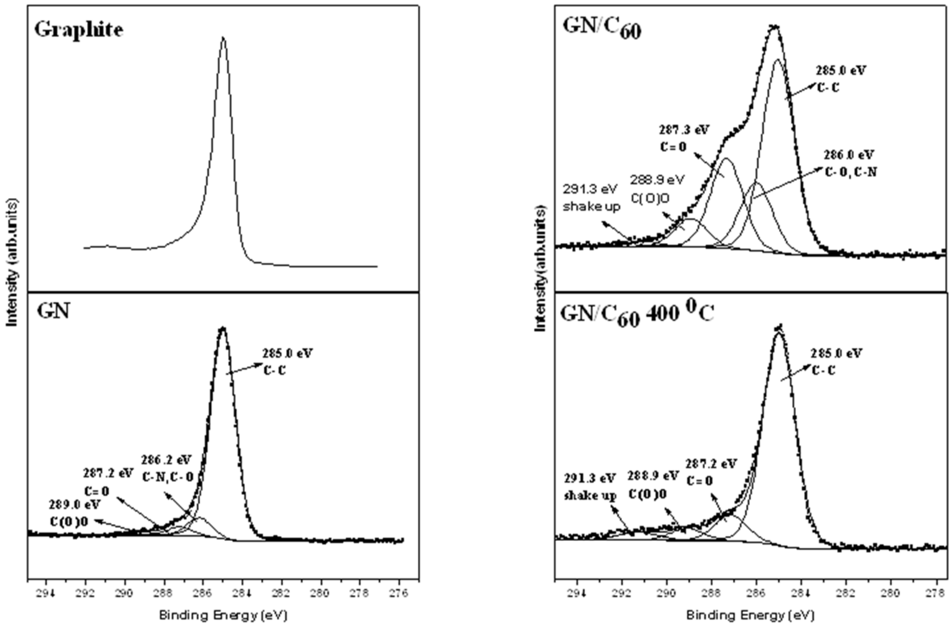

Figure 5.3. The C 1*s* core level region of the XPS spectra of natural graphite, graphite nitrate, and graphite nitrate intercalated with C_{60} (GN/C_{60}) before and after heating at 400 °C under vacuum.

not importantly affect the graphene lattice since less than 8% of graphite results functionalized by oxygen and nitrogen containing groups creating defects on the lattice. These findings are in accordance with those obtained by Raman Spectroscopy (see below). On the other hand, the C 1s core level region of the XPS spectrum of intercalated GN/C_{60} (before heating) reveals the successful intercalation of fullerene whose fingerprint is the shake-up feature centered at 291.3 eV.[28,29] Moreover, the same distinct carbon peaks of GN are also observed in the GN/C_{60} hybrid, however, the relative intensities of these four C1*s* components are quite different from those of GN. In fact, in the GN/C_{60} hybrid, the spectral intensity of the C2, C3 and C4 species seems to be increased with respect to that of the C1 species. 16.5% of the total C1*s* intensity arises from the carbon bound to nitrogen and carbon bound to oxygen (C2), 22.4% comes from the carbonyl groups (C3), while 6.6% stems from the carboxyl groups (C4). This phenomenon could be explained due to the important exfoliation deduced from the XRD data, which causes the photoemission signal of the C2, C3 and C4 functionalized carbon groups situated mainly at the edges of the carbon sheets to be less attenuated. In addition, after annealing of the GN/C_{60} material at high temperature (400 °C) under vacuum, a significant reduction of the oxygen/nitrogen containing functional groups is evident from the decreased intensities of the C2, C3 and C4 species, attesting to the good quality of the graphene sheets, while the shake-up peak at 291.3 eV remains, confirming the presence of C_{60} molecules between the graphene layers. In detail, after heating the hybrid material 81.7 % of the total C 1s intensity corresponds to carbon-carbon bonds of the aromatic ring of graphite, as well the fullerene molecules. Based on the XPS intensities, one also deduces that the oxygen level of the hybrid nanostructure approaches 3 atomic%; in comparison with other intercalation methods of graphite reported up to now,[30] this oxidation level is extremely low.

Since an element's photoemission intensity is directly proportional to its atomic percentage in the probed volume, from the carbon and nitrogen 1s intensities in GN and GN/C_{60} reported in Table 5.1 one can calculate the intercalation yield. The ratio between the carbon to nitrogen intensities (I_{C1s}:I_{N1s}) is 12.1 in the pristine GN, and increases to approximately 15.8 after intercalation of C_{60}. Assuming that this increase in carbonaceous material is due to the insertion of fullerene into the graphite nitrate matrix ($C^{+}_{48}\bullet NO_3^{-}\cdot 2HNO_3$) and hence neglecting the possibility of inserting toluene together with C_{60}, we can estimate the intercalation yield as one C_{60} molecule on every 155±5 carbon atoms of graphite nitrate.

Table 5.1. Chemical composition of GN and GN/C_{60}

GN

	Atomic Percentage%	Error %
C	79.6	1.6
O	13.8	0.8
N	6.6	0.8

Ratio C/N 12.1

GN/C_{60}

	Atomic Percentage%	Error %
C	72.8	1.5
O	22.6	1.3
N	4.6	0.6

Ratio C/N 15.8

5.3.3 Raman spectroscopy

Raman spectroscopy is a widely used tool for the characterization of carbonaceous materials and exhibits similar features for all types of carbons in the spectral range between 800 cm^{-1} and 2000 cm^{-1}. Typically, the spectra show the so-called G band (around 1580 cm^{-1}) assigned to the E_{2g} vibrational mode of carbon atoms in a hexagonal lattice,[31] as well as the D band (at around 1350 cm^{-1}), which is indicative of the degree of disorder in the symmetry of the graphite lattice due to the presence of defects.[32] Figure 5.4 presents the Raman spectra of the pristine graphite and GN, as well as of the GN/C_{60} hybrid. The starting graphite material can be classified as defect free and well-ordered since the D band is absent. After intercalation of nitrate molecules/anions the sharp G peak splits in two peaks at 1580 cm^{-1} and 1610 cm^{-1}, respectively. The splitting of the G band upon intercalation arises primarily from the symmetry changes since every graphitic layer is now adjacent to an intercalant layer on one side and to a graphene sheet on the other.[33,34] Upon intercalation of C_{60} the intensity ratio of these two bands changes and they broaden considerably: the G band centered at 1580 cm^{-1} dominates the spectrum and the split peak has become so broad that it is visible only as a small shoulder. In addition, in the Raman spectrum of GN/C_{60}, a new peak located at 1445 cm^{-1} assigned to the prominent pentagonal pinch mode ($A_g(2)$) of C_{60} reveals

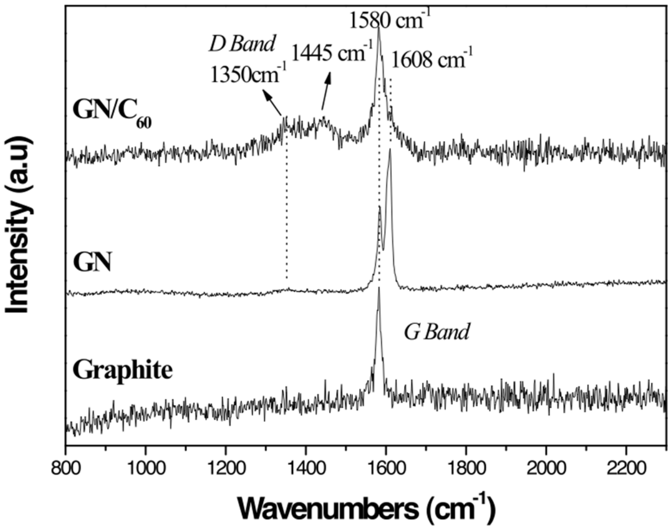

Figure 5.4. Raman spectra of Graphite, GN and GN/C_{60} at room temperature with a laser excitation line at 532 nm.

the presence of fullerene in the final hybrid material. In fact, this peak is down-shifted 24 cm^{-1} from the Ag(2) mode of fullerite (1469 cm^{-1}).[35] This shifted value is typical for C_{60} adsorbed on surfaces where the molecule interacts only weakly, such as H-terminated Si[36] or CO pre-covered Cu(001)[37], *i.e.* where neither covalent bonding nor charge transfer occur. One can also see that a small amount of structural disorders is introduced upon intercalation of fullerenes, which translates into the appearance of a small D band (1350 cm^{-1}); however, the low relative intensity of the D band with respect to the G band (I_D/I_G ~0.3) is an indication of a fairly well ordered, defect-poor intercalated material.[31] A contribution to the existence of the D band may also come from any remaining toluene adsorbed acting as a donor, transferring electrons to the graphene sheets[38,39].

5.3.4 Thermogravimetric (TGA) analysis

To investigate the stability of GN and GN/C_{60}, thermogravimetric (TGA) analysis was performed. We first compared pure graphite and graphite nitrate before and after heating the sample at 100 °C under air; the results are shown in Figure 5.5. Pristine graphite decomposed at temperatures above 680 °C, while GN displayed a 23.3% weight loss up to 100 °C, which was related to the removal of nitrate molecules/anions, and water molecules from the interlayer space of graphite and combusted at lower temperatures (570 °C) than pristine graphite. In the TG curve of GN collected after heating the sample at 100 °C, the first weight loss step is absent and the combustion of the graphite lattice was taking place at the same temperature as for GN that had not been heated, indicating that nitrate anions were efficiently removed from the graphene galleries without influencing the carbon structure. The lower temperature (with respect to pristine graphite) at which graphitic layers of GN and heated GN started to decompose

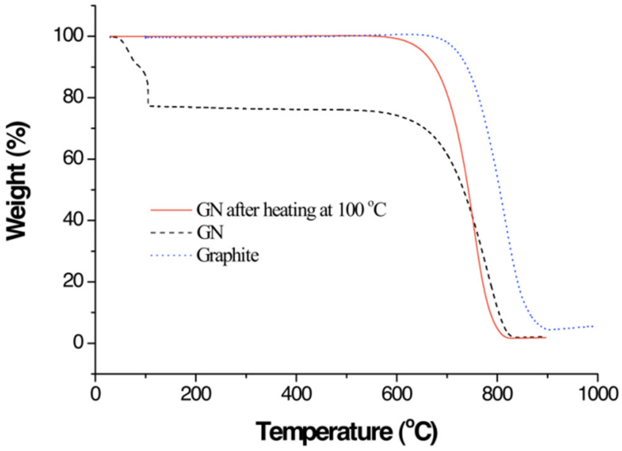

Figure 5.5. Thermogravimetric analysis curves of pristine graphite, graphite nitrate and graphite nitrate after heating at 100 °C (in air)

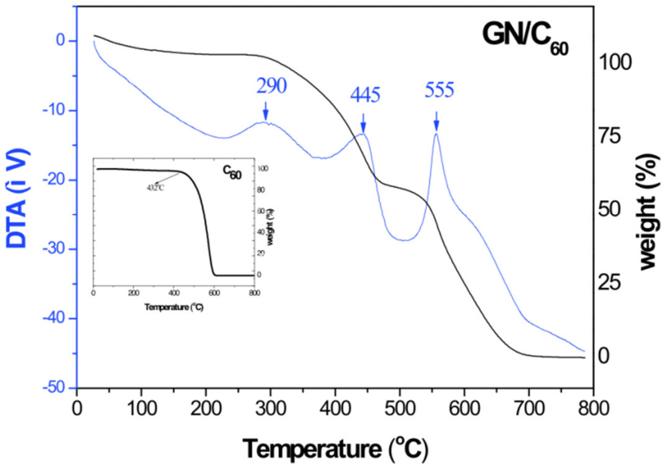

Figure 5.6. DTA/TGA curves of graphite nitrate intercalated with C_{60} (GN/C_{60}). Inset: TGA curve of pure C_{60}.

indicated that opening the interlayer space through intercalation facilitates the access to oxygen even after the intercalant has been evacuated.

After the intercalation of C_{60} into GN, TGA and differential thermal analysis (DTA) were carried out (Figure 5.6) to define the characteristics of this hybrid pillared material. GN/C_{60} showed a 6% weight loss up to 150 °C, related, as for GN, to the removal of both nitrate species and intercalated water. Above this temperature, in the DTA curve exhibits three exothermic peaks. A 17% weight loss between 230 °C and 380 °C, with the exothermic peak centered at 290 °C, is attributed to the removal of oxygen-containing species (see XPS spectra discussed above) from the edges of the graphene sheets and of any toluene co-inserted with

C_{60} via adsorption. Toluene is acting as a donor, transferring electrons to graphene.[38,39] The second exothermic peak centered at 445 °C is assigned to the oxidation of intercalated fullerene molecules based on the comparison with the TGA curve of pure fullerene (see inset Figure 5.7). From the weight loss curve between 380 °C and 500 °C, we estimated that about 25 wt% of the total mass corresponds to fullerene molecules incorporated in the hybrid. These results are in accordance with the XPS data where we observe an increase of the I_{C1s}:I_{N1s} ratio of approximately 25%. Finally, for temperatures above 500 °C, the exothermic peak centered at 555 °C originates from the combustion of high purity graphite.[40] This temperature is lower than that of pristine GN (see Figure 5.6) and an explanation for this acceleration of the combustion might be that because of the fast temperature rise the graphene layers have no time to re-stack via Van Der Waals interaction.[40] From the TG curve, the total amount of the graphene-based matrix is estimated to be 52 wt% of the overall mass of the hybrid material.

5.4 Conclusions

In conclusion, we demonstrated the successful intercalation of pure fullerene in high quality graphite nitrate derived from reaction of pristine graphite with fuming nitric acid. The nitrate anions play the role of co-intercalant enabling C_{60} molecules (using toluene as solvent) to penetrate between the graphene layers. Heating to temperatures where the nitrate anions diffuse out of the structure yields fullerene-pillared graphene.

The presence of intercalated fullerene molecules between the graphene sheets is deduced from X-ray diffraction as well as from Raman, and the spectroscopic techniques demonstrate that the quality of the graphene layers is not compromised by the intercalation. A quantification of the interaction yield was derived from thermogravimetric analysis and X-ray photoemission data, giving 25 at% fullerene molecules intercalated in the pillared structure.

The present method opens new perspectives for the intercalation of various guest molecules in graphite also because graphite nitrate allows for functionalization processes following the very well established carbon chemistry. Pillaring structures based on graphene (using different type of organic/or inorganic pillars in between the graphene layers) may lead to new types of porous materials suitable as catalysts, catalytic supports or adsorbents for gas storage applications.

References

[1] Geim, A. K.; Novoselov, K. S. *Nat Mater.* **2007**, 6, 183-191.

[2] Meng, G.; Jung, Y. J.; Cao, A.; Vajtai, R.; Ajayan, P. M. *Proceedings of the National Academy of Sciences of the United States of America* **2005**, 102, 7074 -7078.

[3] Zhao, X. B.; Xiao, B.; Fletcher, A. J.; Thomas, K. M. *J. Phys. Chem. B* **2005**, 109, 8880-8888.

[4] Collins, G. P.; Bradley, K.; Ishigami, M.; Zettl, A. *Science* **2000**, 287, 1801-1804.

[5] Frackowiak, E.; Béguin, F. *Carbon* **2001**, 39, 937-950.

[6] Rodríguez-Reinoso, F. *Carbon* **1998**, 36, 159-175.

[7] Kayiran, S. B.; Lamari Darkrim, F.; Levesque, D. *J Phys Chem B* **2004**, 108, 15211-15215.

[8] Steele, B. C. H.; Heinzel, A. *Nature* **2001**, 414, 345-352.

[9] Davis, M. E. *Nature* **2002**, 417, 813-821.

[10] Serp, P.; Jośe Lúís Figueiredo, J. L. '*Carbon Materials for Catalysis*' (John Wiley & Sons, Inc, **2009**).

[11] Stankovich, S.; Dikin, D. A.; Dommett, G. H. B.; Kohlhaas, K. M.; Zimney, E. J.; Stach, E. A.; Piner, R. D.; Nguyen, S. T.; Ruoff, R. S. *Nature* **2006**, 442, 282-286.

[12] Pinnavaia, J. T. *Science* **1983**, 220, 365-371.

[13] Gournis, D.; Jankovič, L.; Maccallini, E.; Benne, D.; Rudolf, P.; Colomer, J.; Sooambar, C.; Georgakilas, V.; Prato, M.; Fanti, M.; Zerbetto, F.; Sarova, G. H.; Guldi, D. M. *J. Am. Chem. Soc.* **2006**, 128, 6154-6163.

[14] Khan, A. I.; O'Hare, D. *J. Mater. Chem.* **2002**, 12, 3191-3198.

[15] Liu, Z. -H.; Wang, Z. -M.; Yang, X.; Ooi, K. *Langmuir* **2002**, 18, 4926–4932.

[16] Liu, P.; Gong, K.; Xiao, P.; Xiao, M. *J. Mat. Chem.* **2000**, 10, 933–935.

[17] Pruvost, S.; Hérold, C.; Hérold, A.; Lagrange, P. *Carbon* **2004**, 42, 1825–1831.

[18] Bourlinos, A. B.; Gournis, D.; Petridis, D.; Szabó, T.; Szeri, A.; Dékány, I. *Langmuir* **2003**, 19, 6050–6055.

[19] Rüdorff, W. Z. *Phys. Chem.Abt. B* **1939**, 45, 42–68.

[20] Fuzellier, H. J.; Melin, J.; Herold, A. *Mater. Sci. Eng.* **1977**, 3, 91-94.

[21] Savoskin, M. V.; Yaroshenko, A. P.; Whyman, G. E.; Mysyk, R. D. *J. Phys. Chem. Sol.* **2006**, 67, 1127–1131.

[22] Moreh, R.; Shahal, O.; Kimmel, G. *Phys. Rev. B* **1986**, 33, 5717–5720.

[23] Touzain, P. *Synthetic. Met.* **1979**, 1, 3-11.

[24] Inagaki, M. *J. Mater. Res.* **1989**, 4, 1560–1568.

[25] Savoskin, M. V.; Yaroshenko, A. P.; Mysyk, R. D.; Vaiman, G. E.; Vovchenko, L. L.; Popov, A. F. *Theo. Exp. Chem.* **2004**, 40, 92–97.

[26] Lotya, M.; Hernandez, Y.; King, P. J.; Smith, R. J.; Nicolosi, V.; Karlsson, L. S.; Blighe, F. M.; De, S.; Wang, Z.; McGovern, I. T.; Duesberg, G. S.; Coleman, J. N. *J. Am. Chem. Soc.* **2009**, 131, 3611-3620.

[27] Gournis, D.; Georgakilas, V.; Karakassides, M. A.; Bakas, T.; Kordatos, K.; Prato, M.; Fanti, M.; Zerbetto, F. *J. Am. Chem. Soc.* **2004**, 126, 8561–8568.

[28] Leiro, J.A.; Heinonen, M. H.; Laiho, T.; Batirev, I. G.; *J. Electron. Spectrosc.***2003**, 128, 205–213.

[29] Kumar, A.; Singh, F.; Govind; Shivaprasad, S. M.; Avasthi, D. K.; Pivin, J. C. *Applied Surface Science* **2008**, 254, 7280–7284.

[30] Viculis, L. M.; Mack, J. J.; Mayer, O. M.; Hahn, H. T.; Kaner, R. B. *J. Mat. Chem.* **2005**, 15, 974–978.

[31] Nemanich, R.J.; Solin, S. A. *Phys. Rev. B***1979**, 20, 392–401

[32] Katagiri, G; Ishida, H.; Ishitani, A. *Carbon* **1988**, 26, 565–71.

[33] Afanasov, I. M.; Shornikova, O. N.; Kirilenko, D. A.,; Vlasov, I. I.; Zhang, L.; Verbeeck, J.; Avdeev, V. V.; Van Tendeloo, G. *Carbon* **2010**, 48, 1862–1865.

[34] Dresselhaus, M. S.; Dresselhaus, G. *Adv. Phy.***2002**, 51, 1–186.

[35] Haddon, R. C.; Hebard, A. F.; Rosseinsky, M. J.; Murphy, D. W.; Duclos, S. J.; Lyons, K. B.; Miller, B.; Rosamilla, J. M.; Fleming, R. M.; Kortan, A. R.; Glarum, S. H.; Makhija, A. V.; Muller, A. J.; Eick, R. H.; Zahurak, S. M.; Tycko, R.; Dabbagh, G.; Thiel, F. A. *Nature* **1991**, 350, 222-223.

[36] Dumas, P.; Gruyters, M.; Rudolf , P.; He, Y.; Yu, L. M.; Gensterblum, G.; Caudano, R.; Chabal, Y. *J. Surf. Sci.* **1996**, 368, 330-336.

[37] Rudolf, P.; Raval, R.; Dumas, P.; Williams, G. P. *Appl. Phys. A* **2002**, 75, 147–153.

[38] Kaverzin, A. A.; Strawbridge, S. M.; Price, A. S.; Withers, F.; Savchenko, A. K.; Horsell, D. W. *Carbon* **2011**, 49, 3829–3834.

[39] Boukhvalov, D. W. *Surf. Sci.* **2010**, 604, 2190–2193.

[40] Pang, L. S. K.; Saxby, J. D.; Chatfield, S. P. *J. Phys. Chem.* **1993**, 97, 6941-6942.

Chapter 6

Towards novel multi-functional pillared layered nanostructures: effective intercalation of adamantylamine in graphene oxide and smectite nanoclays

This Chapter describes a new approach for the synthesis of multi-functional materials by the intercalation of adamantylamine (ADMA) molecules into the interlayer space of graphite oxide, montmorillonite and laponite clay. We demonstrate that the hybrid materials thus created have great potential for employment in environmental remediation and biomedicine because they are highly effective in the removal of organic pollutants (e.g. chlorophenols) from aqueous solutions and exhibit remarkable cytotoxic behaviour.

6.1 Introduction

Diamondoids have been extensively studied in recent years due to their successful applications in diverse fields of nano- and biotechnology[1] which rely on the physical and chemical properties[2] imparted by their unique (cage-like) structure of tricyclic saturated hydrocarbons. Thus, a huge number of adamantane derivatives and composites have been prepared and analysed. Many applications have been reported in the literature for these “molecular diamonds” including their use in nanotechnology as templates, or molecular building blocks for the synthesis of novel catalysts[3] high temperature polymers,[4] or hybrid nanostructures.[5-7] In the pharmaceutical industry they are employed in drug delivery and as drug targeting agents,[8] as well as in antiviral drugs (influenza A)[9] and in the treatment of Parkinson and Alzheimer.[10] To further extend the use of diamandoids, host guest chemistry can help to tune or protect the properties of these molecules. In this context, adamantylamine (ADMA), a crystalline adamantane derivative with a covalently attached amino group, is expected to be an ideal pillaring/building block to be incorporated in layered host materials such as layered aluminosilicate clays or graphene oxide (GO), giving rice to new hybrid multifunctional nanostructures.

Layered materials represent a diverse and largely untapped source of two-dimensional (2D) nanosystems with high specific surface area and exceptional physicochemical properties that are important for applications such as catalysis, sensing, environmental remediation, biotechnology, and energy storage.[11-16] The nature of the microenvironment between the 2D nanometer-sized sheets regulates the topology of the intercalated molecules and affects possible supramolecular rearrangements or reactions, such as self-assembling processes that are usually not easily controlled in solution.[17] Smectite clays and graphene oxide are two archetypical layered materials which have long been investigated. Smectite clays are layered minerals consisting of aluminosilicate nanoplatelets, with a unique combination of swelling, intercalation and ion exchange properties that make them valuable nanostructures[18] for use as catalysts,[19] templates in organic synthesis,[20] building blocks for composite materials,[21] or adsorbents of inorganic and/or organic pollutants.[22,23] In most of the cases the intercalation process is a simple ion-exchange procedure between the hydrated cations present in the galleries of the clay and organic/or inorganic cation moieties. Unlike the intercalation of graphite, the one of smectite clays does not involve necessarily charge transfer between the host and the guest species. One the other hand, graphite oxide (GO) is an oxygen rich derivative of graphite decorated with hydroxyl, epoxy, and carboxyl groups on the basal planes and edges of carbon sheets.[24] These functional groups are created by strong oxidation and distributed randomly on the GO sheets, generating aliphatic regions (sp^3-carbon atoms). Due to the existence of such hydrophilic moieties, GO presents similar properties with smectite clays in that it is prone to swelling and intercalation. Both GO and intercalated GO are being considered for numerous applications such as supercapacitors,[25] high mobility transistors,[26] lithium batteries,[27] hydrogen storage, absorbers for organic moieties[28] and for the removal of pollutants (*e.g.* chlorophenols) from aqueous solutions. In contrast to clays, the intercalation process of GO involves covalent bonding of guest molecules to the oxygen-containing groups on the GO surfaces (nucleophilic substitution reactions). It has been demonstrated that, under proper conditions, GO can be exfoliated in water forming colloidal suspensions of single graphene oxide sheets.[29]

In this chapter, we report on the intercalation of adamantylamine into two types of layered matrices, graphene oxide and smectite nanoclay. Intercalation of ADMA in montmorillonite proceeds through a simple cation exchange reaction while in the case of GO, the adamantane derivative is inserted in the graphene interlayers and is covalently bonded via chemical grafting on the epoxy groups on the GO surfaces.

6.2 Experimental section

Host layered materials. Graphene oxide was produced from graphite powder using a modified Staudenmaier's method.[30] (see chapter 2.2.1). The clays used in this work were a natural Wyoming montmorillonite (SWy-2) (see chapter 2.2.2) with cation exchange capacity (CEC) of 78 meq/100 g clay, and a synthetic trioctahedral hectorite, Laponite RD (Lap), produced by Laporte Industries Ltd. with structural formula $Na_{0.8}[Mg_{5.4}Li_{0.4}]Si_8O_{20}(OH)_4$, a CEC of 48.1 meq/100 g clay and average particle size 20 nm. SWy-2 was fractionated to <2 μm by gravity sedimentation and purified by standard methods in clay science (see chapter 2.2.2).

Preparation of clay-adamantylamine hybrids. a. Intercalation of montmorillonite: 300 mg of Na-SWy-2 dispersed in 100 mL distilled deionized water were reacted with 50 mg of 1-adamantylamine (97%, Aldrich) dissolved in 20/1 (v/v) ethanol/water. This amount corresponds to 1.5 times the CEC of SWy-2 montmorillonite. 5 drops of HCl 1M were then added and the mixture was stirred at room temperature for 24 hours. The residue was separated by centrifugation, washed three times with distilled deionized water and air-dried by spreading over a glass plate (product: **SWy-2/ADMA**). **b. Intercalation of laponite**: 300 mg of laponite dispersed in 100 mL distilled deionized water were reacted with 30 mg of 1-adamantylamine (97% Aldrich) dissolved in 20/1 (v/v) ethanol/water. This amount corresponds to almost 1.5 times the CEC of Laponite. The residue was separated by centrifugation, washed three times with distilled deionized water and air-dried by spreading over a glass plate (product: **Lap/ADMA**).

Preparation of graphene oxide-adamantylamine hybrid. In a typical experiment, 300 mg 1-adamantylamine were dissolved in ethanol (50 mL) and added dropwise to a dispersion of GO in distilled deionized water (100 mg GO in 50 mL) under vigorous stirring. Upon addition of adamantylamine the GO solid swelled instantly. The reaction continued for 24 h at room temperature. The GO derivative was isolated by centrifugation and washed three times with 1:1 (v/v) ethanol/water and dried in air (**GO/ADMA**).

Characterization Techniques

X-ray diffraction**:** (see chapter 2.1.2 b)

Infrared spectra: (see chapter 2.1.4)

For optical absorption measurements we used a Perkin Elmer Lambda-35 UV-vis (10 mm quartz cells, (200-900 nm) spectrometer.

X-ray photoelectron spectroscopy: See chapter 2.1.1. Here evaporated 150 nm thick gold films supported on mica were used as substrates. All the samples were dispersed in distilled deionized water, and after stirring and sonication for 30 min, a small drop of the dispersion was left to dry in air on the substrate. An electron flood gun providing 0.3 eV kinetic energy electrons in combination with a gold grid about 1mm above the sample (in the case of clays and clay nanocomposites) was used to compensate for sample charging. All binding energies of GO and SWy-2/ADMA were referenced to the C 1s core level of the C-C bond set to the nominal value of 285.0 eV,[31] while in the case of smectite clay, all binding energies were referenced to the Si 2p core level of clay at 102.8 eV.[32]

For nitrogen adsorption-desorption isotherms: (see chapter 2.1.7)

Cell lines and cell culture: Leiomyosarcoma cells from Wistar rats after chemical carcinogenesis (LMS), human lung cancer cells (A549) and normal human foetal lung fibroblasts (MRC-5), were used in this study. Cells were cultured in culture medium DMEM (Dulbecco's Modified Eagles Medium) enriched with 10% foetal bovine serum (FBS), 100 IU/mL penicillin, 100 μg/mL streptomycin and 1.4 mM L- Gloutamin, at 37 ℃, with 5% CO_2. All materials were provided by Costar and PAA.[33,34]

MTT assay: Cell growth inhibition was analysed using the MTT assay shown in Figure 6.1. Briefly, 3×10^3 LMS and A549 and 5×10^3 MRC-5 cells were cultured overnight on 96-well plates and media containing different concentrations (μg/mL) of Lap and Lap/ADMA dissolved in sterilized water, were added. Control wells had only the sterilized water dose equalling amount added to the test well. After incubation for 48 h, 50 μL of MTT were added in each well from a stock solution (3 mg/mL), and incubated for additional 3 h. The yielded purple formazans were re-suspended in 200 μL of DMSO, using a multi-channel pipette. The solution was spectrophotometrically measured (540 nm, subtracted background absorbance measured at 690 nm) using a microplate spectrophotometer (Multiskan Spectrum, Therno Fisher Scientific, Waltham, USA). All the experiments were performed in triplicate.

Adsorption experiments of chlorophenols: *(a) Swelling of materials*. 10 mg of GO or GO/ADMA were swelled for 20 h in methanol under stirring in glass vials. Then, distilled deionized water was added to a

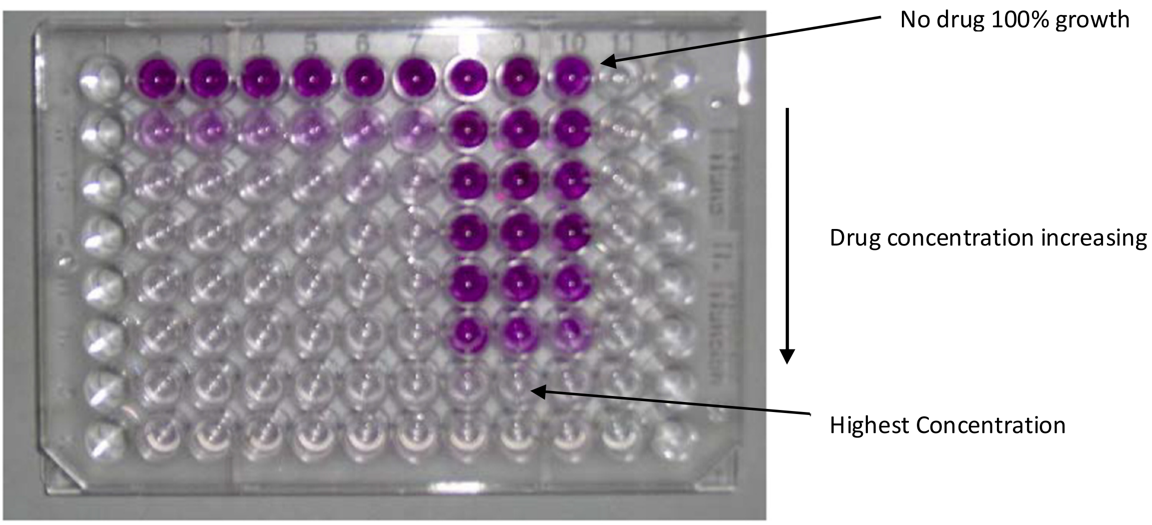

Figure 6.1 A typical 96-well plate after an MTT assay. The first row represents non treated cells (control). Increasing amounts of viable cells resulted in increased purple colouring.

final MeOH:H_2O 70:30 (v/v). 10 mg of SWy-2 or SWy-2/ADMA were swelled for 20 h in distilled deionized water (pH=4.5) under stirring in glass vials. After 20 h methanol was added so the final volume ratio MeOH: water = 70:30 (v/v). This methanol:H_2O mixture was chosen for both materials, since the goal of this experiment was to compare the performance of the clay and GO-based materials. *(b) Adsorption.* The solutes used were 2,4,6-trichlorophenol (2,4,6-TCP) pentachlorophenol (PCP) and 2,4-dichlorophenol (2,4-DCP) purchased from Aldrich (purity 97%). Stock solutions of 0.8 mM 2,4-DCP, 2,4,6-TCP and PCP were prepared in MeOH: H_2O in a ratio 70:30 v/v respectively. Adsorption experiments were performed in batch. In 10 mg of swelled dispersion, standard additions of 2,4-DCP, 2,4,6-TCP or PCP were performed at concentrations ranging between 7 μM and 70 μM. The pH of the reaction mixture was adjusted using NaOH to pH=5.3 for both 2,4-DCP and 2,4,6-TCP and 4.5 for PCP to ensure the presence of protonated form of the phenols since the pK_a of 2,4-DCP is 6.79, the pK_a of 2,4,6-TCP is 6.23 and the pK_a of PCP is 4.7.[35] Screening the experiments showed that the adsorption was completed in 90 min. Thus, our measurements were performed after 2 h of incubation to ensure adsorption equilibrium. Then the samples were centrifuged and UV-Vis spectra of supernatants were measured in quartz cuvettes 6Q, 1x1cm. Controls were run for chlorophenols solutions every 2 h with no solid material in the reaction mixture. The UV-Vis spectra were recorded using a Perkin-Elmer Lambda-35 double beam spectrometer.

6.3 Results and discussion

Since clay is a natural material, some ions are always substituted by other cationic species: typically Al^{3+} for Si^{4+} in the silica tetrahedral layers and Mg^{2+} for Al^{3+} in the alumina octahedral layer. These substitutions leave the clay platelets negatively charged and charge neutrality is achieved by (hydrated) cations (usually sodium)

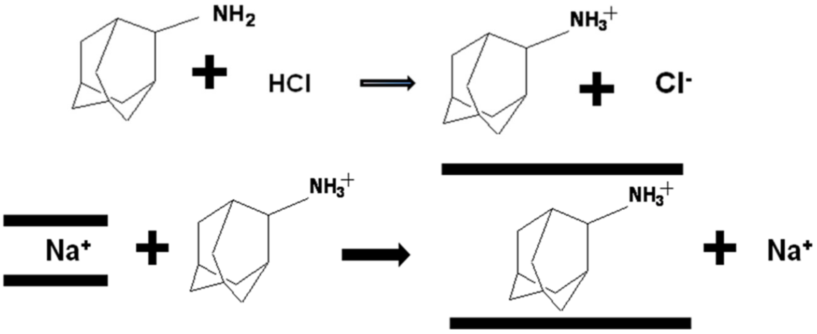

Scheme 6.1 Schematic representation of the intercalation process of adamantylamine (ADMA), after the protonation of the amine end groups, into the inter-lamellar space of the clay. The bold lines represent the negatively charged clay platelets.

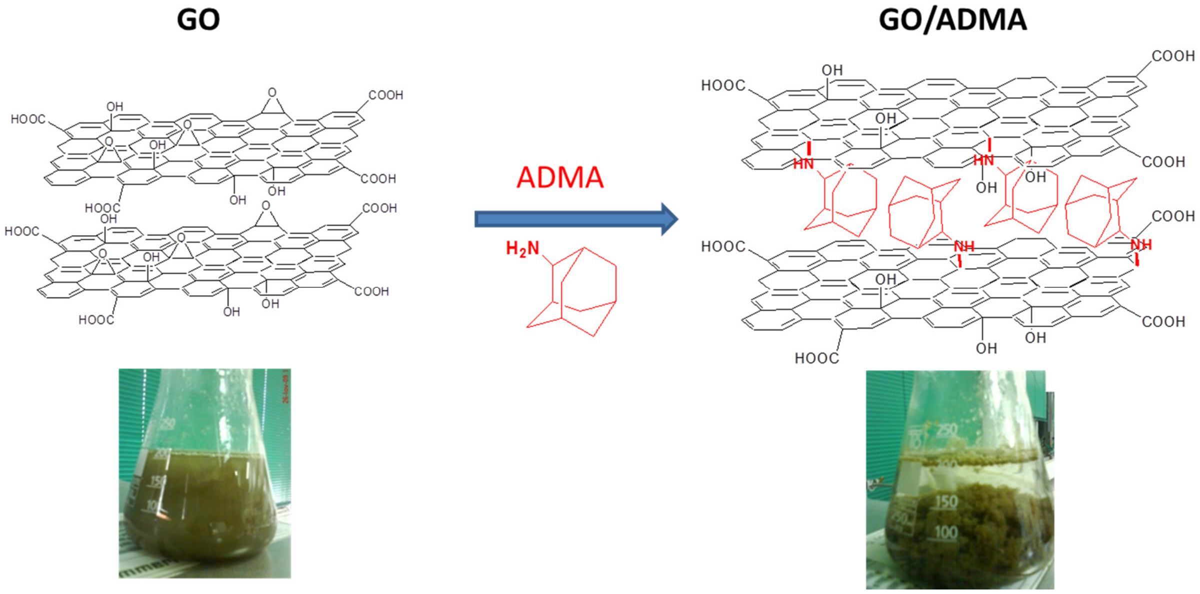

Scheme 6.2 Schematic representation of the synthesis procedure of GO/ADMA

present in the interlayer space. Synthetic clays, like LAP are artificially fabricated to have similar properties. These charge balancing cations can be substituted by organic/or inorganic cationic species and this constitutes an easy way for intercalation of water soluble cationic moieties in the interlayer galleries of clay minerals.[18a] The incorporation of adamantylamine into the interlayer space of the clay involves an initial protonation of the terminal amine groups in order to form cationic adamantane species. The intercalation of positively charged adamantane molecules, readily dispersed in aqueous solution, is achieved by ion-exchange of the charge balancing monovalent Na^+ cations with the diamondoid derivative according to the reaction (Scheme 6.1).

Contrary to clay minerals, GO does not contain charge balance cations, thus intercalation is obtained by functionalization of the GO surface and/or adsorption of molecules held between the galleries by van der Waals interactions. The oxidation and subsequent (partial) exfoliation by chemical treatment has been established first in 1962 (see also Chapter 2).[36,30] ADMA was intercalated in oxidized graphene leading to new pillared hybrid structures. A schematic representation of the reactions is presented in Scheme 6.2. A water dispersion of GO was used as the host material, while the ADMA was diluted with distilled deionized water and then added to the GO solution. An immediate flocculation of GO particles was observed, a phenomenon induced by the insertion of adamantylamine into the GO galleries through covalent bonding via the amine functionality of the adamantane derivative (see XPS data below). The interaction of primary aliphatic amines with GO is taking place mainly through chemical grafting of the amine end groups onto the GO surfaces via a ring opening reaction of the epoxy groups of GO.[29]

6.3.1 X-ray diffraction

X-Ray diffraction is one of the most powerful characterization techniques to demonstrate the success of the intercalation reaction because it allows estimating the interlayer d_{001} spacing between GO sheets. The XRD patterns of GO/ADMA, SWy-2/ADMA and Lap/ADMA are displayed in Figure 6.2. The insertion of adamantylamine between the aluminosilicate and graphene oxide layers causes an increase of the

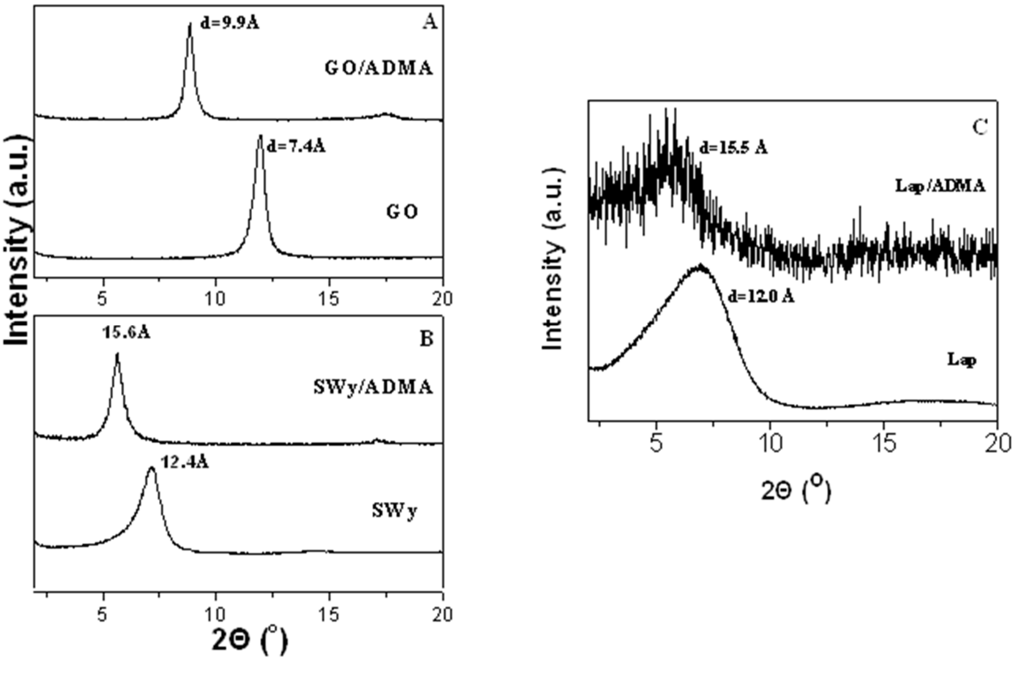

Figure 6.2 XRD patterns of the hybrid pillared systems (A) SWy-2/ADMA, (B) GO/ADMA and (C) Lap/ADMA in comparison with pristine layered matrices (Lap, SWy-2 and GO)

interlayer distance. More specifically, for intercalation in SWy-2 clay (Figure 6.2 B), the basal d_{001}-spacing, which is 12.4±0.3 Å in the initial montmorillonite clay, becomes 15.6±0.4 Å after the modification, which corresponds to an interlayer separation of 15.6-9.6 = 6 Å, where 9.6 Å represents the thickness of a clay layer.[37] The results for laponite (Figure 6.2 C) are similar to those for montmorillonite: the basal d_{001}-spacing, which is 12.0±0.3 Å in the initial laponite clay, becomes 15.5±0.4 Å after the intercalation of adamantylamine; this corresponds to an interlayer separation of 15.5-9.6 = 5.9 Å. This value is in accordance with the size of the adamantylamine molecule if we assume an orientation perpendicular to that of the aluminosilicate platelets.[38] In the case of GO/ADMA (Figure 6.2 A), the 001 diffraction peak centred at ~12° in pristine GO shifts to lower angles corresponding to a d_{001}-spacing of 10.4±0.3 Å. Taking into account the thickness of a graphene oxide layer (6.1±0.2 Å),[39] this corresponds to an interlayer separation of $\Delta = 10.4 - 6.1 = 4.3$ Å occupied by the ADMA pillaring moieties. This value implies that the flexible amine groups of the adamantane must adopt an inclined orientation in the GO galleries.[40]

6.3.2 FTIR spectroscopy

An additional tool for the characterization of hybrid pillared materials is FTIR spectroscopy, which can confirm the successful incorporation of the adamantane derivative in the layered matrices. Figure 6.3 displays the FTIR spectra of SWy-2 and GO before and after the pillaring process. In the case of SWy-2/ADMA, the spectrum displays all the characteristic bands arising from aluminosilicate clay mineral, at 465 cm^{-1} (Si-O-Si and Si-O bending vibrations), 524 cm^{-1} (Si-O-Si bending), 778 cm^{-1} (Si-O deformation), 797 cm^{-1} (Si-O and Si-O-Al stretching), 884 cm^{-1} (Al-Fe-OH deformation), 918 cm^{-1} (Al-

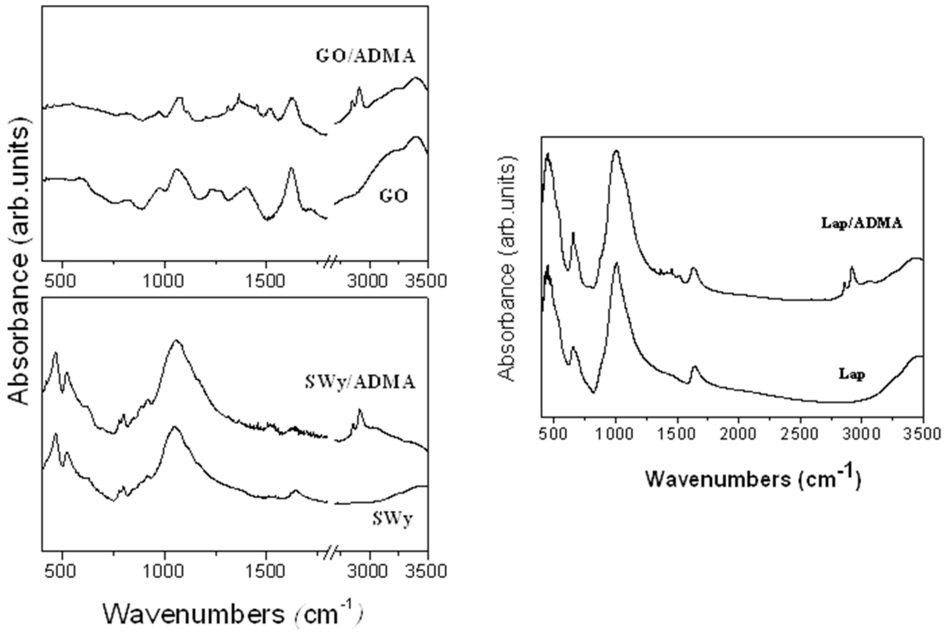

Figure 6.3 FTIR spectra of the hybrid pillared systems SWy-2/ADMA, GO/ADMA (left) and Lap/ADMA (right); the FTIR spectra of pristine SWy-2 and GO are plotted for comparison.

OH-Al bending), 1047 cm^{-1} (Si-O-Si stretching) and 1639 cm^{-1} (H_2O bending). In addition, the presence of adamantylamine in the hybrid material is revealed by the bands centred at 2863 cm^{-1} and 2921 cm^{-1} corresponding to stretching vibrations of C-H, as well as from the peak at 1520 cm^{-1}, due to N-H vibrations. Analogously the FTIR spectrum of Lap/ADMA after the pillaring process displays not only the characteristic bands arising from the aluminosilicate clay but also a peak at approximately 1515 cm^{-1}, due to N-H vibrations testifying the intercalation of the adamantylamine moieties in between the clay sheets. Moreover, in the case of GO/ADMA the same peaks originating from the ADMA molecules are also present in the spectrum, together with the characteristic bands arising from pristine GO at 3410 cm^{-1} (hydroxyl stretching vibration of C-OH groups), 1621 cm^{-1} (C=O stretching vibrations of the -COOH groups), 1396 cm^{-1} (assigned to the O-H deformations of the C-OH groups) and 1062 cm^{-1} (C-O stretching vibrations).[41]

6.3.3 X-ray photoelectron spectroscopy

To verify the presence and integrity of the adamantylamine cycloalkanes within the layered nanostructures, as well as to analyse the chemical environment of ADMA, we employed X-ray photoelectron spectroscopy (XPS). The C 1s XPS spectrum of GO/ADMA (Figure 6.4) reveals the characteristic contribution of C-C/C-H bonds of the GO lattice and adamantane cyclohexane ring centred at a binding energy of 285.0 eV, which amount to 54.3% of the total carbon 1s intensity. The peak at 286.3 eV is due to C-O/C-N bonds and represents 23.8 % of the total carbon 1s intensity. Finally two components at 287.9 eV and 289.6 eV are attributed to carbonyl (C=O) and carboxyl (O-C=O) groups, respectively, which are created on the basal planes and at the boarders of the carbon sheets after the acid treatment.

The N 1s core level region of the XPS spectrum of GO/ADMA, plotted in Figure 6.5, exhibits two main peaks, located at 399.8 eV and 401.5 eV. They arise from the amine end groups of ADMA chemically grafted to the epoxy groups of GO,[42] and from protonated amines ionically bonded to the carboxylic acid anionic groups of GO, respectively. In fact, the corresponding spectrum of pristine ADMA, plotted in the same figure for comparison, is deconvoluted into two photoelectron peaks, one at 400.1 eV, which is attributed to the amine groups of the organic molecule[43] and a second one at 401.5 eV due to protonated amines. After intercalation no amine peak is found but a contribution typical of C-N-C bonds at 399.8 eV, indicating the successful functionalization of ADMA in the GO galleries, while the protonated groups remain at the same binding energy value.

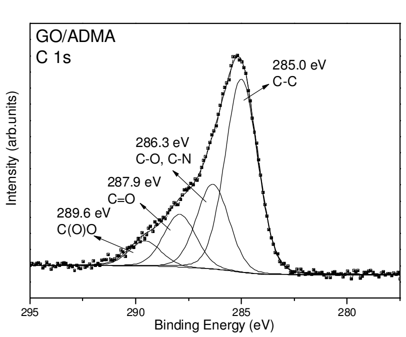

Figure 6.4 C 1s core level region of the X-ray photoelectron spectra of GO/ADMA

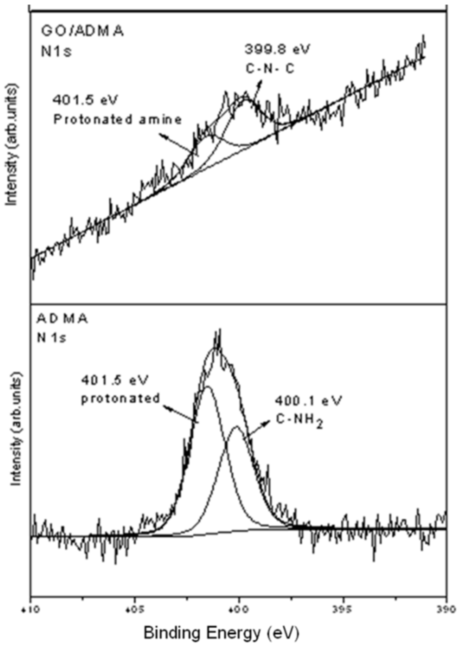

Figure 6.5 Comparison of the N 1s core level region of the XPS spectra of adamantylamine and of the GO/ADMA hybrid

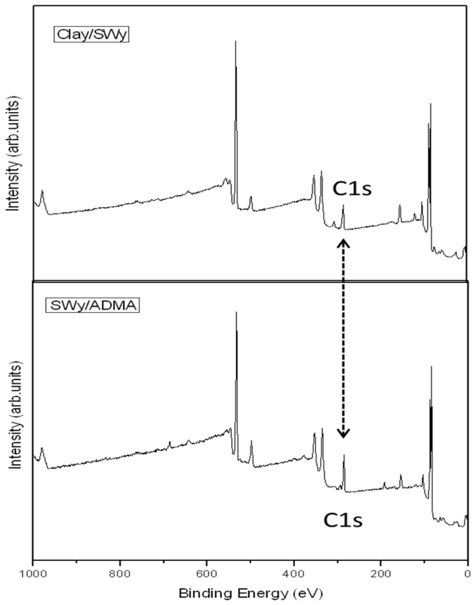

Figure 6.6 XPS survey spectra of montmorillonite clay before (SWy-2) and after intercalation of adamantylamine (SWy-2/ADMA).

XPS measurements were also carried out for the SWy-2/ADMA hybrid system. The survey spectra of SWy-2 and SWy-2/ADMA are shown in Figure 6.6. Characteristic photoelectron and Auger peaks of O, Si, Al, and Mg are clearly distinguishable in the spectrum of pristine montmorillonite clay. A small carbon peak appears, mainly due to contamination from adventitious carbon species always present on the outer surface of air exposed materials, but also due to soil organic matter present in natural clay minerals. After the insertion of ADMA a pronounced increase in the intensity of the carbon signal is observed and confirms the presence of adamantylamine inside the clay galleries. Quantitatively, the incorporation of ADMA molecules in the clay is determined by measuring the ratio between the carbon 1s and the silicon 2p core level photoemission intensities before and after the intercalation process, as shown in Figure 6.7. The C 1s / Si 2p intensity ratio increased from 1.42±0.06 before the incorporation of adamantylamine to 2.79±0.11 after the introduction of ADMA. The presence of the amine terminal groups on adamantane is deduced from the N 1s photoelectron spectrum, presented in Figure 6.8.

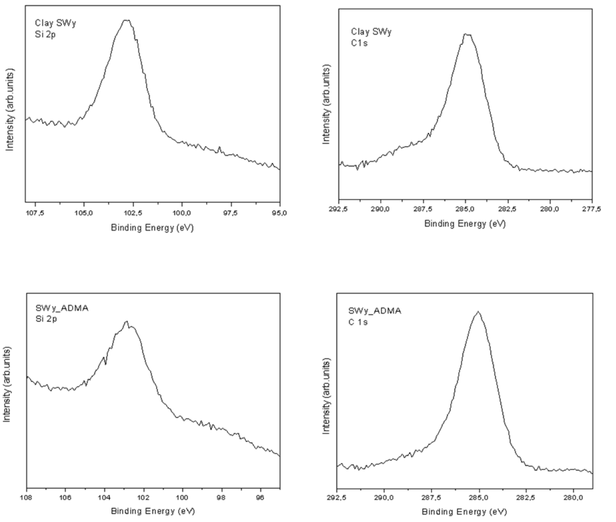

Ratio C/Si 1.42 ±0.06

Ratio C/Si 2.79 ±0.11

Figure 6.7 C 1*s* and Si 2*p* core level regions of the X-ray photoelectron spectra of SWy -2 and SWy-2/ADMA. The calculated intensity ratio C 1s/Si 2p is indicated.

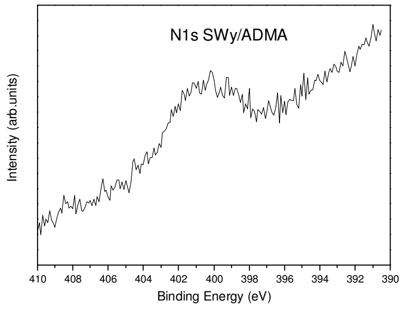

Figure 6.8 N 1s core level region of the X-ray photoelectron spectrum of SWy-2/ADMA

6.3.4 Thermogravimetric and differential thermal analysis

Thermogravimetric (TGA) and differential thermal analysis (DTA) of pure graphite, graphene oxide and the GO/ADMA are displayed in Figure 6.9. The DTA curve of graphite exhibits one exothermic peak at 700 ℃ due to the combustion of carbon layers, while in the case of graphene oxide we

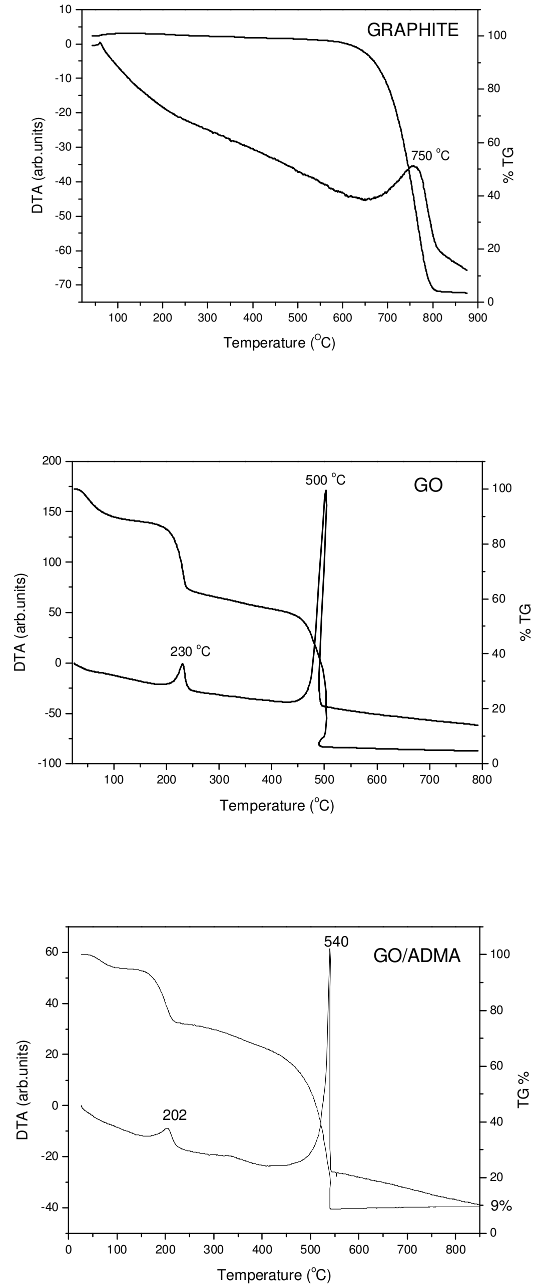

Figure 6.9 Thermogravimetric (TGA) and differential thermal analysis (DTA) of pure graphite, of graphene oxide and of the GO/ADMA hybrid.

have the presence of two exothermic peaks centred at 250 ℃ and 500 ℃, which correspond to a 30% and a 50% weight loss, respectively. These peaks are attributed to the removal of oxygen containing functional groups, created after the acid treatment of graphite (first peak), and to carbon combustion

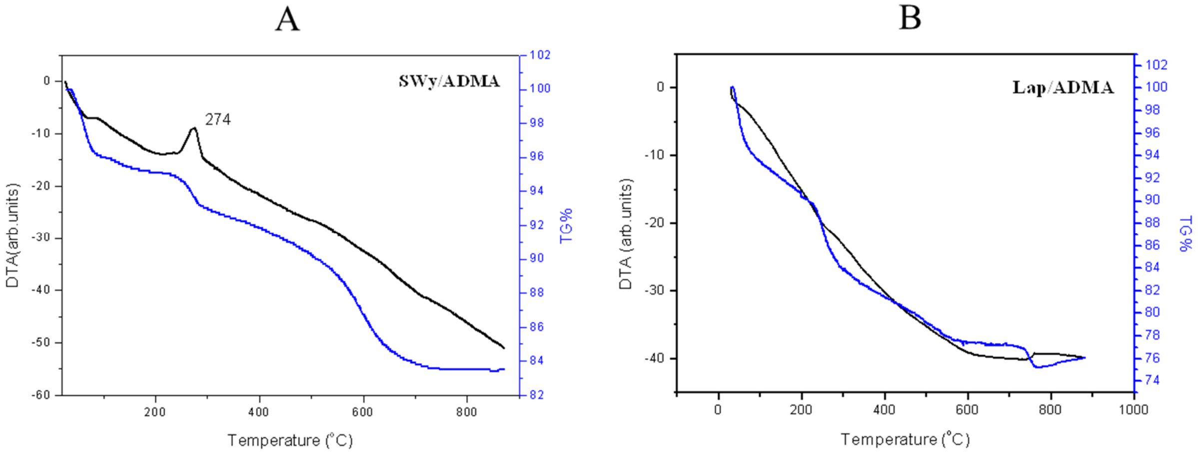

Figure 6.10 (A) DTA and TGA curves of SWy-2/ADMA and (B) DTA and TGA curves of Lap/ADMA

(second peak).[44] In the case of GO/ADMA, the DTA curve exhibits one exothermic peak at ~201 °C with 30% weight loss, ascribed to the removal of oxygen functional groups, while the combustion of the carbon layers appears at 540 ℃. The weight loss observed in the temperature range 280–400 °C originates from the combustion of the amino groups of adamantylamine and represents ~8% of the total mass of the material.

In the thermogravimetric analysis of the hybrid system SWy-2/ADMA shown in Figure 6.10 A, we observe at 100 °C a weight loss of about 5%, attributed to the removal of physisorbed water. Above 100 °C and up to 400 °C a weight loss (with the exothermic peak centred at 274 ℃) in the range of 3-4% occurs, which is due to the calcination of the amino groups of adamantylamine. Moreover, between 400 ℃ and 700 ℃ another weight loss 8.5% is observed, which is due to combustion of the cycloalkane of adamantylamine. Based on the latter two weight losses, we estimate that the amount of intercalated adamantylamine in the hybrid material corresponds to ~12,5 wt % of the total mass. Thermogravimetric (TGA) and differential thermal analysis (DTA) of Lap/ADMA are displayed in Figure 6.10 B. In the thermogravimetric analysis of the hybrid system we observe at 100 °C a weight loss of about 6.5%, attributed to the removal of physisorbed water. Above 100 °C and up to 400 °C a weight loss of 12 % which is due to the calcination of the amino groups of adamantylamine. Finally, between 400 ℃ and 750 ℃ another weight loss of 8 % is observed, which is due to combustion of the cycloalkane of adamantylamine. The two observed thermogravimetric weight losses between that range (400 ℃ and 750 ℃) is due to the different orientation of the adamantylamine molecules in the interlayer space of the laponite clay.

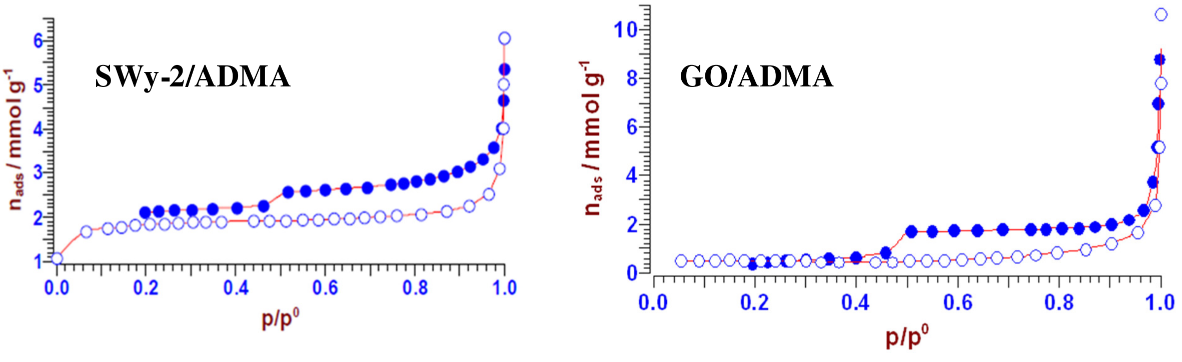

Figure 6.11 N_2 adsorption (filled circles)-desorption (open circles) isotherms from (left) montmorillonite clay intercalated with adamantylamine (SWy-2/ADMA) and (right) graphite oxide intercalated with adamantylamine (GO/ADMA) (measured according to the BET analysis).

Table 6.1 Specific surface area values for graphite oxide (GO), GO intercalated with adamantylamine (GO/ADMA), montmorillonite clay (SWy-2) and montmorillonite clay intercalated with adamantylamine (SWy-2/ADMA)

	Specific Surface Area (S_{BET}) (m^2g^{-1})
GO	9
GO/ADMA	37
SWy-2	65
SWy-2/ADMA	135

6.3.5 Nitrogen adsorption-desorption measurements

Nitrogen adsorption-desorption measurements (at 77 K) were performed on both hybrid materials in order to determine the porosity in each case. The adsorption-desorption isotherms are plotted in Figure 6.11 and Table 6.1 shows the specific-surface-areas (S_{BET}) obtained from these curves through BET analysis (as explained in appendix C of this thesis) for the intercalated hybrid nanostructures GO/ADMA and SWy-2/ADMA, as well as the S_{BET} values calculated for pristine GO and SWy-2 (isotherms not reported here). The specific surface area of pure GO (~9 m^2 g^{-1}) is small indicating that N_2 can only adsorb on the external surfaces of GO, while the interlayer space of GO is inaccessible to the gas. The extremely low S_{BET} value points to a "paraffin-like" behaviour of the material,[45] which is also evident from the appearance of the material. However, for the GO/ADMA hybrid the specific surface area is four times higher (37 m^2 g^{-1}) than for GO, supporting the hypothesis that adamantylamine acts as pillaring species. In fact, this result implies that nitrogen adsorbs not only on the external surface but in the pores between the adamantine pillars. The specific surface area was even larger (135 m^2 g^{-1}) in the case of SWy-2/ADMA.

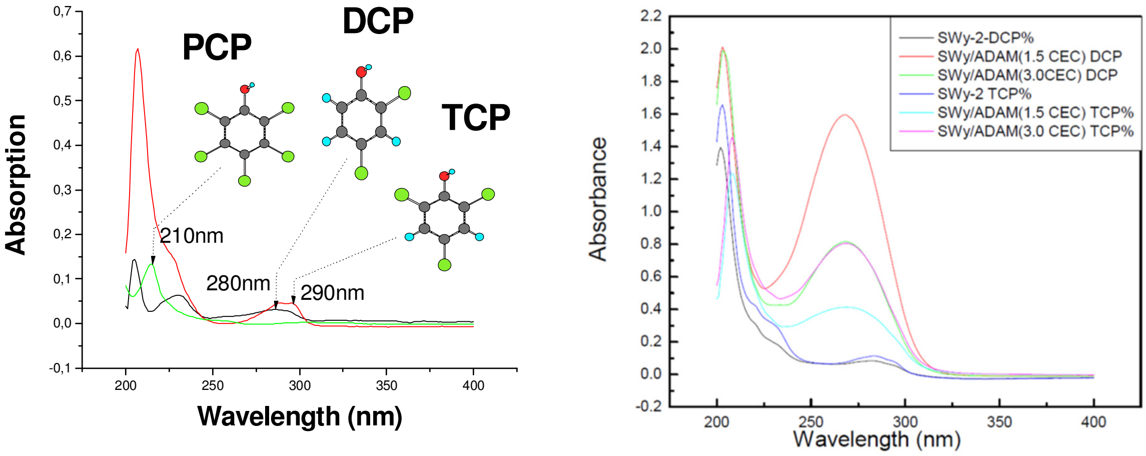

Figure 6.12 Left panel: UV-Vis spectra of 20 μM 2.4.6-trichlorophenol (TCP, red curve), 2.4-dichlorophenol (DCP, black curve) and pentachlorophenol (PCP, green curve) in MetOH:H_2O 70:30 v/v. The arrows mark the peaks used for quantitative analysis of adsorption. **Right panel:** UV-vis spectra of 2.4.6-trichlorophenol (TCP) and 2.4-dichlorophenol (DCP) adsorbed on SWy-2/ ADAM prepared with 1.5 and 3.0 CEC).

6.3.6 Suitability of the SW-2/ADMA hybrid material for environmental remediation: adsorption of phenolic compounds†

a. SWy-2/ADMA

In view of possible applications for these new hybrid materials, we tested whether SWy-2/ADMA is capable of adsorbing organic pollutants (phenol derivatives) from solution. For these experiments SWy-2/ADMA hybrids were prepared with an amount of adamantylamine equal to 1.5 and 3.0 times the CEC of the clay.

The left panel of Figure 6.12 presents UV-Vis spectra for 2,4,6-TCP and 2,4-DCP and PCP. Quantification of the chlorophenols was done using the peak at 280 nm for 2,4-DCP, 290 nm for 2,4,6-TCP and 210 nm for PCP marked by arrows. By comparing these UV-Vis spectra for solutions with known phenol concentrations with the corresponding spectra recorded after adsorption on pristine SWy-2 and on the two types of SWy-2/ADMA hybrids – see examples in the right panel of Figure 6.12-, we could calculate the concentration of chlorophenol adsorbed in each case and compile the adsorption isotherms.

In Figure 6.13 the adsorption isotherms of 2.4.6-trichlorophenol (TCP), 2.4-dichlorophenol (DCP) and pentachlorophenol (PCP), in the starting material (SWy-2) and in two types of SWY-2/ADMA are shown. The adsorption isotherms show a plateau at increased chlorophenol:clay ratios which defines the maximum adsorption capacity of the material, listed in Table 6.2. As evident from the isotherms, TCP and DCP phenols adsorb in the interlayer space of the pristine clay as well as in the pores of SWy-2/ADMA while the adsorption of PCP remained zero in all cases. From Table 6.2 we notice that the adsorption of the various phenols followed a consistent trend for all materials:

DCP>TCP>PCP.

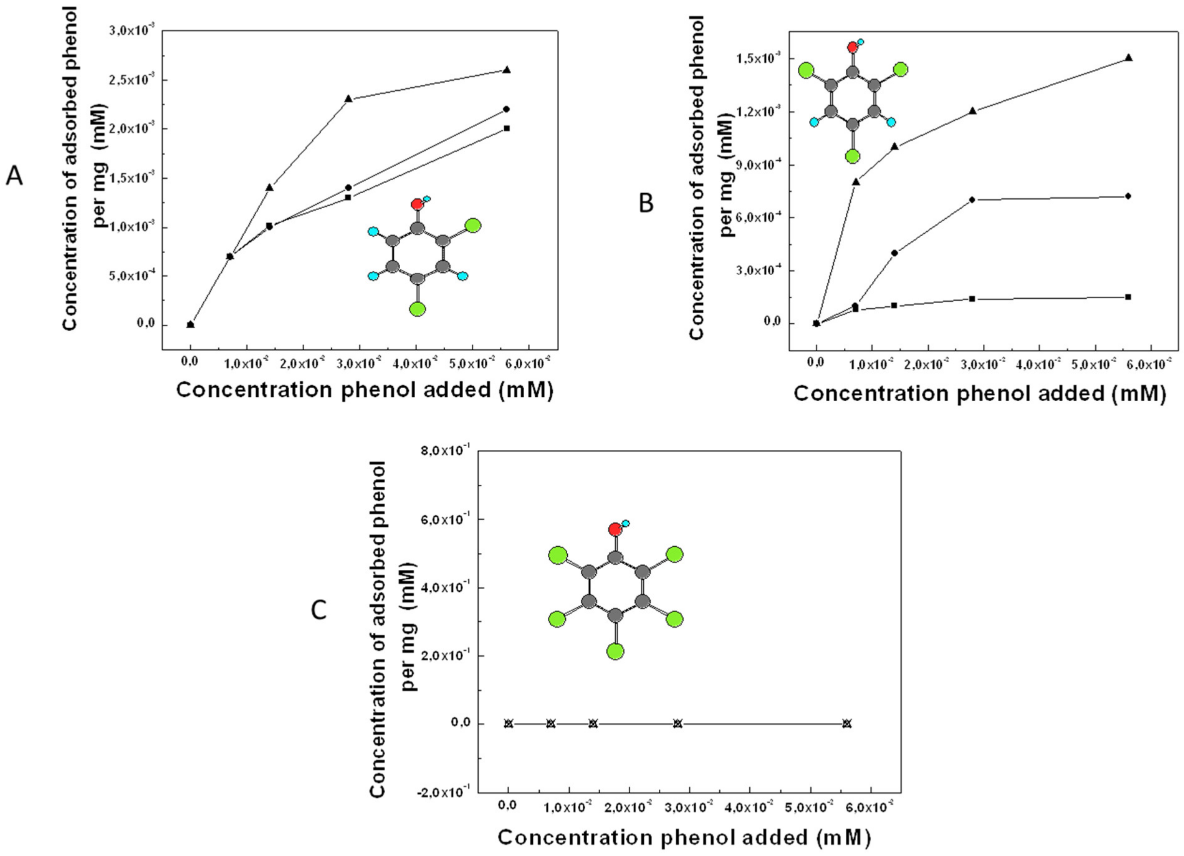

Figure 6.13 (A) Langmuir adsorption isotherms of 2,4-DCP on pristine SWy-2 clay (■), SWy-2/ADMA prepared with 1.5 CEC and (●)SWy-2/ADMA prepared with 3.0 CEC (▲), (B) Adsorption isotherms of 2,4,6-TCP on pristine SWy-2 clay (□), SWy-2/ADMA prepared with 1.5 CEC (○) and SWy-2/ADMA prepared with 3.0 CEC (△), (C) Adsorption isotherms of PCP on pristine SWy-2 clay (☒), SWy-2/ADMA prepared with 1.5 CEC (⊗), and SWy-2/ADMA prepared with 3.0 CEC (⨻).

Table 6.2 Maximum adsorption capacity for chlorophenol [mM per mg] of montmorillonite clay and graphene oxide and of their derivatives SWy-2/ADMA and GO/ADMA.

Chlorophenol	SWy-2	SWy-2/ADMA prepared with 1.5 CEC of adamantylamine	SWy-2/ADMA prepared with 3.0 CEC of adamantylamine	GO	GO/ADMA
2,4-DCP	20×10^{-4}	22×10^{-4}	27×10^{-4}	0	32×10^{-4}
2,4,6-TCP	2×10^{-4}	7×10^{-4}	15×10^{-4}	0	1.3×10^{-4}
PCP	0	0	0	0	0

The uptake of DCP was significantly higher than for TCP. Strikingly the adsorption of PCP remained zero in all cases; the adamantane-modified clays showed improved adsorption capacity *vs.* the unmodified ones. For example the uptake of DCP by the pristine SWy-2 clay was 19 μM/mg but improved to 22 μM/mg for SWy-2/ADMA prepared with 1.5 CEC of adamantylamine and to 27 μM/mg for SWy-2/ADMA prepared with 3.0 CEC of adamantylamine.

In the case of DCP, we observed initially the same adsorption behaviour for the pristine clay and for SWy-2/ADMA prepared with 1.5 CEC of adamantylamine (10^{-2} mM DPC), but as the amount of phenol increases, the intercalated clay is a better absorber than the pristine one. This trend reverts when the concentration of adamantylamine in the hybrid is increased: SWy-2/ADMA prepared with 3.0 CEC of adamantylamine adsorbs significantly higher amounts of DCP for all concentrations of the added phenol and shows a 40% enhanced uptake compared to the pristine clay at the highest phenol concentrations.

For TCP phenol the two hybrids with 1.5 CEC and 3.0 CEC of adamantylamine, respectively both present a higher adsorption than the starting clay. It is obvious that the amount of adsorbed phenol scales with the amount of adamantylamine used in the preparation of the hybrid since the SWy-2/ADMA prepared with 3.0 CEC of adamantylamine displays a 50% higher adsorption than the hybrid material synthesized with 1.5 CEC of adamantylamine.

Comparing the three types of chlorophenols we conclude that the intercalated clays possess higher capability of adsorption for DCP than for TCP while the adsorption of PCP is almost negligible. This difference could be explained by the molecular size of the three phenols: 2.4.6-trichlorophenol and pentachlorophenol are larger so they might block the pores of the pillared hybrid and thereby hamper the adsorption of further molecules (see physical model below).

b. GO-ADMA

In parallel with SWy-2/ADMA we studied the adsorption of organic pollutants (phenol derivatives) from solution on GO/ADMA. To determine the rate of the adsorption also in this case the UV-vis spectra of the adsorptions of DCP, TCP and PCP on graphene oxide and graphene oxide intercalated with adamantylamine were measured (see experimental section and above). By comparing these curves with characteristic curve for solutions with known phenol concentrations, we can calculate the concentration of chlorophenol adsorbed in each case in GO-ADMA hybrid.

Figure 6.14 presented the resulting adsorption isotherms of 2.4.6-trichlorophenol (TCP), 2.4-dichlorophenol (DCP) and pentachlorophenol (PCP) by modified graphene oxide with adamantane in contrast with the unmodified graphene oxide. As shown by the experimental results, the initial, unmodified graphite oxide layers appear to have no adsorption capacity, whereas, the modification of graphite oxide results to the adsorption of chlorophenols. GO-adamantane appears to adsorb selectively DCP while TCP or PCP was minimal. It is to be noted that 2.4-DCP is removed in a higher amounts in comparison to 2.4.6-TCP. This can be explained by the molecular size of two phenols. Thus the data in Figure 6.14 reveal that GO/ADMA can ace as highly-selective sorbent of DCP. In Table 6.2 the maximum adsorption capacity for DCP was 32 μM/mg for GO/ADMA, which was significantly higher than that for SWy-2/ADMA (prepared with 3.0 CEC).

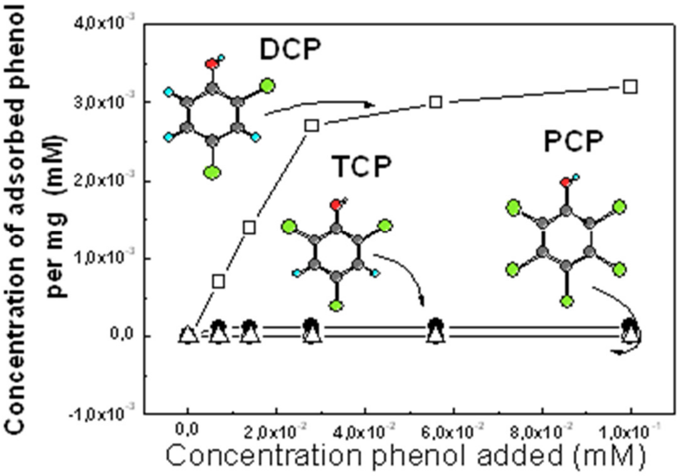

Figure 6.14 Langmuir adsorption isotherms of 2,4-DCP on pristine GO (■) and on GO/ADMA (□); of 2,4,6-TCP on pristine GO (○) and on GO/ADMA (●); of PCP on pristine GO (△) and on GO/ADMA(▲).

Table 6.3 Molecular volume (Å^3) Chemical structure and space filling surface of different phenols (calculated with ChemDraw7.0)

	Molecular volume (Å³)	**Chemical structure**	**Space filling surface**
Pentachlorophenol	83.21	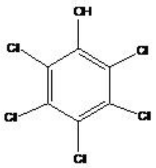	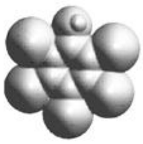
2,4,6-Trichlorophenol	67.92	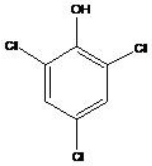	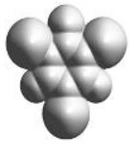
2,4-Dichlorophenol	60.23	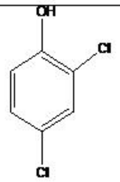	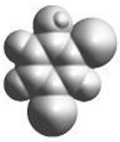
Adamantane	79.34	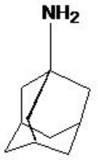	

c. Physical Model

The observed differences in the uptake of PCP, 2,4,6-TCP and 2,4-DCP can be attributed to the difference in the molecular size of the phenols. Comparing the adsorptive capacity of two chlorophenols by modified clays, 2,4-DCP appears to be adsorbed much better than 2,4,6-TCP. The molecular volume of 2.4-DCP is 60.3 $Å^3$, whereas that of 2,4,6-TCP is 67,9 $Å^3$ and the one of PCP 83,2 $Å^3$ (Table 6.3). Thus the more bulky PCP is adsorbed less by the intercalated clays and not at all by GO/ADMA, while DCP seems to be able to penetrate in the interlamellar space of both SWy-2/ADMA and GO/ADMA. This can be explained if we take into account the change in the interlamellar space as depicted in Figure 6.2. The interlayer distance of the pristine SWy-2 clay is 2.8±0.3 Å and becomes 6±0.4 Å in SWy-2/ADMA. On the other hand, the interlayer distance of pristine graphite oxide is 1.3 Å, which is much narrower than that of the initial SWy-2 clay, and becomes 4.3 Å after modification with adamantylamine. Despite this increase in the GO-adamantane only DCP can be accommodated and this results in the observation for significant adsorption of DCP in contrast to TCP and PCP.

6.3.7 Cytotoxicity of Lap/ADMA and GO/ADMA[‡‡]

Another possible future application of the intercalated layered structures is their use as potent cytotoxic agents. We chose laponite and intercalated laponite for these tests because, as mentioned in the introduction, this synthetic clay with small platelet size is frequently used in biomedical applications. Parallel to Lap and Lap/ADMA we also test GO and GO/ADMA for cytotoxic behavior. The IC50 (μg/mL) values for cell proliferation (MTT assay) after 48 h of treatment with ADMA, Lap and Lap/ADMA for LMS cells were 79±7.2 μg/mL, 132±19.1 and 39±9.3μg/mL respectively (Table 6.4), whereas IC50 (μg/mL) values for A549 cells were 122±13.7, 205±20.7 μg/mLand 91±5.0 μg/mL, respectively (Table 6.4). It is noteworthy to mention that Lap and Lap/ADMA exhibited cytotoxic activity on MRC-5 cells in concentration higher than 200 μg/mL. The IC50 (μg/mL) values for cell proliferation (MTT assay) after 48 h of treatment with ADMA, GO and GO/ADMA for LMS cells were 79±7.2, 295±57.7 and 154±31.8 respectively (Table 6.4), whereas IC50 (μg/mL) values for A549 cells were 122±13.7, 259±48 μg/mL and 192±27.6 0 μg/mL, respectively (Table 6.4). Figure 6.15 represents the diagram of IC50 values of ADMA, Lap and Lap/ADMA on LMS, A459 and MRC-5 cells while Figure 6.16 displays the diagram of IC50 values of ADMA,, GO and GO/ADMA respectively. What we observe is that Lap, Lap/ADMA, GO, GO/ADAM and ADMA exhibited antiproliferative activity against LMS and A549 cells. There was no cytotoxic effect during control experiment, using sterilized water. All substances, except ADMA, presented significantly lower toxicity on MRC-5 cells and among all, Lap/ADMA is the most cytotoxic agent against cancer cell lines.There is a statistically significant difference between all cell lines treated with ADMA and Lap/ADMA compared to the Laponite clay ($p<0.05$).In addition, Lap/ADMA showed a significant higher cytotoxicity ($p<0.05$) compared to that of Lap (starting material) and ADMA against both LMS and A459 cells (Figure 6.15). Accordingly there is a statistically significant difference between all cell lines treated with ADMA and GO/ADMA compared to the GO ($p<0.05$). In this case GO/ADMA showed slight lower cytotoxicity ($p<0.05$) compared

---

[‡‡] Cytotoxicity tests performed by I. Verginadis, University of Ioannina.

[†] Enviromental remediation tests performed by E. Serestatidou, University of Ioannina.

to that of ADMA and significantly higher compared to pure GO (Figure 6.16). On the other hand MRC-5 cells stayed unaffected in the case of GO/ADMA compare to GO, whereas for ADMA MRC-5 cells importantly reduced compared with GO.

Table 6.4 IC50 values of ADAM, LAP, LAP/ADMA, GO and GO/ADMA against LMS, A549 and MRC-5

IC50 (μg/L)	*LMS*	*A549*	*MRC-5*
ADMA	79 ± 7.2	122 ± 13.7	149 ± 38.6
LAP	132 ± 19.1	205 ± 20.7	288 ± 41.8
LAP/ADMA	39 ± 9.3	91 ± 5.0	307 ± 32.2
GO	295 ± 57.7	259 ± 48	480 ± 39.6
GO/ADMA	154 ± 31.8	192 ± 27.6	425 ± 52.6

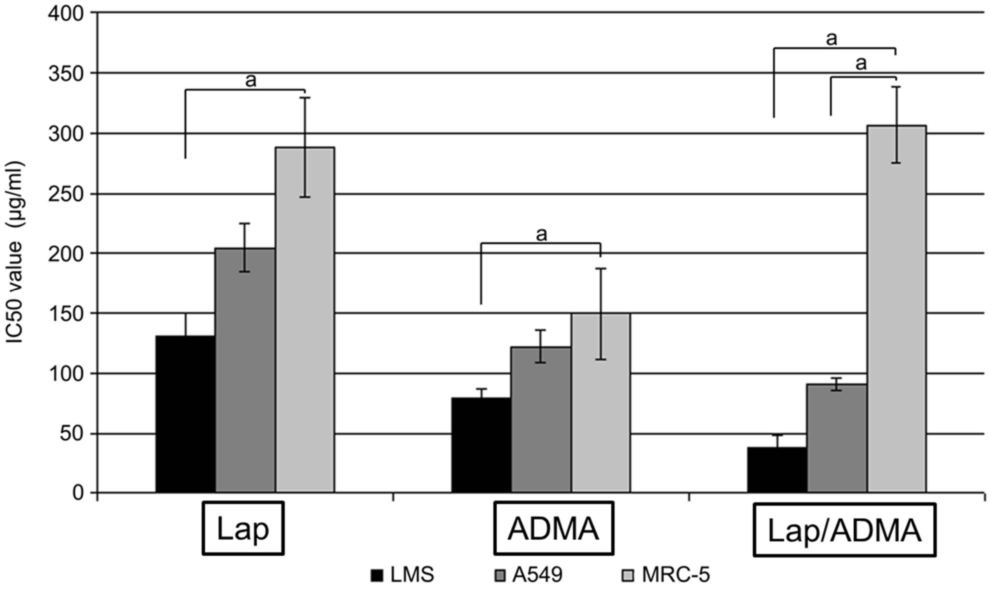

Figure 6.15 IC50 (μg/mL) values of Lap and Lap/ADMA on LMS, A549 and MRC-5 cells, compared with laponite clay (Lap). Comparison of the IC50 (μg/mL) values for Lap, ADMA and Lap/ADMA on LMS, A549 and MRC-5 cells. A statistically significant difference compared to MRC-5 cell line ($p<0.05$) between ADMA and Lap/ADMA;statistically significant difference between groups (Lap,ADMA and Lap/ADMA)

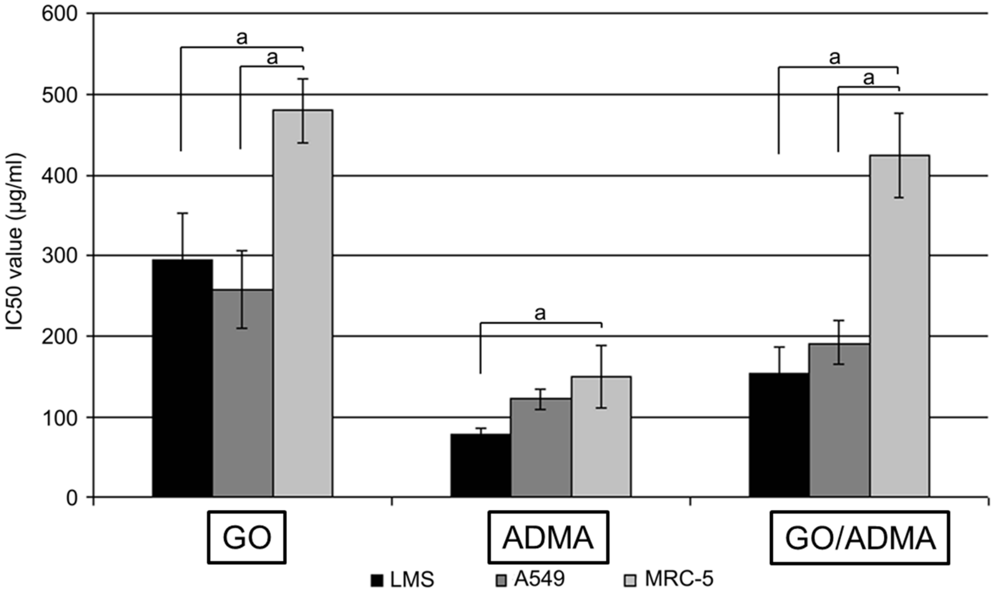

Figure 6.16 IC50 (µg/mL) values of ADMA and GO/ADMA on LMS, A549 and MRC-5 cells, compared with graphite oxide (GO). Comparison of the IC50 (µg/mL) values for GO, ADMA and GO/ADMA on LMS, A549 and MRC-5 cells. A statistically significant difference compared to MRC-5 cell line ($p<0.05$) between ADMA and GO/ADMA; statistically significant difference between groups GO, ADMA and GO/ADMA.

6.4 Conclusions

We successfully achieved the intercalation of adamantylamine into the interlayer space of layered structures. The host materials that we used in our study were graphite oxide, montmorillonite and laponite clay. X-ray diffraction measurements demonstrate the successful intercalation of adamantylamine into all three host matrixes, while X-ray photoelectron spectroscopy, FTIR spectroscopy as well as thermogravimetric and differential thermal analysis illustrate the type of interactions between the host materials and the intercalated molecules as well as the intercalation yield. Porosimetry measurements quantified the specific surface area for each of the hybrid nanostructures. UV-vis spectra demonstrated that the hybrid material obtained by intercalation of adamantylamine into montmorillonite clay has an excellent potential for environmental remediation because of it is capable of adsorbing significant quantities of organic pollutants. Finally the hybrid nanostructures obtained by intercalation of adamantylamine into laponite clay were investigated for its cytotoxicity against cancer cell lines and one normal cell line. The findings revealed that Lap and Lap/ADMA exhibited antiproliferative activity against LMS and A549 cells, while found to be significantly less toxic on MRC-5 cells. We established a controllable and reproducible method for the synthesis of multi-functional material capable for diverse applications in the fields of energy storage, environmental and biomedical applications.

References

[1] Ali Mansoori, G.; *Adv. Chem. Phys.* John Wiley & Sons, Inc.: **2008**; pp 207-258.

[2] (a) McIntosh, G. C.; Yoon, M.; Berber, S.; Tománek, D. Phys. Rev. B - 2004, 70, 045401; (b) Merkle, R. C. Nanotechnology 2000, 11, 89-99; (c) Rawls, R. *Chem. Engin. News* **2002**, 80, 13.

[3] Zones, S. I.; Nakagawa, Y.; Lee, G. S.; Chen, C. Y.; Yuen, L. T. *Microp. Mesop. Mater.* **1998**, 21, 199-211.

[4] Meador, M. A. *Annual Review of Materials Science* **1998**, 28, 599-630.

[5] Siegel, R. W.; Hu, E.; Roco, M. C. *Nanostructure Sci. & Tech.* - A Worldwide Study. Prepared under the guidance of the IWGN, NSTC, **1999**, WTEC, Loyola Collage in Maryland.

[6] Mansoori, G. A. Principles of Nanotechnology: *Molecular Based Study of Condensed Matter in Small Systems*, World Scientific Pub. Co., New York, NY, **2005**.

[7] Mansoori, G. A.; George, T. F.; Zhang, G.; Assoufid, L., *Molecular Building Blocks for Nanotechnology*: From Diamondoids to Nanoscale Materials and Applications: Preface. 2007; Vol. 109.

[8] Ramezani, H.; Mansoori, G. A., *Diamondoids as molecular building blocks for nanotechnology.* **2007**; Vol. 109, pp 44-71.

[9] Anderzej O., *ActaBiochemical Polonica*, **2000**, 47, 1-7.

[10] J. G. Hardman, L. E. Limbird, Goodman & Gilman's: *The pharmacological basis of therapeutics.* 10th Edn. McGraw-Hill Book Co., New York, NY, **2001**.

[11] Clearfield, A. *Chem. Rev.* **1988**, 88, 125-148.

[12] Whittingham M. S.; Jacobson, A. J. Intercalation Chemistry, Academic, New York, 1982.

[13] Vaccari, A. *Appl. Clay Sci.* **1999**, 14, 161–198.

[14] Darder, M.; López-Blanco,; M. Aranda, P.; Leroux, F.; Ruiz-Hitzky, E. *Chem. Mater.* **2005**, 17, 1969–1977.

[15] Choi, J. D.; Choi, G. M. *Sensors and Actuators, B: Chemical* **2000**, 69, 120–126.

[16] Zhang, L. L.; Zhao, S.; Tian, X. N.; Zhao, X. S. *Langmuir* **2010**, 26, 17624–17628.

[17] Khatua, B. B.; Lee, D. J.; Kim, H. Y.; Kim, J. K. *Macromolecules* **2004**, 37, 2454–2459.

[18] a) Pinnavaia, T. J. *Science* **1983**, 220, 365-371; (b) Konta, *J. Appl. Clay Sci.* **1995**, 10, 275-335; (c) Lagaly, G. *Sol. State Ionics* **1986**, 22, 43-51.

[19] (a) Ballantine, J. A. NATO-ASI Ser. C **1986**, 165, 197 –212.(b) Cornelis, A.; Laszlo, P. *NATO-ASI Ser. C* **1986**, 165, 213-228.

[20] (a) Georgakilas, V.; Gournis, D.; Petridis, D. Angewandte Chemie - International Edition 2001, 40, 4286-4288; (b) Georgakilas, V.; Gournis, D.; Bourlinos, A. B.; Karakassides, M. A.; Petridis, D. Chemistry - *A Eur. J.* **2003**, 9, 3904-3908.

[21] (a) Kloprogge, J. T. *J. Porous Mat.* **1998**, 5, 5-41; (b) Gil, A.; Gandía, L. M.; Vicente, M. A. *Catalysis Reviews – Sci. Engin.* **2000**, 42, 145-212; (c) Ma, Y.; Tong, W.; Zhou, H.; Suib, S. L. *Micropor. Mesopor. Mater.* **2000**, 37, 243-252; (d) Ohtsuka, K. *Chem. Mater.* **1997**, 9, 2039-2050; (e) Shichi, T.; Takagi, K. *J. Photoch. Photob. C: Photochemistry Reviews* **2000**, 1, 113-130.

[22] Wolfe, T. A.; Demirel, T.; Baumann, E. R. *Clays & Clay Minerals* **1985**, 33, 301–311.

[23]. Boufatit, M.; Ait-Amar, H.; Mc Whinnie, W. R. *Desalination* **2008**, 223, 366–374.

[24] (a) Lerf, A.; He, H.; Forster, M.; Klinowski, J. *J. Phys. Chem. B* **1998**, 102, 4477-4482; (b) Kovtyukhova, N. I. *Chem. Mater.* **1999**, 11, 771-778; (c) Kovtyukhova, N. I.; Martin, B. R.; Mbindyo, J. K. N.; Smith, P. A.; Razavi, B.; Mayer, T. S.; Mallouk, T. E. *J. Phys. Chem. B* **2001**, 105, 8762-8769.

[25] Jeong, H. K.; Jin, M.; Ra, E. J.; Sheem, K. Y.; Han, G. H.; Arepalli, S.; Lee, Y. H. *ACS Nano* **2010**, 4, 1162-1166.

[26] Ang, P. K.; Wang, S.; Bao, Q.; Thong, J. T. L.; Loh, K. P. *ACS Nano* **2009**, 3, 3587–3594.

[27]. Kumar, A.; Reddy, A. L. M.; Mukherjee, A.; Dubey, M.; Zhan, X.; Singh, N.; Ci, L.; Billups, W. E.; Nagurny, J.; Mital, G.; Ajayan, P. M. *ACS Nano* **2011**, 5, 4345–4349.

[28] Lv, W.; Tang, D. -M.; He, Y. -B.; You, C. -H.; Shi, Z. -Q.; Chen, X. -C.; Chen, C. -M.; Hou, P. -X.; Liu, C.; Yang, Q. -H. *ACS Nano* **2009**, 3, 3730–3736.

[29] (a) Bourlinos, A. B.; Gournis, D.; Petridis, D.; Szabo, T.; Szeri, A.; Dekany, I. *Langmuir* **2003**, 19, 6050-6055; (b) Gengler, R. Y. N.; Veligura, A.; Enotiadis, A.; Diamanti, E. K.; Gournis, D.; Jozsa, C.; van Wees, B. J.; Rudolf, P. *Small* **2010**, 6, 35-39.

[30] Staudenmaier, L. *Ber. Deut. Chem. Ges.* **1898**, 31, 1481–1487.

[31] Lotya, M.; Hernandez, Y.; King, P. J.; Smith, R. J.; Nicolosi, V.; Karlsson, L. S.; Blighe, F. M.; De, S.; Zhiming, W.; McGovern, I. T.; Duesberg, G. S.; Coleman, J. N. *J. Am. Chem. Soc.* **2009**, 131, 3611-3620.

[32] Ebina, T.; Iwasaki, T.; Chatterjee, A.; Katagiri, M.; Stucky, G. D. *J. Phys. Chem. B* **1997**, 101, 1125-1129.

[33] Evangelou, A.; Kalpouzos, G. ; Karkabounas, S.; Liasko, R.; Nonni, A.; Stefanou, D.; Kallistratos, G. *Cancer Letters* **1997**, 115, 105-111.

[34] Jacobs-Lorena, M.; Colombo, B.; Baglioni, C. *Biochimica et Biophysica Acta* (BBA) - Nucleic Acids and Protein Synthesis **1970**, 224, 174-183.

[35] Ribeiro, A.; Neves, M.H.; Almeida, M.F.; Alves, A.; Santos L. *J. Chromatography A* **2002**, 975, 267-274.

[36] (a) Brodie, B. C. *Ann. Chim. Phys.* **1860**, 59, 466–472; (b) Hummers Jr, W. S.; Offeman, R. E. *J. Am. Chem. Soc.* **1958**, 80, 1339.

[37] Theng, B. K. G. *The Chemistry of Clay Organic Reactions;* Adam Higler: London, **1974**.

[38] Tiwari, R. N.; Chang, L. *J. Appl. Phys.* **2010**, 107, 103305.

[39] Dekany, I.; Kruger-Grasser, R.; Weiss, A. *Colloid Polym. Sci.* **1998**, 276, 570-576.

[40] (a) Johnston, A. G.; Leigh, D. A.; Murphy, A.; Smart, J. P.; Deegan, M. D. *J. Am. Chem. Soc.* **1996**, 118, 10662-10663; (b) Leigh, D. A.; Murphy, A.; Smart, J. P.; Slawin, A. M. Z. *Angewandte Chemie* (International Edition in English) **1997**, 36, 728-732; (c) Seel, C.; Vögtle, F. *Chem.-Eur. J.* **2000**, 6, 21-24.

[41] Lee, D. W.; De Los Santos V, L.; Seo, J. W.; Felix, L. L.; Bustamante D, A.; Cole, J. M.; Barnes, C. H. W. *J. Phys. Chem. B* **2010**, 114, 5723-5728.

[42] Herrera-Alonso, M.;Abdala, A. A.; McAllister, M. J.;Aksay, I. A.;Prud'homme, R. K.*Langmuir* **2007**, 23, 10644–10649.

[43] Moulder, J.F.; Stickle, W. F.; Sobol, P. E.; Bohmen, K. D. *Handbook of X-ray photoelectron spectroscopy*; Perkin-Elmer Corporation: Eden Prairie, MN, **1992**.

[44] Becerril, H. A.; Mao, J.; Liu, Z.; Stoltenberg, R. M.; Bao, Z.; Chen, Y. *ACS Nano* **2008**, 2, 463-4.

[45] Vaia, R.A.; Teukolsky, R.K.; Giannelis, E.P. *Chemistry of Materials* 1994, 6, 1017-1022.

Chapter 7

A simple road for the transformation of few-layer graphene into MWNTs[§§]

In this chapter we report for the first time the direct formation of multiwall carbon nanotubes (MWNT) by ultrasonication of graphite in dimethylformamide (DMF) upon addition of ferrocene aldehyde (Fc-CHO). The tubes appear strictly at the edges of graphene layers containing Fe clusters, while similar attempts of Fc with benzyl aldehyde or other Fc derivatives do not induce formation of nanotubes. Higher amounts of Fc-CHO added to the dispersion do not increase significantly MWNT formation. Increasing the temperature reduces the amount of formation of MWNTs and shows the key role of ultra-sound induced cavitation energy. It is concluded that Fc-CHO behaves as a radical trap, reducing the concentration of radical reactive species that slice graphene into small moieties; then it localizes itself at the edges of graphene and templates the rolling up of a sheet to form a nanoscroll where it remains trapped; finally it accepts and donates unpaired electron to the graphene edges and converts the less stable scroll into a MWNT. This new methodology matches the concept that CNTs are rolled up graphene layers. The proposed mechanism is general and will lead to control the production of carbon nanostructures by simple ultrasonication treatments.

7.1 Introduction

Carbon is a most versatile element that occurs in allotropic forms as diverse as diamond, graphite, and the more recently discovered nanostructures of fullerenes, nanotubes (CNTs) and graphene.[1] The production of graphene by micromechanical cleavage[2] triggered an enormous experimental activity. Many studies demonstrated that graphene monolayers possess novel structural,[3] electrical[4] and mechanical[5] properties. Additionally, graphene can be thought as a 2D building block for carbon nanostructures of other

---

[§§] This chapter is based on: Quintana, M.; Grzelczak, M.; Spyrou, K.; Calvaresi, M.; Bals, S.; Kooi, B.; Van Tendeloo, G.; Rudolf, P.; Zerbetto, F.; Prato, M.; 2012. A Simple Road for the Transformation of Few-Layer Graphene into MWNTs. J. Am. Chem. Soc (in Press).

dimensionalities. It can be wrapped into 0D buckyballs, rolled into 1D nanotubes, or stacked into 3D graphite.[6] Recently, in situ TEM experiments demonstrated the direct transformation of flat graphene sheets into fullerene cages where etching of the edge carbon atoms promotes folding into fullerenes.[7]

CNTs are often described as rolled-up graphene layers. Matching this concept to experiments where the layers fold into CNTs is still a great challenge. To date large-scale mass CNT production has only been achieved by stochastic synthetic processes such as arc discharge,[8] laser ablation,[9] and chemical vapor deposition (CVD),[10] which require post-synthetic separation and purification treatments.[11]

During the last few years, ultrasonication has become an extremely powerful tool in the synthesis, modification and manipulation of carbon nanomaterials.[12] Under appropriate conditions, ultrasounds can functionalize CNTs, open their caps, or even fracture them completely.[13] In addition to surface modifications, carbon nanotubes can be prepared directly from organic solvents with the assistance of ultrasounds.[14-16] Graphite ultrasonication produces exfoliation in many solvents, if the free energy of mixing is negative[17] and the solvent is able to stabilize colloidal graphene.[18] It is accepted that ultrasounds break the graphitic basal structure and produce graphitic carbon fragments of variable sizes, which are later intercalated by solvent molecules.[19] To complicate matters, ultrasounds generate cavities whose implosion releases sufficient energy to form high-energy intermediates and free radicals that can drive chemical reactions.[20,21] Chemical attack reduces the size of the graphene sheets and is therefore detrimental to the physical properties that are usually sought after. Graphene dispersions produced by exfoliation of graphite in organic solvents, such as N-methyl-2-pyrrolidone (NMP) and N,N-dimethylformamide (DMF), first reached concentrations up to 0.01 mg/ml and 1 wt% monolayer.[17] Increasing sonication time, the concentration increased up to 1.2 mg/ml and 4 wt% monolayer.[22] The resulting graphene sheets presented higher concentration of defects and size reduction proportional to the sonication time. Previous studies demonstrated that sonication in DMF produces $\bullet CH_3$ and $\bullet CH_2N(CH_3)CHO$ radicals.[23] These radicals form either through reaction of the solutes with ultrasound-generated •H and •OH radicals, or by direct pyrolysis of weak bonds. In air-saturated sonicated solutions, the radicals convert to the corresponding peroxyl radicals, such as $\bullet OOCH_2N(\bullet CH_3)CHO$.[24] By virtue of their longer lifetimes and higher selectivity, the latter species are likely responsible for the damage of the graphene layers. To avoid oxidation, antioxidant molecules, for instance natural flavonoids, can be employed to effectively scavenge the free radicals generated during sonication.[24]

7.2 Results and discussion

In the present work, we sonicated graphite in DMF in the presence of ferrocene aldehyde (Fc-CHO),[25] a reducing agent that can inhibit reactions promoted by oxygen, peroxides and radicals. Ferrocene derivatives are used in the synthesis of CNTs as catalysts and carbon source.[26] Addition of Fc-CHO reduces the effect of long sonication times on graphene sheets and produces the controlled cutting of graphene sheets close to the edges. The direct formation of multiwalled carbon nanotubes (MWNT) is here observed for the first time. It occurs by sealing unstable pieces of graphene sheets of limited size.[26,27] A schematic representation of the experimental procedure is presented in Figure 7.1.

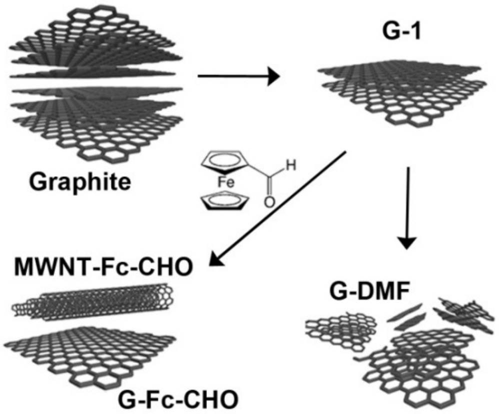

Figure 7.1 Ultrasound-assisted synthesis of carbon nanostructures.

7.2.1 Experimental section[***]

Samples were prepared using the ultrasonic tip processor GEX 750. All samples were sonicated in cycles of 30 s on / 30 s off for 1 or 3 h periods of time at the lower power of the ultrasonic tip (20%, 112.5 W). During ultrasonication, samples were kept in an ice bath to avoid overheating. As a starting material, we produced G-1: 10 mg of graphite crystals were ultrasonicated in 30 ml of DMF during 1 h in order to induce partial exfoliation of graphite. (G-1). After sonication, dispersions were left to stabilize for 5 min and then the liquid phase was removed by pipetting. Dispersions were copiously washed by filtration with fresh DMF to remove all possibly altered DMF formed during ultrasonication. Special attention was paid to keep the samples wet during the filtration processes. G-1 dispersion was used as starting material for the further experiments. As control experiment, we performed a 3 h sonication of G-1 without the addition of the antioxidant molecules (G-DMF). Sonicated DMF was always removed by filtration and the wet precipitate was re-dispersed in 10 ml of fresh DMF. Then, in a different set of experiments 40 mg of Fc-CHO were added to G-1. Dispersions were further sonicated for 3 h, under the same experimental conditions. The resulting dispersions are named D-Fc-CHO. This product was copiously washed by filtration with fresh DMF in order to remove antioxidant and by-product molecules. Samples were re-dispersed in a bath ultrasonicator (few seconds) in 10 ml of fresh DMF. Centrifugation of all dispersions was carried out at 3000 rpm during 30 min. A precipitate was observed only for G-1. Two liquid fractions, of 5 ml each, of the D-Fc-CHO dispersion were collected and analyzed. UV-vis spectroscopy was used to measure the absorption at 660 nm. The concentration of the final dispersion was calculated using the absorption coefficient α= 2460 mL/mg•m,[17] resulting in 0.031±0.003 mg/mL. The dispersed material was investigated by transmission electron microscopy (TEM), Figure 7.2a. TEM analysis of G-1 (30 micrographs) indicates the presence of graphene flakes with lateral size of typically a few μm, consisting of several layers.

[***] Synthesis by Mildred Quintana and Marek Grzelczak.

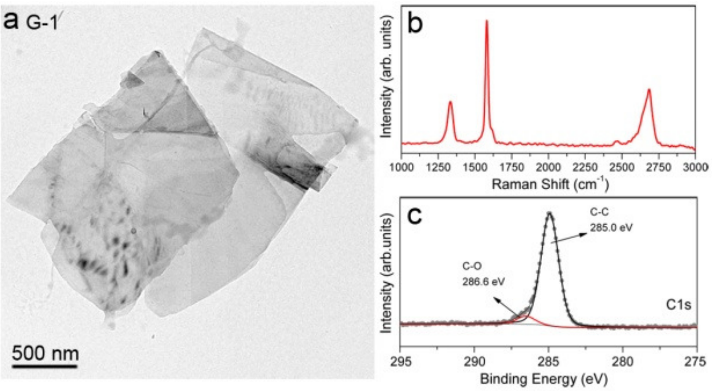

Figure 7.2 Starting material. TEM micrographs of solution cast **G-1**(a). Raman spectra excited at 633 nm for **G-1** (b). C 1s core level region of the X-ray photoemission spectrum of **G-1** (c).

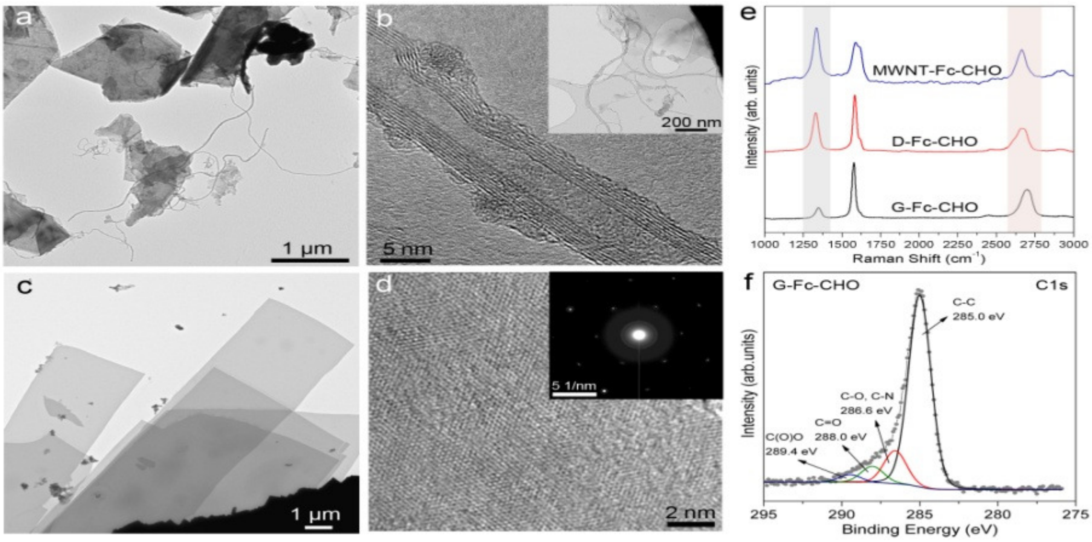

Figure 7.3 Carbon nanostructures produced by the addition of Fc-CHO during ultrasonication of **G-1**. a) TEM micrograph of solution cast **D-Fc-CHO**. b) HR-TEM of **D-Fc-CHO** where a MWNT on a graphene lattice is observed; in the inset, a panoramic TEM micrograph of **MWNT-Fc-CHO** is shown. c) Representative TEM micrograph of **G-Fc-CHO**. d) HR-TEM image of **G-Fc-CHO**; the inset shows the corresponding diffraction pattern. e) Comparison of the Raman spectra of **MWNT-Fc-CHO**, **D-Fc-CHO** and **G-Fc-CHO** collected exciting at 633 nm, the D and 2D bands are high-lighted. f) C 1s core level photoemission line of **G-Fc-CHO**.

D-Fc-CHO was obtained by sonication of G-1 with the addition of Fc-CHO (Figure 7.3). After washing and re-dispersing the product in 10 mL of fresh DMF, the concentration of the sample was calculated from the optical absorption as described above for G-1 and found to be 0.029±0.003 mg/mL. When analyzed by TEM, the presence of very long MWNTs (2 ± 0.5 µm) was observed in D-Fc-CHO as shown in Figure 7.3a. The formation of the tubular structures is seen exclusively at the edges of graphene layers (Figure 7.4).

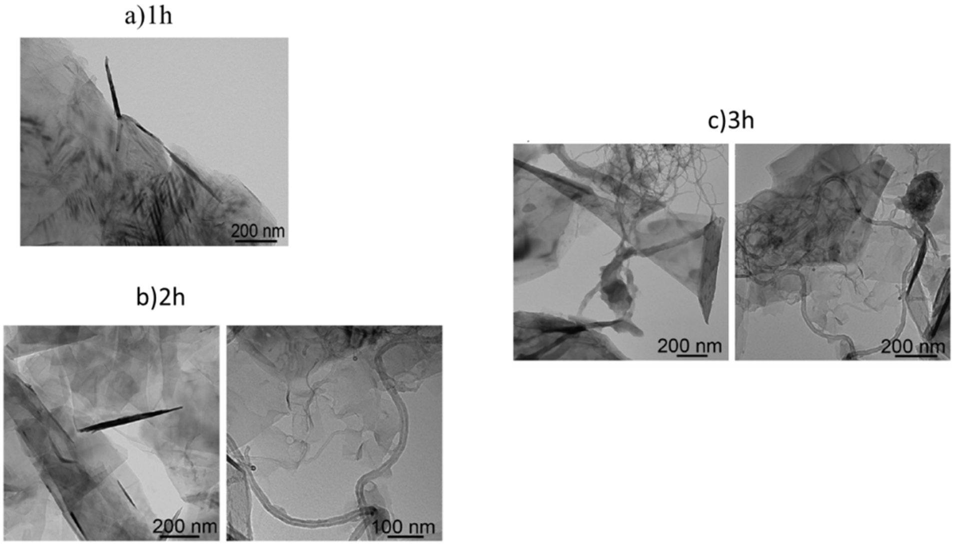

a)1h

b)2h

c)3h

Figure 7.4 MWNTs formation on the edges of the graphene layers. Evolution as a function of sonication time is shown.

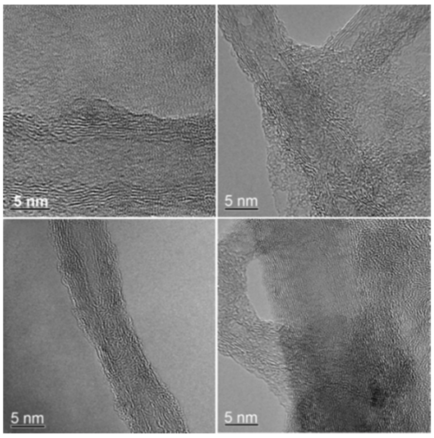

Figure 7.5.MWNT formation on the edges of graphene layers. Evolution as a function of sonication time is shown.

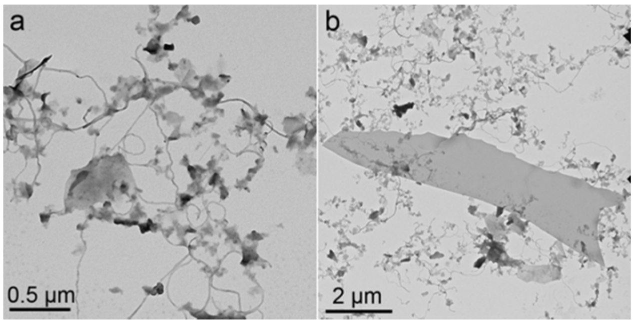

Figure 7.6.MWNTs produced by the addition on Fc-CHO mixed with graphene layers.

7.2.2 High resolution-transmission electron microscopy

Further analysis of the sample by HR-TEM proved the existence MWNTs. In some micrographs it is possible to distinguish the rolling up of the graphene edges while in others completely isolated MWNT are seen (Figure 7.5). The Raman spectrum of D-Fc-CHO is shown in Figure 7.3e. The ID/IG value of 0.72 and the 2D band at 2666 cm^{-1} imply a disordered material. After centrifugation, the concentration of the supernatant was again calculated from the optical absorption to amount to 0.007±0.002 mg/mL. TEM images of this supernatant, MWNT-Fc-CHO, show preponderantly the presence of MWNT, but small graphene fragments are still noticeable (Figure 7.6). The tube surfaces observed by HR-TEM reveal semi-crystalline MWNT showing disordered, distorted fringes surrounding the hollow core. The distance between the graphene sheets was found to be 0.35±0.01 nm. These structures are similar to as-grown MWNT obtained by chemical vapor deposition before annealing (Figure 7.3b Inset).[28] The HR-TEM of these structures after annealing at 500 ºC for 30 min, showed the symmetric, evenly spaced line patterns that have been interpreted as images of coaxial, nested graphitic tubes (Figure 7.3b).[29] Alternatively, the same images were attributed to graphitic scroll structures.[30] As previously reported, scroll segments, consisting of rolled-up graphene sheets, may coexist with nested tube segments inside a continuous tubular structure. The implication is that MWNT originate during the sonication process from the scrolls by Carbon-Carbon bond rearrangement.[31]

7.2.3 Raman spectroscopy and X-ray photoelectron spectroscopy

Further characterization of the sample by Raman spectroscopy captured the fingerprint of different carbon nanostructure.[32] For MWNT-Fc-CHO, the symmetrical shape of the 2D peak (no shoulder as in graphite) evidences the existence of MWNT since the sample does not contain the perfect structure of crystalline graphite due to the strong curvature of small diameter nanotubes (Figure 7.3e). The ID/IG value of 1.36 agrees with the semicrystalline structure observed by HR-TEM. The concentration of the lower part of the dispersion, G-Fc-CHO, was 0.012±0.003 mg/mL. When this sample was deposited on a TEM grid, graphene sheets with lateral size of few microns were found. A representative TEM micrograph is reported in Figure 7.3c, additional micrographs can be seen in Figure 7.7a. HR-TEM characterization confirms the presence of crystalline graphene, which was later corroborated by the analysis of the electron diffraction patterns. An example of this, inset in Figure 7.3d, shows what appears to be a single graphene.[33] The occurrence of a small D band at 1346 cm^{-1} and the ID/IG value of 0.33 are attributed to the edges of the graphene sheets. The 2D-band is symmetrical and roughly consists of one component, typical of monolayer or few-layer graphene (Figure 7.3e). The C 1s core-level photoemission line of G-Fc-CHO, presented in Figure 7.3f, gives insight into the chemical composition of this material: it shows, apart from the main component at 285.0 eV binding energy assigned to the aromatic carbon (77.2±1.3 % of the total amount of carbon), also contributions from carbon singly bound to oxygen or nitrogen at 286.6 eV (13.2±0.3 % of the total amount of carbon), as well as from carbonyl at 288.0 eV and carboxyl groups at 289.4 eV binding energy. The latter amount to 6.6±0.1 % and 3.1±0.1 %, respectively, of the total amount of carbon. The O 1s peak of D-Fc-CHO (Figure 7.7b) demonstrates the presence of different oxidation states of carbon after the reaction. The peak at 532.4 eV of binding energy is attributed to oxygen singly bound to carbon, while the peaks at 531.1 eV and 533.5 eV stem from carbonyl and carboxyl groups, respectively. A minor amount of Fe, about 0.3 at%, was identified and probably is due to residual iron, close to the edges.

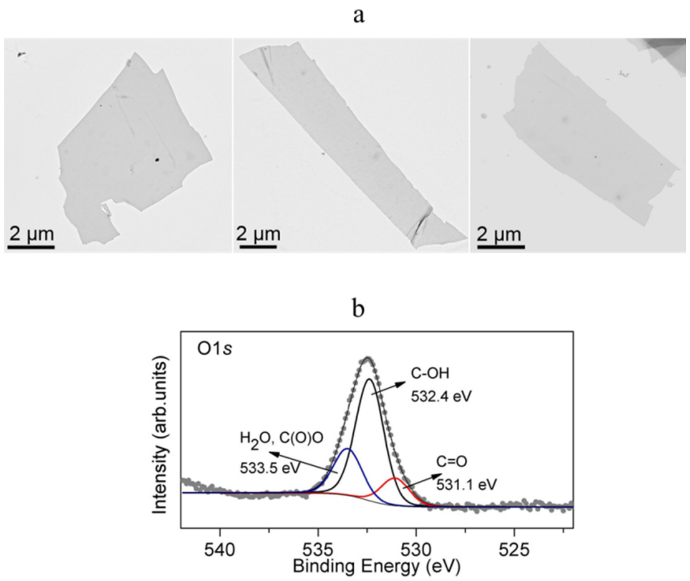

Figure 7.7 (a) TEM images of graphene sheets of G-Fc-CHO, (b) O 1s XPS peak of D-Fc-CHO

To test the possibility of producing larger quantities of MWNT, we added larger amounts of ferrocene aldehyde to the initial dispersion. No significant additional MWNT formation was observed by TEM and the treatment resulted in further oxidation of the sample as confirmed by Raman spectroscopy and XPS analysis. The implication is that the mechanism of formation of MWNTs entails an interaction of Fc-CHO with graphene layers that must reach a plateau in terms of concentration.

As a control experiment we sonicated G-1 without the addition of Fc-CHO under the same experimental conditions of G-Fc-CHO. Figures 7.8 a,b display representative TEM and Raman spectra of G-DMF; the shape and intensity of the 2D band at 2650 cm^{-1} for G-DMF are significantly different from those of pristine graphite. Conversely, the 2D band of G-DMF shows a low intensity band associated with damage of graphene.[34] The ID/IG value of 0.99 for G-DMF, identify the material as highly damaged graphene comparable to graphene oxide (GO).[35] Figure 7.8c shows the C 1s core level photoemission line of G-DMF. In the C 1s line of G-DMF the component at 285.0 eV, due to aromatic carbon, is reduced to 41.6±0.5 %, while the C-O bonds at 286.2 eV account now for 34±0.3 % of the total carbon amount and smaller peaks at 287.8 eV (15.8±0.2 %) and 289.3 eV (8.5±0.2 %) are assigned to carbonyl and carboxyl groups, respectively. A slightly increased amount of nitrogen (2.5 at%) was also observed for G-DMF as compared to G-1 (Figure 7.2). Such an increase in the degree of oxidation of G-DMF may result from oxidative processes promoted by free radicals generated during ultrasonication. Hence, the addition of Fc-CHO minimizes the oxidation of G-1 treated under the same experimental conditions than G-DMF, decreasing the conversion of C-C bonds to other C-X species (X= O or N) by more than 1/3. All the analyses identify D-Fc-CHO as a significantly less damaged material than G-DMF. From microscopy and Raman analysis, oxygenated groups are most abundant in the MWNT-Fc-CHO sample. Five other control experiments were carried out. In the same conditions of ultrasonication, we used (i) Fc, (ii) benzaldehyde, (iii) Fc together with benzaldehyde, (iv) Fc-COOH, and (v) $FcCON(CH_3)_2$. In no case MWNTs were observed in the reaction mixture. The experimental details and the characterization of the

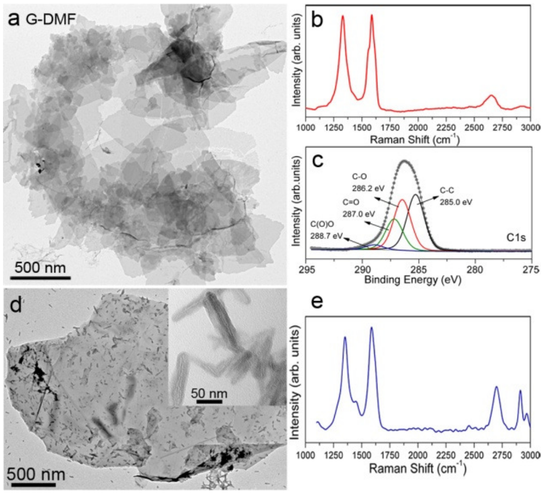

Figure 7.8 Control experiment performed by the sonication of G-1 without the addition of Fc-CHO (**G-DMF**) TEM micrograph of drop-cast **G-DMF** (a). Raman spectra of drop-cast **G-DMF** (b). C 1s core level photoemission line of **G-DMF** (c). Influence of temperature on the graphene exfoliation in the presence of the Fc-CHO. **G-Fc-CHO** (d) prepared by ultrasonication at room temperature. Raman spectra of drop-cast **G-Fc-CHO** (e) dispersion onto silicon oxide substrates, excited at 633 nm.

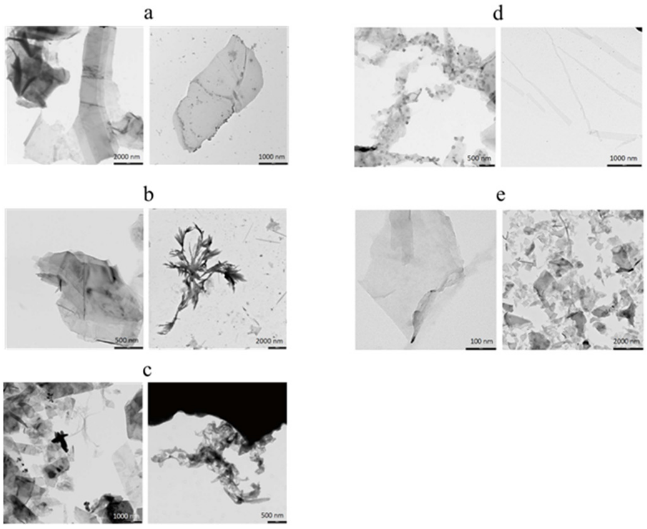

Figure 7.9 Control experiments preparation. G-1 dispersion was used as a starting material for the control experiments. As control experiment, we performed a 3 h sonication of G-1 adding (a) Fc, (b) benzaldehyde, (c) Fc together with benzaldehyde, (d) Fc-COOH, and (e) FcCON(NH_3)$_2$. The product was washed by filtration with fresh DMF in order to remove antioxidant and by-product molecules. Samples were re-dispersed in a bath ultrasonicator (few seconds) in 10 mL of fresh DMF. Centrifugation of all dispersions was carried out at 3000 rpm during 30 min. Two liquid fractions, of 5 mLeach, of the D-FC-CHO dispersion were collected and analyzed.

products in these control experiments are reported in Figure 7.9.

The key role of the cavitation energy in these processes is demonstrated by increasing the temperature of the process to room temperature (25 ℃). After ultrasonication of the G-Fc-CHO dispersion, we did not observe the formation of MWNT, but only of carbon nanoscroll-like structures, Figures 7.9d and 7.9e. The lack of formation of MWNT is due to the fact that the higher temperature decreases the energy density of cavitation[36] and allows terminal radical reaction pathways to dominate.

The experimental findings together with the control experiments allow us to conceive a possible mechanism for the formation of carbon nanotubes based on the multiple role of Fc-CHO. Defects caused by various factors, including chemical functionalization[37] or physical adsorption,[38] play a crucial role in the spontaneous twisting and folding and in the disruption of the aromatic bond network of graphene nanoribbons.[39] Rolling of the sheets starts from the edges[40,41] and entails an energy barrier that must be overcome. Fc-CHO templates the formation of MWNT by lowering the barrier for rolling nanoribbons. Encapsulation of metallocene molecules in nanotubes is a highly exothermic process.[42] Formation of ferrocene nanorods, attributed to π–π stacking of ferrocene molecules, on the surface of graphene sheets has been observed experimentally.[43] We performed a combination of Molecular Mechanics and Molecular Dynamics calculations for an increasing number of Fc-CHO molecules deposited on the nanoribbon obtained by unzipping a (8,8) CNT (See Table 7.1 and Figure 7.10). The length of the tube

Table 7.1 Energy barrier for a SWNT (8,8)rolling up with different number of Fc-CHO

N° of Fc-CHO molecules	Energy barrier for a SWNT (8,8) rolling	Stabilization energy of the Fc-CHO molecule (Kcal mol^{-1})
0	120.3	
1	102.5	17.8
2	86.0	16.5
3	72.0	14.0
4	63.3	8.7

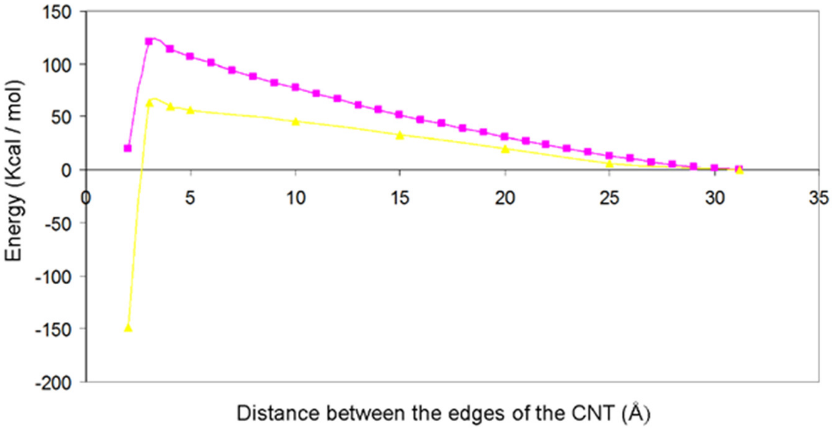

Figure 7.10 Minimum energy path (MEP) for the rolling up of the graphene nanoribbon in the absence (purple line) and in the presence of four Fc-CHO molecules (yellow line)

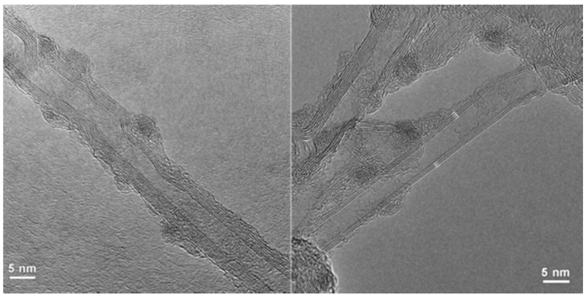

Figure 7.11 TEM images of MWNTs after annealing treatment

was 24.5 Å. In the absence of Fc-CHO, the activation barrier for folding the nanoribbon is 120.3 kcal mol^{-1}. Introduction of the first Fc-CHO molecule decreases the barrier by 17.8 kcal mol^{-1}. The energy decrease is further lowered for the introduction of each subsequent Fc-CHO molecule. When 4 Fc-CHOs template the process, the barrier is nearly halved to 63.3 kcal mol^{-1}.

Crucial for templating the folding of graphene sheets by Fc-CHO is the presence of iron inside the MWNTs as detected by TEM (Figure 7.11). It confirms that incorporation of Fc-CHO occurs and strongly vouches for their templating activity and supports the idea that this is the starting mechanism in the formation of the MWNT.

In the five control experiments MWNTs were not observed in the reaction mixture. Fc, benzaldehyde, Fc together with benzaldehyde, Fc-COOH, and FcCON(CH_3)$_2$ may still be able to exert in some templating activity or roll up the sheets but must lack part of the properties of Fc-CHO that produce MWNTs.

7.3 Quantum chemical calculations[†††]

We performed quantum chemical calculations (Table 7.2) that showed that Fc-CHO has the highest electron affinity (EA) of a set of molecule that comprised also Fc-COOH, Fc-CON(CH_3)$_2$, Fc, and benzaldehyde. Since Fc-CHO is the only molecule that produces CNTs, these calculations confirm that its radical scavenging activity is superior to that of the others and can be of primary importance in the MWNT formation. The large spin density located on the aldehydic group of Fc-CHO (Figure 7.12) further shows its role in the antioxidant activity.

Table 7.2 Electron affinities (EAs)

Molecule	*EA (Kcal/mol)*
Fc-CHO	-50.0
Fc-COOH	-44.4
Fc-CON(CH_3)$_2$	-32.0
Fc	-31.5
Benzaldehyde	-26.6

[†††] Calculations performed by Matteo Calvaresi and Francesco Zerbetto , University of Bologna.

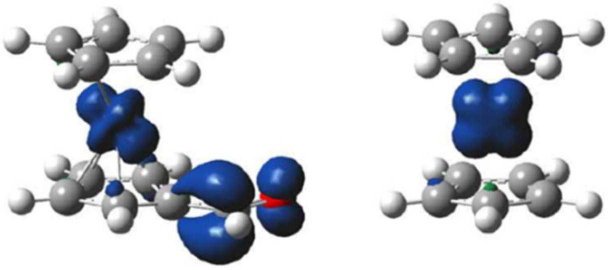

Figure 7.12 Isosurfaces spin densities of Fc-CHO (left) and Fc (right) radical molecules plotted using an isovalue of 0.004 ea_0^{-3}.

A final feature to consider is that in graphene the reactivity of edges is at least twice as large as the reactivity of the bulk atoms.[44] This observation concurs with scanning tunneling spectroscopy measurements that evidenced a higher electronic density of states near the Fermi level at the edges[45] and theoretical calculations that predicted that edge states occur in any graphene sheet.[46]

From all these observations, we suggest that during ultrasonication different scenarios may occur:

a) in the absence of antioxidants, the radical species are strong enough to oxidize the graphene sheet; this process starts at the edges and at inner defects and slices graphene sheets in small pieces;

b) in the presence of Fc-CHO, the concentration of radical reactive species is considerably reduced; some radical attacks to the edges still occur and loosen the sheets;

c) Fc-CHO then acts in a different way; it localizes itself at the edges of graphene and templates the rolling up of a sheet to form a nanoscroll where it remains trapped; the localization implies that a limiting number of Fc-CHO can roll up the sheet, in agreement with the experimental finding that higher amounts of ferrocene aldehyde do not provoke additional MWNT formation;

d) Fc-CHOs inside the scroll then act as active bumpers in a pinball machine; they accept and donate unpaired electron with the graphene edges and convert the less stable scroll into a MWNT.

While step *(d)* is only putative, it makes chemical sense. This mechanism explains the formation of long tubes during the ultrasonication process.

7.4 Conclusion

To sum up, we studied the effect of adding Fc-CHO during exfoliation of graphite in DMF with the help of ultrasonication treatment. The formation of MWNTs was observed when this antioxidant was added. A considerably reduction of the degree of oxidation of the exfoliated graphene sheets was demonstrated by XPS and Raman spectroscopy analyses. Higher concentrations were determined, from the UV-vis absorption at 660 nm, of the dispersions and larger graphene sheets were observed by TEM and HR-TEM. Our results allow us to propose a radical attack mechanism controlled by the presence of the antioxidant molecules and the different reactivity of diverse graphene edges. Templating activity of Fc-CHO facilitates the nanoribbons rolling. These results are expected to be useful to understand how solvents disperse graphene and in advancing the controlled synthesis of carbon nanotubes. This procedure can also reach higher yields of liquid-phase exfoliation graphene.

References

[1] Rao, C. N. R.; Seshadri, R.; Goviandaraj, A.; Sen, R. *Mat. Sci. Eng. R.* **1995**, 15, 209-262.

[2] Novoselov, K. S.; Geim, A. K.; Morozov, S. V.; Jiang, D.; Zhang, Y.; Dubonos, S. V.; Grigorieva, I. V.; Firsov, A. A. *Science* **2004**, 306, 666-669.

[3] Meyer, J. C.; Geim, A. K.; Katsnelson, M. I.; Novoselov, K. S.; Booth, T. J.; Roth, S. *Nature* **2007**, 446, 60-63.

[4] Castro, N.; Guinea, F.; Peres, N. M. R.; Novoselov, K. S.; Geim, A. K. *Rev. Mod. Phys* **2009**, 81, 109-162.

[5] Frank, I. W.; Tanenbaum, D. M.; van der Zande, A. M.; McEuen, P. L. *J. Vac. Sci. Technol.* **2007**, 25, 2558-2561.

[6] Geim, A. K.; Novoselov, K. *J. Nat. Mater.* **2007**, 6, 183-191.

[7] Chuvilin, A.; Kaiser, U.; Bichoutskaia, E.; Besley, N. A.; Khlobystov, A. N. *Nat. Chem.* **2010**, 2, 450-453.

[8] Joumet, C. ; Maser, W. K. ; Bernier, P. ; Loiseau, A. ; Lamy de la Chapelle, M. ; Lefrant, S.; Deniard, P. ; Lee, R. ; Fischer, J. E. *Nature* **1997**, 388, 756-758.

[9] Terrones, M. *Int. Mat. Rev.* **2004**, 49, 325-377.

[10] Hafner, J. H.; Bronikowski, M. J.; Azamian, B. R.; Nikolaev, P.; Rinzler, A. G.; Colbert, D. T.; Smith, K. A.; Smalley, R. E. *Chem. Phys. Lett.* **1998**, 296, 195-202.

[11] Haddon, R. C.; Sippel, J.; Rinzler, A. G.; Papadimitrakopoulos, F. *MRS Bulletin* **2004**, 29, 252-259.

[12] Skrabalak, S. E. *Phys. Chem. Chem. Phys.***2009**, 11, 4930-4942.

[13] Kaempgen, M.; Lebert, M.; Haluska, M.; Nicolso, N.; Roth, S. *Adv. Mater.***2008**, 20, 616-620.

[14] Jeong, S.-H.; Ko, J.-H.; Park, J.-B.; Park, W. J. *J. Am. Chem. Soc.***2004**, 126, 15982–15983.

[15] Li, C. P.; Teo, B. K.; Sun, X. H.; Wong, N. B.; Lee, S. T. *Chem. Mater.***2005**, 17, 5780-5788.

[16] Li, C.-P.; Wong, N.-B.; Lee, C.-S.; Lee, S.-T.; Teo, B. K. *J. Am. Chem. Soc.* **2002**, 124, 14856-14857.

[17] Hernandez, Y.; Nicolosi, V.; Lotya, M.; Blighe, F. M.; Sun, Z.; De, S.; McGovern, I. T.; Holland, B.; Byrne, M.; Gun'Ko, Y. K.; Boland, J. J.; Niraj, P.; Duesberg, G.; Krishnamurthy, S.; Goodhue, R.; Hutchison, J.; Scardaci, V.; Ferrari, A. C.; Coleman, J. N. *Nat. Nanotechnol.***2008**, 3, 563-568.

[18] Shin, C.-J.; Lin, S.; Strano, M. S.; Blankschtein, D. *J. Am. Chem. Soc.***2010**, 132, 14638-14648.

[19] Cravotto, G.; Cintas, P. *Chem. Eur. J.***2010**, 16, 5246-5259.

[20] Gedanken, A. *Ultrason. Sonochem.***2004**, 11, 47-55.

[21] Suslick, K. S.; Choe, S.-B.; Cichowlas; A. A.; Grinstaff, M. W. *Nature* **1991**, 353, 414-416.

[22] Khan, U.; O΄Neil, A.; Loyta, M.; De, S.; Coleman, J. N. *Small* **2010**, 6, 864-871.

[23] Misik, V.; Riesz, P. *Free Radical Biol. Med.* **1996**, 20, 129-138.

[24] Wang, J.; Huang, L.Y.; Chen, G. A.; Huang, J. L. *Chem. Lett.***2005**, 34, 1514-1515.

[25] Fukuzimi, S.; Shimoosako, K.; Suenobu, T.; Watanabe, Y. *J. Am. Chem. Soc.* **2003**, 125, 9074-9082.

[26] Cao, A.; Dickerel, P. L.; Sawyer, W. G.; Ghasemi-Nejhad, M. N.; Ajayan, P. M. *Science* **2005**, 310, 1307-1310.

[27] Ugarte, D. *Nature* **1992**, 359, 707-709.

[28] Kosaka, M.; Ebbesen, T. W.; Hiura, H.; Tanigaki, K. *Chem. Phys. Lett.* **1995**, 233, 47-51.

[29] Iijima, S. *Nature* 1991, 354, 56-58.

[30] Zhang, X. F.; Zhang, X. B.; Van Tendeloo, G.; Amelinckx, S.; Op de Beeck, M.; Van Landuyt, J. *J. Cryst. Growth* **1993**, 130, 368-382.

[31] Berber, S.; Tománek, D. *Phys. Rev. B* **2004**, 69, 233404.

[32] Ferrari, A. C.; Robertson, J. *Phys. Rev. B* **2000**, 61, 14095-14107.

[33] Meyer, J. C.; Geim, A. K.; Katsnelson, M. I.; Novoselov, K. S.; Obergfell, D.; Roth, S.; Girit, C.; Zettl, A. *Solid State Commun.* **2007**, 143, 101-109.

[34] Ferrari, A. C.; Meyer, J. C.; Scardaci,V.; Casiraghi,C.; Lazzeri, M.; Mauri, F.; Piscanec, S.; Jiang, D.; Novoselov, K. S.; Roth, S.; Geim, A. K. *Phys. Rev. Lett.* **2006**, 97, 187401.

[35] Subrahmanyam, K. S.; Vivekch, S. R. C.; Govindaraj, A.; Rao, C. N. R. *J. Mater. Chem.***2008**, 18, 1517-1523.

[36] Shah, Y. T.; Pandit, A. B.; Moholkar, V. S. *In Cavitation Reaction Engineering: P. Ch. (Plenum Chemical Engineering Library)*, TP156, C38548, 1999.

[37] Ramanathan, T.; Abdala, A. A.; Stankovich, S.; Dikin, D. A.; Herrera-Alonso, M.; Piner, R. D.; Adamson, D. H.; Schniepp, H. C.; Chen, X.; Ruoff, R. S.; Nguyen, S. T.; Aksay, I. A.; Prud'Homme, R. K. ; Brinson, L. C. *Nat. Nanotech.* **2008**, 3, 327-331.

[38] Yu, D.; Liu, F. *Nano Lett.* **2007**, 7, 3046-3050.

[39] Bets, K. V.; Yakobson, B. I. *Nano Res.* **2009**, 2, 161-166.

[40] Gass, M. H.; Bangert, U.; Bleloch, A. L.; Wang, P.; Nair, R. R.; Geim, A. K. *Nature Nanotech.* **2008**, 3, 676-681.;

[41] Ivanovskaya, V. V.; Zobelli, A.; Wagner, P.; Heggie, M. I.; Brid-don, P. R.; Rayson, M. J.; Ewels, C. P. *Phys. Rev. Lett.* **2011**, 107, 065502

[42] Plank, W.; Pfeiffer, R.; Schaman, C.; Kuzmany, H.; Calvaresi, M.; Zerbetto. F.; Meyer, J. *ACS Nano*, **2010**, 4, 4515–4522.

[43] Zhu, J.; Sun, K.; Sim, D.; Xu, C.; Zhang, H.; Hng H. H.; Yan, Q. *Chem. Commun.* **2011**, 47, 10383-10385.

[44] Sharma, R.; Huun, B.; Perera. C. J.; Strano, M. S. *Nano Lett.* **2010**, 10, 398-405.

[45] Klusek, Z.; Kozlowski, W.; Waqar, Z.; Datta, S.; Burnell-Gray, J. S.; Makarenko, I. V.; Gall, N. R.; Rutkov, E. V.; Tontegode, A. Y.; Titkov, A. N. *Appl. Surf. Sci.* **2005**, 252, 1221-1227.

[46] Wimmer, M.; Akhmerov A. R.; Guinea, F. *Phys. Rev. B* **2010**, 82, 045409.

[47] Moulder, J. K.; Stickle, W. F.; Sobol, P. E.; Bomben K. D. *In Handbook of X-ray photoelectron Spectroscopy*; Eden Prairie: Minnesota, 1992.

Chapter 8

Pillaring of GO with [$A1_{13}(O)_4(OH)_{24}(H_2O)_{12}{}^{7+}$] Keggin ions and derived hybrids

In this chapter we report the successful intercalation of Aluminium species into the interlayer space of graphite oxide, after interaction with Keggin ion [$A1_{13}(O)_4(OH)_{24}(H_2O)_{12}{}^{7+}$], and subsequent heating of this hybrid nanostructure up to 370 °C. X-ray diffraction demonstrates the intercalation of the Al clusters, and the subsequent behaviour of the derived intercalated structure upon heating, while X-ray photoelectron spectroscopy identifies the type of Aluminium clusters incorporated between the graphene oxide layers.

8.1 Introduction

Graphene-based nanocomposites materials triggered the interest of the scientific world due to their outstanding physical, chemical and electronic properties.[1,2] However, the need of a controllable, high yield production of graphene, to meet the demand for bulk synthesis of mesoporous materials with accessible pores of molecular dimensions, lead to the development of new routes for making this stable 2-D nanomaterial. Graphene oxide (GO) is considered to be one of the most promising materials for the bulk production of graphene-based composite nanostructures.[3] The oxygen functional groups of GO, namely mostly epoxy, hydroxyl and carboxyl groups on the surface and at the edges of carbon sheets[4,5]) allow for the creation of hybrid nanocomposites materials for diverse applications such as adsorbents, energy storage, gas separation, building blocks for catalysts, GO-polymer composites, battery electrode materials.[6-14] The Keggin ion, a molecular inorganic compound with the formula $A1_{13}(O)_4(OH)_{24}(H_20)_{12}{}^{7+}$ or (Al_{13}) in short, is the most important polyoxocation formed in aluminium polycation chemistry, with many applications in geochemistry, sensing activities, catalysis, environmental chemistry, water treatment, material science and pharmacy.[15,16] In this chapter we report on the successful intercalation of GO by Aluminium clusters of variable size and subsequent behavior of the graphene flakes upon thermal treatment. These hybrid nanostructures are promising candidates for application such in gas storage, catalysis, biosensors, and biomedical devices.

8.2 Experimental section

Host layered material. Aqueous dispersions of graphene oxide were produced using a modified Staudenmaier's method[2] from graphite powder (see chapter 2.2.1)

Synthesis of Keggin ion.[‡‡‡] The chemicals used in preparing the solutions; $AlCl_3.6H_2O$ 99% (Aldrich) and NaOH 98.3% (Merk). The Al_{13} polyoxocations were synthesized as follows: 100 mL of 0.2 M aluminium chloride solution contained in the glass reactor was heated and was kept at 80°C, 240 mL of 0.2 M NaOH solution was slowly added under continuous stirring and accurate temperature control. The Al_{13} solution was allowed to cool down to room temperature in about 24 h. The solution pH ranged from 3.7 to 3.9, depending on the rate of stirring and residual Al_{13}^+.

Preparation of Keggin ion pillared graphene (PILGOK). In a typical experiment, 66 mL Al_{13} solution mixed with 12 mL NaOH solution 6M and added dropwise to a suspension of GO in distilled deionized water (100 mg GO, 50 mL) under vigorous stirring. Upon addition of the Al_{13} solution, the GO solid swelled instantly. The reaction continued for 24 h at room temperature. The GO derivatives was isolated by centrifugation and washed two times with distilled deionized water and dried in air. Finally, the sample was heated at 200 °C for 2 h in air.

Powder X-ray Diffraction (XRD). (see chapter 2.1.2 b)

FTIR spectroscopy. (see chapter 2.1.4)

Raman spectroscopy. (see chapter 2.1.3)

Thermal analysis. Thermogravimetric (TGA) and differential thermal (DTA) analysis were performed using a Perkin Elmer Pyris Diamond TG/DTA. Samples of approximately 5 mg were heated in air from 25 °C to 850 °C, at a rate of 5 °C/min.

X-ray Photoelectron Spectroscopy (XPS).(see chapter 2.1.1) All binding energies were referenced to the C 1s core level of the C-C bond set to the nominal value of 285.0 eV[1].

8.3 Results and discussion

The oxidation and subsequent exfoliation of graphite by chemical treatment is widely known for a very long time.[2,3] Graphite oxide possesses a lamellar structure of graphene sheets decorated with various oxygen-containing functional groups like hydroxyl, epoxy, and carboxyl, on the surface and at the edges of carbon sheets. Our starting material was graphite powder and GO was produced by the Staudenmaier's method[17]. GO was then intercalated with Keggin ion ($[Al_{13}O_4(OH)_{24}(H_2O)_{12}]^{+7}$) to synthesize novel intercalated layered nanostructures. In detail a water solution of the inorganic Al_{13} was added to the GO dispersion. An immediate flocculation of the graphene oxide particles was observed (Scheme 1). Apparently the flocculation was induced by the insertion of Al clusters into the GO galleries, through hydrogen bonding or electrostatic interactions with the oxygen functional groups of GO. Finally, the

---

[‡‡‡] Synthesis by E. Diamanti, University of Ioannina.

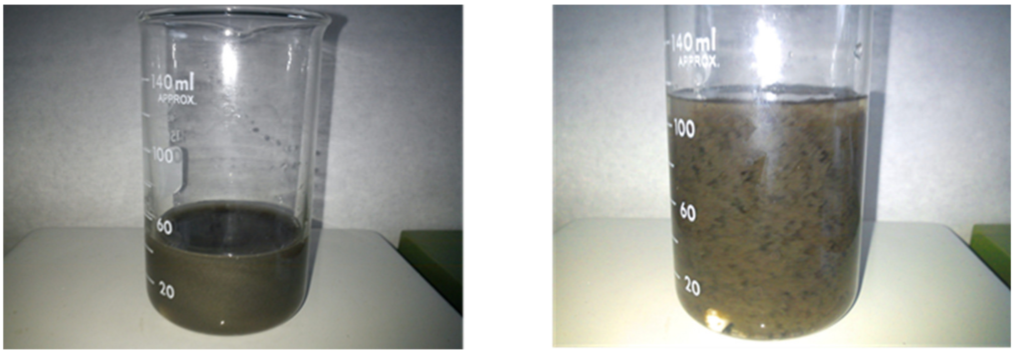

Figure 8.1 (left) Dispersion of graphite oxide (GO) in water, (right) flocculation after the insertion of Keggin ion derivatives into the GO matrix.

samples were heated to 200 °C and to 375 °C for 2 h in air in order to investigate the thermal stability and structure of the hybrid material.

8.3.1 X-ray diffraction

The X-ray diffraction (XRD) patterns of pristine graphite (G), graphene oxide (GO) and PILGOK are presented in Figure 8.2. The pattern for pure graphite reveals a peak at 26.6° corresponding to a basal spacing $d_{002} = 3.3$ Å. The diffraction pattern of GO, on the other hand, exhibits a 001 reflection peak[4,18] at

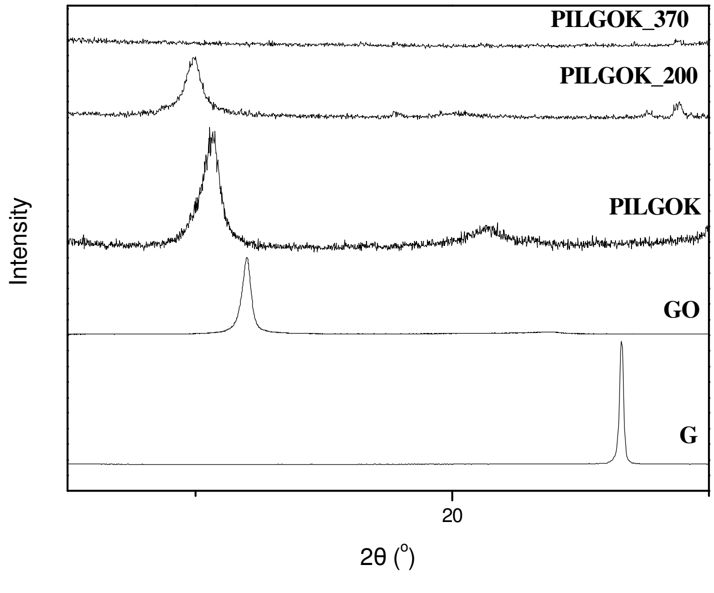

Figure 8.2 Comparison of the X-ray diffraction data of graphite (G), graphite oxide (GO), graphene oxide intercalated with $Al_{13}(O)_4(OH)_{24}(H_2O)_{12}^{7+}$ at ambient conditions (PILGOK), after heating to 200 °C (PILGOK_200) and to 370 °C (PILGOK_370)

12.0^{o} corresponding to a basal spacing d_{001}=7.3 Å, confirming the successful oxidation of graphite after the acid treatment. After the intercalation of Al_{13} polycations, the 001 reflection was shifted to lower angles testifying to an increased basal spacing of 8.3 Å (Figure 8.2 top curve). The increase in the d_{001} distance is due to the insertion of Al derived molecules which are located in the GO interlamellar space, where they are believed to hydrogen bonded or interact ionically with the basal carboxylic groups of the graphene surfaces. Taking into account the thickness of the graphene oxide layers 6.1 Å,[19] we estimate an interlayer separation of $\Delta = 8.3 - 6.1 = 2.2$ Å for Al_{13}derivatives. After heating at 200 °C the basal spacing of GO increased from 8.3 Å to 8.9 Å (Figure 1b middle curve) indicating that the pillared structure remains stable at this temperature. The small increase in the d_{001}-spacing is attributed to disorder of the graphitic platelets (turbostratic effect).[20] After heating PILGOK to 370 °C the d_{001} diffraction peak completely disappears, (Figure 8.2 top curve) indicating that we have no longer an ordered layered structure but that the material is now completely exfoliated.

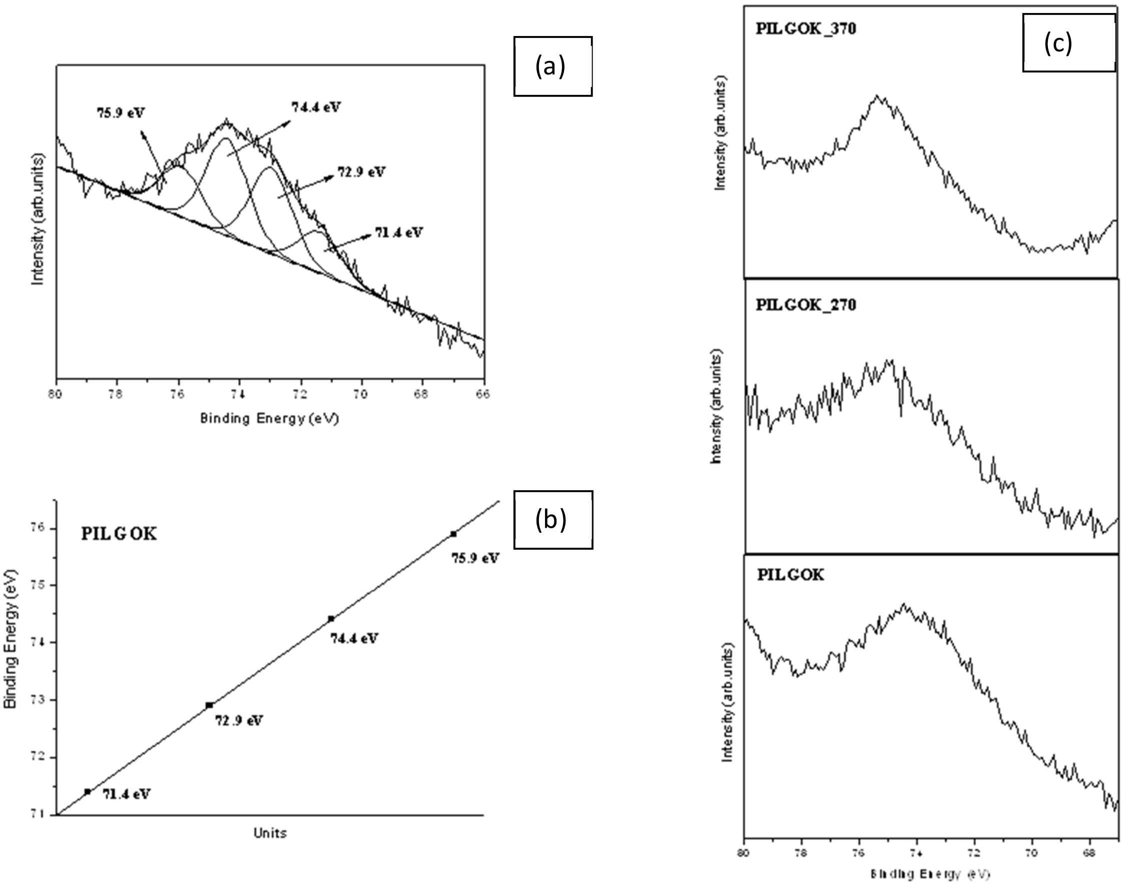

Figure 8.3 (a) X-ray photoelectron spectrum of the Al 2p core level region of graphite oxide intercalated with Al derivatives (PILGOK) (b) Different oxidation states of aluminium can be expressed by the straight line of the four different shifts in the binding energy of the Al 2p core level photoemission peak (c) Al 2p core level region of the XPS spectrum of intercalated graphite oxide at ambient conditions (bottom panel, PILGOK), and after heating to 200 °C (central panel, PILGOK_200) and to 370 °C (top panel, PILGOK_370).

Table 8.1 Atomic percentage % of PILGOK at ambient conditions

	Atomic Percentage %	**Error at%**
C	79.2±1.6	2
Al	14.8±1.2	8
O	6.0± 0.7	8

8.3.2 X-ray photoelectron spectroscopy

X-ray photoelectron spectroscopy was performed on PILGOK in order to verify the presence and integrity of the Al structures in the interlayer space of graphene oxide and to evaluate the nature of the graphene-based nanostructure upon thermal treatment (at 200 °C and at 370 °C) . The carbon 1*s* core level emission (C-C/C-H) at 285.0 eV was used as a reference and all binding energies where shifted consequently as to compensate for any possible charging effect. The atomic percentages of carbon, oxygen and aluminium in the intercalated material are displayed in Table 8.1. Figure 8.3 shows the Al 2p core level region of the PILGOK photoelectron spectrum which indicates that various types of Al clusters co-exist in the graphite oxide galleries. When we fitted the spectrum with a minimum number of components, we could conclude that different Al species are present; based on their binding energies we identify them as Al (70.2 eV), AlO(OH) (72.8 eV), AlOOH (74.3 eV) and finally Al_2O_3 (75.9 eV).[21-24] Heating to 200 °C and to 370 °C clearly affects the intercalated material as seen from the comparison of the Al 2p XPS of the freshly synthesized sample with the ones obtained after heating in Figure 8.3(c): some components are slightly shifted to lower binding energy due to change of the environment.

8.3.3 Thermogravimetric and differential thermal analysis

Thermogravimetric (TGA) and differential thermal analysis (DTA) data of pure graphite, graphene oxide, and intercalated graphite oxide (PILGOK) are shown in Figure 8.4. The DTA curve of graphite (Figure 8.4a) exhibits one exothermic peak at 700 °C due to the combustion of carbon layers, while graphene oxide shows two exothermic peaks centred at 250 °C and 500 °C, which correspond to 30% and 50% weight losses, respectively. The first of these peak is attributed to the removal of oxygen containing functional groups, created after the acid treatment of graphite, while the second one refers to carbon combustion and occurs at a lower temperature than for graphite because GO is a more open structure.[4,25] For PILGOK the DTA curves exhibits one exothermic peak at ~200 °C associated with a 30% weight loss and ascribed to the removal of oxygen functional groups, while the combustion of the carbon layers appears now already at 375 °C. Finally from the remaining weight of the PILGOK samples after heating to 900 °C the wt% of inorganic Al species can be calculated: we find that the Al containing species account for ~8% of the total mass, in agreement with the XPS data analyzed above.

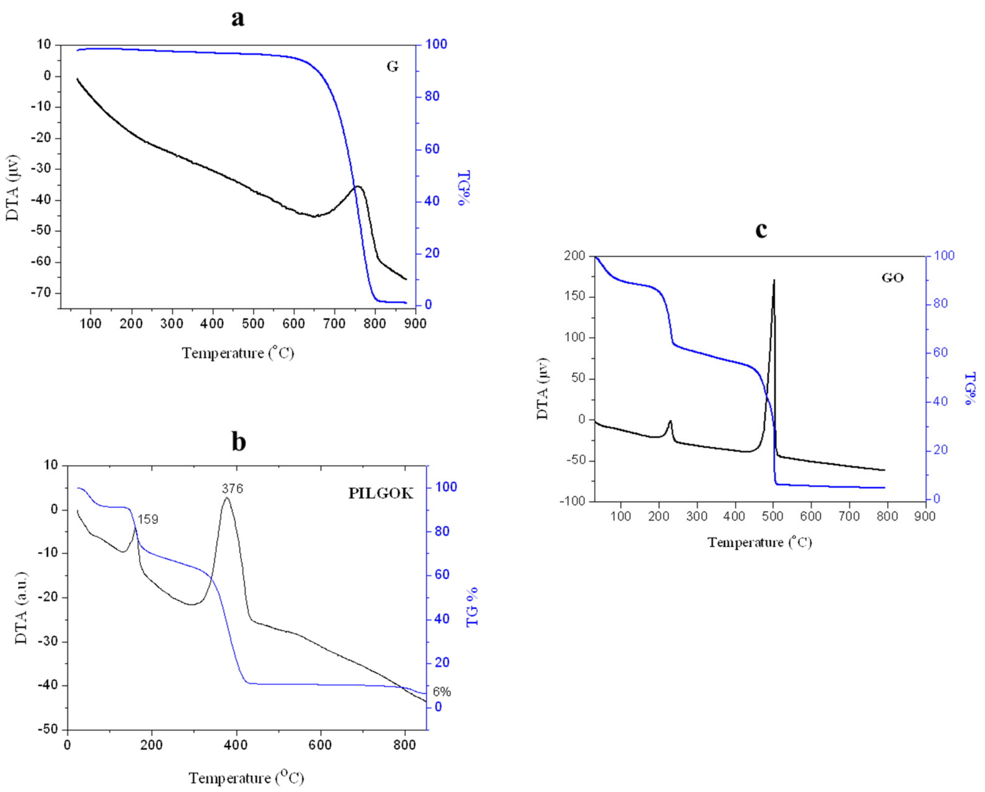

Figure 8.4 DTA and TGA curves of pristine graphite (a), GO (c), and PILGOK (b)

8.4 Conclusions

After the intercalation of graphite oxide (GO) with Keggin ions $[A1_{13}(O)_4(OH)_{24}(H_20)_{12}]^{7+}$, X-ray diffraction and X-ray photoelectron spectroscopy data indicate that Al moieties are present between the graphene oxide layers, not as a Keggin ions but as smaller Al clusters. These clusters cause an expansion of the distance between graphene oxide planes by 2.2 Å. Heating to 200 °C further increases this distance by 0.6 Å because of turbostratic disorder. Additional heating to 370 °C leads to full exfoliation of graphite composite and yields a nanomaterial which is promising for applications like catalysis, gas or liquid separation and energy storage.

References

[1] Geim, A. K.; Novoselov, K. S. *Nat. Mater.* **2007**, 6, 183–191.

[2] Y. J. Gan, L. T. Sun and F. Banhart, Small, 2008, 4, 587–591.

[3] Verdejo, R.; Bernal, M. M.; Romasanta, L. J.; Lopez-Manchado, M. A. J. *Mater. Chem.* **2011**, 21, 3301–3310.

[4] Bourlinos, A. B.; Gournis, D.; Petridis, D.; Szabo, T.; Szeri, A.; Dekany, I. *Langmuir* **2003**, 19, 6050–6055.

[5] Kovtyukhova, N. I.; Ollivier, P. J.; Martin, B. R.; Mallouk, T. E.; Chizhik, S. A.; Buzaneva, E. V.; Gorchinskiy, A. D. *Chem. Mater.* **1999**, 11, 771–778.

[6] Seredych, M.; Bandosz, T. J.; J. *Colloid Interface Sci.* **2008**, 324, 25–35.

[7] Morishige, K.; Hamada, T. *Langmuir* **2005,** 21, 6277–6281.

[8] Matsuo, Y.; Hatase, K.; Sugie, Y.*Chem. Mater.***1998**, 10, 2266–2269.

[9] Matsuo, Y.; Matsumoto, Y.; Fukutsuka, T.; Sugie, Y. *Carbon* **2006**, 44, 3134–3135.

[10] Szabo, T.; Tombacz, E.; Illes, E.; Dekany, I. *Carbon* **2006**, 44, 537–545.

[11] Kotov, N. A.; Dekany, I.; Fendler, J. H. *Adv. Mater.***1996**, 8, 637–641.

[12] Wang, D.; Kou, R.; Choi, D.; Yang, Z.; Nie, Z.; Li, J.; Saraf, L. V.; Hu, D.; Zhang, J.; Graff, G. L.; Liu, J.; Pope, M. A.; Aksay, I. A. *ACS Nano* **2010**, 4, 1587–1595.

[13] Pumera, M. *Energy & Environmental Science* **2011***,* 4, 668–674.

[14] James S. L.*Chem. Soc. Rev.* **2003,** 32, 276-288.

[15] Wang, G.; Zhou, J.; Li, J. *Biosens. Bioelectron.* **2007**, 22, 2921–2925.

[16] Deschaume, O.; Shafran, K. L.; Perry, C. C.*Langmuir* **2006**, 22, 10078–10088.

[17] Staudenmaier, L. *Ber. Dtsch. Chem. Ges.* **1898**, 31, 1481–1487.

[18] Nethravathi, C.; Viswanath, B.; Shivakumara, C.; Mahadevaiah, N.; Rajamathi, M. *Carbon* **2008**, 46, 1773-1781.

[19] Dekany, I.; Kruger-Grasser, R.; Weiss, A. *Colloid Polym. Sci.* **1998**, 276, 570-576.

[20] Dresselhaus, M.S. In Supercarbon: Synthesis, Properties and Applications; Yoshimura, S., Chang, R. P., *Eds. Springer Series in Materials Science*, Vol. 33; Springer: New York, **1998**.

[21] Zhitomirsky, V. N.; Kim, S. K.; Burstein, L.; Boxman, R. L. *Applied Surface Science* **2010**, 256, 6246–6253.

[22] *Handbooks of Monochromatic XPS Spectra* volume 2, XPS International, Mountain View California, 94040, USA, **1997**.

[23] McCafferty, E.; Wightman, J. P.*Surf. Interf. Analys.***1998**, 26, 549–564.

[24] Bou, M.; Martin, J. M.; Le Mogne, T.; Vovelle, L.*Appl. Surf. Sci.* **1991**, 47, 149–161.

[25] Becerril, H. A.; Mao, J.; Liu, Z.; Stoltenberg, R. M.; Bao, Z.; Chen, Y. *ACS Nano* **2008**, 2, 463-470.

Chapter 9

Interaction between organic polycyclic aromatic molecules and graphite oxide: A study of the intercalation process

In this chapter we report for the first time the intercalation mechanism of cyclic aromatic molecules into graphite oxide. We investigate two molecules of this family, aniline and naphthalene amine. We observe that aniline molecules prefer to covalently bind to the graphene oxide matrix via chemical grafting, while naphthalene amine binds with the graphene oxide surface through π-π electrostatic interactions. The presence of intercalated aromatic molecules between the graphene oxide (GO) layers is demonstrated by X-ray diffraction (XRD), while the type of interaction between the graphene oxide (GO) and polycyclic organic molecules is illustrated by X-ray photoelectron spectroscopy (XPS). The present work opens new perspectives for the interaction of various aromatic molecules with graphite oxide and the so-called "intercalation chemistry".

9.1 Introduction

Graphene is a one-atom thick layer of sp^2 hybridized carbon atoms, tightly packed in a hexagonal crystal lattice and the main basic building block of other graphitic nanostructures (like graphite, fullerenes and nanotubes). The extraordinary/unusual properties of graphene[1,2] promise well for numerous, very different applications in electronics and spintronics, but also as reinforcement in polymer composites, constituent of composite materials, sensors and so on.[3-10] To realize this potential, efficient approaches for the production of large quantities of graphene are needed; currently one of the most promising is the chemical exfoliation of graphite passing the oxidation of the graphene sheets in order to form graphene oxide.[11-13] Graphene oxide (GO) is a layered material achieved through strong oxidation of graphite[14-17]. GO is characterized by the presence of oxygen–containing moieties, mostly hydroxyl and epoxy groups, but also carboxyl groups both on the surface and at the edges of the carbon sheets. These groups convert hydrophobic graphite into highly soluble graphite oxide in several polar and nonpolar solvents including water.[18,19]By now the attachment of functional groups is exploited by the well-established intercalation chemistry[20,21,22]leading to graphene-based hybrid materials for polymer composites, electrochemical sensors and biosensors, fillers in composite materials for engineering applications, supercapacitors, energy storage and environmental applications.[23,24,25,26,27,28,29]

The adsorption of organic molecules on carbon surfaces has been studied extensively for many years.[30,31,32] However, up to now, a mechanism for covalent or non-covalent functionalization of graphene sheets through chemical grafting or π-π interactions respectively, using aromatic molecules has not been reported in the literature. Studies on carbon nanotubes (CNTs) have shown strong adsorption affinity with many organic contaminants including polycyclic aromatic hydrocarbons[33,34,35,36] where the high adsorptive interactions of CNTs and aromatic molecules derive from the π-π electron donor-acceptor interaction between the graphene sheets (donors) and the CNTs (acceptors).[37] In this chapter we demonstrate for the first time the mechanism, by which two aromatic molecules, aniline and naphthalene amine, interact with the graphite oxide matrix and form new intercalated hybrid nanostructures. The structure and properties of this new class of materials may lead to potential promising applications such as environmental or electronic and adsorbents in water treatment, catalysis, solid state gas sensors and energy storage devices.

9.2 Experimental section

Materials. Preparation of graphite oxide (GO):(see chapter 2.2.1)

Preparation of GO intercalated with aniline (GO_A): A sample of 100 mg of graphite oxide was dispersed in 100 mL of distilled deionized water (H_2O) and the dispersion was stirred for 24 h at ambient conditions. Afterwards we increased the pH of the solution to 10 by adding (dropwise) NaOH 0.5 M. Then 0.3 ml of aniline were added (dropwise) to 20 mL of distilled deionized H_2O and the solution left stirring for 24 h while being mildly heated at 40 °C. Finally the solution of aniline was added to the one of GO. After stirring for 48 h, the GO_A aggregates were washed with distilled deionized water three times, separated by centrifugation and air-dried by spreading on glass plates.

Preparation of GO intercalated with naphthalene amine (GO_NA): In a similar experiment al procedure 100 mg of graphite oxide were dispersed in 100 mL of distilled deionized H_2O and the mixture was stirred for 24 h in air. The pH was increased to 10 by adding (dropwise) NaOH 0.5 M. A solution of naphthalene amine (300 mg) in distilled deionized H_2O (20 mL) was then added dropwise to the GO dispersion and the mixture was stirred for 24 h in ambient conditions. The final solution was washed with distilled deionized H_2O three times, separated by centrifugation and air-dried by spreading on glass plates.

Characterization techniques. X-ray photoelectron spectroscopy (XPS): (see chapter 2.1.1). All binding energies were referenced to the C 1s core level line[38] of the C-C bond at 285.0 eV and are given ±0.1 eV.

X-ray diffraction (XRD): (see chapter 2.1.2)

9.3 Results and discussion

9.3.1 X-ray diffraction

The intercalation of aniline and naphthalene amine molecules into the interlayer space of graphite oxide was demonstrated by X-ray diffraction measurements. Figure 9.1 displays the XRD pattern of graphite oxide (GO), and graphite oxide after reaction with aniline (GO_A) and naphthalene amine (GO_NA) respectively. We observe a shift to lower angles of the diffraction peak for both the GO_A and GO_NA hybrid nanostructures as compared to GO, indicating a larger distance between the graphene layers and therefore pointing to the successful intercalation of the aromatic species. In detail, for GO_A the basal d_{001}increased to 8.6±0.3 Å while for GO_NA the d_{001} space amounted to 8.1±0.3 Å. Taking into account the interlayer distance of GO (6.1 Å)[39] we estimate the opening of the graphene oxide layers after the insertion of the aromatic amines: in the case of aniline intercalation this additional opening amounts to ~2.5 Å, while for naphthalene amine intercalation it is ~2.0 Å. To explain the type of interaction between the aromatic molecules and the graphene sheets, we employed X-ray photoelectron spectroscopy.

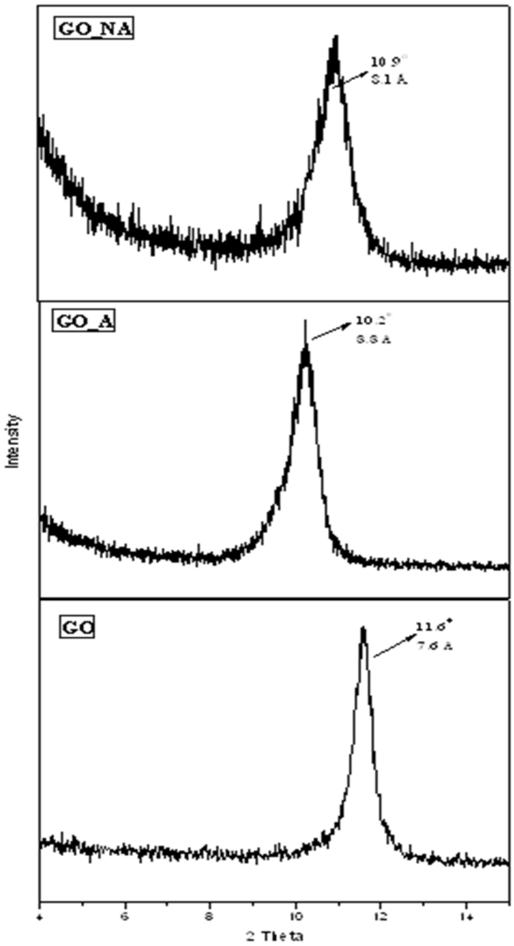

Figure 9.1 Comparative XRD of graphite oxide (GO), graphite oxide intercalated aniline (GO_A) and graphite oxide intercalated naphthalene amine (GO_NA).

9.3.2 X-ray photoelectron spectroscopy

Figure 9.2 (left panel) shows the C 1s core level region of the XPS spectrum of GO, which displays four contributions at 285.0 eV, 285.9 eV, 287.2 eV and 288.3 eV binding energy. The peak at 285.0 eV originates from carbon-carbon bonds of the hexagonal lattice, and accounts for 22.8 % of the total carbon intensity. The contribution at 287.2 eV is due to the C=O functional groups and accounts for

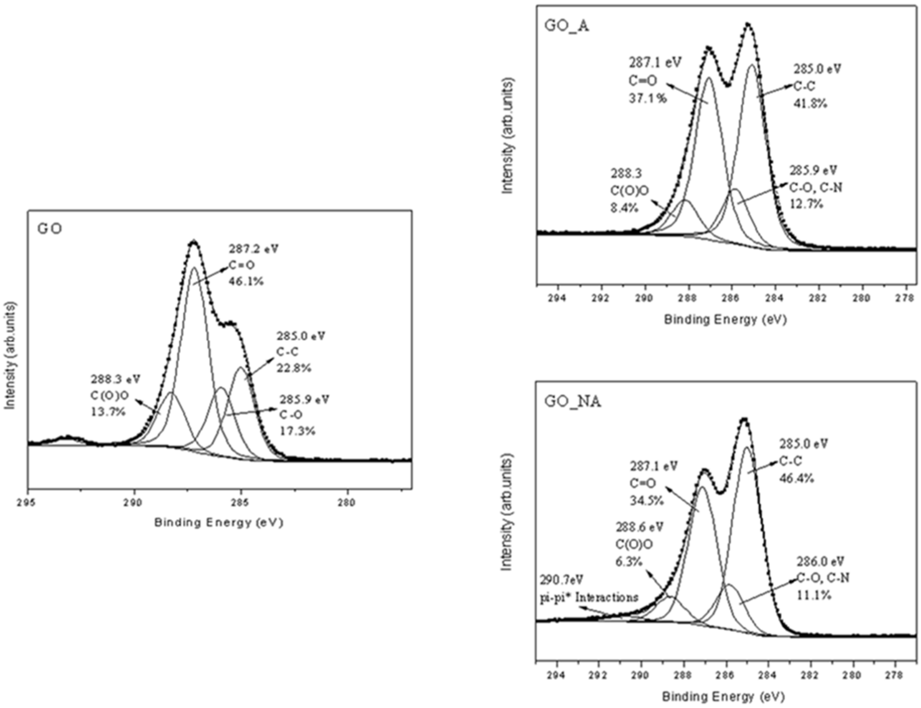

Figure 9.2 X-ray photoelectron spectra of the C 1s core level region of graphite oxide (GO), graphite oxide intercalated with aniline (GO_A) and graphite oxide intercalated with naphthalene amine (GO_NA).

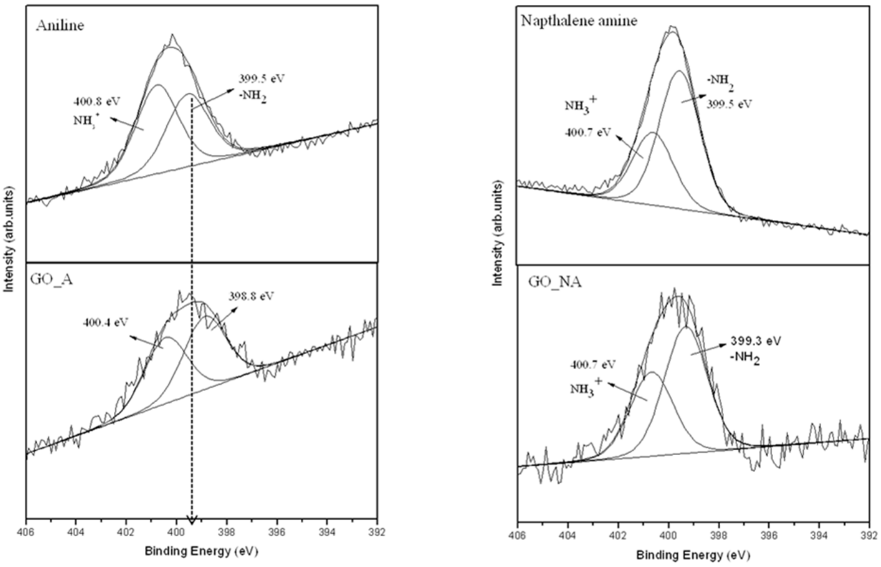

Figure 9.3 X-ray photoelectron spectra of the nitrogen 1s core level region of aniline, graphite oxide intercalated with aniline (GO_A), and graphite oxide intercalated with naphthalene amine (GO_NA).The spectrum of a drop cast film of naphthalene amine is also shown for comparison.

46.1 % of the total carbon intensity. Two peaks centered at 285.9 eV and 288.3 eV arise from the C-O and C(O)O bonds, representing 17,3 % and 13.7 % of the total carbon 1s peak intensity, respectively.

After the intercalation of aniline and naphthalene amine into the GO galleries, the chemical composition of the resulting hybrid nanostructures changed in comparison with the starting material. In the carbon 1s spectra of GO_A and GO_NA (shown in the right panel of Figure 9.2) we observe a significant increase of the intensity of the peak due to C-C bonds centred at 285.0 eV. More specifically the relative intensity of this contribution rises to 41.8% for GO_A and to 46.4% in the case of GO_NA, demonstrating the presence of a carbonaceous material co-existing with the GO lattice. The peaks at 285.9 eV (12.7 %) for GO_A and 286.0 eV (11.1 %) for GO_NA hybrids correspond to the C-O bonds of the GO lattice as well from the C-N functional groups of the aromatic species. Finally, in the case of GO_A two more peaks at 287.1 eV (37.1 %) and 288.3 eV (8.4%) reveal the presence of carbonyl and carboxyl groups, respectively in our final material. On the other hand, for GO_NA in addition to the peaks corresponding to the carbonyl groups at 287.1 eV (34.5%) and to the carboxyl groups at 288.6 eV (6.3%) we clearly observe the existence of the shake up satellite peaks from the π-π transitions of the benzene rings and the graphite sheets at 290.7 eV,[40] in contrast with the GO_A nanostructure, where this peak is absent. From this we can conclude that naphthalene amine prefers to bind between the graphene sheets via π-π interactions, while aniline chemically binds to the functional groups of graphene oxide via ringopening reactions of the epoxy groups of GO.[41,42] The ratio of the total intensities of the carbon 1s to oxygen 1s photoemission lines for GO, GO_A and GO_NA is presented in Table 9.1. This ratio increased after intercalation of aniline from 1.62 to 2.12 and after intercalation of naphthalene amine from 1.62 to 2.91.

Additional significant information on the type of interaction of aniline and naphthalene amine with the graphene oxide sheets comes from the N 1s core level region of the photoelectron spectra of GO_A and GO_NA (shown in Figure 9.3). The spectrum of both the aniline and the naphthalene amine intercalated structures can be deconvoluted into two main peaks placed at ~399.5 eV and ~400.8 eV binding energy, which correspond to amine groups and protonated amines of the aromatic species, respectively.[43] For GO_A and GO_NA we see clear differences stemming from how aniline and naphthalene amine interact with the graphene oxide layers. In the case of GO_A, the photoelectron peak attributed to amine groups of aniline is shifted to lower binding energies (398.8 eV), pointing to the creation of a chemical bond with the epoxy groups of GO (C-N-C bond)[44,45,46]. Taking into account the size of aniline and combining the informing about the covalent bonding with the XRD data, we conclude that these molecules must have an inclined orientation when inserted between the graphene sheets. For GO_NA we do not observed any significant change on the N 1s XPS spectrum with respect to that of a drop cast film of naphthalene amine (presented in the right top panel of Figure 9.3 right). This matches with interpretation of the C 1s XPS spectrum of GO_NA because in the case of π-π interactions the amine functional groups do not participate in any interactions but are present as free groups inside the graphene galleries (scheme 9.2).

Table 9.1 Ratio of the total intensities of the carbon 1s to oxygen 1s photoemission lines for GO, GO_A and GO_NA

GO	GO_A	GO_NA
1.62±0.03	*2.12±0.06*	*2.91±0.06*

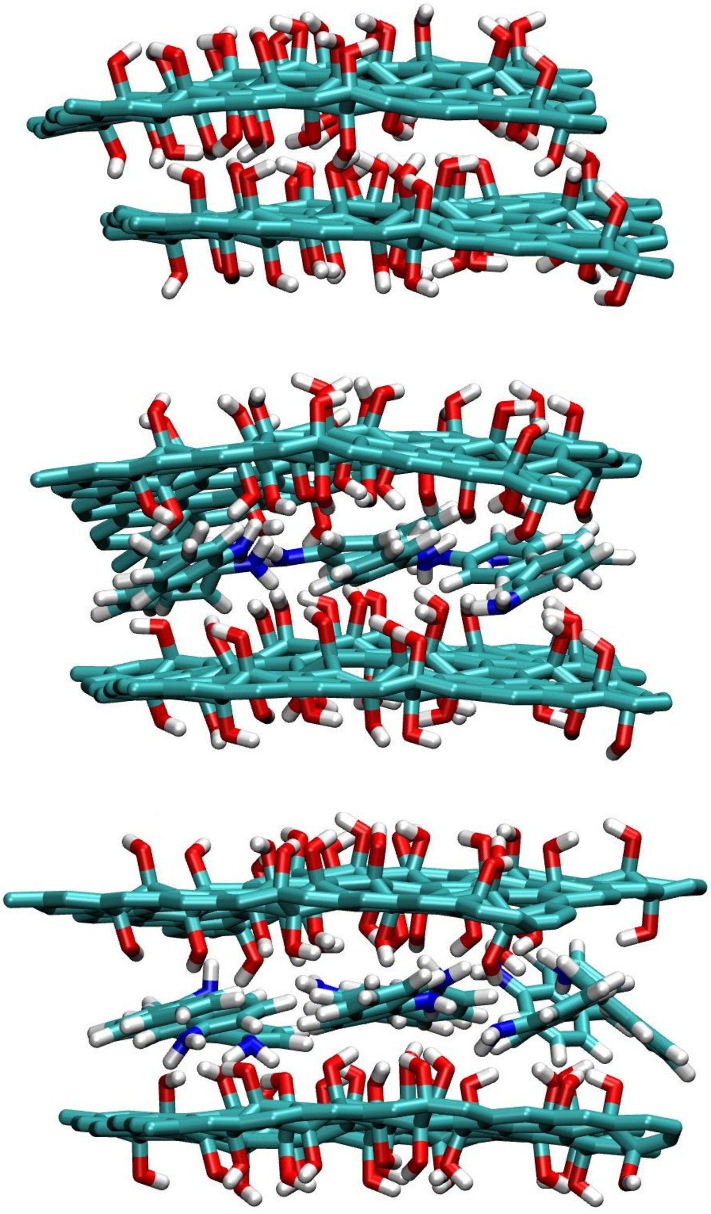

Figure 9.4 Conformation of GO (top), of aniline when intercalated between graphite oxide sheets (centre) and of naphthalene amine when intercalated between graphite oxide sheets (bottom) as resulting from the simplified molecular dynamics simulations [see text below].

9.4 Molecular dynamics simulations

To get further insight into the interaction of of anilene and naphthalene amine with GO, Francesco Zerbetto's group at the University of Bologna has been performing molecular dynamics simulations. For the time being only the results from the first short trial run ("quick and dirty", 1 ns) are available, where to simplify the calculation time only OH groups were introduced on GO. The results of these simulations are shown in Figure 9.4 and seem to support the experimental findings. Some interesting issues arose and will have to be tackled in the next steps: 1) the interlayer distance in GO depends on the amount of water, however, here no water was included. In the future, the calculation will have to be repeated with the amount of water determined from the thermogravcimetric analysis discussed above). 2) The simulations found that aniline is much more mobile between the GO layers than naphthalene amine, which implies that it is able to locate the most reactive point(s) of GO. Organic chemistry also suggests that aniline is more basic than naphthalene amine and should therefore be more reactive with the epoxy groups.

9.5 Conclusions

In this study we have observed the successful intercalation of common organic polycyclic aromatic compounds between the layers of graphite oxide (GO), and examined in detail the mechanism by which each molecule interacts with the graphene oxide surface. We demonstrate that the type of interaction for aniline and naphthalene amine with the graphene oxide layers differs according to the size of the aromatic molecules. More specifically we have shown that aniline covalent binds with the graphite oxide matrix through chemical grafting, while naphthalene amine prefers to adsorb on the surface of graphene oxide by π-πinteractions. This novel class of hybrid materials opens new horizons in intercalation chemistry and may drive potential applications in electronics, energy storage and environmental remediation.

References

[1] Novoselov, K. S.; Geim, A. K.; Morozov, S. V.; Jiang, D.; Zhang, Y.; Dubonos, S. V.; Grigorieva, I. V.; Firsov, A. A. *Science* **2004**, 306, 666-669.

[2] Geim, A. K.; Novoselov, K. S. *Nat. Mater.* **2007,** 6, 183–191.

[3] Wu, J.; Pisula, W.; Müllen, K.*Chem. Rev.* **2007**, 107, 718–747.

[4] Balandin, A. A.; Ghosh, S.; Bao, W.; Calizo, I.; Teweldebrhan, D.; Miao, F.; Lau, C. N. *Nano Lett.* **2008**, 8, 902–907.

[5] Kim, K. S.; Zhao, Y.; Jang, H.; Lee, S. Y.; Kim, J. M.; Kim, K. S.;Ahn, J. -H.; Kim, P.; Choi, J. -Y.; Hong, B. H. *Nature* **2009**, 457, 706–710.

[6] Bae, S.; Kim, H.; Lee, Y.; Xu, X.; Park, J. -S.; Zheng, Y.; Balakrishnan, J.; Lei, T.;Ri Kim, H.; Song, Y. I.; Kim, Y. -J.; Kim, K. S.; Özyilmaz, B.;Ahn, J. -H.; Hong, B. H.;Iijima, S. *Nat. Nanotechnol.* **2010**, 5, 574–578.

[7] Tombros, N.; Jozsa, C.; Popinciuc, M.; Jonkman, H. T.;Van Wees, B. J. *Nature* **2007**, 448, 571–574.

[8] Stankovich, S.; Dikin, D. A.; Dommett, G.H. B.; Kohlhaas, K. M.; Zimney, E. J.; Stach, E. A.; Piner, R. D.; Nguyen, S. T.; Ruoff, R. S. *Nature* **2006**, 442, 282–286.

[9] Brey, L.; Fertig, H. A. *Phys. Rev.B* **2006**, 73 (23), 235411.

[10] Schedin, F.;Geim, A. K.;Morozov, S. V.; Hill, E. W.; Blake, P.;Katsnelson, M. I.;Novoselov, K. S. Nat. Mater. **2007**, 6, 652–655.

[11] Stankovich, S.; Dikin, D. A.; Dommett, G. H. B.; Kohlhaas, K. M.; Zimney, E. J.; Stach, E. A.; Piner, R. D.; Nguyen, S. T.; Ruoff, R. S. *Nature* **2006**, 442, 282–286.

[12] Verdejo, R.; Barroso-Bujans, F.; Rodrı´guez-Pe´rez, M. A.; de Saja, J. A.; Lo´pez-Manchado, M. A. *J. Mater. Chem.* **2008**, 18, 2221–2226.

[13] Segal, M. *Nat. Nanotechnol.* **2009** , 4 , 612-614.

[14] Boehm, H. P.; Clauss, A.; Fischer, G. O.; Hofmann, U. *Z. Naturforsch. B* **1962**, 17, 150-153

[15] Brodie ,B. C. *Ann. Chim. Phys.* **1860**, 59, 466-472.

[16] Staudenmaier, L. *Ber. Deut. Chem. Ges.* **1898**, 31, 1481-1487.

[17] Hummers, W. S.; Offeman, R. E.*J. Am. Chem. Soc.* **1958**, 80, 1339.

[18] Bourlinos, A. B.; Gournis, D.; Petridis, D.; Szabo, T.; Szeri, A.; Dekany, I. *Langmuir* **2003**, 19, 6050–6055.

[19] Dreyer, R. D.; Park, S.; Bielawski, C. W.; Ruoff, R. S. *Chem Rev Soc* **2010**;, 39, 228–40.

[20] Bissessur, R.; Liu, P.K. Y.; Scully, S. F. *SyntheticMet.* **2006**, 156, 1023–1027.

[21] Meng, N.; Zhang, S.-Q.; Zhou, N.-L.; Shen, J. *Nanotechnology* **2010**, 21, 185101.

[22] Hagenmuller, P. *J. Phys. Chem. Solids* **1998**, 59, 503–506.

[23] Stankovich, S.; Dikin D. A.; Dommett, G. H. B.; Kohlhaas, K. M.; Zimney, E. J.; Stach, E. A. *Nature* **2006**, 442, 282–286.

[24] Shao, Y.; Wang, J.; Wu, H.; Liu, J.;Aksay, I. A.; Lin, Y.*Electroanalysis* **2010**, 22, 1027–36.

[25] Wang, Y.; Shi, Z.; Huang, Y.; Ma, Y.; Wang, C.; Chen, M.; Chen, Y.*J. Phys.Chem. C* **2009**, 113, 13103–13107.

[26] Chen, W.; Duan, L.; Zhu, D. *Environ.Sci. Technol.* **2007**, 41, 8295–8300.

[27] Wang, L.; Lee, K.; Sun, Y. -Y.; Lucking, M.; Chen, Z.;Zhao, J. J.; Zhang, S. B. *ACS Nano* **2009**, 3, 2995–3000.

[28] Guo, J.; Wang, R.;Tjiu, W. W.; Pan, J.; Liu, T. *J. Hazard.Mater.* **2012**, 225-226, 63–73.

[29] Jin, Z.;Lomeda, J. R.; Price, B. K.; Lu, W.; Zhu, Y.; Tour, J. M.*Chem Mater* **2009**, 21, 3045–3047.

[30] Zhu, D.;Pignatello, J. J.*Environ. Sci. Technol.* **2005**, 39, 2033–2041.

[31] Xu, Y.; Bai, H.; Lu, G.; Li, C.; Shi, G.; *J. Am. Chem. Soc.***2008**, 130, 5856–5857.

[32] Rochefort, A.; Wuest, J. D. *Langmui r***2009**, 25, 210–215.

[33] Yang, K.; Zhu, L.; Xing, B. *Environ. Sci. Technol.* **2006**, 40, 1855–1861.

[34] Chen, W.; Duan, L.; Zhu, D. *Environ. Sci. Technol.* **2007**, 41, 8295–8300.

[35] Chen, R. J.; Zhan, Y. G.; Wang, D. W.; Dai, H. J. *J. Am. Chem. Soc.* **2001**, 123, 3838. (b) Nakashima, N.; Tomonari, Y.; Murakami, H. *Chem. Lett.* ***2002***, 31, 638-639.

[36] Nakayama-Ratchford, N.; Bangsaruntip, S.; Sun, X.; Welsher, K.; Dai, H. J. *J. Am. Chem. Soc.* **2007**, 129, 2448-2449.

[37] Chen, W.; Duan, L.; Zhu, D.*Environ. Sci. Technol.* **2007**, 41, 8295–8300.

[38] Lotya, M.; Hernandez, Y.; King, P. J.; Smith, R. J.; Nicolosi, V.; Karlsson, L. S.; Blighe, F. M.; De, S.; Wang, Z.; McGovern, I. T.; Duesberg, G. S.; Coleman, J. N. *J. Am. Chem. Soc.* **2009**, 131, 3611-3620

[39] Dekany, I.; Kruger-Grasser, R.; Weiss, A. *Colloid Polym. Sci.* **1998**, 276, 570-576.

[40] Biniak, S.; Szymanski, G.; Siedlewski, J.; Swiatkowvski, A. *Carbon* **1997**, 35, 1799-1810.

[41] Bourlinos, A. B.; Gournis, D.; Petridis, D.; Szabo, T.; Szeri, A.; Dekany, I. *Langmuir* **2003**, 19, 6050-6055.

[42] Gengler, R. Y. N.; Veligura, A.; Enotiadis, A.; Diamanti, E. K.; Gournis, D.; Jozsa, C.; van Wees, B. J.; Rudolf, P. *Small* **2010**, 6, 35-39.

[43] Moses, P. R.; Wier, L. M.; Lennox, J. C.; Finklea, H. O.; Lenhard, J. R.; Murray, R. W. *Anal Chem***1978**, 50, 576–85.

[44] Ektessabi, A. M.; Hakamata, S. *Thin Solid Films* **2000**, 377-378, 621–625.

[45] Shin, J. -W.; Jeun, J. -P.; Kang, P.-H. *Macromol.Res.* **2010**, 18, 227–232.

[46] Herrera-Alonso, M.; Abdala, A. A.; McAllister, M. J.;Aksay, I. A.; Prud'homme, R. K. *Langmuir* **2007**, 23, 10644–10649.

Appendix A

Clays

A.1 History

"Clay" has been defined differently by geologists, mineralogists and soil scientists through time. Historically the word clay was used to define small inorganic particles smaller than <2 μm portion of soil (heterogeneous mixture of fluids and particles like clays, sand), without any reference to composition or crystallinity. The most recent definition classifies clays as a group of phyllosilicate (phyllo = sheet like structure) minerals based on hydrous aluminium or magnesium silicates that have layered (sheet) structure. Clays were mentioned already in Ancient Greece for their applications in ceramics (bricks) and, exceptionally, as pigments. Herodot (430 B.C) and Xenofon (355 B.C), refer to Babylonian walls made of brick (Figure A.1),and Aristotle (384-322 B.C) mentions clay in his general theory about bodies "quarried'' and bodies "mined"; the first reference to clay as part of mineralogy comes from Theophrastus (372-287 B.C).[1]

The definition of clay was first formalized by Agricola in his famous handbook of mineralogy, with the title 'De Natura Fossilium' (1546). Finally in 1995 both the nomenclature committees of AIPEA and CMS report the definition of clay and clay mineral. According to these reports the term clay refers to "*a naturally occurring material composed primarily of fine-gained minerals which is generally plastic at appropriate water contents and will harden when dried or fired. Although clay usually contains phyllosilicates, it may contain other materials that impart plasticity and harden when dried or fired. Associated phases in clay may include materials that do not impart plasticity and organic matter.*" and to clay minerals as "*phyllosilicate minerals and minerals which impart plasticity to clay and which harden upon drying or firing*"

A.2 General Description

Every clay mineral contains two types of sheets. The main structural unit is the tetrahedral sheet of silicon oxide (SiO_4). Silicon (Si) is located in the centre of the tetrahedral and connected covalently with four oxygen (O) atoms at the edges. Every tetrahedral unit shares three of the oxygens with neighbouring tetrahedra leading to the creation of a 2-dimensional (2-D) sheet (Figure A.2 above). The second significant structural unit of clays is the octahedral unit, which consists of Al^{+3}, Mg^{+2} or $Fe^{+2,+3}$ placed in the centre of the octahedral and connected with six oxygen (O) or hydroxyl (OH) groups at the edges. Every octahedron shares four O with neighbouring octahedra, resulting in the creation of an octahedral sheet as illustrated in Figure A2.

.[2]

Figure A.1. Original walls of ancient Babylon.

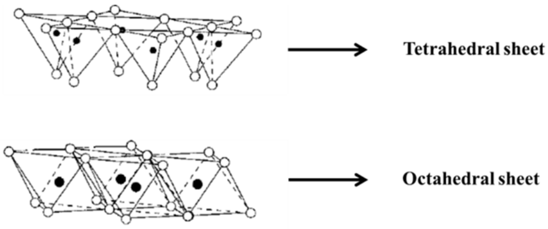

Figure A.2. Schematic representation of tetrahedral and octahedral sheets where the black spots refer to Si and Al/or Mg atoms, respectively and white spots represent the oxygen atoms.

Clays can be classified in categories based on many criteria. The most common classifications of phyllosilicate minerals consider the type of sheets (2:1 or 1:1), their structural formula, and the cation exchange capacity (will be discussed in detail below). These properties categorize them in subgroups. In this project we worked with montmorillonite, a clay mineral that belongs to the family of smectite clays.

Smectite clays are a class of layered aluminosilicate minerals with a unique combination of swelling, intercalation and ion exchange properties that make them valuable nanostructures in different fields of high interest.[3,4] Their structure consist of an octahedral alumina layer fused between two tetrahedral silica layers as sketched in Figure A.3.

In the tetrahedral sheet Al^{+3} can replace Si^{+4} creating a negative charge. Occasionally Fe^{+3} cations are also present in the tetrahedral lattice. In the octahedral sheets negative charging may occur by substitution of Mg^{+2} for Al $^{+3.}$ Many other transition metals have been found in the octahedral sheets including Fe^{+2}, Fe^{+3}, Mn^{+2}. Because of the negative charge on the clay lattices due to isomorphous substitutions, charge neutrality is obtained by compensating cations between the basal planes. They are monovalent or sometimes divalent and surrounded by water molecules, (hydrated cations) as shown in Figure A.4.

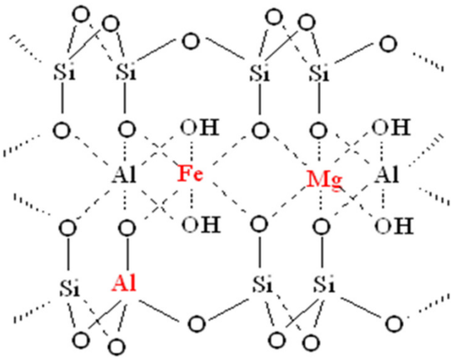

Figure A.3. Schematic representation of montmorillonite clay.

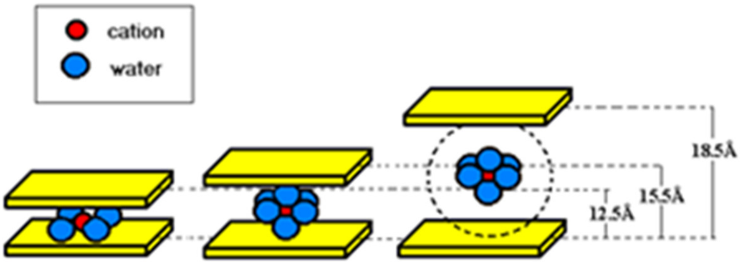

Figure A.4. Swelling properties of clay minerals.

The quantity of cations between the clay sheets, which is characteristic for each class of clay mineral, is called cation exchange capacity (CEC), and expressed in meq of exchange cations per mass of clay (see Figure A.5). For these systems, intercalation is equivalent with ion exchange, and unlike for graphite intercalation compounds, does not involve necessarily charge transfer between host and guest species. Clays have the natural ability to adsorb organic or inorganic guest cationic species (and even neutral molecules) from solutions, and it is this cation "storage" that allows for clay minerals to be used as catalysts,[5,6]templates[7,8] in organic synthesis, or as building blocks for composite materials.[9-14] The nature of the microenvironment between the aluminosilicate sheets regulates the topology of the intercalated molecules and affects possible supramolecular rearrangements or reactions, such as self-assembling processes that are usually difficult to control in solution.[9–16]

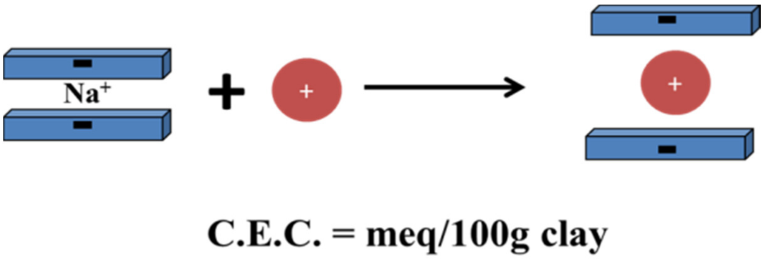

Figure A.5. Intercalation process on a clay mineral by ion exchange.

References

[1] Pabst, W.; Kořánová, R. *Acta Geodynamica et Geomaterialia* **2009**, 6, 87–100.

[2] Guggenheim, S.; Martin, R.T. *Clays and Clay Minerals* **1995**, 43, 255–256.

[3] (a) Pinnavaia, T. J. *Science* **1983**, 220, 365. (b) Konta, J. *Appl. Clay Sci.***1995**, 10, 275. (c) Lagaly, G. *Solid State Ionics* **1986**, 22, 43.

[4] Newman, A. C. D. *Chemistry of Clays and Clay Minerals*; Mineralogical Society Monograph, No. 6; Longman: London, **1987**.

[5] Ballantine, J. A. *NATO-ASI Ser., Ser. C* **1986**, 165, 197.

[6] Cornelis, A.; Laszlo, P. *NATO-ASI Ser., Ser. C* **1986**, 165, 213.

[7] Georgakilas, V.; Gournis, D.; Petridis, D. *Angew. Chem., Int. Ed.***2001**, 40, 4286.

[8] Georgakilas, V.; Gournis, D.; Bourlinos, A. B.; Karakassides, M. A.; Petridis, D. *Chem.Eur. J.* **2003**, 9, 3904.

[9] Theng, B. K. G. *Chem. Clay Org. React.***1974**, Adam Hilger: London.

[10] Kloprogge, J. T. *J. Porous Mater.* **1998**, 5, 5.

[11] Gil, A.; Gandia, L. M.; Vicente, M. A. *Catal. Rev. Sci. Eng.***2000**, 42, 145.

[12] Ma, Y.; Tong, W.; Zhou, H.; Suib, S. L. *Micropor. Mesopor. Mat.* **2000**, 37, 243.

[13] Ohtsuka, K. *Chem. Mater.***1997**, 9, 2039.

[14] Shichi, T.; Takagi, K. J. *Photochem. Photobiol., C***2000**, 1, 113.

[15] Gournis, D.; Georgakilas, V.; Karakassides, M. A.; Bakas, T.; Kordatos, K.; Prato, M.; Fanti, M.; Zerbetto, F. *J. Am. Chem. Soc.* **2004**, 126, 8561.

[16] Gournis, D.; Jankovic, L.; Maccallini, E.; Benne, D.; Rudolf, P.; Colomer, J. F.; Sooambar, C.; Georgakilas, V.; Prato, M.; Fanti, M.; Zerbetto, F.; Sarova, G. H.; Guldi, D. M. *J. Am. Chem. Soc.* **2006**, 128, 6154.

Appendix B

X-ray photoelectron spectroscopy

B.1 History

The idea and subsequent development of X-ray photoelectron spectroscopy, XPS in short, is strongly connected to the discovery of the photoelectric effect by Heinrich Hertz in 1887, in which X-rays were used as exciting photon source.[1] The photoelectric phenomenon, sketched in Figure B.1(a), was ideally explained later in 1905 by Albert Einstein, who suggested the wave-particle duality of light that can only be understood using the quantum theory (Nobel Prize 1921). Two years later in 1907, P.D. Innes experimented using a Roentgen tube, Helmholtz coils, a magnetic field hemisphere and photographic plates in order to record broad bands of emitted electrons as a function of velocity, and this was the first XPS spectrum ever recorded.[2] Other researchers, such as Moseley, Rawlinson and Robinson, independently performed various experiments trying to figure out the details in those broad bands. After a non-productive scientific period due to the second world war, Kai Siegbahn and his group at the University of Uppsala, Sweden, made a significant step concerning improvements in the equipment and finally in 1954 is recorded the first high-energy resolution XPS spectrum of cleaved sodium chloride (NaCl), which revealed the potential of XPS. A few years later, in 1967, Siegbahn published an ample study on XPS resulting on the immediate recognition of the values of XPS.[3] In co-operation with Siegbahn, Hewlett-Packard in the USA produced the first commercial monochromatic XPS instrument in 1969. Siegbahn received the Nobel Prize in 1981 for his wide efforts to develop XPS into a useful analytical tool. Since then, XPS is one of the most important techniques for surface analysis.

B.2 General description

X-ray photoelectron spectroscopy is a quantitative spectroscopic technique that supplies useful information about the elemental composition, as well the chemical environment and electronic state of the elements composing a probed volume reaching from the surface to a depth of several nm (<10nm) into the sample.[1]The sample to be analyzed is bombarded with a monochromatic X-ray beam of known energy, hν, giving rise to the emission of electrons with kinetic energy (E_k), where $E_k<h\nu$, owing to the photoelectric effect (Figure B.1(b)).

The kinetic energy of the ejected electrons (photoelectrons) can be measured by an electron energy analyzer, and from this the binding energy of the electron is defined by the equation:

$$E_k=h\nu-E_b-\Phi_{sp}$$

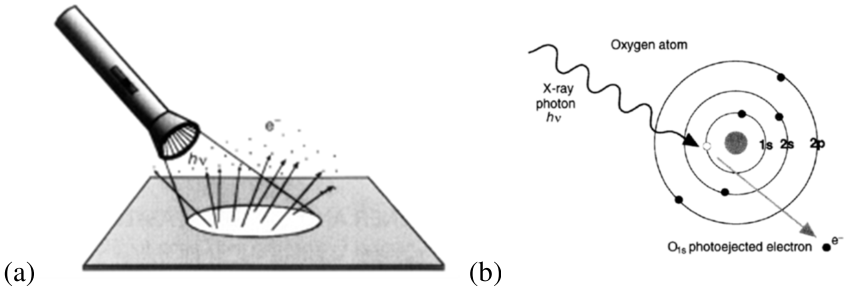

Figure B.1(a) Schematic representation of the photoelectric effect. (b) Photoelectric effect as an analytical tool.

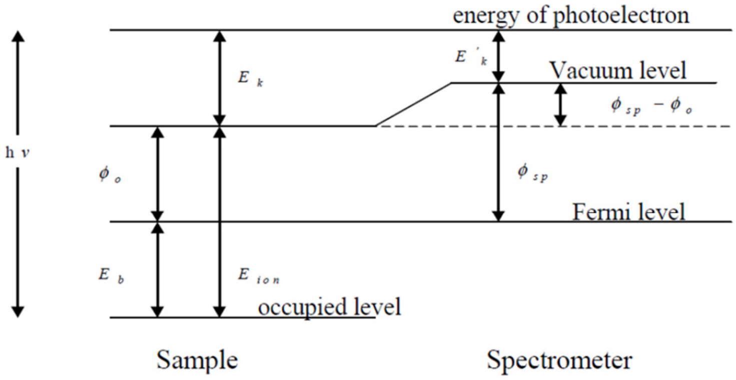

$$h\nu = E_b + E_k + \phi_0$$

Figure B.3 Schematic diagram of the photoemission process. The surface is irradiated with X-rays of known energy, hν, and electrons of kinetic energy E_k are ejected. Φ_o is the work function of the sample, and these electrons reach the detector with work function Φ_{sp} where their kinetic energy E_k is measured.

where hν represents the energy of the incident X-ray beam, Φ_{sp} is the spectrometer work function, the minimum amount of energy one electron needs to escape from the surface. A detailed representation of the photoemission process which also takes into account the sample work function, Φ_o, is shown on an energy level diagram in Figure B.2 for a sample in electrical contact with the spectrometer.

In this thesis we are interested in ejected photoelectrons coming from the core levels, which do not participate in any kind of chemical bonding. As sketched in Figure B.1(b) each element is characterized by a specific electronic configuration and will therefore give rise to a unique set of electrons with specific binding energies (E_b) in the X-ray photoelectron spectrum. Such a spectrum, which reports the number of photoelectrons as a function of the binding (or kinetic) constitutes a fingerprint of the elements compose the surface as shown in Figure B.3, where several core levels of gold, carbon, oxygen, nitrogen and iron are identified. The electrons that escape without energy loss contribute to the characteristic peaks, while those that undergo inelastic energy loss contribute to the background of the spectrum.[4] The relative intensity of a core level peak is mainly governed by the atomic photoemission

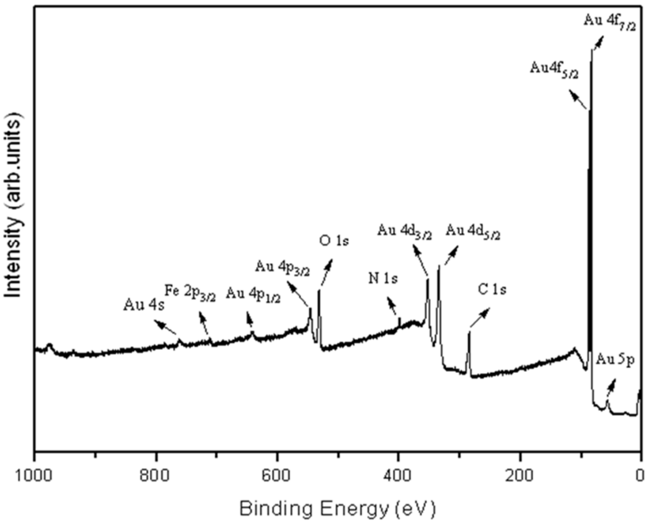

Figure B.3 A typical XPS spectrum, in which core levels of gold, carbon, iron and oxygen can be identified.

cross-section. In particular, since the cross-section of H and He when excited with X-rays is too small,[5] these elements cannot be detected by XPS.

The elemental composition of the surface is derived from the area under the core level peaks. The atomic concentration (C_A) of the element A is usually calculated as:

$$C_A = \frac{I_A / S_A}{\sum_i I_i / S_i}$$

where I_i is the area under the peak of the element i, which is proportional to the amount of i, and S_i is the relative sensitivity factor, a corrective factor that takes into account the excitation energy, the electron mean free path, the cross section and the instrumental efficiency.

B.3 Ultra-high vacuum (UHV) requirements

For the photo electrons to reach the energy analyzer after the photoemission process, avoiding any scattering inside the chamber, the mean free path should be much bigger than the dimensions of the spectrometer. This can be achieved by working in Ultra-high Vacuum (UHV) in the measuring chamber. UHV not only allows the electrons to move unperturbed into the spectrometer analyzer, it also prevents the first atomic layers of the sample from being covered by contaminant during the measuring time. In practice, the majority of experiments are carried out with a base pressure of 10^{-10} Torr, which is also the pressure we worked with most of the times.

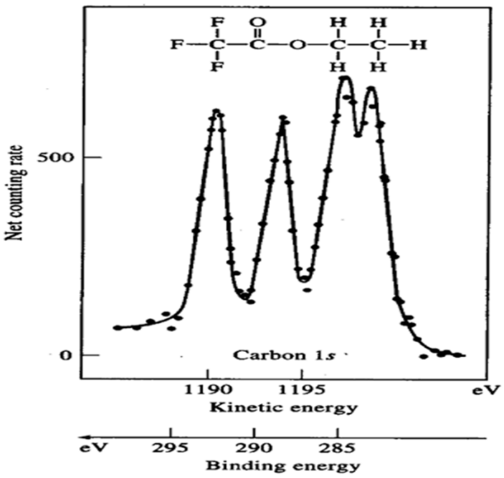

Figure B.4. C 1s core level region of the X-ray photoelectron spectrum of ethyl trifluoroacetate. Different binding energies correspond to the different chemical environment of the carbon atoms in the molecule. Adapted from Gelius et al.[7] J. Electron Spectrosc.Copyright 1974.

B.4 The chemical shift

The exact binding energy of an electron depends not only upon the core level involved in the photoemission process, but also on the oxidation state of the atom and the local chemical and physical environment. Core level binding energies are in fact determined by the Coulomb interaction of the electron with other electrons and the electrostatic interaction with the nuclei. Any change in the chemical environment of the element corresponds to different energy levels, giving rise photoelectrons with slightly different kinetic energies. As a consequence, variations in the elemental binding energies – called the chemical shifts – can be used to identify the chemical state or the chemical groups of the material being analyzed.[6] The presence of the chemical shifts gives XPS the alternative name: Electron Spectroscopy for Chemical Analysis (ESCA). Figure B.4 presents an example of chemical shift in the C 1s core level of ethyl trifluoroacetate measured in the gas phase.[7]Thestructure of the molecule is presented above the XPS spectrum. The reason we chose this molecule for the illustration of the chemical shift is that the peaks of the spectrum correspond ideally to the different chemically shifted of carbon 1s components.

The four different peaks correspond to four different shifts: the peak at the highest binding energy (~ 293.0 eV) is attributed to carbon bound to three fluorine atoms (CF_3-), while the other three peaks due to C(O)O , C-C and C-H bonds. Higher electron density around the photoemitting atom translates into lower binding energy. To quantify the elemental composition of the sample, the area under the core level peaks is calculated. Since photoelectrons from different core levels are detected with different efficiency, one has to take into account the relative sensitivity factor of each element, a corrective factor S_i that takes into account the excitation energy, the electron mean free path, the cross section and the instrumental efficiency of the element. The atomic concentration (C_A) of the element A is usually calculated as:

$$C_A = \frac{I_A / S_A}{\sum_i I_i / S_i}$$

where Ii is the area under the peak of the element i, which is proportional to the amount of i.

References

[1] Briggs, D.; Seah, M. P. '*Practical Surface Analysis by Auger and X-ray Photoelectron Spectroscopy'*, (John Wiley & Sons, Norwich, **1983**).

[2] Jenkin, J. G.; Leckey, R. C. G.; Liesegang, J. *J. Electron Spectrosc.***1977**, 12, 1.

[3] Seigbahn, K.; Nordling, C.; Fahlman, A.; Nordberg, R.; Hamrin, K.; Hedman, J.; Johansson, G.; Bergmark, T.; Karlsson, S.; Lindgren, I.; Lindberg, B.*Nova Acta Reg. Soc. Sci. Upsaliensis* **1967**, 20, 1.

[4] J. F. Watts: '*An Introduction to Surface Analysis by XPS and AES*', John Wiley &Sons Ltd. The Atrium, Southern Gate, Chichester, **2003**.

[5] Scofield, J. H. *J. Electron Spectrosc.***1976**, 8, 129.

[6] Moulder, J. K.; Stickle, W. F.; Sobol, P. E.; Bomben, K. D. '*Handbook of X-ray photoelectron Spectroscopy*', Physical Electronics, (Inc. Eden Prairie, Minnesota, **1995**).

[7] Gelius, U.; Basilier, E.; Svensson, S.; Bergmark T.; Siegbahn K.*J. Electron Spectrosc.* **1974**, 2, 405.

Appendix C

Porosimetry measurements

C.1 Introduction

Physical and synthetic materials which have the natural ability to adsorb on their surface molecules or atoms (in gas or liquid phase), thus they are described as adsorbent materials. When this adsorption arises from weak Van der Waals interactions (20-50 KJ/mol), it is called physisorption, while in the case of creation of chemical bonds (200-400 KJ/mol) between the adsorbate atoms (atoms that already have been adsorbed) and surface atoms of the solid, the process is called chemisorption.

The phenomenon of adsorption depends strictly on the surface area of the adsorbent; the larger the surface area of the solid, the higher the quantity of molecules adsorbed. At this point we have to point out that the term ‘surface’ refers also to the internal surface of the pores of the material.

The porosity describes the pore space in a material (Sing et. al.1985).[1] It defines the internal surface of the porous structure and as a consequence determines the surface area. An open pore is a cavity that communicates with the surface. In addition to the open pores on the surface, a porous material also possesses closed pores, which are inside the structure and do not interact with the surface. The closed and open pores are called interparticular porosity of the solid. Pores are classified as macropores when the pore diameter exceeds 50 nm, mesopores for pore diameter between 2 – 50 nm and micropores for (pore diameter < 2 nm as described in Figure C.1.[1]

Surface area and porosity are key physical parameters that determine the performance and behaviour of solids and powders in applications such as catalysis, separation and purification of gases and liquids, and energy storage.[2-5]

C.2 Porosimetry measurements

The definition of the surface area, as well of the pore size of a material, includes a process based on the physical adsorption of an inert gas on its surface. The molecules of the inert gas adsorb on the surface layer-by-layer. That means that when the whole surface of the material covered with the adsorbate, the second layer starts to grow on top of the first one and so on. The surface of the material is calculated from the first layer of the molecules that covers the surface, while the pore size is estimated from the whole volume of molecules that are adsorbed.

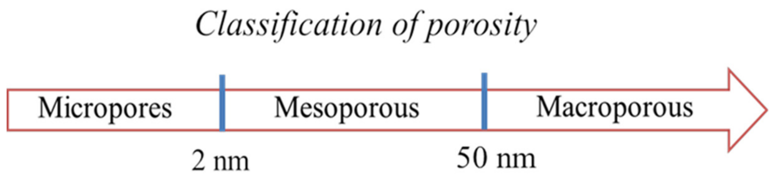

Figure C.1. Schematic representation of classification of the pore size (IUPAC1984)

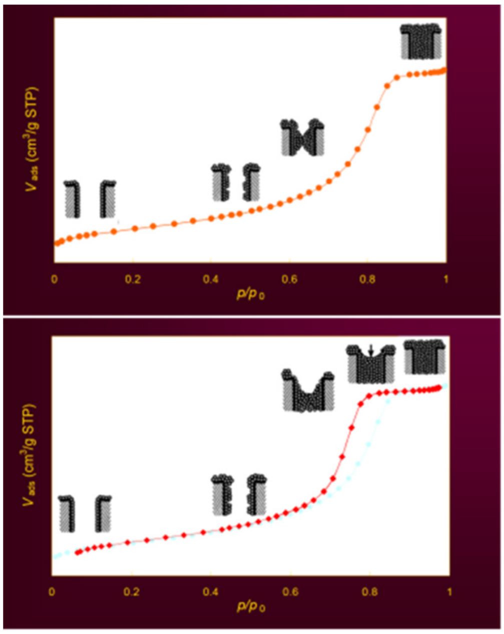

Figure C.2. Adsorption (above) and desorption (below) isotherms in different stages (S.J. Gregg and K.S.W. Sing, Adsorption, Surface Area and Porosity, 1982).

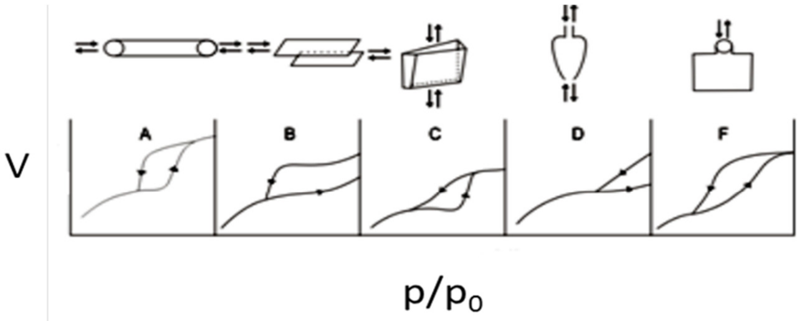

Figure C.3 The geometrical structure of the pores depending on the shape of the hysteresis loop of the adsorption-desorption isotherm (S.J. Gregg and K.S.W. Sing, Adsorption, Surface Area and Porosity, 1982).

During the adsorption of the molecules (gas phase) from the adsorbent (solid phase), a dynamic equilibrium is established between the two phases. This equilibrium depends on the temperature of the system, the concentration of the gas that has not been adsorbed (or the saturated vapour pressure, p_0) and the volume of the gas phase that has been adsorbed. As a consequence this equilibrium can be expressed with different diagrams depending on which parameter is constant every time. Here we are interested in the adsorption isotherms which give the volume of the adsorbate (per mass unit of the adsorbent) versus the pressure, while keeping the temperature constant (Figure C.2). For porous materials, the adsorption-desorption isotherms display a hysteresis loop. The shape of the hysteresis loop depends on the geometrical structure of the pores (Figure C.3). The physical explanation of this phenomenon is that the desorption of the adsorbate take place in lower values of p/p_0 than the values of pressure that acquired for the adsorption in the same temperatures. In other words: there is a hysteresis loop in the isotherms for absorption and desorption because of the difference in pressure during these two processes.

C.3 Specific Surface Area

The method of Brunauer, Emmett and Teller (BET) is a successful model that explains the adsorption of gas molecules on a solid surface for the measurement of the specific surface area.[6] This theory is an extension of the Langmuir theory*, a theory that provides information for monolayer molecule adsorption that does not describe most real cases. The specific surface area is calculated according to the BET equation (Brunauer et. al. 1938), taking into account that there is no restriction for the number of layers of adsorbate and the layers do not interact between each adsorption layer. The resulting BET equation is given by:

$$P\frac{P}{V(P_0-P)}=\frac{1}{V_m c}+\frac{c-1}{V_m c}\left(\frac{P}{P_0}\right)$$

where V is volume adsorbed, V_m volume of a monolayer, P sample pressure, P_0 saturation pressure and c constant related to the enthalpy of adsorption (BET constant). The specific surface area (SBET) is then calculated from V_m by the following equation:

$$S_{BET}=\frac{V_m n_a a_m}{mV_L}$$

where n_a is the Avogadro constant, a_m the cross sectional area occupied by each nitrogen molecule, m the weight of the sample and V_L the molar volume of nitrogen gas (22414 cm^3). The theory is based on the assumption that the first adsorbed layer involves adsorbate/adsorbent bonding energies, and the following layers the energies of the adsorbate/adsorbate interaction.

$$*\frac{1}{V}=\frac{1/P}{KV_m}+\frac{1}{V_m}\textit{Langmuir equation}$$

C.4 Total pore volume and pore size distribution

The method of Barrett, Joyner, and Halenda is a procedure for calculating pore size distributions from experimental isotherms using the Kelvin model of pore filling. It applies only to the mesoporous and small macropore size range.

The macropores are determined with mercury (Hg) porosimetry while the mesopores with nitrogen (N_2) porosimetry. From the desorption curve and based on the Kelvin equation in N_2 porosimetry, we estimate the radius of the porous from the pressure of the isotherm. The Kelvin equation is used to calculate the relative pressure of nitrogen in equilibrium with a porous solid, and applied to the size of the pores where capillary condensation takes place. The equation was presented in its original form by Thomson (1871).

$$\ln \frac{P}{P_0} = -\frac{2\gamma V_L}{rRT} \cos \theta$$

In the Kelvin equation, p is the equilibrium vapour pressure of a liquid in a pore of radius r, P_0 the equilibrium pressure of the same liquid on a plane surface, γ surface tension of the liquid, V_L molar volume of the liquid, θ the contact angle with which the liquid meets the pore wall, R the gas constant and T absolute temperature. When the meniscus of condensate is concave, capillary condensation will proceed in pores of radius r as long as the adsorptive pressure is greater than pressure p.

References

[1] Sing, K. S. W.; in Fraissard, J. P; Conner, C. W. Eds., *Dordrecht, South Holland, The Netherlands: Kluwer Academic Publishers*, **1997**, p. 6.

[2] Frackowiak, E.; Béguin, F. *Carbon* **2001**, 39, 937-950.

[3] Rodríguez-Reinoso, F. *Carbon* **1998**, 36, 159-175.

[4] Kayiran, S. B.; Lamari Darkrim, F.; Levesque, D. *J. Phys.Chem. B* **2004**, 108, 15211-15215.

[5] Steele, B. C. H.; Heinzel, A. *Nature* **2001**, 414, 345-352.

[6] Brunauer, S.; Emmett, P. H.; and Teller, E. *J.Am.Chem.Soc.* **1938**, 6, 309–319.

Summary

Carbon is the most versatile element with the greatest number of known allotropic forms like diamond, graphite and the most recently synthesized fullerenes, nanotubes and of course graphene. Due to their special properties all these allotropes have had a great scientific and technological impact in time and opened new horizons in different fields such as nanoelectronics, transistors, sensors, gas separators, catalysis, supercapacitors, and energy storage materials. Aim of this PhD project was the successful manipulation of graphene and its derivatives in order to create efficient hybrid nanostructures for multi-functional applications.

Several methods are available for the preparation of graphene. The first attempt came from Brodie, who was the first to exfoliate graphite, through strong oxidation, leading to graphene oxide sheets. More than a century after the creation of graphene oxide, the revolutionary method of micromechanical cleavage by K.S Novoselov and A.K.Geim's lead to isolated graphene sheets and revealing the outstanding properties of this exotic 2-D flat monolayer. However micromechanical cleavage is not suitable for controllable production and has an extremely low yield of graphene, hence new methods have been investigated. Among the best is the chemical vapor deposition (CVD) and epitaxial growth, facilitating the high yield production of graphene; but the good quality is hampered by the creation of defects in the lattice. In chapter 3 we review an alternative way for the production of graphene, namely chemical exfoliation of graphiteand distinguished the production of graphene oxide (GO) and all the other methods that do not involve chemical oxidation of graphene. The approach followed aimed at providing the reader with an overview of the advantages and disadvantages of each method in terms of quality, yield, structural integrity and electronic properties.

The organic functionalization of carbon nanotubes by the 1,3-dipolar cycloaddition of azomethide ylides opens new perspectives for the production of soluble and easy to handle CNTs. After the discovery of graphene a huge effort has been devoted to the chemical modification of the first stable 2-D monolayer ever found, which may help for future applications, like the utilization of graphene as robust scaffold in the construction of composite materials. In chapter 4 of this thesis we report our approach for the organic functionalization of few layer graphene by the dipolar cycloaddition method and show that functionalizing groups are distributed evenly over the sheets and their edges.

Chapter 5 is devoted to the intercalation of pure graphite with fullerene. The intercalation includes the utilization of a co-intercalant, which is introduced between the sheets of graphite first, helping to increase the interlayer distance between the graphene layers and consequently to intercalate C_{60}. The co-intercalant used in our case was nitric acid, leading to the creation of graphite nitrate (GN). The nitric acid molecules adsorb between the graphene layers with weak interactions, without affecting significantly the graphene lattice and help the fullerene molecules to intercalate by π-πstacking with the graphene layers. Heating of the final material at relatively low temperatures (100 ℃) removes the co-intercalated leaves only fullerene inside the graphite matrix. The quality of the intercalated graphite is high as demonstrated by Raman measurements. This method is a new approach for the intercalation of graphite as it does not require any oxidation treatment and subsequent reduction of the graphene lattice.

In Chapter 6 we present a new method for the creation of novel multi-functional hybrid systems through the successful intercalation of adamantylamine into the interlayer space of graphite oxide and two types of clays, natural montmorillonite clay and synthetic laponite clay. The final hybrids were characterized by a combination of X-ray diffraction, X-ray photoelectron spectroscopy, FTIR spectroscopy, thermogravimetric and differential thermal analysis in order to fully investigate their chemical structure. We

could show that these pillared materials are highly suitable for the removal of organic pollutants (chlorophenols) from water, and display significant anticancer activity in cell cultures. The proposed synthesis method will lead to the controllable bulk production of intercalated layered materials for environmental remediation and medical applications.

In Chapter 7 we describe for the first time an innovative and reproducible method for the direct formation of multi-wall carbon nanotubes by ultrasonication of graphite in dimethylformamide upon addition of ferrocene aldehyde. Ultrasonication of graphite produces sufficient energy for exfoliation in different solventsbut also creates free radicals on the graphene sheets. Ferrocene aldehyde has a double role: firstly it acts as a radical trap reducing the damage on the exfoliated graphite sheets and secondly it localizes at the edges of few layer graphene causing the sheets to roll up and form carbon nanoscrolls; the latter convert into multi-wall carbon nanotubes thanks to the ultrasound energy. The proposed method will lead to the controllable production of carbon nanostructures by simple ultrasonication treatments.

Chapter 8 is devoted to the intercalation of aluminium clusters into the interlayer space of graphite oxide and the subsequent behaviour of the derived intercalated structure upon heating. After the synthesis of Keggin ion $[A1_{13}(O)_4(OH)_{24}(H_2O)_{12}{}^{7+}]$, we intercalated the aluminium polycation between the layers of graphene oxide. X-ray diffraction and X-ray photoelectron spectroscopy testify to the success of our method. This hybrid material is promising for applications like catalysis, gas or liquid separation and energy storage.

Finally in chapter 9 we report the intercalation of organic cyclic aromatic molecules in the interlayer space of graphite oxide. We studied two aromatic molecules (aniline and naphthalene amine) and investigated the type of bonding with the graphitic sheets. Aniline binds on the graphene oxide layer via covalent bonding to the epoxy groups, while naphthalene amine prefers to attach to the graphene surface through π-πinteractions. This new class of hybrid materials opens the horizons for the intercalation chemistry of aromatic molecules into graphene-based nanomaterials.

Therefore the aim of this thesis, namely the synthesis and manipulation of novel pillared materials based on graphene, was successfully achieved, opening the way for further investigation of their properties and for their utilization in innovative applications.

Samenvatting

Koolstof is het meest veelzijdige element met het grootste aantal bekende allotrope vormen zoals diamant, grafiet en de meest recente gesynthetiseerde fullerenen, nanobuizen en natuurlijk grafeen. Door hun speciale eigenschappen hebben deze allotropen een grote wetenschappelijke en technologische impact gehad in de geschiedenis. Ook hebben deze eigenschappen nieuwe inzichten opgeleverd op verschillende gebieden zoals nano-elektronica, transistors, sensoren, gasscheiders, katalyse, supercondensatoren en energieopslag materialen.

Het doel van dit promotieonderzoek was het succesvol manipuleren van grafeen en de derivaten om operatieve hybride nanostructuren voor multifunctionele toepassingen te creëren.

Er is een aanzienlijk aantal methoden beschikbaar voor de bereiding van grafeen. De eerste poging is afkomstig van Brodie, hij was de eerste die door middel van sterke oxidatie grafiet deed exfoliëren wat leidde tot grafeen oxide vellen.

Meer dan een eeuw na het creëren van grafeen oxide leidde de revolutionaire methode van micromechanische splitsing door K.S Novoselov en A.K Geim tot geïsoleerde grafeenvellen en het onthullen van de buitengewone eigenschappen van deze exotische 2-D vlakke monolaag.

Echter het ontbreken van een regelbare productie en de zeer lage opbrengst van grafeen resulteerde in het onderzoeken van nieuwe methoden. Onder de beste methoden behoren chemical vapor desposition (CVD) en epitaxiale groei, dat het makkelijker maakt om een hoge opbrengst van grafeen te produceren maar de goede kwaliteit wordt belemmerd door het ontstaan van defecten in de structuur. In hoofdstuk 3 wordt een alternatieve manier voor de productie van grafeen beoordeeld, namelijk chemische exfoliatie van grafiet. Dit deel is onderverdeeld in twee categorieën: de productie van grafeen oxide (GO) en alle andere methoden waarbij geen sprake is van chemische oxidatie van grafeen. De volgende aanpak is bedoeld om de lezer een overzicht te geven van de voor- en nadelen van elke methode in termen van kwaliteit, rendement, structurele integriteit en elektronische eigenschappen.

De organische functionalisering van koolstof nanobuisjes door de 1,3-dipolaire cycloadditie van azomethide ylides opent nieuwe perspectieven voor de productie van oplosbare en gemakkelijk te hanteren CNTs. Na de ontdekking van grafeen is er heel veel aandacht besteed aan de chemische modificatie van de eerste stabiele 2-D monolaag ooit gevonden, die kunnen helpen bij toekomstige toepassingen zoals het gebruik van grafeen als een robuuste steun bij de constructie van composietmaterialen. In hoofdstuk 4 van dit proefschrift beschrijven we onze aanpak voor de organische functionalisatie van enkele laag grafeen door de dipolaire cycloadditie methode die met groot succes is gebruikt voor de functionalisering van koolstof nanobuisjes.

Hoofdstuk 5 is gewijd aan de intercalatie van zuiver grafiet met fullereen. De intercalatie omvat het gebruik van een co-intercalant, die eerst wordt geïntroduceerd tussen de bladen van grafiet, om mee te helpen aan het verhogen van de tussenlaag afstand en dus het intercalatie proces van C_{60}.

In ons geval hebben wij de co-intercalant salpeterzuur gebruikt, dat leidde tot de creatie van grafiet nitraat (GN). De geïntercaleerde salpeterzuur moleculen adsorberen tussen de lagen grafeen met zwakke interacties, zonder een significante invloed te hebben op de grafeen structuur en het helpt de fullereenmoleculen te intercaleren met de grafeenlagen door π-πstacking.

Verwarming van het uiteindelijke materiaal bij relatief lage temperaturen (100 ℃) verwijdert de co-geïntercaleerde en laat alleen de fullerenen in de grafietmatrix. De kwaliteit van het geïntercaleerde is hoog zoals is aangetoond bij Raman metingen. Deze methode is een nieuwe benadering voor de intercalatie van grafiet omdat het geen oxidatiebehandeling vereist en de daaropvolgende reductie van de grafeenstructuur.

In hoofdstuk 6 presenteren we een nieuwe methode voor het creëren van nieuwe multifunctionele hybride systemen na de succesvolle intercalatie van adamantylamine (ADMA)in de tussenlaagruimte van grafietoxide en twee soorten klei , natuurlijke montmorilloniet klei en synthetische laponite klei.

De uiteindelijke hybriden werden gekenmerkt door een combinatie van X-ray diffractie (XRD), X-ray foto-elektron spectroscopie (XPS), FTIR spectroscopie, thermogravimetrische en differentiële thermische analyse om de volledige chemische structuur te onderzoeken.

We kunnen laten zien dat deze pillared materialen zeer geschikt zijn voor het verwijderen van organische verontreinigende (chloorfenolen) uit water en toont significant antikanker activiteit in gekweekte cellen. De voorgestelde synthesewerkwijze leidt tot de regelbare bulkproductie van geïntercaleerde gelaagde materialen voor milieusanering en medische toepassingen.

In hoofdstuk 7 beschrijven we voor het eerst een innovatieve en reproduceerbare methode voor de directe formatie van multiwand carbon nanobuisjes door ultrasonicatie van grafiet in dimethylformamide met toevoeging van ferrocene aldehyde. Ultrasonicatie van grafiet produceert voldoende energie voor exfoliatie in verschillende oplosmiddelen en creëert daarbij vrije radicalen op de grafeenvellen. Ferrocene aldehyde heeft een dubbele rol. Ten eerste gedraagt het zich als een val voor vrije radicalen en daarmee reduceert het de schade aan de gefolieerde vellen. Ten tweede lokaliseert het zich op de randen van few layer grafeen waardoor de vellen oprollen en zo carbon nanoscrolls vormen die converteren in multiwand carbon nanobuisjes. De beschreven methode zal leiden tot een controleerbare productie van carbon nanostructuren door middel van eenvoudige ultrasonicatie behandelingen.

Hoofdstuk 8 is gewijd aan de intercalatie van aluminiumclusters in de ruimtes tussen de grafietoxide lagen en het daaropvolgende gedrag van de afgeleide geïntercaleerde structuur bij verhitting. Na de synthese van Keggin ion $[\mathrm{A1}_{13}(\mathrm{O})_4(\mathrm{OH})_{24}(\mathrm{H_2O})_{12}{}^{7+}]$ hebben we de aluminium polycatie tussen de grafeenoxide lagen geïntercaleerd. Door middel van röntgenstraal diffractie en röntgen foto-elektron spectroscopie kan het succes van onze methode worden aangetoond.

Tot slot in hoofdstuk 9 doen we verslag van de intercalatie van polycyclische aromatische moleculen in de tussenruimtes van de grafietoxide lagen. We hebben het type binding van twee soorten aromatische moleculen (aniline en naftaleen amine) met de grafeenvellen onderzocht. Analine bindt zich aan de grafeen oxidelaag via covalente binding aan de epoxy groepen terwijl naftaleen amine zich bij voorkeur bindt aan het grafeenoppervlak door middel van π-π interactie. Deze nieuwe klasse van hybride materialen verbreedt de horizon voor de intercalatie-chemie van aromatische moleculen aan grafeen gebaseerde nanomaterialen.

Gezien de resultaten is het doel van dit proefschrift, namelijk de synthese en manipulatie van nieuw op grafeen gebaseerde pillared materialen, succesvol behaald en maakt het ruim baan voor verder onderzoek naar de eigenschappen en het gebruik in innovatieve toepassingen.

Curriculum Vitae

Spyrou Konstantinos

Education

2008-2012:	University of Groningen, the Netherlands Ph.D. research in the group of Surfaces and Thin Films, under the supervision of Prof. dr. P. Rudolf.
2007-2008	University of Ioannina, Greece Diploma Thesis Research project: ‘’Attachment of magnetic nanoparticles on carbon nanotubes filled with superconducting single-crystalline tin nanowires: Synthesis and characterization”
2007-2008	University of Ioannina, Greece Diploma in Materials Science and Engineering Admission after National Introductory Examinations
2007	Graduated from 1st Lycceum (high school) of Ioannina, Greece

List of publications

1. Gengler, R.Y.N.; Spyrou, K.; Rudolf, P. 2010. A roadmap to high quality chemically prepared graphene. Journal of Physics D: Applied Physics 43, 374015.

2. Quintana, M.; Spyrou, K.; Grzelczak, M., Browne, W. R.; Rudolf, P.; Prato, M. Functionalization of graphene via 1,3-dipolar cycloaddition. ACS Nano 2010, 4, 3527–3533.

3. Quintana, M.; Grzelczak, M.; Spyrou, K.; Calvaresi, M.; Bals, S.; Kooi, B.; Van Tendeloo, G.; Rudolf, P.; Zerbetto, F.; Prato, M.; 2012. A Simple Road for the Transformation of Few-Layer Graphene into MWNTs. J. Am. Chem. Soc. (In Press).

4. Quintana, M.; Grzelczak, M.; Spyrou, K.; Kooi, B.; Bals, S.; Van Tendeloo, G.; Rudolf, P.; Prato, M. 2012. Production of large graphene sheets by exfolition of graphite under high power ultrasounds in the presence of tiopronin. Submitted to Chem. Commun.

5. Spyrou, K.; Kang L.; Gengler R. Y. N.; Diamanti, E.; Gournis, D.; Prato, M.; Rudolf, P. A novel route towards high quality fullerene-pillared graphene. (Ready for submittion)

6. Spyrou, K.; Diamanti, E.; Potsi. G; Velalopoulou, A.; Verginadis, G.; Deligianakis, G.; Gournis, D.; Rudolf, P. Towards novel multi-functional pillared layered nanostructures: effective intercalation of adamantylamine pillaring species in graphene oxide and montmorillonite nanoclay. (In preparation)

7. Spyrou, K.; T. Tsoufis, Gournis, D.; Zerbetto F.; Rudolf, P. The interaction between organic polycyclic aromatic molecules and graphite oxide: A new study towards intercalation. (In preparation)

8. Spyrou, K.; Diamanti, F.; Rudolf. P, Gournis, D. Pillaring of GO with $[A1_{13}(O)_4(OH)_{24}(H_2O)_{12}{}^{7+}]$ Keggin ions and derived hybrids (In preparation)

9. Dimos K.; Papayannis K. D.; Diamanti K.E.; Baikousi. M, Spyrou K.; Rudolf P.; Gournis D.; Karakassides A. M.; Carbon-based materials abnormal thermal behavior. (ready for submittion)

SOME WORDS OF GRTITUDE

It was summer of 2008 when I received an offer for a PhD position from the University of Groningen…..ups if I start like this I want another 50 pages to finish my thesis. In any case I don't like to talk about myself, I never do it. But knowing that during my defense date you will be a bit bored watching me answering questions it is the best opportunity to show my appreciation for some people.

I would like to express my recognition to Prof. Petra Rudolf for her valuable help and support all these years. I still remember the first day we met, while I was searching the entire Zernike complex trying to find the group of surfaces and thin films. I would never forget her warm welcome that made me feel less stressed. Whenever I needed help you were there for me leading me, with your valuable knowledge. Your office was always open for me when I needed advices, even when you were really busy telling me that my students are the most important part. Petra it was a great pleasure for me working next to you. Thank you for believing in me.

A special appreciation for my second promotor Prof. Dimitrio Gourni. Dimitri If I tried to tell you how much I appreciate you, I'd be talking the rest of my life. You are the best example for me in order to continue in this field. (Το ότι έχω φτάσει ως εδώ το οφείλω σε σένα).

I gratefully thank Prof. Mauricio Prato. It was an honor for me to collaborate with such a great scientist.

Special thanks to the two of my paranymph: Luca and Konstantinos who are willing to take care of all the preparations.

Yvonne is the best secretary a group could ever have with a big smile, great sence of humour and always willing to help.

Over my PhD I have collaborated with many people, to whom of course I own the biggest part of my thesis. In particular I wish to thank Prof. Zerbetto F from University of Bologna, Prof. Kooi, Browne, W. R. and Tsoufis T. from University of Groningen, Prof. Bals S. and Prof Van Tendeloo, G. from University of Antwerp, Mildred Q. and Grzelczak M. from the university of Trieste, Regis G from University of Groningen., Prof. Deligianakis, G. Evmorfia Diamadi, Verginadis, G.; Potsi. G. Seristatidou E. from University of Ioannina.

Leaving in a lab the bigger part of my day is like having a second house. And as every house has a family I also had one all these years. I would like to thank all the people from my group. Regis I appreciate all the support in the lab, but also for the nice talks in the office 0066 where we spend days and nights. Tatiana thank you from the bottom of my heart for all your help during these years. From the first day I arrived you integrate me as part of the PhD family and you make me feel like home. You're a good friend. Luca and Stefano even If we were working in different aspects we were close to each other sharing good and bad moments and of course I cannot forget our going out nights. Aleksey I appreciate all the help I receive from you whenever I need it in the lab, wishing you the best for the future. Meike, Peter, Lumi, Martina, Naureen, Juan Carlos, Moritz, Kathrin, Fey, Ahn, thank you all for the nice time we spend in the lab. Finally I am grateful for the tecknicians Luc and Hans who helped me many times with problems in the lab.

I wish to thank the members of the reading committee, Professors P. Mauricio, J. A. Loontjens and K.U.Loos for their willingness to read my thesis and for the valuable suggestions. I appreciate your input that improved my thesis in many ways.

I have met a lot of people during my stay in Groningen, from all over the world. These people hug me from the first time and integrate me in the big family of the university and of Groningen. Friday nights and party themes will be unforgettable. I would like to thank all of them one by one for their friendship and all the support and good times we had together. Tano and Jesus (My best Mexican friends), Maurizio (watch out!) Andrea and Alessio (Fridays were never the same), Luminita, Maria Jesus, Maria Jose, Santi (I will never forget your amazing parties), Luminita, Philippo and Dorota, Giulio, Johanne, Alina (for the fruitful discussions), Orcun, Ilias, Elke, Juan Carlos (3 months are enough to consider you as good friend), Panos (Πάνο σε ευχαριστώ για τη βοήθεια σου όλα αυτά τα χρόνια), Nikos Dalavouras (Νίκο σε ευχαριστώ για την ωραία παρέα το πρώτο χρόνο που ήρθα στο Groningen), Luminta Fediuc, Bi Rongrong (my studenthouse friends) .

I would like also to thank all the members of the football team. 4 years of early wake up on Sundays after hangovers, thousands of fights with strong Dutch players and of course a lot of fun. Elmer (captain), Johan, Julio, Stefano, Manfred (the unbreakable midfielder), Andrey (Crazy Russian), Bas, Dumaz, Peter, David, Oscar, Julien, Phillip, Yasen, Andrea, Mark, Guiseppe, Ivan. Keep scoring….

A special blessing to ACLO, my second house. Thousands of hours with the Triathlon team, the fitness, the swimming pool, the spinning courses, the futsal team. Sports make you feel better and I cannot imagine my life without them! In this part I would like to thank Bauke for the nice trainings.

A special thanks to my two Groningen sisters Maria Ivanova and Evi Katsoula (Love you both), Dimitris Arvanitis, Evelina and Doris (Δημήτρη, Εβελίνα, Δόρη και Εβη δε θα ξεχάσω ποτέ πόσο πολύ μου σταθήκατε από τη πρώτη στιγμή που ήρθα στην Ολλανδία και επίσης για τα ωραία ταξιδάκια στην Ευρώπη).Jantina thank you for the nice moments we spend together and the wonderful spiritual talks.

My best friends Λευτέρη, Κώστα, Πάρη, Σπύρο, Λεωνίδα, Λευτέρη, who are standing next to me 23 years in good and bad moments. I have to add in this family a new member Βασίλης who support me 4 years in the Netherlands. I cannot imagine if I could make it without them. “Σας ευχαριστώ πολύ για όλα και που είστε στη ζωή μου”. I am very lucky that at the end of my PhD I found Konstantinos and Savas spending nice moments. (Αν και σας ξέρω λιγο καιρό σας θεωρώ πολύτιμους φίλους και σας ευχαριστώ για όλες τις ωραίες στιγμές που περάσαμε μαζι ευελπιστώντας να επακολουθήσουν και άλλες).

To all the members of my beautiful family who were of great help by their ways of giving and creating my confidence in myself and of what came out of me. The family that has truly been a good example of love, hard working, honesty and decency. Μπαμπά, Μαμά, Αποστόλη, Τούλα, Νίκο, Χαρούλη σας ευχαριστώ πολύ για όλη τη βοήθεια όλα αυτά τα χρόνια. Θεία Σοφία, Ελένη, Βίκυ, Γιάννη, Θεία Ρούλα, Ελένη, Έφη, Σοφούλα, Γιώργο, Κώστα, Θεία Γιαννούλα σας ευχαριστώ!

From the first day of my PhD till the last I gave my soul in order to retrieve knowledge.